City University London

ACTIVE VIBRATION CONTROL OF CIVIL ENGINEERING STRUCTURES

BY

PANAGIOTIS RENTZOS

A THESIS SUBMITTED FOR THE DEGREE OF DOCTOR OF PHILOSOPHY

CITY UNIVERSITY, LONDON
SCHOOL OF ENGINEERING AND MATHEMATICAL SCIENCE

CONTROL ENGINEERING RESEARCH CENTRE

DECEMBER 2007

To

my parents

TABLE OF CONTENTS

LIST OF FIGURES

LIST OF TABLES

Acknowledgements

First and foremost, this arduous journey en route to a PhD would not have been possible without the kind support and guidance of my supervisor Dr. G. Halikias. His patience, tolerance, kindness and encouragement were the most important factors that led to the completion of this work.

I would also like to thank Professor N. Karcanias for assisting me in developing the ideas and formulation in the *pendulum* chapter, and also Professor K. Virdi and Dr. E. Milonidis who were always keen to help me.

Studying towards a PhD would have been impossible if it had not been for my family. I sincerely thank my parents and brother for their constant moral and financial support.

I would also like to acknowledge the state of Luxembourg for partially financing my project.

My overall experience at City University was enjoyable. We shared a nice, amicable, and co-operative environment with my friends in the office and our supervisors. I would like to thank all of them and Edyta.

"I grant the powers of discretion to the University Librarian to allow this thesis to be copied in whole or in part without any further reference to me. This permission covers only single copies made for study purposes, subject to normal conditions of acknowledgment".

Abstract

This thesis is in the area of active vibration control of Civil Engineering structures subject to earthquake loading. Existing structural control methods and technologies including passive, active, semi-active and hybrid control are first introduced. An extensive analysis of a frame-pendulum model is developed and analysed to investigate under what conditions effective energy dissipation is achieved in Tuned Mass Damper systems and the limitation of these devices under stiffness degradation when the structure enters the inelastic region.

Linear Quadratic Gaussian and H-infinity active control schemes are designed, simulated and assessed for buildings, modelled as lumped parameter systems, including base and actuator dynamics. Various aspects of the designs are extensively evaluated using multiple criteria and loading conditions and validated in large-scale benchmark problems under practical limitations and implementation constraints.

A novel design method is proposed for minimising peak responses of regulated signals via a deadbeat parametrisation of all stabilising controllers in discrete-time. The method incorporates constraints on the magnitude and rate of the control signal and is solved via efficient Linear Programming methods. It is argued that this type of optimisation is more relevant for structural control, as failure occurs when maximum member displacements are exceeded.

The problem of stiffness matrix estimation from experimental data is formulated as an optimisation problem and solved under various conditions (positive definiteness, tri-diagonal structure) via an alternating convex projection scheme. Both static and dynamic loading is considered. The method is finally incorporated in an adaptive control scheme involving the redesign in real-time of an LQR (Linear Quadratic Regulator) active vibration controller. It is shown that the method is successful in recovering the stability and performance properties of the nominal design under conditions of significant uncertainty in the stiffness parameters.

CHAPTER 1

INTRODUCTION

1.1. Introduction

Protecting structures from environmental hazards such as earthquakes and wind loads has always been a challenge in civil engineering. Strong earthquakes can have devastating effects even for countries like the USA and Japan that have the economic and technologic ability to design structures safely for such loads. Designing structures strong enough to resist earthquakes that are likely to occur at most once in their lifetime is uneconomic. Earthquake engineering design is always evolving and current codes of practice are based on concepts of inelastic energy absorption and controlled damage. In modern design practice emphasis is placed on giving structures elasticity rather than strength by allowing for larger deformations during earthquakes. This has resulted in fewer buildings collapsing and reduced number of deaths, but has increased the economic costs due to damaged buildings. There is growing demand for designing buildings that can not only prevent them from collapsing, but also minimises damage by reducing vibrations from earthquakes, wind loads and also heavy traffic, waves or deliberate acts.

A novel idea for protecting structures is the use of structural control. This involves the use of damping devices or active mechanisms that help suppress undesired vibrations of civil engineering structures. Given that seismic design methods are already based on energy absorption concepts, it is surprising that it took so long for this method to be developed in the area of structural engineering, since similar techniques (e.g. suspensions) have been used for a long time in the automotive industry. Passive systems are mechanisms in structures that dissipate energy. In Civil Engineering applications the most common passive damping device is a tuned-mass-damper (TMD). This dissipates energy by placing a mass on the top of a building, oscillating with the same frequency as the building's resonant frequency (fundamental mode).

A different method is active control, where actuators capable of producing large forces are placed inside a building to counteract external forces, e.g. due to earthquakes or wind loading. The most common mechanism is the active mass driver (AMD). A large mass, placed on top of the building, is being driven by actuators counter-balancing the movement of the building from the earthquake. What began as a theoretical state of the art method is slowly gaining acceptance by the industry and is progressively used more frequently in structures. The first structure to implement active structural control was the Kyobashi Seiwa building in Tokyo [Lynch 1993] in 1989. This 10-storey building had two controllers placed on the roof counteracting the first two modes of vibration whose mass was about 1% of the total mass of the building. The actuators were suspended like a pendulum and used hydraulic pumps to transfer energy. The devise was used to control the building during large winds and small to moderate earthquakes.

An active control mechanism consists of an actuator, a control mechanism, a (mathematical) control law and sensors to record the motion of specific parts of the structure [Hatada and Smith 1997]. An actuator is placed at a certain position in the structure, and when a disturbance occurs (e.g., earthquake, high wind, etc.) the sensor records it and sends the signal to the computer, which in turn analyses the data and triggers the actuator. The actuator generates the appropriate forces that attempt to minimise or suppress vibrations thus stabilising the building. In the sense described above, active control is more demanding than passive because a poorly designed system may lead even to instability.

There are several disciplines required to design a good active structural system and several major areas where active research in structural control is taking place. These include:

- Structural dynamics and the theory of vibrations; the underlying theory behind why and how structural control works.

- "Intelligent" mechanical systems that require the minimum possible energy to be efficient and can effectively transfer energy from the

actuator to the control device with minimal losses (tuned mass dampers, active mass drivers, hybrid control devices, smart material etc).

- Control systems design; including accurate modelling of disturbance-structure-controller interaction, appropriate optimal/robust control design algorithms and any other issue arising in control engineering problems (e.g. instrumentation, actuators-sensors placement, etc).

- Evaluation of the overall control system via computer simulations and validation of simulations via experimental work.

The thesis is mainly focused on theoretical aspects of control systems design necessary for structural control. Since structural control is a new application area of feedback control, the existing techniques (and algorithms) and design methods have to be re-examined and their applicability in structural control reassessed.

Control Systems is the area of engineering that deals with the analysis and synthesis of dynamic system responses. The main objective of control engineering is to modify the "open-loop" dynamics of the system by manipulating its input and output variables, so that the "compensated system" has improved dynamic-response characteristics in terms of stability margins, disturbance rejection or noise immunity. Typically, the controller is implemented in a closed-loop (feedback) configuration, automatically adjusting its input signals using measurement information arising from its outputs, so that the overall system operates automatically. In the context of active structural control the measured information is typically provided by strain-gauges, displacement sensors or accelerometers placed at strategic locations on the structure. This information is sampled and fed to the controller, which consists of an algorithm implemented inside a computer. The algorithm generates digital signals that, after being converted back to analogue form, are applied to the inputs of the actuator (typically an electro-mechanical or hydraulic device), which generates an appropriate force or torque to counteract the external effects due to the earthquake or wind load.

Modelling is central in control systems design. Buildings are usually idealised as linear time-invariant lumped spring-mass-damper systems. The control device requires appropriate modelling and by interacting with the structure a new increased order model is obtained. The effect of disturbances on a structure and the way they propagate and affect its response are also essential aspects in modelling the combined earthquake-structure-controller system. Material non-linearities, external perturbations and uncertainties of structural parameters are also common and need to be taken into account in the modelling process. Physical systems can never be exactly approximated by mathematical models, but the closer the representation the more accurate conclusions can be drawn about the system's expected behaviour.

In the context of active structural control the objective is to suppress vibrations arising from external disturbances (Earthquake or Wind load) by effectively absorbing energy and improving the damping of the structure. In contrast to more straightforward active control applications (e.g. automotive active suspension systems), civil engineering structures are significantly more complex systems dynamically. This is mainly due to the presence of a large number of vibration "modes" (longitudinal, lateral, torsional), which are typically coupled. Complexity also arises from the interaction between the structure and its surrounding soil (in the case of earthquakes) and due to non-linear effects, especially in the presence of large forces/displacements when parts of the structure enter the inelastic region. Modelling accurately the disturbance signal (Earthquake or Wind load) in terms of its strength, frequency and energy content and its interaction with the structure gives rise to an additional source of complexity.

Over the last few years a wide range of design methodologies have been proposed in the area of structural control, including non-linear/sliding-mode control, pole-placement and observer-based methods, adaptive control, fuzzy/neural-based methods, reliability-based control and optimal control [Housner et al 1997]. Optimal control appears to be the design method increasingly favoured by most researches, mainly due to important recent theoretical advances in this field and to the design flexibility that this method offers. The two most important optimal control paradigms, around which most other optimal-control methods cluster, are LQR/LQG optimal control and H_∞ optimisation methods which are examined thoroughly in this work. In addition, new design optimal

algorithms are proposed to account for different objectives and assessed via analytical and simulation results.

1.2. Thesis main contributions

- Under cycling loading, present during earthquakes, steel ceases to have elastic properties. This results in the change of strength and stiffness of steel elements and reduction in the frequency of vibration of the structure. Simulation results based on the frame-pendulum system are used to describe the dynamic behaviour of an inelastic steel structure employing passive control.

- Prior knowledge of the characteristics of the input disturbance signal in control systems design is beneficial for the design of the feedback controller and the optimisation of its response. Here, an identification filter obtained by analysing the spectral characteristics of a real earthquake signal is obtained and incorporated to an LQR design procedure, which is subsequently analysed and simulated. The results show that improved levels of performance can be achieved with this method and suggest the importance of using any such a-priori information, whenever it is available.

- A novel design method is proposed and developed that aims to reduce maximum peak responses of regulated inputs, an objective especially appropriate for structural engineering applications. The resulting optimisation problem involves the parametrisation of all discrete finite settling-time stabilising controllers and is solved using linear programming. The controller is designed for a variety of input signals and the obtained simulation results are compared with those obtained by other methods. Particular care has been taken to make the design method realistic by incorporating appropriate constraints on the magnitude and rate of the resulting control signal. Other practical issues have also been addressed, e.g. controller model reduction, addition of pre-whitening filters, optimising the design by considering different disturbance models, computational issues arising from the Linear Programming algorithm, etc.

- A novel method is proposed for estimating poorly or partially known stiffness matrices of structures from online data recorded from its dynamic response. The method relies on the solution of an optimisation (distance) problem over the cone of positive-definite matrices. The estimation method can be applied to structural stiffness matrices arising in civil engineering applications, including a special form of tri-diagonal structure corresponding to the models developed in this work. Various techniques are developed for the solution of the optimisation problem, convergence is formally established and comparisons between the different methods are made through simulations.

- Structures affected by earthquakes or other environmental loads often require reinforcement in terms of structural control. If the stiffness of such a structure has degraded at unknown levels, there is difficulty in designing a suitable controller. This problem can be overcome by performing on-line estimation of the uncertain stiffness parameters during an earthquake. After an acceptable number of measurements have been obtained, the estimator should ideally converge to the true stiffness parameters which can then be used to re-design the controller. In the thesis the estimation technique described in the previous paragraph is combined with an on-line LQR tuning control method, resulting in a robust adaptive design algorithm. Simulation results demonstrate the ability of this method to suppress vibration and stabilise a structure (which otherwise would be unstable if the wrong initial parameters were used for control design), even in the presence of considerable levels of uncertainty in the stiffness parameters.

- The control techniques investigated in this work are applied for two industry-standard benchmark problems which have been proposed recently to evaluate different control design schemes. The benchmark problems involve the control design of two real large-scale structures under stringent practical requirements and assessed with multiple performance criteria. The relative advantages of each design method examined are analysed and discussed.

1.3. Thesis Outline

Chapter 2 reviews the literature on existing structural control methods. The chapter is focused on describing practical aspects of mechanical control systems and their use. The main control methods, i.e. passive, active, hybrid and semi-active control are introduced. The potential merits and drawbacks of each method are explained and an example of a real structure employing a control mechanism corresponding to each method is presented.

In chapter 3 the control-design methods used throughout the thesis are presented, starting from basic definitions and building up to more advanced topics, which form the foundations of the techniques used in subsequent chapters. A brief introduction of the preliminaries of control systems theory is given, followed by topics related to systems modelling and mathematical systems' representations. Examples are given of simple mass-spring-damper models, their transfer functions and state-space representations. Concepts of discrete-time control, controllability, observability, and systems' representation in terms of time-domain and frequency-domain techniques (Bode plots) are also included here. Classical control methods such as pole placement, Linear Quadratic Regulators (LQR) and Kalman filters are discussed in more detail. The H_∞ control problem is formally stated and its solution is outlined using the Youla parametrisation approach.

The next chapter analyses a passive control system, namely a frame with a pendulum providing energy dissipation. The aim here is to establish whether the pendulum, which is a natural system without any external interference, can reduce directly or indirectly the vibrations of the frame. Three possible mechanisms for achieving this are suggested and analysed with the help of linear and non-linear simulations. General rules are established on how to tune the parameters to obtain optimal results. The second part of this chapter deals with the concept of inelastic material behaviour. When steel exceeds its elastic limit its stiffness degrades permanently or temporarily. This results in changes of the characteristic period of vibration of the structure. By using a simple non-linear

stiffness model the effectiveness of the developed passive control system is analysed and discussed.

In chapter 5, a detailed design of an active controller is presented. The objective here is to establish how active control can be designed and implemented in practice. A 3-storey building is modelled, including base dynamics and employing an active tendon control mechanism. The control design method used is based on Linear Quadratic Regulator (LQR) theory which is analysed in depth. A multi-objective controller is designed and tuned by including appropriate penalty terms and subsequently augmented with a Kalman state estimator (LQG). The LQR controller is evaluated for many different scenaria using extensive simulations: Passive, impulsive, sinusoidal and real earthquake responses of acceleration, displacement and inter-storey drifts are presented and analysed, both in the time and frequency domains. Finally, an identification filter is included emphasising performance in the frequency range where the spectral density of the earthquake signal is large (i.e. the frequency range where most of the energy of the earthquake signal is concentrated) and an LQR controller is re-designed and re-assessed.

In chapter 6, as a continuation of the work in the previous chapter, an H_∞ controller is designed. The same structural model is used for design purposes and the simulation results are evaluated including passive, impulsive, sinusoidal and earthquake responses, as before. In the design problem formulation frequency-dependent weighting functions are included in order to emphasise specific frequency ranges appropriate to each design objective, in addition to scalar penalty terms also used in LQR. The results of LQR and H_∞ control designs are compared in terms of peak/RMS responses and damping properties. Conclusions are drawn about the validity of the two design methods for this specific case study and also their general applicability in the area of structural control.

Chapter 7 presents a novel design approach aiming to minimise the maximum peak response of regulated signals (rather than their energy or RMS values). This is a more relevant design objective for structural control, since structural failure occurs when the maximum deformation capacity of members is exceeded. The method is formulated in discrete-time and uses a parametrisation of all closed-loop finite settling time stabilising controllers. This leads to a linear programming optimisation problem. The problem formulation allows the designer to set constraints on the maximum control signal and its

rate. The designer has also the choice of setting the exact settling time of the response. After the derivation of the design algorithm, the optimal controller is obtained and simulated for various inputs. Comparisons are made with the results of the LQR design, for a full evaluation of the method.

Chapter 8 deals with the estimation of positive (semi-) definite stiffness matrices. By applying a set of forces F and measuring the resulting displacements X, the stiffness matrix of a structure can be obtained. The "Procrustes algorithm" is proposed as an optimisation tool for estimating K when there are measurement errors in F or X and (possibly) a-priori knowledge of the structure of the K matrix. Three special forms of stiffness matrices are common among Civil engineering structures; these include general positive (semi-) definite matrices, triadiagonal positive (semi-) definite matrices, and triadiagonal positive (semi-) definite matrices with additional redundancy between their elements, arising in models of buildings. All three cases are examined by using the Procrustes algorithm, developing analytic solutions or combining with existing optimisation methods (e.g. convex alternating projections algorithm). The estimation can be computed using either static loading, or from the structure's dynamic response in the presence of an external disturbance. Finally, a case study is presented where an active control system is employed by a structure without exact knowledge of its stiffness matrix. The aim here is to determine whether such a system can be stabilised, by re-designing the controller at every sampling step using the updated information of the stiffness parameters provided by the estimation procedure.

Chapter 9 applies the control design algorithms used in previous chapters in two benchmark problems, followed by the evaluation of the results of each method. Here, all the practical aspects related to the implementation of real schemes are included in the analysis, such as time delays, saturation of control signals, quantisation effects in digital control, large-scale models and their approximation, multiple design objectives, etc. The control methods are evaluated mainly in terms of peak and RMS responses of acceleration, displacement and inter-storey drift variables. Two benchmark problems involve the control design for two real buildings, the first being a 3-storey structure and the second a 76 storey tower designed for resistance to wind loading.

The last chapter outlines the main conclusion of this work and suggests directions of future research based on open issues resulting from the present work.

CHAPTER 2

LITERATURE SURVEY ON STRUCTURAL CONTROL

2.1. Introduction

Earthquakes' action is a natural disaster responsible for many casualties and economic loss. Although seismic design has been increasingly improved over the years and the majority of buildings can resist high earthquakes, casualties are still high and the question of achieving good results subject to economic considerations is important. Currently the codes of practice (in Europe and USA) state the following [Eurocode 8 1998]:

For small earthquakes:	A structure should be able to withstand the earthquake without any damage.
For moderate earthquakes:	Some structural damage is allowed as long as it is repairable after the earthquake.
For large earthquakes:	Heavy structural damage can occur without collapse and loss of life even if after the earthquake the building is uninhabitable.

The current way of seismic design, which satisfies the above requirements, is to design buildings in the inelastic range. This means that a structure can resist only a specific amount of the applied force (20-25 %) but does not fail because it has high ductility. This method fulfils the requirements set out by the code of practice, and has managed to limit the number of casualties. As a result the death toll after an earthquake is significantly reduced but the economic loss has increased due to damaged buildings. New methods have developed that minimise the effect of earthquakes and make the

buildings usable even after high earthquakes. Active control of structures is a promising new field that fulfils these criteria.

The idea of passive control for minimising the effects of earthquakes is very attractive since, without withstanding the whole energy of an earthquake, a passive device can be installed that dissipated high amounts of energy thus making a structure economic and safe. The main advantage of this system is that it remains undamaged even after a relative large earthquake. However, it soon became apparent that such a system cannot fully protect a structure from very large earthquakes. Since the idea of controlling structures existed, the new concept of actively controlling structures was born, in which energy could be injected to a building to help it withstand earthquake forces. In the following paragraphs a detailed review of the most-commonly used control methods is given. These include passive, active, semi-active and hybrid control.

2.2. Passive Control

A passive control system is one in which structural vibrations are reduced using a passive control device imparting a force upon the structure. By the term passive control two main types are meant, base isolation and mechanic energy dissipation systems. These include: metallic yield dampers, friction dampers, viscoelastic dampers, viscous fluid dampers, tuned mass dampers (the framework of active control), tuned liquid dampers, etc. [Housner et al 1997], which will be described in later sections.

2.2.1. Base isolation

The concept of base isolation dates 50 years back but it was not since recently that it was applied in its current form. It is not a widely used method, mainly because it is not sufficiently tested for large earthquakes. The theory of base isolation relies on the idea that the superstructure would not be subjected to large accelerations if it was partially "disconnected" from the foundations of the building. Hence the earthquake force would not be transferred from the ground to the upper floors of the building. Base isolation manages to keep the structure rigid, by inserting a layer of rubber under the ground

floor, so that the energy of the earthquake is dissipated and the superstructure exhibits reduced accelerations. The main disadvantage of this method is that high ground displacement can occur, but if two buildings are separated by a sufficient distance. it can be very efficient. Base isolation cannot minimise disturbances arising from higher modes but increases the damping of the fundamental mode of the structure and therefore provides a safe solution in many cases.

There are two basic types of isolation systems. The system that has been adopted most widely in recent years is typified by the use of elastomeric bearings [Kelly 1991]. This isolation system deflects the earthquake energy through the dynamics of the system instead of absorbing it. A layer of low horizontal stiffness is added between foundations and building, aiming at decoupling it from the horizontal components of the earthquake. This results in decreasing the fundamental frequency of the structure and removing it from the dominant earthquake frequencies and also increases the fundamental mode contribution, minimising effects from higher modes [Chang et al 2001]. The higher modes, that can produce displacements, do not participate in the motion because they are orthogonal to the first mode. The first dynamic mode produces large deformations on the isolated system while keeping the structural responses low. This base isolation approach is valid even when no damping is present, although some damping is beneficial. Recently, a significant amount of research in this area involves ways to increase damping [Tsai et al 2003], the problems with this issue lying in the highly non-linear mechanical behaviour of high damping rubber bearings. Apart from this topic, significant amount of research concentrates on the design and implementation of more practical base-isolation systems that can be used in practice; this mainly consists of testing various schemes for choosing the appropriate material required and gaining acceptance from the industry.

The second type of base isolation uses the sliding system, where a friction-pendulum is a sliding system using a special interfacial material sliding on stainless steel [Kelly 1991]. This works by limiting the transfer of shear across the isolation interface. The friction pendulum system uses a spherical sliding interface to provide restoring stiffness while the friction between the sliding interfaces dissipates energy. It results in increasing the structure's fundamental period and moving it away from the earthquakes' dominant frequency content. There are several systems [Wang 2002] employing

friction-pendulum systems, among others the San Francisco International airport, Greece's centralised liquefied natural gas storage tanks, the Benicia-Martinez bridge and three buildings in China.

Base isolation on its own does not have any control associated with it and therefore will not be examined further. However, it can be combined with several active or semi-active control systems and therefore a basic understanding of the concept is needed. For further information on the topic of base isolation see [Tsai et al 2003]. A typical example of a base isolation system is shown in figures 2.1 and 2.2.

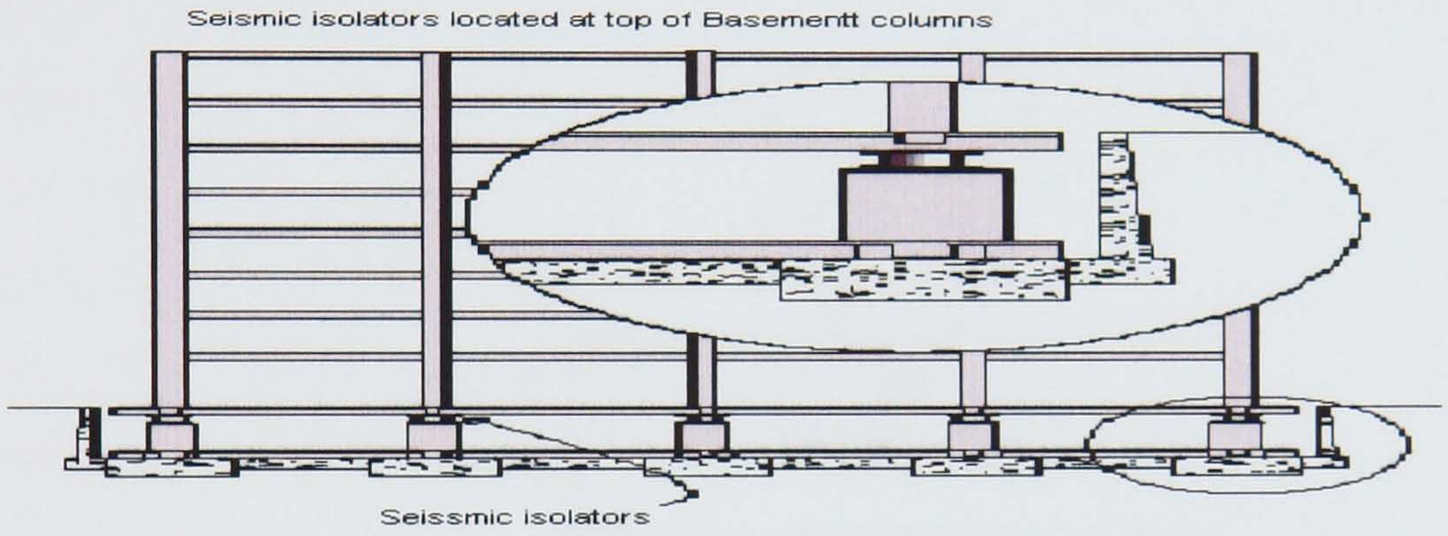

Figure 2.1 Seismic isolators located at top of basement column. Source: [DIS]

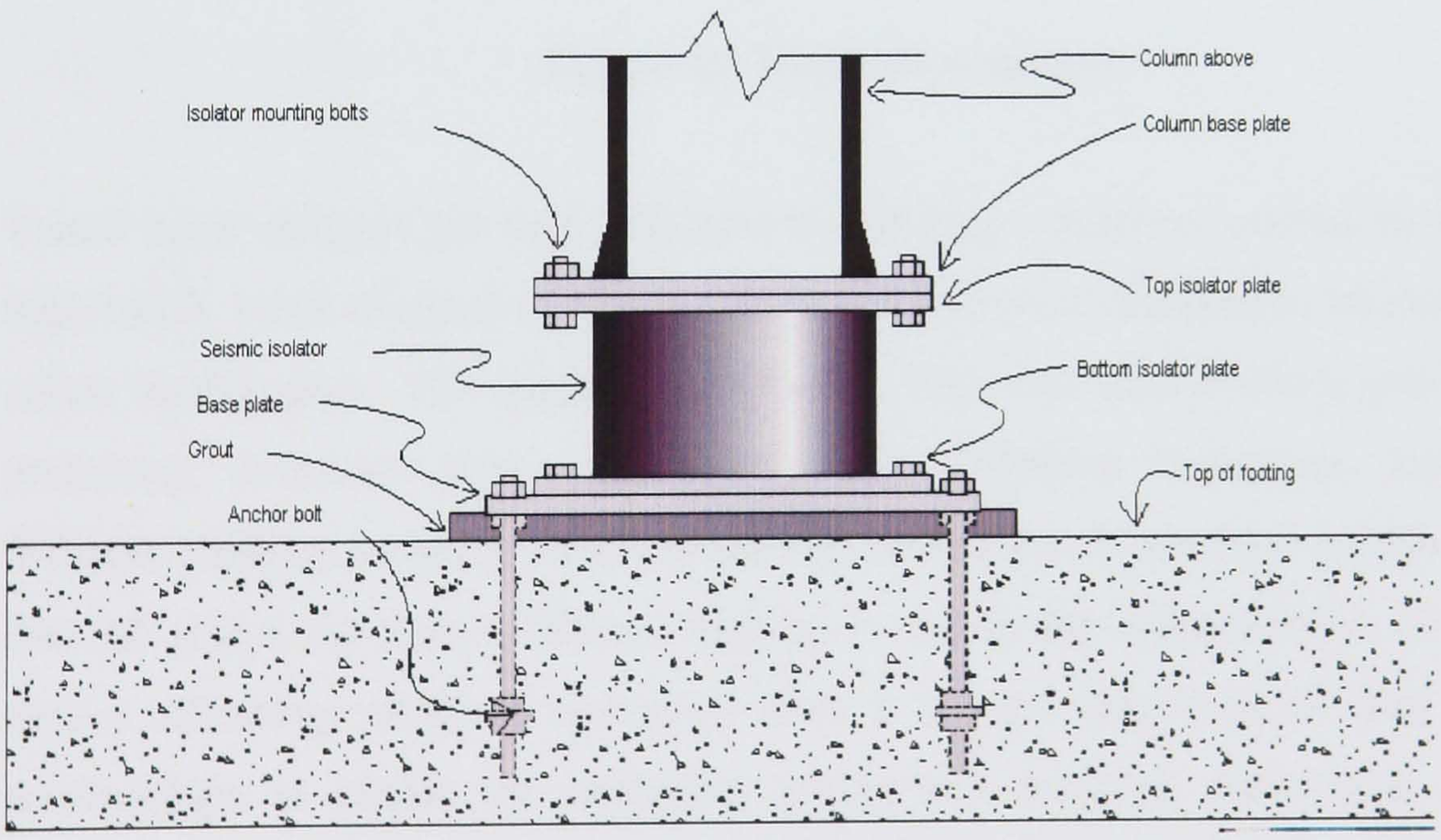

Figure 2.2 Seismic isolator. Source:[DIS]

2.2.2.Mechanic energy dissipation systems

Tuned mass dampers: The concept of tuned mass dampers dates back to the 1940's. Tuned mass dampers can stabilise the heights of tall buildings against violent motion. The presence of a tuned mass forces a comparitavely lightweight building structure to overcome the inertia of a giant concrete block placed in such a way that the block only begins to move in one direction just as the building begins to move in the other, thus dampening the building's oscillatory motion. Shown schematically in Figure 1, a TMD is a modular device composed of a spring, mass, and dashpot. These three components can each be implemented in a number of different ways, as illustrated in figure 2.3.

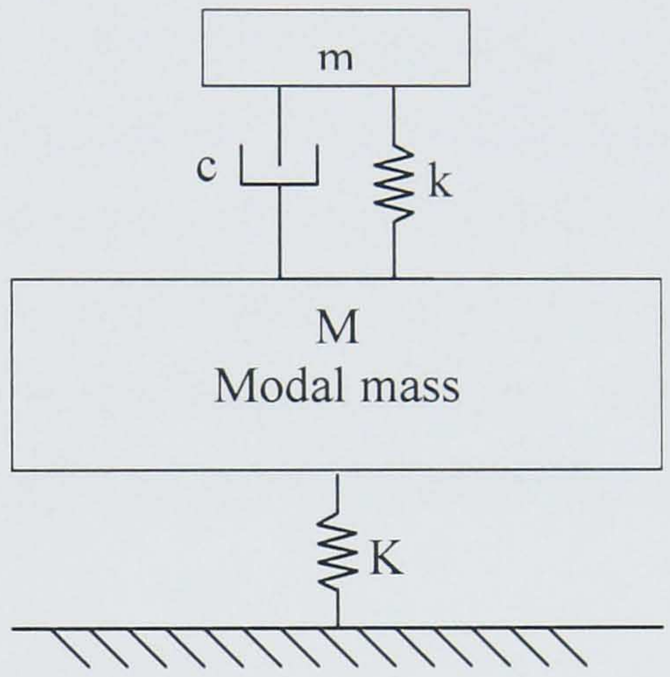

Figure 2.3 Tuned mass damper

Tuned mass dampers are very effective in reducing vibrations excited by high winds, high traffic loads or gyms inside buildings and minimise inhabitants discomfort during minor earthquakes. The question is whether they can also produce good results in protecting structures from large earthquakes. Different researchers have reported different findings in terms of the efficiency of TMD's. It has been widely recognised that the reason for these different findings is due to the characteristics of the ground motion affecting vibration reduction; thus it is very important to find appropriate relationships to obtain the optimum, tuning and damping parameters, an area of significant current research interest [Singh et al 2002]. Also a TMD can only decrease the fundamental (the normal mode of vibration having the lowest frequency) mode's response. An answer to this problem is the use of several TMDs [Li 2002], [Li 2003],

[Li and Liu 2002], each tuned at different modes to represent all dominant modes of vibration.

Another area of research in TMDs is the form of the actual mechanism with several different types of systems being proposed (spring-mass type, pendulum type, circular track type, ring-like pendulums etc.). Other considerations on TMD's include the actual mass that can be placed on the top of a building, the movement of a TMD that would be enough to stabilise the building and minimising the friction of a TMD.

Among all the different mechanical energy dissipation systems, TMD is the most attractive one since its use is economic and proven for other vibration mitigation apart from large earthquakes. Therefore it could be more efficient to improve TMD's rather than develop and use other more sophisticated methods. TMD's are very commonly used together with other active control systems and hybrid systems, and it has even been suggested that a TMD would be very efficient if combined with a base isolation system. The base isolation would act to increase the contribution of the fundamental mode and the TMD would decrease the amplitude of vibrations. Extensive work on the area of TMD control has been reported by several researchers including [Johnson et al 2003] and [Singh et al. 2002].

Tuned liquid Dampers(TLD): Tuned liquid dampers are systems that add damping to a structure by the adverse motion of water. The advantage of this method is that the liquid can provide a very large force in very economic terms (low energy, low cost of material and maintenance). The disadvantage is that the motion of water is very difficult to describe and model. Although TLD's have been used for suppression of wind vibrations, their use in cases of earthquakes is in question due to the very large force that will have to be applied. The behaviour of liquids is very difficult to model, especially when at increased motion waves occur that tend to destabilise the system. Therefore, a lot of theoretical and experimental work needs to be carried out in order for this method to gain acceptance for earthquake resistance.

Configuration: A TLD consists of a rectangular container filled with two immiscible fluids that dampen the response through the motion of the interface. Another popular TLD is a Tuned Liquid Column Damper (TLCD) which consists of a tube filled with

water. The fundamental period of the system depends on the length of column of water. The dissipation term is non-linear and depends on the coefficient of head loss (figures 2.4, 2.5). The concept of using water to actively control a structure is attractive but due to its very unpredictable behaviour, especially at sudden loads that would be present in active control, it is very difficult to use for large earthquakes [Housner et al. 1997].

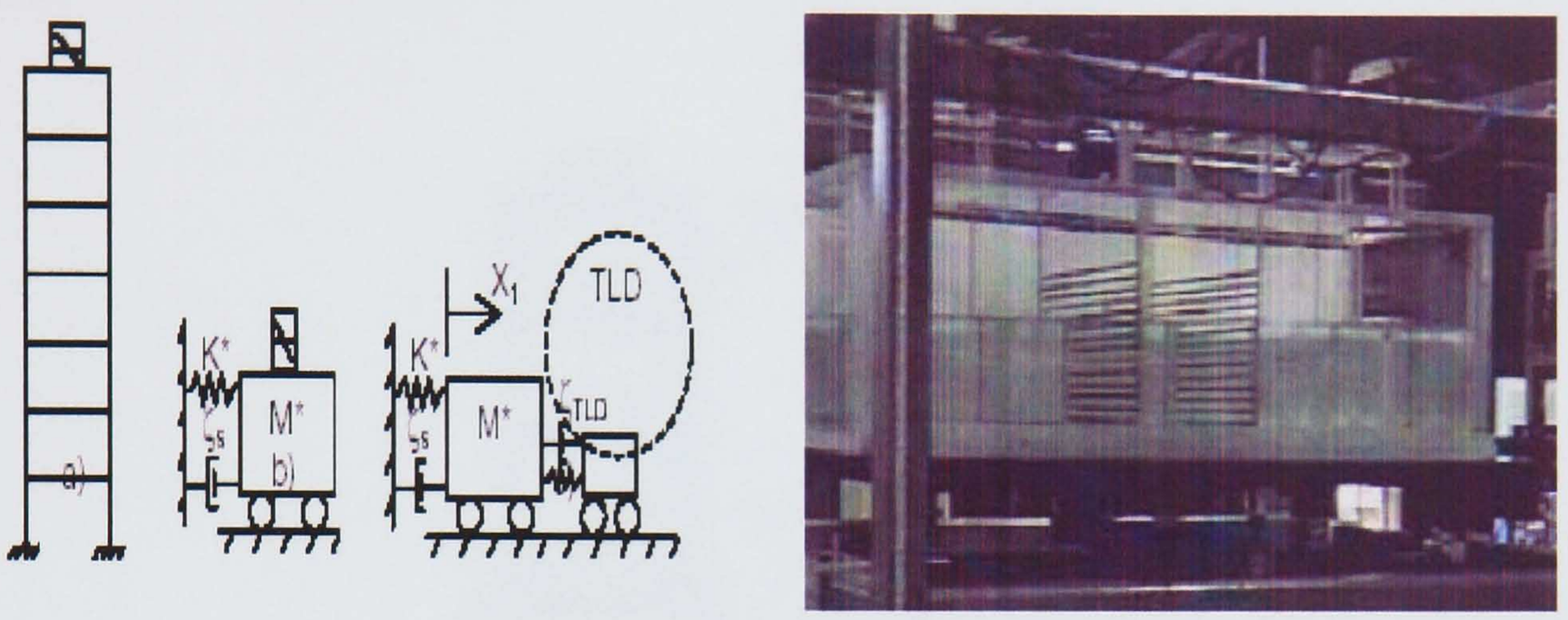

Figure 2.4-2.5 Tuned liquid damper. Source: [Damatty 2002]

Fluid viscous dampers: Fluid Viscous dampers (FVD) have also been used to add damping into structures. The concept is not new and FVD's are being used in the military and aeronautical engineering industry. The concept is that a cylinder piston is filled with a viscoelastic fluid (figure 2.6). Energy is dissipated due to the movement of the piston inside the highly viscous fluid. The viscous nature of the device is ensured by orifices along the piston. Taylor Devices' Fluid Viscous Dampers have gained acceptance recently and are used for seismic protection on new or existing buildings. FVD's are relatively small and can be placed in several parts of the structure depending on what extend and number they are needed.

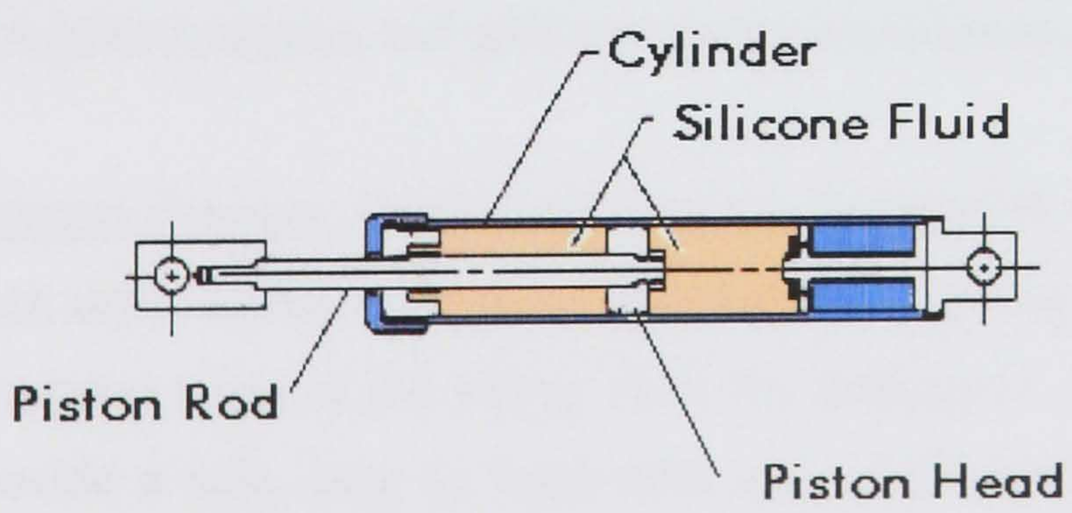

Figure 2.6. Diagram of a Fluid Viscous Damper. Source:[Constantinou 1994]

Although the behaviour of FVD's is more linear and easier modelled than that of TLD's, at strong earthquakes the FVD develops excessive damping forces, which tend to destabilise the system. Therefore significant amount of research is currently carried out at a theoretical level to establish non-linear laws modelling its behaviour [Hsiung and Chopra 2002]. Usually FVD are placed like bracings in structures in one or several floors.

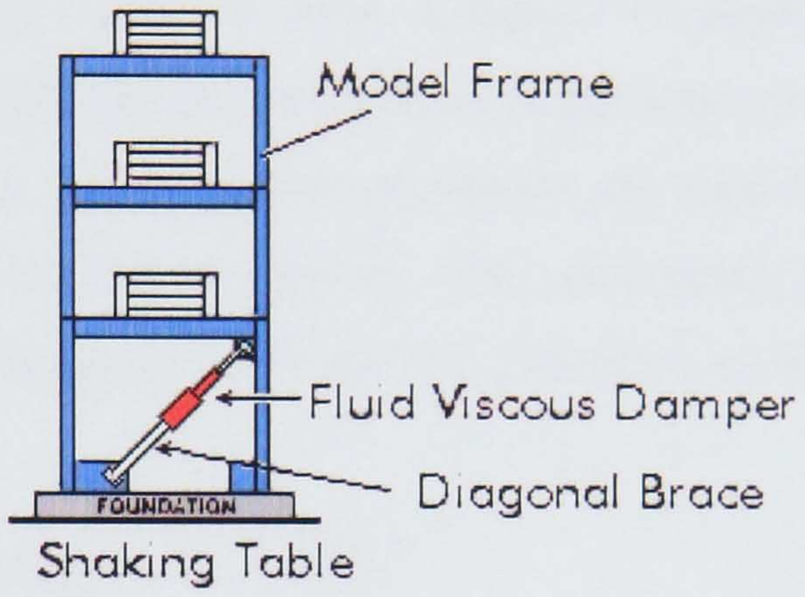

Figure 2.7 Fluid Viscous Damper. Source: [CONST]

Metallic yield dampers: Current seismic codes are based on inelastic energy absorption from damping. Damping can be added by other means, one of which is by placing metallic yield dampers (MYD). Such devices use mild steel plates with triangular shapes so that the yielding is spread uniformly throughout the material. Several different devices are used, some of which are U-strip energy dissipators and torsional and flexural beams [Housner et al. 1997]. MYD is a safe method of guaranteed results but of limited strength.

Metallic yield dampers cannot be used as active control devices but could be combined with other mechanisms to reduce the movement from environmental loads. Because their interaction could hardly change the behaviour of the active mechanism, they should be treated as two different control mechanisms.

Friction dampers: Friction dampers are designed to have moving parts that slide over each other during a strong earthquake. When sliding occurs, friction is created, which dissipates some of the energy from the earthquake. Like metallic yield dampers they provide a safe, easy to implement and of guaranteed results answer to earthquake protection. They can minimise the devastating effects on buildings of earthquakes by some margin. Friction dampers can be easily implemented at minimal cost since they

are of similar structural material and do not take much space [Almazan et al. 2001]. Friction dampers could be implemented together with other control mechanisms like viscoelastic devices, although they are of limited use as active structural control mechanisms.

Viscoelastic dampers Viscoelastic dampers are used to dissipate energy at all deformation levels. They were first used for civil engineering purposes in the twin towers in the World Trade Centre in 1969. A typical viscoelastic damper is made of copolymers or glassy substances and consists of viscoelastic layers bonded with steel plates and hysteretic loops. The behaviour of viscoelastic material under cyclic loading depends on frequency, strain and temperature. The relationship between shear stress (τ) and shear strain (γ) with frequency (ω) is given by [Housner et al. 1997]:

$$\tau(t) = G'(\omega)\gamma(t) + \frac{G''(\omega)\gamma(t)}{\omega}$$

where,

$G'(\omega)$ is the shear storage modulus and,

$G''(\omega)$ is the shear loss modulus of the viscoelastic material

In contrast to other energy dissipation systems, theoretical results and complex relationships are needed to maximise the effects of viscoelastic dampers. An advantage is that their behaviour is linear and that they can be used in several classes of systems.

2.2.3. Overview of passive control

Passive systems have the following advantages:

1 They are inexpensive systems that can be incorporated in the structure without much difficulty.
2 There is no or limited maintenance cost.
3 They do not need any external power.
4 They constitute a safe method, functioning at all times, which reduces vibrations by a limited amount.

5 They are stable.

6 They assure that no structural damage occurs during small or moderate earthquakes.

The main disadvantage of passive control is that it has a limited capability of reducing vibrations because it dissipates energy and does not counteract forces. This means that, on its own, it might not provide enough protection against large earthquakes.

Structural control implementations: Dampers are not only used at skyscrapers in regions of severe natural hazards. Recently in London the millennium bridge was built, a prestigious and famous work, as the name suggests, and high financial help was provided for its successful completion. The millennium bridge was closed for the public for almost two years due to the large vibrations that it exhibited. Dampers were added to reduce the effect of vibrations and the bridge was re-opened to the public.

The day that it was opened 80,000-100,000 people crossed the bridge. The maximum sway of the bridge was 70mm, which was not related to wind loading but was generated simply from the large amount of people walking on it. This phenomenon is now called synchronous lateral excitation. The solution was to place a number of viscous dampers under the deck, around the piers and the south landing to control the lateral motions. Tuned mass dampers were also placed under the deck as a precaution.

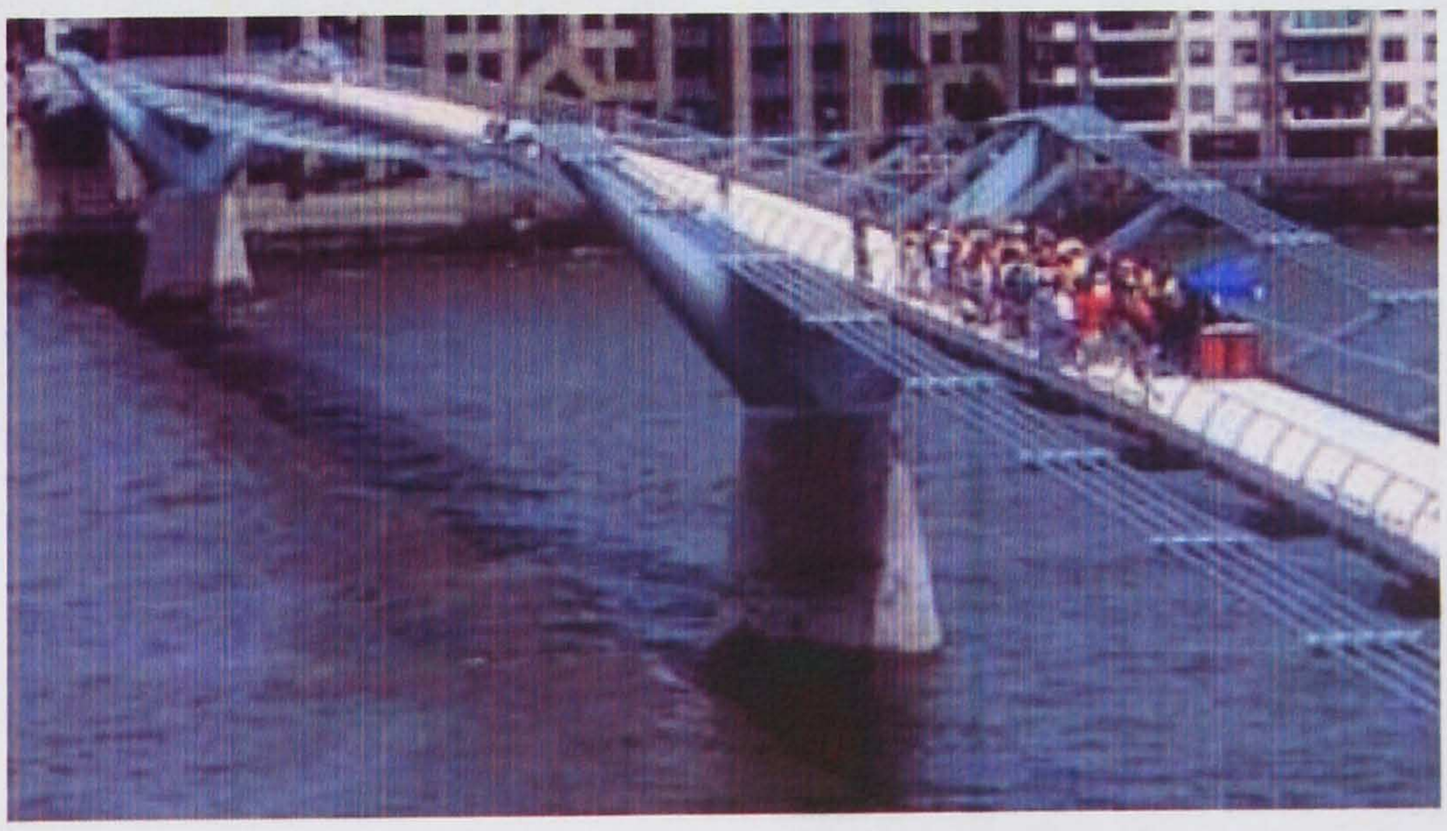

Figure 2.8. Millennium bridge Source: [Arup n.d.]

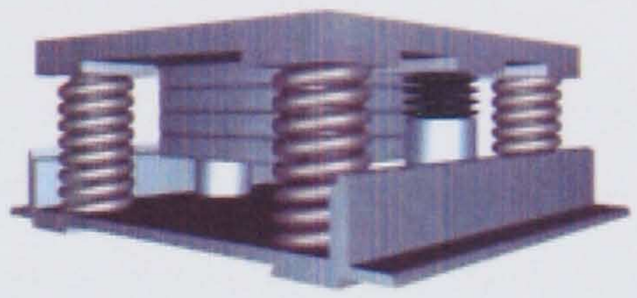

Figure 2.9. Dampers on millennium bridge Source: [Arup n.d.]

The most famous TMD is installed in the tallest building on earth, which is the Taipei 101 in Taiwan (figures 2.10, 2.11), having 101 floors above ground as the name suggests. It is in a region of very strong earthquakes and typhoons. A TMD (figure 2.10) is installed to reduce vibrations. It is a steel pendulum suspended from the 88th to the 92nd floor with a force of 662 metric tonnes. It has a 5.5m diameter, which is the largest damper sphere in the world. The structural frame is able to resist the earthquakes by itself but the TMD is added for increased security and to increase inhabitant comfort during earthquakes and strong winds.

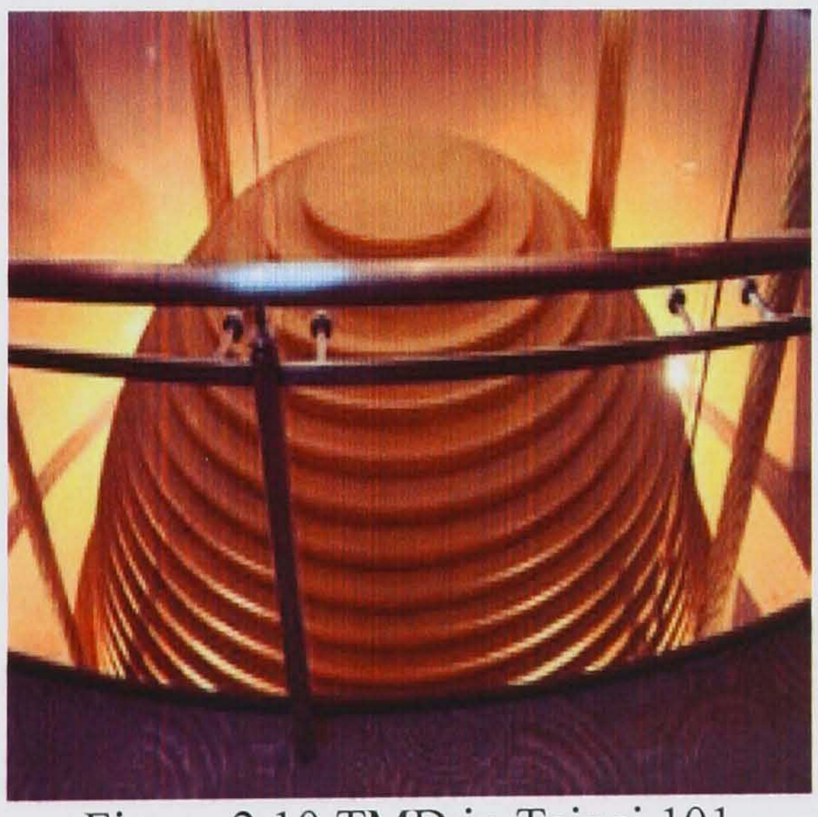

Figure 2.10 TMD in Taipei 101
Source: [Wiki n.d]

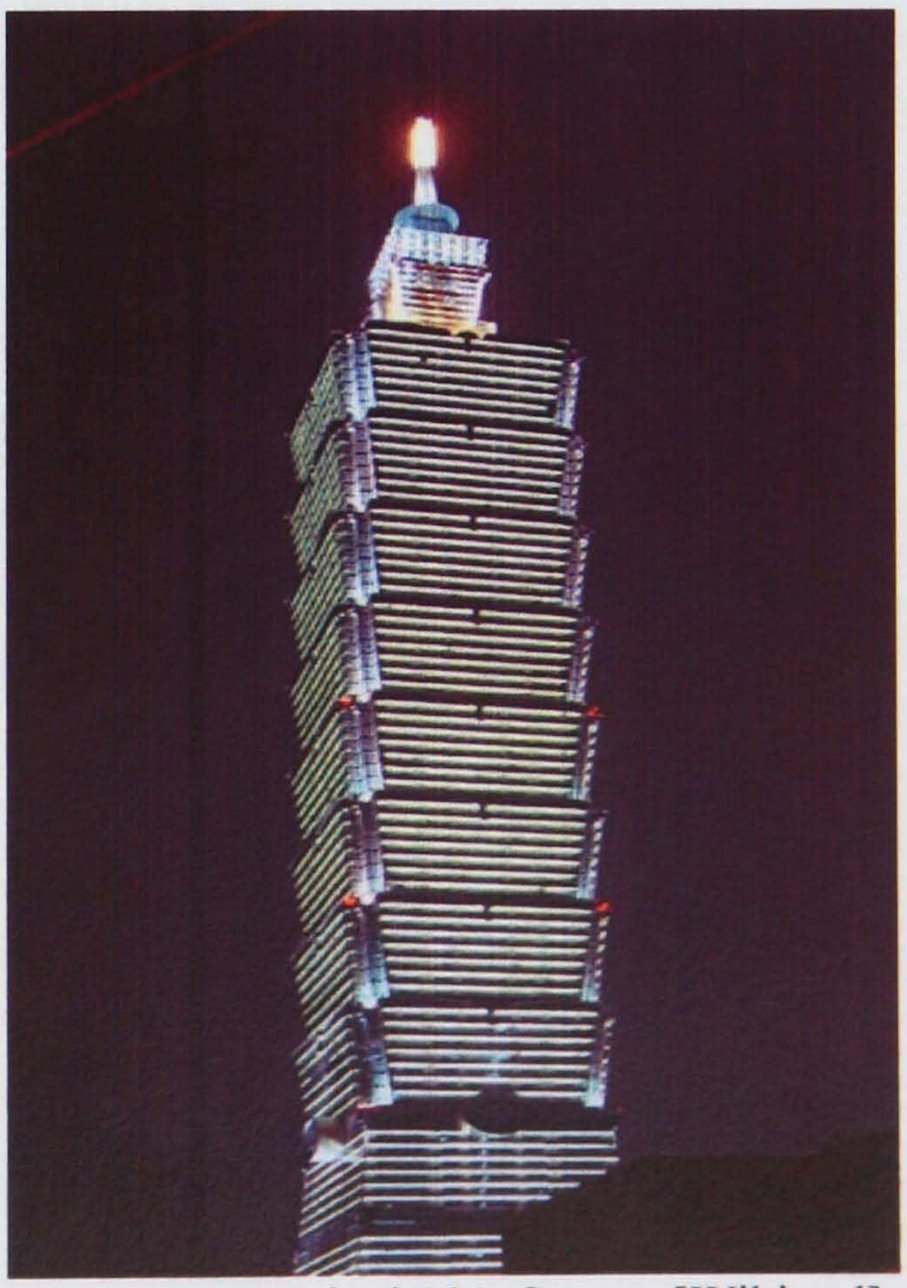

Figure 2.11 Taipei 101. Source [Wiki n.d]

2.3. Active control

Active control is a new idea to protect structures. An active control mechanism consists of an actuator, a control mechanism, a (mathematical) control law and sensors to record the motion of specific parts of the structure [Hatada and Smith 1997]. An actuator is placed at a certain location in the structure, and when there is a disturbance (earthquake, high wind, etc.) the sensor records it and sends the signal to the computer, which in turn analyses the data and triggers the actuator. The actuator acts and generates the appropriate forces that would minimise or suppress the vibration and stabilise the structure. In contrast to passive control, active control minimises the disturbance from its source and is therefore considered to be more effective.

The first structure to implement active structural control was the Kyobashi Seiwa building in Tokyo [Lynch 1993]. The 10-storey building had two controllers placed on the roof. The first one (4.2 tons) was placed in the roof's centre of mass to control transverse vibration and the second one (1.2 tons) at the edge of the building to control torsional motion. The actuators (active mass drivers) were suspended like a pendulum to minimise friction and air resistance. The device was used to control the building during large winds and small to moderate earthquakes. Finally, the actuators used hydraulic pumps to transfer energy.

The number of actuators employed depends on the modes that have to be targeted. Normally the actuator is tuned at the fundamental mode vibrating in the opposite direction. Usually one actuator for the fundamental mode is used in structures where the first mode has a large contribution. It is likely that tall structures are more flexible hence stabilising one mode is not enough, and thus more actuators may need to be used in this case.

Since the success of the Kyobashi building, the use of active mechanisms or similar devices spread to several buildings (table 2.1). These can be grouped into two kinds of actuators: Active tendon control and Active mass driver described in detail in the next section. The table below lists all the buildings using active control in Japan and South East Asia [Yang n.d] until 2001.

Summary of Actively Controlled Buildings / Towers						
Full-Scale Structure/location			Control	AMD/HMD		Actuation
	Year	Scale of Building	System	No.	tons	Mechanism
Kyobashi Center Bldg./ Tokyo	1989	33m, 400 ton, 11 stories	AMD	2	5	hydraulic
Kajima Technical Research Institute No. 21 Bldg./ Tokyo	1990	12m, 400 ton, 3 stories	AVS			variable orifice hydraulic damper
Sendagaya INTES/ Tokyo	1991	58m, 3280 ton (1st mode),11 stories	AMD	2	72	hydraulic
Shimizu Tech. Lab/ Tokyo	1991	7 stories	HMD	1	4.3	servo motor
Applause Tower (Hankyu Chayamachi Bldg.)/Osaka	1992	162m, 62660 ton, 34 stories	AMD	1	480	hydraulic
Elevator Tech. Lab.	1992	60m	AGS			
Kansai Int. Airport Control Tower/Osaka	1992	86m, 2570 ton, 5 stories	HMD	2	10	servo motor
OAC 200 Bay Tower/Osaka	1992	200m, 56680 ton, 50 stories	HMD	2	200	servo motor
Osaka Resort City 200/Osaka	1992	200m, 56680 ton, 50 stories	HMD	2	230	servo motor
Long Term Credit Bank/Tokyo	1993	130m, 39800 ton, 21stories	HMD	1	195	hydraulic
Nishimoto Kosan Nishikicho Bldg./Tokyo	1993	54m, 2600 ton, 14 stories	HMD	1	22	servo motor
Yokohama Land Mark Tower/Jokohama	1993	296m, 260600 ton, 70 stories	HMD	2	340	hydraulic
Hamamatsu ACT Tower/Hamatsasu	1994	213m, 107534 ton, 45 stories	HMD	2	180	servo motor
Hikarigaoka J-City Tower/Tokyo	1994	112m, 25391 ton, 24 stories	HMD	2	44	servo motor
Hirobe Miyake Bldg./Tokyo	1994	31m, 273 ton, 9 stories	HMD	1	2.1	servo motor
Hotel Phoenix Hotel Ocean 45/Miyasaki	1994	154m, 83650 ton, 43 stories	HMD	2	240	servo motor
MHI Yokohama Bldg./Jokohama	1994	152m, 61800 ton, 34 stories	HMD	1	60	servo motor
NTT Kuredo Motomachi Bldg./Hiroshima	1994	150m, 83000 ton, 35 stories	HMD	1	78	servo motor
Penta-Ocean Exp. Bldg./Tokyo	1994	6 stories	HMD			
Porte Kanazawa (Hotel Nikko Kanazawa)/Kanazawa	1993	131m, 27600 ton, 30 stories	AMD	2	100	hydraulic
Riverside Sumida Central Tower/Tokyo	1994	134m, 52000 ton, 33 stories	AMD	2	30	servo motor
Shinjuku Park Tower/Tokyo	1994	233m, 130000 ton, 52 stories	HMD	3	330	servo motor
Nissei Dowa Phoenix Tower/Osaka	1995	145m, 26800 ton, 29 stories	HMD	2	84	servo motor
Osaka WTC Bldg./Osaka	1995	255m, 80000 ton, 55 stories	HMD	2	100	servo motor
Plaza Ichihara/Chiba	1995	58m, 5760 ton, 12 stories	HMD	2	14	servo motor
Kaikyo-messe Dream Tower/Yamagushi	1996	153m, 5400 ton	HMD	2	10	
Rinku Gate Tower North Bldg./Osaka	1996	255m, 65000 ton, 56 stories	HMD	2	160	servo motor
Herbis Osaka/Osaka	1997	190m, 62450 ton, 40 stories	HMD	2	320	hydraulic
Itoyama Tower/Tokyo	1997	89m, 9025 ton, 18 stories	HMD	1	48	servo motor
Nisseki Yokohama Bldg./Yokohama	1997	133m, 53000 ton, 30 stories	HMD	2	166	
TC Tower/Taiwan	1997	348m, 221000 ton, 85 stories	HMD	2	100	servo motor
Bunka Gakuen New Bldg./Tokyo	1998	93m, 43488 ton, 20 stories	HMD	2	48	servo motor
Daiichi Hotel Ohita Oasis Tower/Ohita	1998	101m, 20942 ton, 21 stories	HMD	2	50	hydraulic
Odakyu Southern Tower/Tokyo	1998	150m, 50000 ton, 36 stories	HMD	2	30	linear motor
Otis Shibayama Test Tower/Chiba	1998	154m, 6877 ton, 39 stories	HMD	1	61	hydraulic
Sotesu Takashimaya Kyodo Bldg./Yokohama	1998	115m, 68954 ton, 27 stories	HMD	2	122	
Century Park Tower/Tokyo	1999	170m, 124540 ton, 54 stories	HMD	4	440	
JR Central towers/Nagoya	1999	Hotel; 226m; Office; 245m 300000ton	HMD	4(H) 2(O)	60(H) 75(O)	servo motor(H) hydraulic(O)
Nanjing Tower/Nanjing	1999	310m	AMD	1	60	hydraulic
Shin-Jei Bldg./Taipei	1999	99m, 22 stories	AMD	3	120	servo motor
Shinagawa Intercity A/Tokyo	1999	144m, 50000 ton, 32 stories	HMD	2	75	
Incheon Int. Airport Air-traffic Control Tower/Korea	2000	100m	HMD	2	12	servo motor
Keio University Engineering Building/Tokyo	2000		Smart Base Isolation	-	-	variable orifice orifice damper
Harumi Island Triton Square/Tokyo	2001	3 buildings (195m, 175m and 155m)	Couple Building Control			2 servo actuator

Table 2.1. SOURCE [Yang n.d]

2.3.1. Active Tendon Control

Active tendon control seems to be theoretically the most powerful control method in active structural control. Tendons are existing parts of a structure and therefore do not need to be added separately. A tendon, usually in the ground floor, cross connecting the two corners of the first floor to the two corners of the ground floor can pull the tendon by an actuator in the ground floor in a direction opposite to the movement of the earthquake (figures 2.13, 2 .14, [Dyke et al. 1994a]).

This method does not work by adding damping or dissipating energy but it applies a force whose direction is opposite to the movement of the building. Since the tendons are usually placed at the ground floor (unlike other passive schemes where the controller is at the top) if the movement of the building at the ground floor is minimised, the response on the rest of the building is minimised proportionally. This is the most accurate method to suppress a disturbance since it counteracts forces on the structure and at the point where the earthquake first encounters the structure.

The actuator is powered usually by a servo controlled hydraulic actuator since this is the most cost-effective method to inject large power. The disadvantage of this control system is that it has very large energy requirements, which makes it very expensive to use. Active tendon control can be combined with other passive energy systems like base isolation to reduce the energy demand by keeping the structure safe.

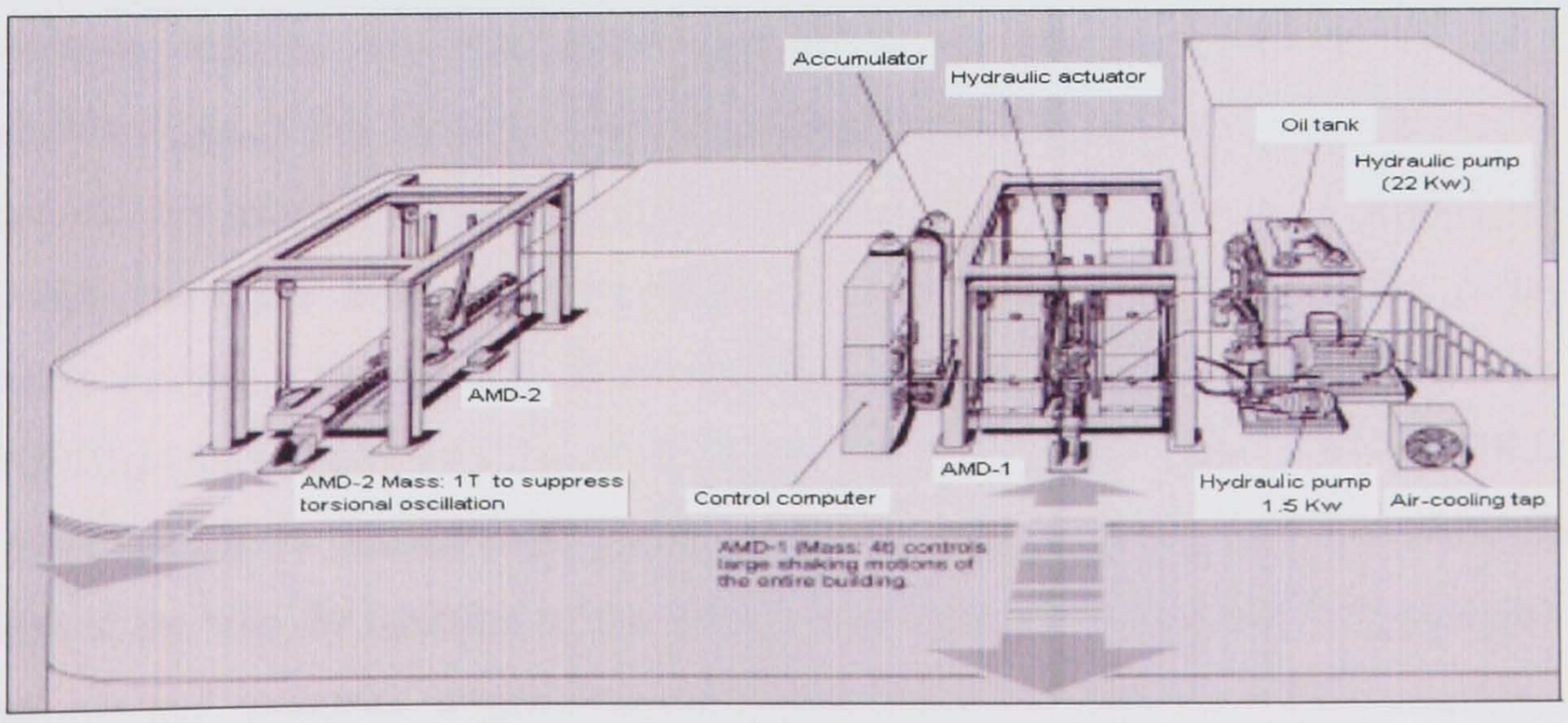

Figure 2.12 First implemented active control actuator. Source: [Lynch 1993]

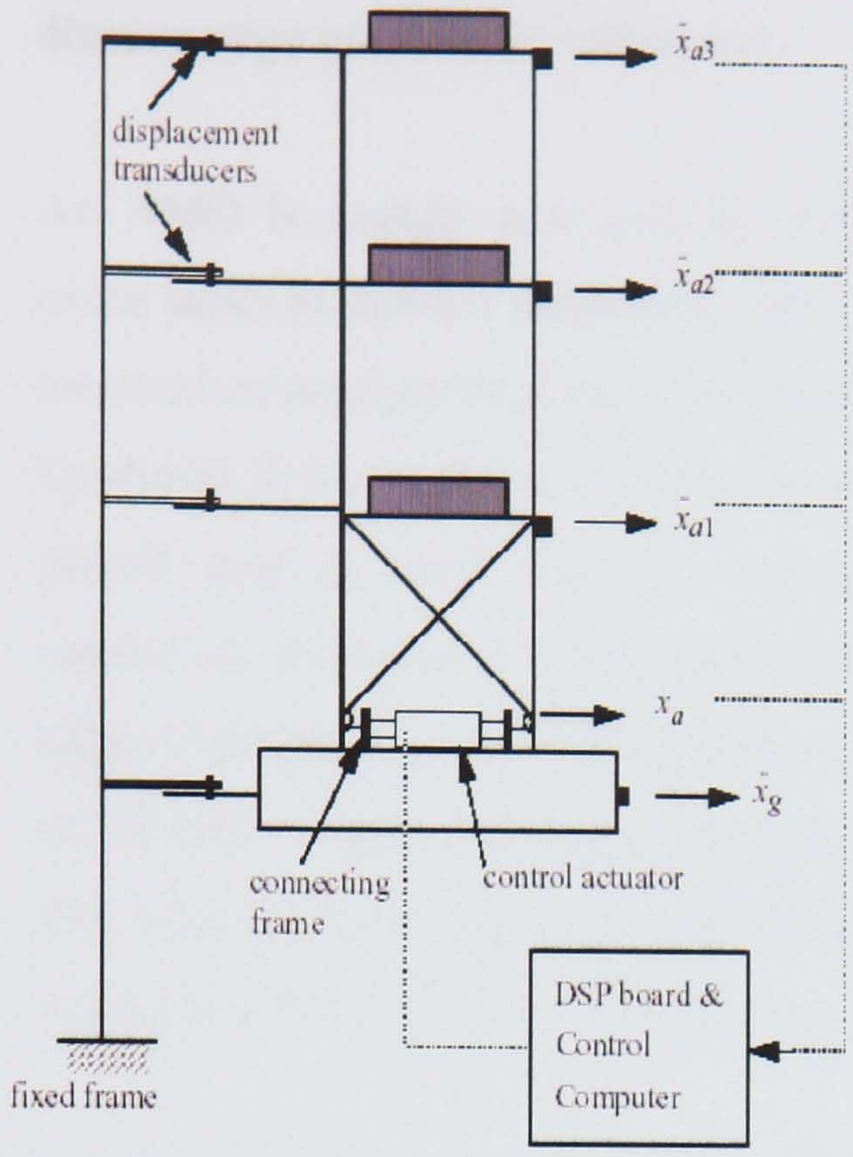

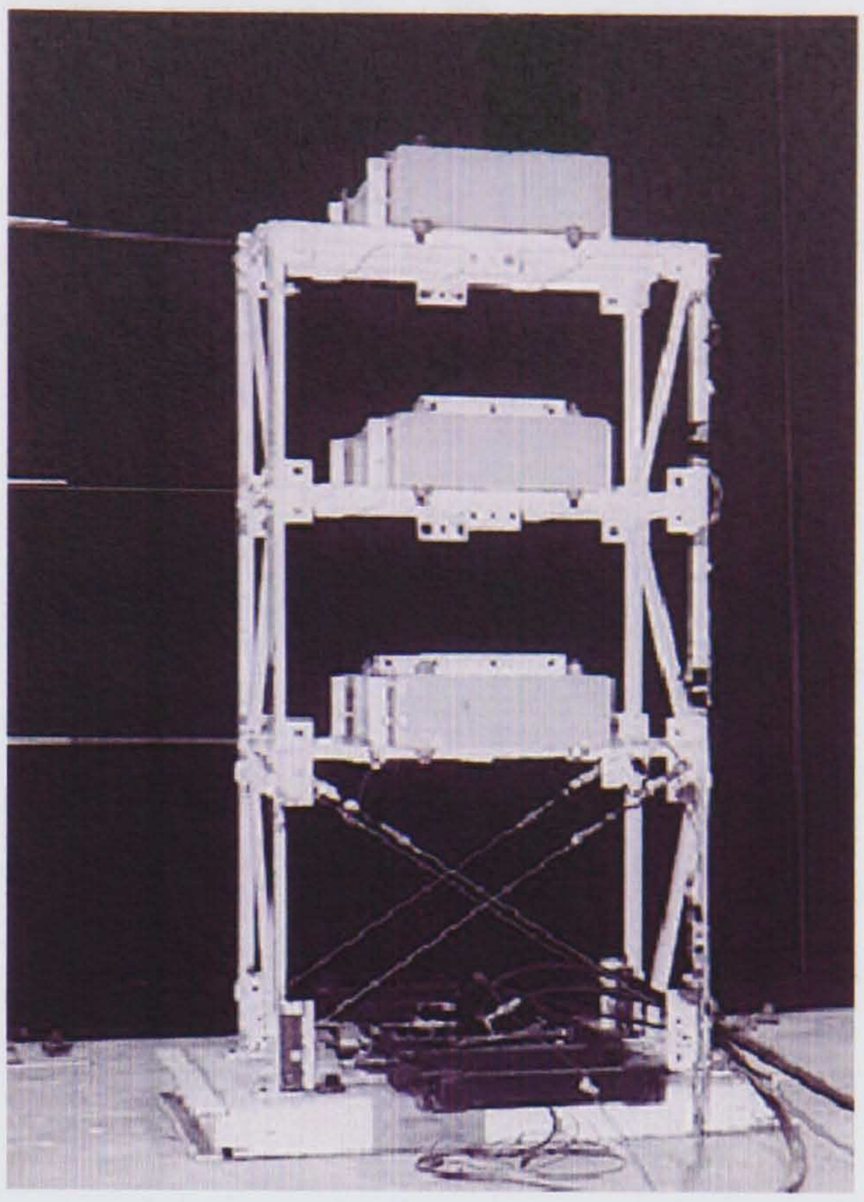

Figures 2.13, 2.14 Active tendon control. Source:[Dyke et al. 1994a]

2.3.2. Active Mass Driver/Damper (AMD)

An active mass driver is a mass, placed at the top of a structure. During movement of the building the mass moves at a direction opposite to that of the building so as to maintain the centre of mass at the same position, thus stabilising the building. The advantages of AMD are that it can be combined with a passive system (TMD) to improve stability and the force requirement is less than that of an ATS. The disadvantage of this method is that since the earthquake is applied to a building from the ground, the actuator force coming from the top may not be able to stabilise it since the waves propagate at opposite directions. In civil engineering terms if the fundamental mode having a large modal mass contribution is the main one (which is excited) a building can be stabilised, but if the higher modes are also significant the AMD has a lower impact. In control engineering terms the problem arises due to a non-minimum zero in the transfer function of the system, characteristic of systems with non-collocated sensors and actuators, which imposes additional phase lag and tends to destabilise the system. Since active control is usually used in high flexible structures, modal

contribution from higher-order modes is typically significant. and therefore this disadvantage needs to be addressed.

An AMD is usually activated by hydraulic pumps (or electric servomotors), which cause jacks to move a suspended mass (figure 2.11). AMD was the first active control mechanism implemented on a structure and therefore has received a lot of attention. The Kyobashi Seiwa building in Tokyo was constructed in 1989. It consisted of two AMD's placed upon the roof. The first one, of 4 tons, was placed at the centre of gravity to control the fundamental mode and the second one, consisting of 1 ton, was placed at the edge of the building to control torsional motion. The control mechanisms represent 1% of the total weight and could produce a force of 3.4 and 2.2 metric tons respectively. The AMD primary goal was to improve habitant's comfort during moderate earthquakes and high winds rather than to withstand extreme earthquakes.

The success of this system has led to the implementation of active control mechanisms for protection from earthquakes and high winds, including attempts to control even extreme earthquake events. More sophisticated systems like the DUOX or TRIGON [Lynch 1993] were designed that would be able to operate at lower energy levels. A very attractive system is the combination of a passive system together with an active control mechanism (hybrid control). A lot of research has been carried out in this area and certain limitations of this approach have been discussed in the previous section.

AMD is the active control area that has received most attention in terms of research. Some papers in the literature include benchmark problems [Spencer et al. 1998], [Baker et al. 1999] where many different control algorithms are compared for several design aspects (root-mean-square values, peak values, maximum displacements, accelerations etc.). Also several researchers have attempted to find the limits of these controllers in terms of saturation levels, when larger forces are applied than those the controller can withstand [D' Amato and Rotea 1999], [Forrai et al. 2003]. Further work on active control is presented in [Zhang and Ivan 2001a], [Zhang and Ivan 2001b], [Min et al. 2001] .

Another difference between active and passive control is that a passive device will be dissipating energy at all times. An active device may have a negative effect and

destabilise a building if the force is applied at the wrong direction or at the wrong time. Therefore the following aspects need to be taken into consideration as well.

1 Time delay
2 Actuator saturation/ Controller saturation
3 Controllability/Observability, sensor/actuator related problems
4 Possibility of power cut-off during earthquake

Time–delay: From the time the earthquake waves reach the surface to the moment the sensor measures it, sends the signal to the computer, the computer processes it and the actuator applies the required force there is inevitably some time delay. New techniques and new sophisticated technology have managed to decrease the delay to 0.1-0.2 ms, which can be significant. A number of papers have been published analysing the effects of time delays in structural control [Soong 1990], [Chu et al. 2001], [Agrawal and Yang 2000], [Alt et al. 2000]. Current structural control design techniques deal with the problem of time-delay satisfactory and some researchers claim that the time-delay can even be used to have a positive effect on the structure [Firdaus et al. 2003].

Actuator saturation: Sometimes the force required by an actuator is larger than the maximum that can be produced. Else, a large force over a short time interval needs to be produced. In such situations the actuator may saturate. The behaviour of the control system is not predictable in this case because the theoretical way by which the controller was designed no longer applies. The problem of actuator saturation has been discussed in [D' Amato and Rotea 1999], [D'Amato and Rotea 1997].

Controllability/Observability, sensor/actuator related problems: Controllability measures how effective a controller is when placed at a specific location on a structure. Observability measures the amount of information that can be obtained from the measured variables if a sensor is placed at a specific location. A formal control theoretic definition is given in the next chapter. The problem of actuator placement in other control mechanisms is often trivial. From the nature of the control system or from practical and construction considerations there may be only one obvious optimum location of an actuator (usually the highest floor). In active tendon control usually the ground floor is considered to be the optimum location but there are other considerations.

like using several active tendon systems (ATS) or having a larger ATS that covers more than one floor. Soong has proposed some simple methods for finding the optimal sensor and controller location in a structure [Soong 1990].

The problem of observability is important because if the mode at which the building is vibrating is not known, the information from only one mode is not sufficient to describe the behaviour of the rest of the structure. A simple solution to this problem is the placement of several sensors (for a building one in each floor) something that is costly and increases system complexity. Nevertheless, the cost of an extra sensor is insignificant. This is not true in the case of controllability, where it is crucial to find the optimal controller location(s), since the cost of an extra actuator (or more power) may be sufficient to make the system uneconomic.

A similar way may be followed to identify the optimal controller locations. First, define a controllability index as:

$$\rho(x) = \left[\sum_{j=1}^{n} \{ g[\Phi_j(x)] y_{j(\max)}(t) \}^2 \right]^{1/2}$$

where:

x = percent of total height of structure

n = number of modes considered

Φ_j = j-th modal shape

y_j = maximum j-th modal response spectrum

$g = \Delta\Phi_j(x) / \Delta x$ (for ATS controller)

Although this method is valid for the above example, more sophisticated methods originating from control theory can be used. As suggested by [RANA], [Hamdan and Nayfesh 1989], a gross measure of controllability of the i-th mode is the norm of f_i where:

$$f_i = \frac{q_i^T B}{\|q_i\|}$$

in which q_i is the i-th left eigenvector of the system matrix A given by $\lambda_i q_i = A^T q_i$ and λ_i is the i-th eigenvalue of A. The author proposed this method for first and second order linear systems but in [Rana et al. 1997] it was extended and used for evaluating the controllability of an active bracing system (similar to ATS) of an 8 floor storey building after appropriate model reduction. Further research in the area of optimal sensor/actuator placement, including QN control and spline function interpolation methods have been reported in [Xing et al. 2001] and [Limongelli 2003], respectively.

The above problems are mostly areas where further research is needed to improve the behaviour of active control systems rather than disadvantages, although they demonstrate that if any of these aspects is miscalculated, the controller might become unstable or ineffective, a problem that does not arise with passive control. The major (if not only) concern is the large energy requirements which might make the controller unable to meet its requirements or very expensive. Furthermore, during an earthquake there might be an electricity cut-off and the controller could cease to operate unless a local generator is in place. This however is more of a practical problem rather than a civil or control engineering design issue.

2.4. Hybrid Control

A hybrid control system has one active and one passive component. The idea behind a hybrid system is that passive control cannot fully protect a structure from extreme earthquakes but active control is too expensive and requires high energy levels. An active system is always on, resulting to a constant energy supply and high cost. In the case of a hybrid system, the passive component is acting at all times, while the active component starts to function only when the disturbance signal arrives. This means that the maintenance cost of the active system is minimal, since it is used only during the periods when earthquakes occur.

Hybrid mass damper: The hybrid mass damper is the most commonly employed actuator in controlling buildings. It comprises of a TMD and an AMD. The energy requirement of this system is relatively low and achieves similar results to those of an AMD. A very attractive system is the inverted pendulum. Tuned at the natural frequency of the building it vibrates with a relatively small force. Many systems have been developed, like multiple active–passive mass dampers that are tuned to more than one natural frequency of the system [Li 2003]. Almost any passive energy systems can be combined with AMD. Hybrid systems are typically more complex since the dynamics of two components are combined (figure 2.15).

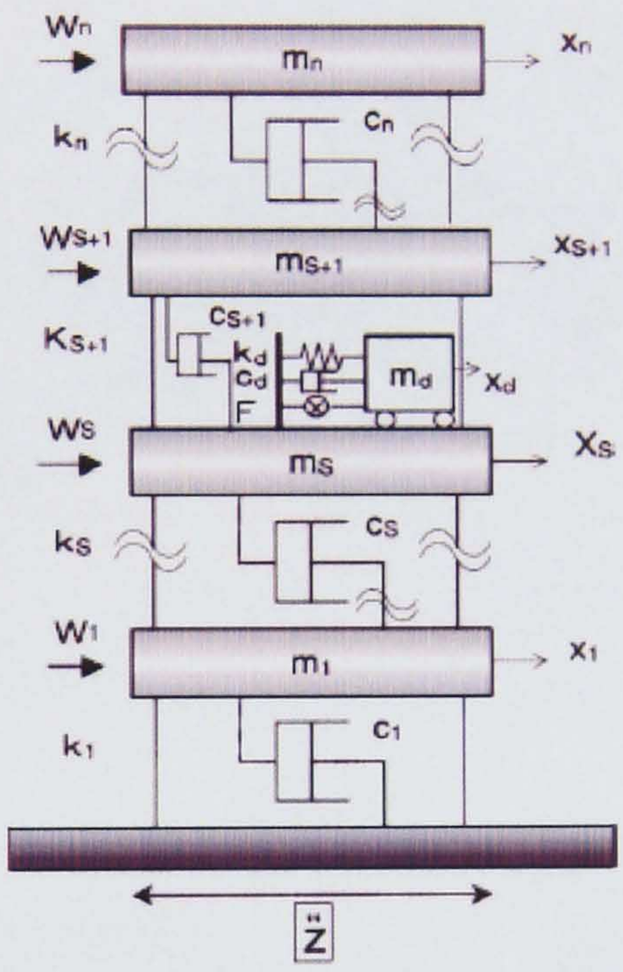

Figure 2.15 Hybrid mass damper

Hybrid base isolation: Base isolation can reduce the inter-storey drift and absolute acceleration on a structure but has a very high base displacement. If combined with an active system (active tendon or AMD) it can reduce the base displacement as well. Base isolation systems exhibit non-linear behaviour and therefore different control algorithms are used as opposed to the traditional LQG and H_∞ methods like fuzzy, neural networks, adaptive non-linear control, etc [Chang et al. 2001].

One of the first buildings to have a hybrid mass damper was the Ando Nishickiko building in Japan, Tokyo. It was designed by the Kajima corporation which also designed the first AMD as well. The building is a 14 storey steel structure. The control

device called DUOX consists of a 20-ton TMD and two AMD resting on the TMD of 2 tons each. The stroke of the TMD and AMD is 50 and 25 cm respectively, and they are targeting the first two modes of vibration. The total mass of the building is 2600 tons, i.e. the DUOX is less than 1% of the total mass of the building. This system is supposed to be more cost-effective than AMD. Also the DUOX system is designed to reduce vibrations due to strong winds and moderate earthquakes.

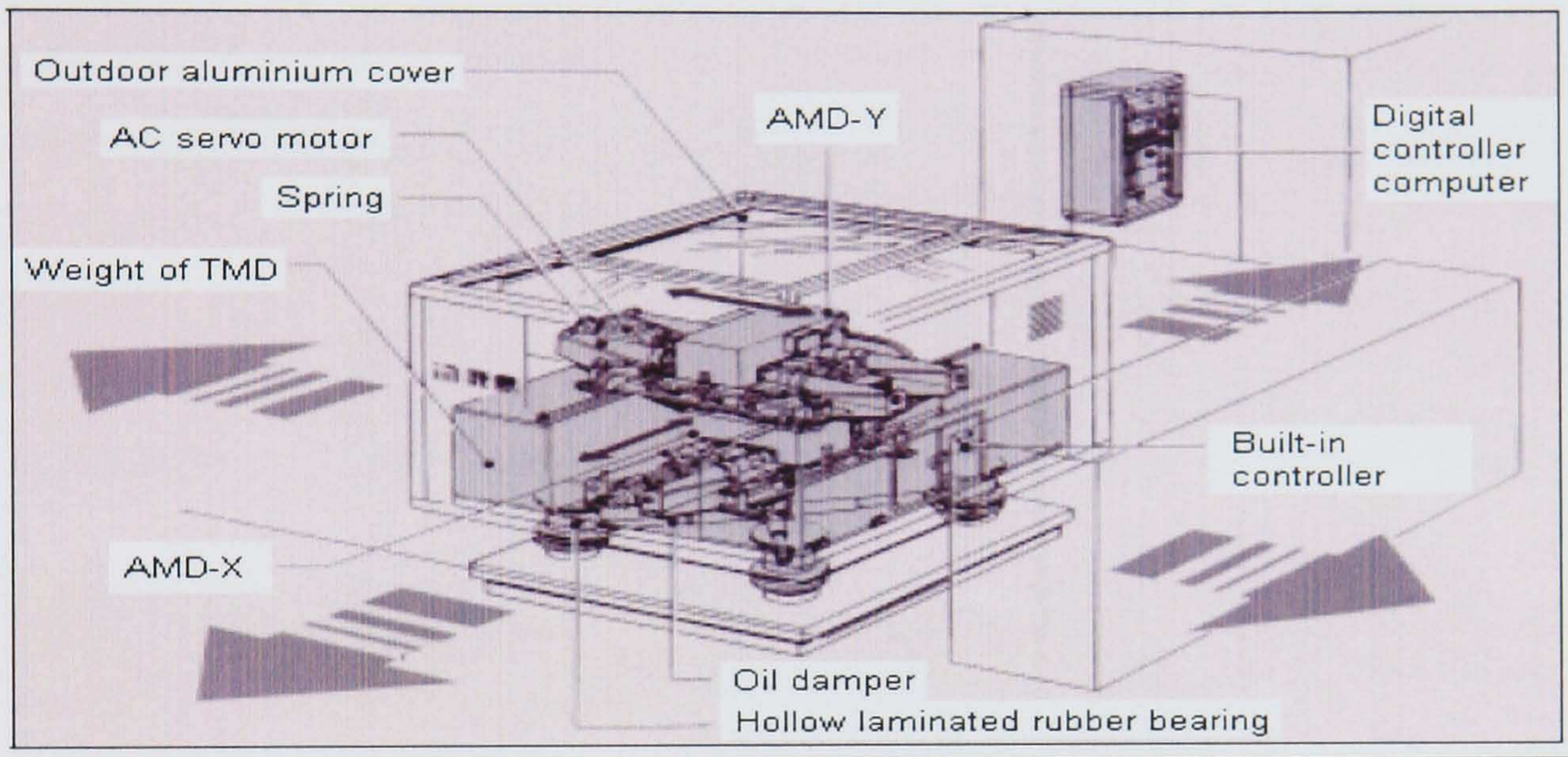

Figure 2.16 Concept of a hybrid mass damper (DUOX system) Source:[_Lynch 1993]

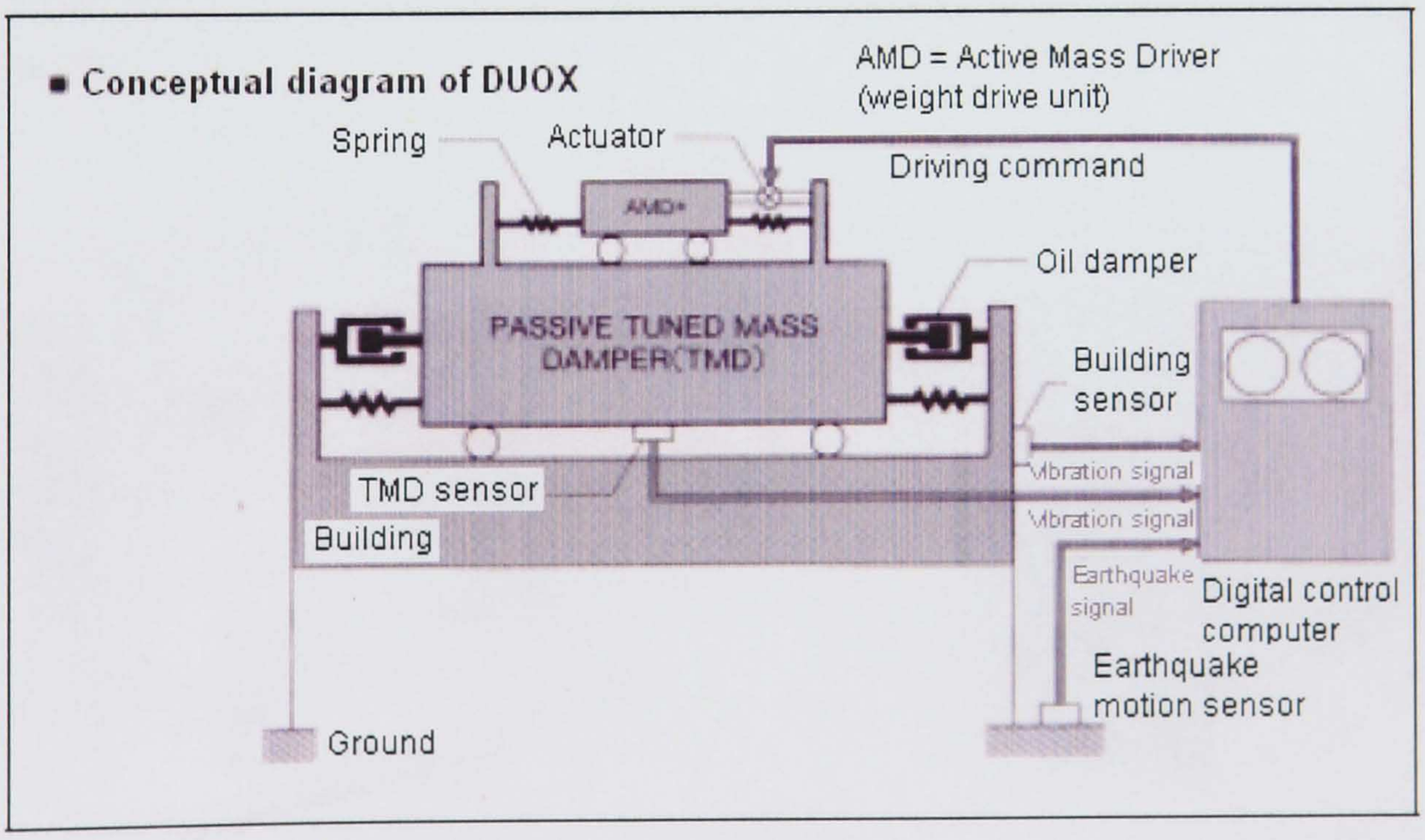

Figure 2.17 Hybrid mass damper (TRIGON system). Source: [Lynch 1993]

2.5. Semi-Active Control

Semi-active control is a mechanism that cannot inject mechanical energy into a system, but has properties that can be controlled to reduce the responses of the system [Spencer and Sain 1997]. In control engineering terms such systems are observable but poorly controllable. They have the advantage that they require a minimal amount of energy but perform much better than passive systems and have the potential to compete with active control systems in terms of performance. They also do not tend to destabilise the system due to small errors. Semi-active schemes have already been implemented with success. It is expected that they will be more frequently used in the future, due to their high efficiency for the low energy they require. A practical difference between active and semi-active control is that in semi-active control several small actuators are implemented in a structure rather than one.

Variable-orifice dampers (VOD): The idea behind a VOD is a variable stiffness device mechanism. "V"-bracing is used and at their apex a variable stiffness device is connected (figures 2.18, 2.19). This device can be locked and therefore be ineffective or unlocked so that the brace can resist lateral loads. The power required to lock and unlock the braces is minimal and can also be produced by a backup generator [Spencer and Sain 1997].

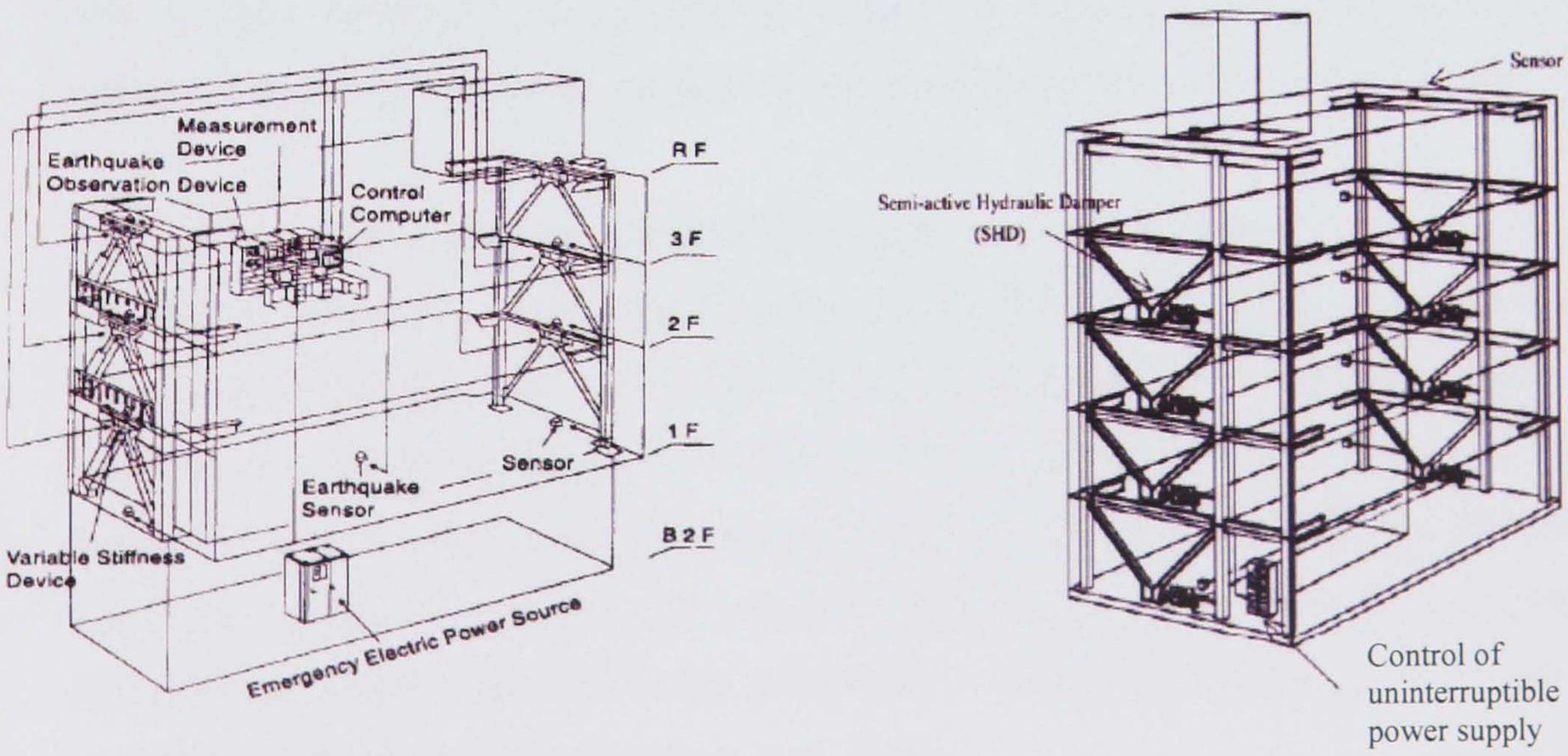

Figure 2.18, 2.19 Semi-active hydraulic dampers. Source: [Spencer and Sain 1997]

Recently the Kajima k-Building was constructed in Tokyo, a 38-story building with 88 variable orifice dampers and two hybrid mass dampers and also the Kajima R-building, a 54 story building with 356 variable orifice dampers and 192 passive dampers.

Variable friction dampers/Controllable tuned liquid dampers: A Variable friction damper consists of a friction shaft that is rigidly connected to the structural bracing. The force in the friction at interface is adjusted by allowing slippage in controlled amounts. Another device is a friction controllable fluid that produces good results if connected with a base isolation system. Controllable tuned liquid dampers utilise the motion of a sloshing fluid or column of fluid to control a structure.

Smart dampers (or controllable fluid dampers): These consist typically of electrorheological (ER) or magnetorheological (MR) fluids. ER and MR are free flowing fluids that within milliseconds after their exposure to electric or magnetic field, become semi-solids of controllable yield strength. The properties of those fluids are shown in figure 2.20. During vibration they change from stiff when the element is at its original position to fluid when the element is at maximum displacement and vice versa. This is done during each vibration which is why a fast response time is necessary.

ER and MR are suspensions of particles in liquids. They are added in fluids without altering their behaviour. When they are exposed to electric or magnetic field, these articles form chains that cease the flow of liquid and transform it into static structure.

The stiffness and yield strength of ER or MR dampers depends on the electric or magnetic field and the concentration of the particles. ER and MR fluids were developed in the 1940s but they were not used for engineering purposes until the 1980's in mechanical engineering. ER initially received more attention since electricity is used more widely than magnetism, but lately MR fluids seem to be increasingly attractive due to the very good properties they posses compared to ER. Their behaviour, however, is non-linear which means that a lot of research is needed before they can be reliably used [Sun et al. 2003], [Djajakesukma et al. 2002].

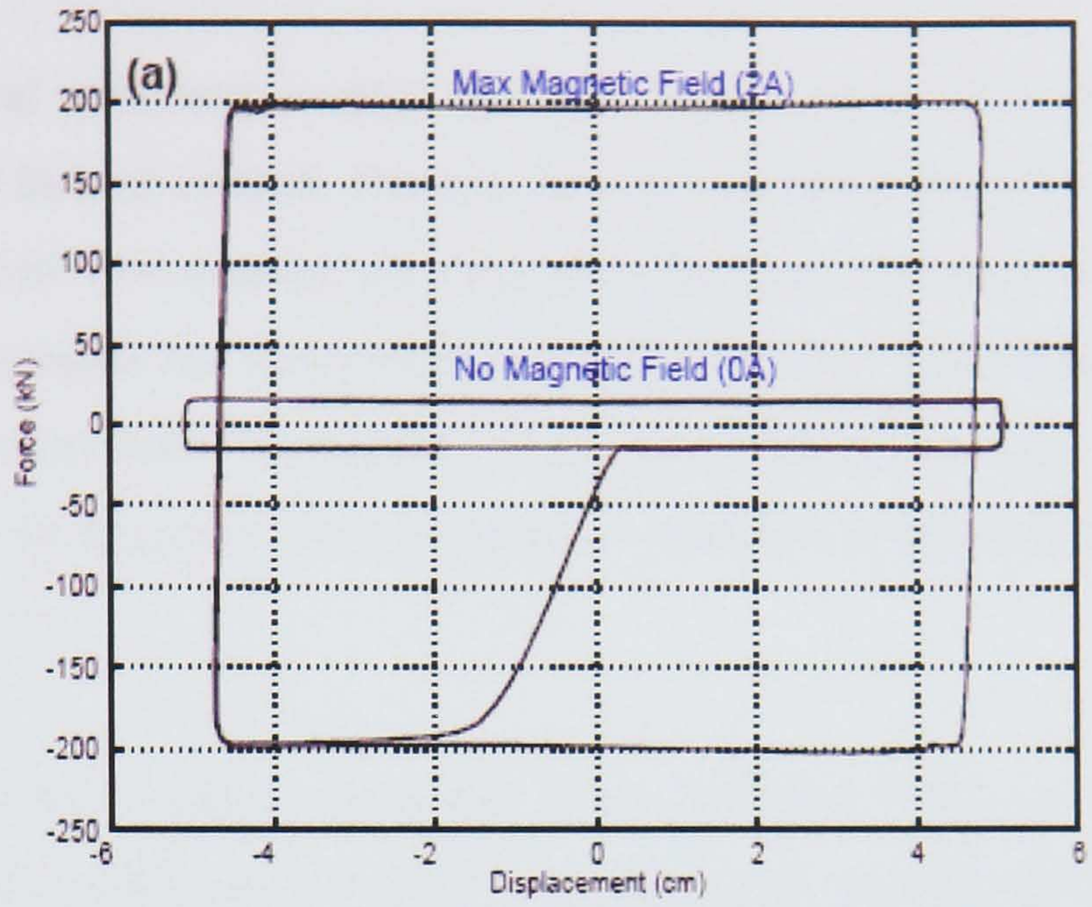

Figure 2.20 Force-displacement graph of MR fluids source:[Spencer and Sain 1997]

Structural control implementation: The first structure with MR dampers has been operating in Japan since 2001. It is the Nihon-Kagaku-Miraikan, the Tokyo National Museum of Emerging Science and Innovation. It has two 30-ton MR fluid dampers installed between the 3rd and 5th floor. The first bridge using smart materials is the Dongting Lake bridge in Hunan, China. It is a cable-stayed bridge that uses two MR dampers on each cable to mitigate cable vibration.

Figure 2.21 Tokyo National Museum of emerging Science and Innovation. Source: Spencer and Sain 1997

Figure 2.22 Dongting Lake bridge, Hunan, China. Source: Spencer and Sain 1997

2.6. Summary

There are several structural control methods, which are divided into passive, active, semi-active and hybrid control. Passive devices are those that dissipate energy. They can be divided into two classes, base isolation and passive energy dissipation systems. Base isolation systems are very robust and effective. The logic behind them is simple, i.e. if the superstructure is isolated from the substructure then the effect of the earthquake will be minimal. Base isolation is effective in minimising the fundamental mode movement.

In contrast to base isolation there are many different types of passive dissipation systems. Here the challenge is to find a creative way to dissipate as much energy as possible. Some systems require just one device, targeting the fundamental mode (e.g. tuned mass damper) and some several devices (e.g. fluid viscous damper). The most common device is the tuned-mass damper. A mass vibrating at the top of the building in the fundamental mode is used to reduce vibrations by dissipating energy.

In active control powerful actuators apply forces aiming at counteracting the induced vibrations. This is the strongest kind of control. Here, full control analysis and modelling is required. An active controller requires a control mechanism, an actuator, sensors and a mathematical control law. The main advantage of active control is its ability to produce large forces and theoretically counteract any earthquake. The drawback is that such actuators, usually hydraulic, require very large forces. Active controllers are dynamic systems and hence require detailed mathematical modelling and control theory for their effective design. Feedback control laws, full robustness analysis and many other control aspects related to control implementation and validation are also required before installing such a system.

Semi-active devices cannot inject any mechanical energy into the system, but have the ability to vary their stiffness characteristics. It has been reported in the literature that semi-active devices can achieve results close enough to active control by using much lower energy requirements. Hybrid systems combine aspects from the above systems. They usually consist of a passive device, which is always on, and a small active device

activated during a strong earthquake. In semi-active and hybrid systems' detailed control analysis is required for their effective design and implementation.

The most effective mechanisms are active control devices since they can apply forces and can resist very large disturbances. Hence, the rest of the thesis will be mainly concentrated in the area of active control. Since the area of structural control is new, much additional research is required before they can be fully accepted by the research and industrial communities. Areas such as modelling, optimal placement of actuators and sensors, controllability and observability, the effects of time delay, robustness, optimal control laws and actuator saturation are only some of the areas requiring further work in the area of active structural control. In passive control most new research is in the area of developing and implementing new or existing ideas in a practical way, whereas for active control fundamental research is required in the area of controller design itself.

CHAPTER 3

CONTROL THEORY

3.1. Introduction

This chapter outlines the main aspects of control theory that will be used in the thesis, by starting from the basic definitions and building up to the required theories and design methodologies. The introductory topics include general concepts of control and automation, classification of systems, open and closed-loop systems, feedback control and some basic concepts of classical control. Special emphasis is placed on state-space equations, including representation of mechanical systems by differential equations and their state-space equivalent form. The next section outlines the concepts of pole placement and controller design including a number of widely-used techniques such as, Linear-Quadratic Regulators (LQR), Linear Quadratic Gaussian (LQG) control and H_2 optimal control. Finally, a method for parametrising all stabilising controllers (Youla parametrisation) is described, which is of great importance to H_2 control and also l_1-optimal control theory which is described in a separate chapter.

3.2. Fundamentals of control theory

The work described in this thesis is in the area of active vibration control of civil engineering structures. In this section we introduce the main concepts in the area of Systems and Control theory, which are used extensively throughout this work. A *system* is an assembly of physical components related in a way to form a unit. *Control* is the science that studies systems, by observing the system's output signals via measurements and regulating the system's response in an appropriate way. For a more formal definition, a system can be considered to be a mathematical model described by a set of interrelated equations and constraints; Control involves the study of these equations, including the ability to manipulate them, in a way that modifies the system's response in

the desired way. Thus, an important part of control is the ability to model a real system mathematically, so that the response of the real system can be adequately determined from the model.

An example of a system is a room having a thermostat to control its temperature. A thermometer measures the temperature and when this drops to a certain level the heating is automatically turned on, until the desired temperature is reached. A typical control system has three main elements. The *Plant* (in this case the room and its heating/cooling properties) the *sensors* (in this case the thermometer that measures the room temperature), and the control system or Controller (in this case the thermostat that switches the heating on and off). A system that needs to be controlled always has an *input* and an *output*. An input signal is the excitation applied to the plant by the controller, in this example the thermostat signal. Output is the response obtained from the plant. The difference between the input and the output signals is the *error* signal, which should be zero in a perfectly controlled system. The system may be subjected to external *disturbances*, e.g. opening a window will alter the room's temperature.

The above system is considered to be in *closed-loop* form because the control action is dependent on the output. An *open-loop* system is one where the control action is independent of the output. In the previous example, if the heating would be switched on and off at the same time every day the system would be open-loop. The vast majority of control systems are closed-loop and use feedback. *Feedback* is a property of the closed-loop system; by comparing the input with the output, the system can take the appropriate corrective action. There is also *feedforward control*, when the system knows in advance (at least partly) the disturbance signal and can counteract it (e.g. partially cancel it). Feedforward control is used rather rarely in real systems. In the previous example, feedforward control would correspond to a situation in which the exact time of a window opening or the exact change of temperature was known, so that corrective action was taken before a significant drop in temperature was detected. In this case, due to the slow dynamics of the system, feedforward would probably not lead to significant performance improvements of the control system; this is in contrast to cases of structures' protection against earthquakes, where prior knowledge about the characteristics of the earthquake signal would be very useful.

Feedback control systems are divided into two classes. The first class corresponds to the "*regulator problem*", where a physical variable needs to be maintained at a constant value. The second class corresponds to the "*servo-mechanism-problem*" where a physical variable which varies in time needs to be tracked, e.g., a robotic arm moving along a pre-determined path. The regulator problem can be shown to be equivalent to the problem of *disturbance rejection*, and will be used throughout this thesis.

3.3 Further systems classification

Throughout this work systems will be described by differential equations arising from mechanics. These can be either ordinary differential equations giving rise to lumped-parameter systems, or partial differential equations arising from continuous mechanics resulting in distributed parameter systems. Another important distinction is between *linear* and *non-linear* systems. Linear systems are typically described by linear differential equations, which can be reduced to systems of first-order differential equations. Linear systems satisfy the principle of superposition and are typically, much simpler to model and control. Another important distinction is between *time-varying* and *time-invariant* systems. The differential equation describing a time-invariant system does not depend explicitly on the time-variable. The majority of systems that will be examined here are *linear-time-invariant (LTI)*. This assumption already implies some degree of approximation, since physical systems will always degrade with time and are to some extend non-linear.

The response $y(t)$ of a linear system to several inputs $u_1(t), u_2(t), \ldots u_n(t)$ acting simultaneously is equal to the sum of the responses of each input acting alone, when all the initial conditions in the system are zero (the system is at rest) [Stubberud et al. 1994]. That is, if $y_i(t)$ is the response due to input $u_1(t)$, then

$$y(t) = \sum_{i=1}^{n} y_i(t) \tag{3.1}$$

Equivalently, a system is linear if its input-output relationship can be described by the *convolution* integral (assuming zero initial conditions):

$$y(t) = \int_0^t w(t,\tau)u(\tau)d\tau \tag{3.2}$$

If further $w(t,\tau) = w(t-\tau)$, the system is time-invariant and $w(t)$ denotes its impulse response. Systems can further be classified as *analogue* or *digital.* A signal dependent on a continuum of values of the time-variable is called a continuous-time signal or analogue signal. A signal defined at discrete instants of time, is called a discrete-time signal. Discrete-time systems often use difference equations rather than differential equations and their transfer function is defined as a function of a unit-delay element, e.g. $u\left(z^{-1}\right)$.

Discrete control

Most of the work carried out in this thesis involves continuous-time (analogue) control but some sections include work involving discrete control. In most applications, discrete-time (or digital control) is applied via a computer or microprocessor on a continouous-time system, sampled at regular intervals kT, for $k = 0,1,2,\ldots T$. In such cases, the sampled system is often represented at the sampling instances by means of a discrete transfer function $G(z)$, depending on the continuous-time plant $G(s)$ and the sampling interval T. The most common representation arises via the so-called ZOH (zero-order-hold) equivalence, in which the response of $G(z)$ to any discrete-time signal coincides to the response of $G(s)$ at the sampling instances to the corresponding continuous piece-wise constant ("staircase") signal resulting by holding the digital samples constant over one sampling period. An important issue of digital control of analogue systems is the choice of sampling frequency rate $f_s = 1/T$. According to the Nyquist criterion in Signal Processing, continuous signals which are sampled and subsequently reconstructed back to analogue form suffer from *aliasing,* unless the sampling rate is chosen to be at least twice as high as their highest frequency component, i.e. $f_s \geq 2f_{\max}$ [Philips and Harbor 1996]. To avoid aliasing in digital control analogue signals are low-pass filtered before sampling and, in practice, the sampling rate is chosen at least 5-10 times higher than the target bandwidth of the closed-loop system.

Discrete-time control involves the design of digital controllers in the *Z*-domain typically using *z*-transform or discrete state-space techniques. The theory of *z*-transforms is similar to that of Laplace transforms applicable to continuous-time system and most classical-control design techniques (e.g. root-locus, Nyquist, Bode, etc) developed for continuous-time systems have their *z*-domain counterparts. The same applies for state-space techniques, with most concepts (stability, controllability, observability) and design methods (state-feedback, observers, LQR/LQG, etc) having developed in both domains. Finally "cross-domain" design approaches also exist (*w*-plane, Tustin`s bilinear transformations), in which a discrete-time system is transformed into a continuous-time "equivalent", a corresponding (continuous-time) controller is designed by analogue techniques and then transformed back into digital form using the inverse transformation.

3.4. Mathematical representation of systems

3.4.1 Transfer Functions

The first part in setting up and solving any control problem involves modeling the corresponding physical system using mathematical equations. For linear time-invariant systems the output (Y) is usually defined in the Laplace-transform domain as a function of the input (U); the ratio $Y(s)/U(s)$ is called a *transfer function* $G(s)$. Thus,

$$Y(s) = G(s)U(s) \tag{3.3}$$

Consider a simple spring-mass-damper system (figure 3.1.) [Philips and Harbor 1996]. The governing dynamic equation is given by a standard differential equation of the form:

$$F(x) = M\frac{d^2x}{dt^2} + C\frac{dx}{dt} + Kx \tag{3.4}$$

where x denotes displacement, M is the mass, K the stiffness and C the damping coefficient. In a control-design situation a typical problem would be to generate an appropriate force $F(t)$ in order to regulate the displacement (x) of the mass. In order to simplify the problem and avoid solving the differential equation directly, the equation is transformed by taking Laplace transforms.

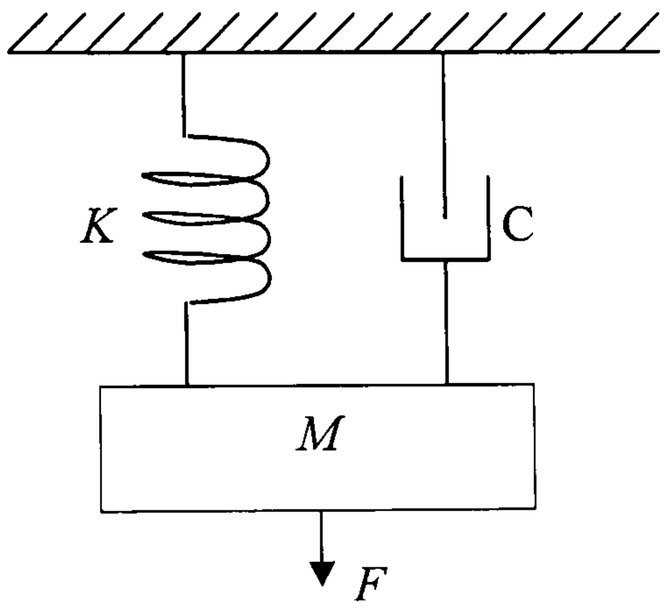

Figure 3.1. 1DOF Spring-mass-damper model

The Laplace transform of a function $f(t)$ is defined as:

$$L\left[f(t)\right] = \int_0^\infty f(t)e^{-st}dt \tag{3.5}$$

Taking Laplace transforms in equation (3.4), assuming zero initial conditions, this can be written as:

$$F(s) = (Ms^2 + Cs + K)X(s) \tag{3.6}$$

and thus:

$$\frac{X(s)}{F(s)} = \frac{1}{Ms^2 + Cs + K} \tag{3.7}$$

Setting $U(s) = F(s)$ as the input and $Y(s) = X(s)$ as the output of the system gives the transfer function of the system as:

$$G(s) = \frac{Y(s)}{U(s)} = \frac{1}{Ms^2 + Cs + K} \tag{3.8}$$

This is the standard procedure used to derive the transfer function of any linear time-invariant system. Equation (3.8) can be generalised for multivariable mechanical systems to structural models of the form:

$$M\ddot{x} + C\dot{x} + Kx = F \tag{3.9}$$

where x is a vector of displacements, M is a mass matrix (typically symmetric and positive definite), C is the damping matrix (typically symmetric), K is the stiffness matrix (typically symmetric and positive definite) and F is the vector of external forces applied to the structure.

3.4.2. State-space models

Another way of representing a dynamic system is as a *state-variable model (state space form)*. The state variable model is a set of 1^{st} order coupled differential equations, usually written in vector-matrix from. An n^{th} order system is written in state-space form using n-first order equations, which preserve the input-output relationship. A state-space model is an "internal" description of the system and as such it contains more information than the transfer function. This additional information involves internal variables that are either unreachable from the input (uncontrollable modes) or do not contribute to the output (unobservable modes). If a state-space model does not contain uncontrollable and unobservable modes it is called *minimal*. Non-minimal modes (i.e. uncontrollable/unobservable modes) appear as pole-zero cancellations in the system's transfer function.

A minimal state-space model of a system can be derived from its transfer function using the following method. Consider the simple spring-mass-damper system in the previous example. The governing dynamic equation is given by (3.4). Clearly, in this case the behaviour of the system is completely specified by two variables, the displacement and the velocity. We thus choose the states:

$$x_1 = y(t) \tag{3.10}$$

$$x_2 = \frac{dy(t)}{dt} = \dot{x} \tag{3.11}$$

Note that:

$$\frac{dy}{dt} = x_2 \tag{3.12}$$

and

$$\frac{d^2y}{dt^2} = \frac{dx_2}{dt} = \left(\frac{F - C\frac{dx}{dt} - Kx}{M} \right) \tag{3.13}$$

using (3.9) and (3.12). By rearranging the equations we obtain:

$$\begin{aligned} \dot{x}_1 &= x_2 \\ \dot{x}_2 &= -\frac{K}{M}x_1 - \frac{C}{M}x_2 + \frac{1}{M}F \\ y &= x_1 \end{aligned} \tag{3.14}$$

These equations are written in the standard state-space form:

$$\begin{pmatrix} \dot{x}_1 \\ \dot{x}_2 \end{pmatrix} = \begin{pmatrix} 0 & 1 \\ -\frac{K}{M} & -\frac{C}{M} \end{pmatrix} \begin{pmatrix} x_1 \\ x_2 \end{pmatrix} + \begin{pmatrix} 0 \\ \frac{1}{M} \end{pmatrix} F \tag{3.15}$$

and

$$y = \begin{bmatrix} 1 & 0 \end{bmatrix} \begin{bmatrix} x_1 \\ x_2 \end{bmatrix} \tag{3.16}$$

which define the state-transition and output equations, respectively. In general, a state space model for a linear time-invariant (LTI) system is of the form:

$$\begin{aligned} \dot{x}(t) &= Ax(t) + Bu(t) \\ y(t) &= Cx(t) + Du(t) \end{aligned} \tag{3.17}$$

where $\dot{x}(t)$ denotes the time-derivative of $x(t)$. In general:

$x(t)$ = state vector (n by 1 vector for an nth-order system)

A = (n by n) system matrix

B = (n by n) input matrix

C = (p by n) output or sensor matrix

D = (p by r) matrix representing direct coupling between input and output (feedthrough)

Also, $u(t)$ and $y(t)$ represent the input and output vectors, respectively.

In some cases it is important to determine (a minimal) state space model of a transfer function and vice versa. The task of obtaining a minimal state-space realisation from the transfer function is called the minimal realisation problem [Hall 2006]. The reverse task (obtaining the transfer function from a state-space realisation) is straightforward and can be performed using the formula:

$$G(s) = C(sI - A)^{-1} B + D \tag{3.18}$$

Note that a system has many (in fact infinite) state-space realisations, i.e. internal descriptions. All these realisations, however, correspond to the same transfer function (since the input-output characteristics of the system must be identical).

3.5. Stability

One of the most important objectives of control design is *stability*. There are many definitions of stability but, roughly, a system is stable if it remains at rest unless excited by an external source and returns to rest if all excitations are removed. More formally,

> *A system is called bounded-input-bounded-output stable if every bounded input results in a bounded output.*

An example of an unstable system is a driver moving the steering wheel on a wet road. The system is unstable once the car goes left and right with increasing amplitude rather than following a steady direction, because the input (the direction of the steering wheel) of the driver is having a negative effect to the output (the actual direction of the car). In theory, the response of the system in figure 3.2 is unbounded, so its *steady-state* (impulse) response (i.e. where the response settles after infinite time) is not defined and

the system is unstable. In contrast, in figure 3.3 the steady-state (impulse) response attains a constant value, therefore the system is stable. In this case the response tends to a constant value (possible zero) and is called *transient* before settling to its limiting value.

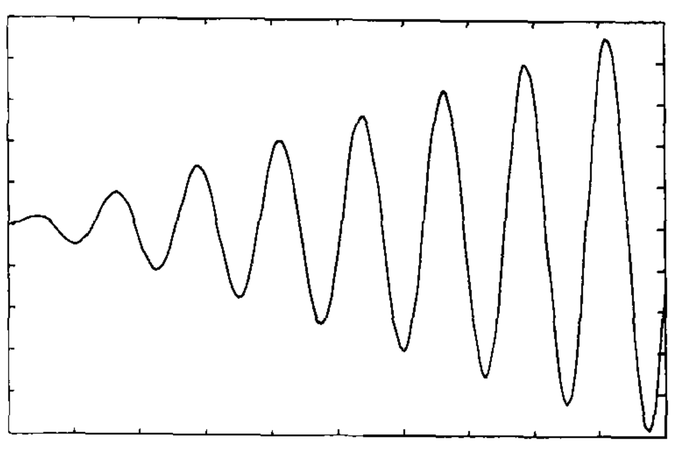

Figure 3.2 Unstable system response

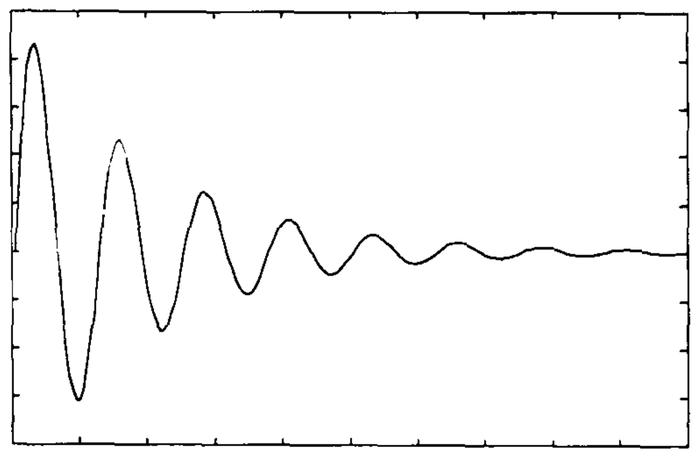

Figure 3.3 Stable system response

The roots of the numerator and denominator polynomials of the transfer function of a linear system define its *zeros* and *poles*, respectively. If any pole lies in the (closed) right-half plane, i.e. if it has a non-negative real part, the system is unstable; for example, the system

$$G(s) = \frac{(s-1)(s+3)}{(s-2)(s+2)} \tag{3.19}$$

is unstable because it has a pole at $s = 2$. There are several other methods to determine the stability of a system, e.g. from the coefficients of the characteristic polynomial (*Ruth-Hurwitz test*), the system's state- space realisation outlined in the following section, etc. Other tests (*Nyquist, Bode, Root Locus*) allow us to determine the stability of a feedback system as some parameter (e.g. gain) varies. Poles and zeros of a multivariable system are normally defined via the transfer function's Smith McMillan from [Antsaklis and Mitchell 1998]

3.5.1. Stability in state-space models

In state space representation the stability of an LTI system can be determined of its "A" matrix. If the real part of an eigenvalue is positive the corresponding mode is unstable. otherwise it is asymptotically stable:

If $\mathrm{Re}(\lambda_i(A)) < 0$ λ_i is a stable mode

If $\mathrm{Re}(\lambda_i(A)) > 0$ λ_i is an unstable mode

Here the system is assumed to be in the standard state-space form of equation (3.17). Recall that the eigenvalues of A are the roots of the characteristic polynomial of A, $\det(\lambda I - A) = 0$.

3.5.2. Controllability, observability

The concepts of *controllability* and *observability* are very important in control systems. In almost all control problems in order to proceed with the design, the assumption that the system is controllable and observable is made. An uncontrollable system (or mode) is one that cannot be affected by the input. For example if a system needs to control the movement of an object in the x-direction, applying a force in the y-direction will not affect the movement in the x-direction, therefore the corresponding system (or mode) is uncontrollable. More formally,

An LTI system is controllable if, for every x^* *and every* $T>0$, *there exists an input function* $u(t)$, $0 < t \le T$, *such that the system state can be steered from* $x(0)=0$ *to* $x(T)=x^*$.

The concept of observability is dual to that of controllability. If some modes cannot be determined from the measurements, the system is unobservable. More formally,

An LTI system is observable if the initial state $x(0)$ *can be uniquely deduced form the knowledge of the input* $u(t)$ *and output* $y(t)$ *for all t between 0 and* $T>0$.

There are several controllability and observability tests for LTI systems, the most common being the "rank test" [Stubberud et al. 1994] which states the following:

An LTI system is controllable if the *controllability matrix* Γ_c has rank n (where n is the number of state variables), where

$$\Gamma_c = \begin{bmatrix} B & AB & A^2B & \cdots & A^{n-1}B \end{bmatrix} \tag{3.20}$$

Similarly, an LTI system is observable if the observability matrix Γ_o has rank n, where:

$$\Gamma_0 = \begin{bmatrix} C \\ CA \\ CA^2 \\ \vdots \\ CA^{n-1} \end{bmatrix} \tag{3.21}$$

Finally a system is called *detectable* if all unstable modes are observable, and *stabilisable* if all unstable modes are controllable.

Thus, a system can be stabilised by state-feedback (output injection) only if it is stabilisable (detectable). Unobservable/uncontrollable dynamics do not show up in the transfer function. If all modes in a state-space realisation of a system are observable and controllable the system is in minimal realisation form.

3.5.3. Bode plots

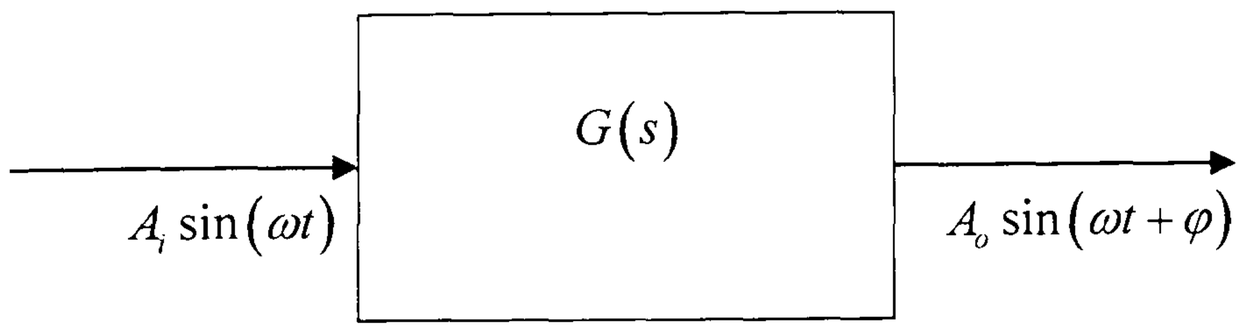

Consider equation (3.3) where the signal $U(t) = A_i \sin(\omega t)$ is applied to the input of an LTI system with transfer function $G(s)$; Provided the system is stable the output, $Y(t)$, is a sinusoid of the same frequency (after all transients have "died out") but in general

of different amplitude and phase, i.e. $Y(t) = A_o \sin(\omega t + \varphi)$ The gain at frequency ω is the ratio of the steady-state amplitude of the output over the amplitude of the input i.e.

$$\text{gain} = \left| \frac{A_o}{A_i} \right| \tag{3.22}$$

A magnitude (gain) Bode diagram is a plot of the gain in dB`s, where *gain in dB=20 log_{10}(linear gain)*, against frequency. Similarly a phase Bode diagram shows the variation of phase φ with ω. Consider the magnitude Bode plot of a system. The highest peak of the graph shows the highest gain and the frequency at which a sinusoidal input will excite the system the most (largest output over input ratio).

3.6. Controller design

3.6.1. Pole placement

As the locations of the poles of a system strongly affect its dynamic (transient) response, one way of modifying the characteristics of the system (under state-feedback) is to place the poles of the closed loop system at desired locations. The technique is called pole placement. It can be shown that if the system is controllable, the poles of the closed-loop system can be placed at arbitrary locations (provided they are symmetric with respect to the real axis). This is a very strong result which shows that under controllability the designer has complete freedom in modifying system's dynamics. Of course, this does not take into account constraints on the magnitude/energy of the required control signal and other practical considerations.

To illustrate the procedure, assume that $u(t) = r(t) - Kx(t)$, where r is a reference input, $u(t)$ is the control input and K is a gain (state-feedback) matrix. Under closed-loop control,

$$\dot{x}(t) = Ax(t) + Bu(t) = Ax(t) + B(r(t) - Kx(t)) = (A - BK)x(t) + Br(t) \tag{3.23}$$

and hence the closed-loop dynamics are now described by the eigenvalues of $A-BK$. The aim is thus to pick K so that the eigenvalues of $A-BK$ have the desired properties. If, for example, we want to stabilise A, we need to pick K so that $A-BK$ is stable (all eigenvalues have negative real part). If, in addition, we want to increase the damping of the system, all eigenvalues of $A-BK$ must be placed in the high-damped (left) region of the left-half plane. A standard procedure for obtaining the required gain matrix for SISO system is via Ackermann's formula [Antsaklis and Mitchell 1998]:

$$K = [0...01]\Gamma_c^{-1}\Phi_d(A) \tag{3.24}$$

where,

$$\Gamma_c = \begin{bmatrix} B & AB & \dots & A^{N-1}B \end{bmatrix} \tag{3.25}$$

and $\Phi_d(s)$ denotes the required characteristic polynomial of the closed-loop system evaluated at $s = A$. Note that Γ_c is assumed to be invertible, i.e. (A, B) must be controllable.

After the system has been identified, modelled and has taken its final form as a transfer function or a state-space model, it needs to be controlled by designing a feedback controller (or else compensator or regulator). The most common type of controller used in classical control is the proportional-plus-integral-plus-derivative (PID) controller. Modern control theory uses more powerful controllers, typically arising from the solution of an optimisation problem. In the context of active vibration control applications, one of the most widely used control-design methodologies arises from the solution of the Linear Quadratic Gaussian (LQG) problem, which is outlined below.

3.6.2 Linear Quadratic Regulators (LQR)-optimal control

Optimal control methods are control design techniques which provide "the best possible" (optimal) solution to an optimisation problem. Thus, in pole placement the aim is normally to stabilise a system, whereas in optimal control the objective is to optimise a performance index (while still keeping the system stable).

LQR (Linear quadratic regulator) is an optimisation method involving a quadratic objective function, corresponding to the weighted energy of all regulated and control variables. In the case of active control design, this formulation gives the designer sufficient flexibility to include all relevant design objectives, e.g. absolute displacements or relative inter-storey drifts, accelerations of each floor of the building, forces or strains developed at critical locations of the structure, constraints on the size of the actuator's signals, etc.

Assume that the plant to be controlled has a state space realisation:

$$\dot{x}(t) = Ax(t) + Bu(t)$$
$$y(t) = Cx(t) + Du(t)$$

The objective in LQR is to select the control input $u(t)$ that minimises the performance index:

$$J_{lqr} = \lim_{T\to\infty} \int_0^T (x^T Qx + u^T Ru)dt \qquad (3.26)$$

over all control signals $u(t)$.

In the above formulation it is required to minimise a performance index consisting of (weighted) energy terms involving the state-variables and the control signals. Thus the performance index balances transient-performance requirements ("fast" state-variables' decay) with control-effort constraints (control energy remains "small"). Normally, the matrices Q and R represent design parameters which shift the emphasis between these two (typically conflicting) objectives. A high value of Q (relative to R) places more emphasis on system performance (dynamic response), and vice-versa.

The standard assumptions of the general LQR problem are as follows:

1. The weighting matrices satisfy $Q = Q^T \geq 0$ and $R = R^T > 0$;
2. The pair (A,B) is stabilisable; and,
3. The pair (A,Q) is detectable.

Under these assumptions, the optimal controller is obtained in the form $u(t) = -K_c x(t)$, where K_c is the optimal state-feedback gain, given by:

$$K_c = R^{-1} B^T P_c \tag{3.27}$$

and P_c is the stabilising solution of the algebraic Riccati equation:

$$A^T P_c + P_c A - P_c B R^{-1} B^T P_c + Q = 0 \tag{3.28}$$

Here "stabilising" refers to the solution for which the closed-loop "A" matrix $A_c = A - BR^{-1}B^T P_c$ is asymptotically stable. It can be shown that under the stated conditions P_c is unique, symmetric and positive semi-definite matrix. Apart from stabilising the system, it may be shown that LQR controllers are also guaranteed to have good stability margins [Maciejowski 1989].

3.6.3. Linear Quadratic Gaussian (LQG) control

The main assumption of LQR is that all state-variables are measurable, which clearly is unrealistic in practice. This is removed by using LQG control (Linear-Quadratic-Gaussian), which is a generalisation of LQR and poses the design problem in a stochastic framework.

In LQG external disturbances are modelled as (filtered) white noise signals, while the objective function to be minimised is a stochastic version of the one used in LQR control. LQG removes the LQR assumption that all states are measurable; instead noisy measurements are assumed, and the overall problem decomposes to two separate sub-problems involving optimal estimation of the state-variables and optimal regulation ("separation" or "certainty-equivalence" principle). This is especially convenient for the designer, since the regulator part of the design remains unaffected. The optimal estimator ("Kalman filter") gives rise to a dynamic controller and is essentially an optimal observer, achieving a balance between the effects of disturbance and sensor-noise signals.

LQG control is a well-established design method, which has been applied successfully in many application domains. Computationally, it is easy to implement (requiring the off-line solution of two algebraic Riccati equations), while the weighting functions can be "tuned" in a systematic way to shift the emphasis between the various objectives included in the quadratic cost function. As mentioned earlier. LQR provides the design automatically with excellent stability margins. Unfortunately, these are no longer guaranteed when the Kalman filter is implemented, although various techniques are available to partially recover them and inject some measure of robustness into the design (Loop Transfer Recovery) [Maciejowski 1989].

The state space equation describing the plant is similar to the LQR formulation. with the addition of two white noise terms, representing process and measurement noise:

$$\begin{aligned} \dot{x}(t) &= Ax(t) + Bu(t) + Ew(t) \\ y(t) &= Cx(t) + Du(t) + v(t) \end{aligned} \tag{3.29}$$

Here $w(t)$ and $v(t)$ are zero-mean stochastic processes, uncorrelated in time (white noise) with known covariance matrices. The initial state is also assumed to be a random vector, with known mean and covariance matrix, and uncorrelated with both $w(t)$ and $v(t)$. The stochastic version of the problem is to find the optimal control signal which minimises the performance index

$$J_{lqg} = E\left\{\int_0^x (x^T Qx + u^T Ru)dt\right\} \tag{3.30}$$

where $E(\cdot)$ denotes statistical expectation, under the standard assumptions of stabilisability of (A,B), detectability of (A,C) and positive semi-definiteness (positive-definiteness) of Q (R). The problem is divided into two sub-problems: the first sub-problem is to obtain the optimal estimator, which minimises the root mean-square value of the state-estimation error, i.e.

$$\min E\{(x-\hat{x})^T(x-\hat{x})\} \tag{3.31}$$

This is solved by the Kalman filter [Davis and Vinter 1985]

$$\frac{d\dot{\hat{x}}}{dt} = A\hat{x} + Bu + L(y - C\hat{x} - Du) \tag{3.32}$$

in which L is the optimal Kalman gain, defined from the solution of an algebraic Riccati equation involving the covariance matrices of v and w; this is actually of the dual form to the algebraic Riccati equation used in the solution of the LQR problem. The second sub-problem involves the solution to the optimal regulator's gain and is identical to the solution of the LQR problem (with all stochastic terms removed). The separation (certainty equivalence) principle guarantees that this decomposition into two separate sub-problems still gives the overall optimal solution to the original problem.

A drawback of this theory is that it may have poor stability margins (the excellent stability margins guaranteed for the LQR controller no longer apply) and therefore several design modifications have been introduced to improve the system robustness (loop-transfer recovery [Maciejowski 1989]). Furthermore, since the Kalman filter replicates the dynamics of the plant, the general issue of model uncertainty and robustness becomes critical. Note that all uncertainties are represented in LQG as noise signals affecting the process dynamics or the measurements, which may not be realistic in practice. Despite these limitations LQG methods have a sound mathematical foundation and have proved effective in many practical designs; overall they produce very good results that are difficult to obtain with classical control methods.

The LQG problem is equivalent to the so-called "H_2 optimal control problem". The aim of this problem is to find a proper real-rational controller $K(s)$ that stabilises the plant $G(s)$ internally and minimises the H_2 norm of the transfer matrix $T_{zw}(s)$ between w (disturbances) and z (regulated signals). The formulation and solution of the H_2 problem is different from LQR but essentially the *two problems are identical*.

3.6.4. Robust -H_∞ control

Robust control is a design methodology which deals systematically with the effects of uncertainty, especially its implications on the stability and performance properties of the feedback system. Model uncertainty is known to be one of the most important

considerations in control systems design. A mathematical model, which is used for control design, can never represent exactly the real physical system which is controlled. resulting in a model mismatch or perturbation. The objective of robust control is to make the design insensitive to this model error.

LQ methods can take into account robust performance objectives only in an ad-hoc way, after the controller has been designed [Maciejowski 1989]). H_∞ optimal control is a more systematic robust control methodology, which can address directly robustness issues in its optimisation framework. This is achieved by imposing (frequency-weighted) bounds on the "size" (norm) of the uncertainty, and optimising for the worst-case perturbation within the assumed uncertainty class. Thus, H_∞ is a "worst-case" or "min-max" design approach, and as such it can be potentially conservative if the assumed size of the uncertainty is overestimated [Zhou and Doyle 1998].

Before proceeding with outlining the method, some mathematical terms need to be defined:

1. A vector *p-norm* is defined as:

$$\|x\|_p = \left(\sum_{i=1}^{n} |x|^p \right)^{1/p} \tag{3.33}$$

For example, the two-norm (or Euclidian norm) $\left(\|x\|_2\right)$ gives the length of a vector.

2. Singular values of a complex matrix A are the square roots of the eigenvalues of AA^*, where A^* denotes the complex conjugate transpose of A, i.e.

$$\sigma_i(A) = \sqrt{\lambda_i(AA^*)} \tag{3.34}$$

If A is a function of frequency, the singular values can be plotted in the frequency domain (Bode plots) and the H_∞ norm is the distance from the x-axis to the peak value of the largest singular value. In H_∞ control, the aim of the controller is to minimise this peak value – in general this is achieved by adjusting the gain at other frequencies, until ideally the plot of the maximum singular value becomes flat and no further reduction is possible. Mathematically the infinity norm of a transfer function is given by:

$$\|G\|_{\infty} = \max_{\omega \in \Re} \bar{\sigma}[G(j\omega)] \tag{3.35}$$

where $\bar{\sigma}$ denotes the largest singular value.

The following graph (figure 3.4) illustrates the generalised regulator problem which is the standard paradigm in H_{∞} optimisation. In this diagram $P(s)$ is the generalised plant, $K(s)$ is the controller and $\Delta(s)$ represents the model uncertainty (perturbation).

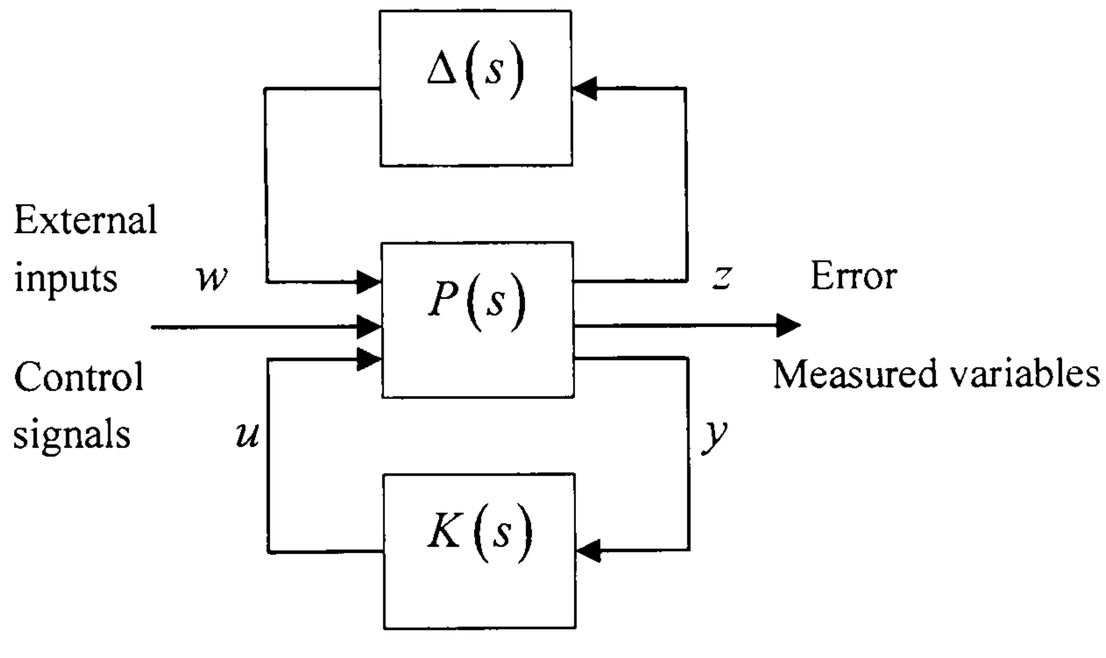

Figure 3.4. Generalised plant including modelled external perturbation

In the diagram:

$w(s)$: all external disturbance signals

$z(s)$: all controlled (regulated) variables (e.g. errors etc.)

$u(s)$: all control signals

$y(s)$: all measured outputs

$\Delta(s)$: model perturbation

$P(s)$: generalised plant (including frequency-weights)

$K(s)$: compensator

The generalised regulator problem is represented by the above block diagram. Set $\Delta = 0$ and partition P conformally with the signals (w, u) and (z, y), i.e.

$$P(s)=\begin{bmatrix} P_{11}(s) & P_{12}(s) \\ P_{21}(s) & P_{22}(s) \end{bmatrix} \tag{3.36}$$

Then we can write:

$$z = P_{11}w + P_{12}u \tag{3.37}$$

$$y = P_{21}w + P_{22}u \tag{3.38}$$

The objective is to design an output-feedback controller $K(s)$ (i.e. such that $u = Ky$) which stabilises the system and minimises the infinity norm of the transfer function between $w(s)$ and $z(s)$. By substituting $u = Ky$ in eq. (3.38) we get,

$$u = K(I - KP_{22})^{-1}P_{21}w \tag{3.39}$$

Substituting this in eq. (3.37) gives

$$z = \left[P_{11} + P_{12}K\left(I - P_{22}K\right)^{-1}P_{21}\right]w \tag{3.40}$$

For simplicity this function will be written as:

$$z = F_l(P, K)w \tag{3.41}$$

(lower linear fractional map of P and K). The H_∞ problem now becomes:

$$\min_{K(s)} \left\| P_{11} + P_{12}K(I - P_{22}K)^{-1}P_{21} \right\|_\infty \tag{3.42}$$

over all realisable controllers $K(s)$ which stabilise the closed-loop system [Maciejowski 1989]. Note that the infinity norm represents the maximum energy transfer between the disturbance signal $w(s)$ and the regulated signal $z(s)$.

In order to proceed to the solution of the H_∞ problem, the Youla parametrisation over all stabilising controllers needs to be performed, established by [Youla et al. 1976]. This is outlined in the next section.

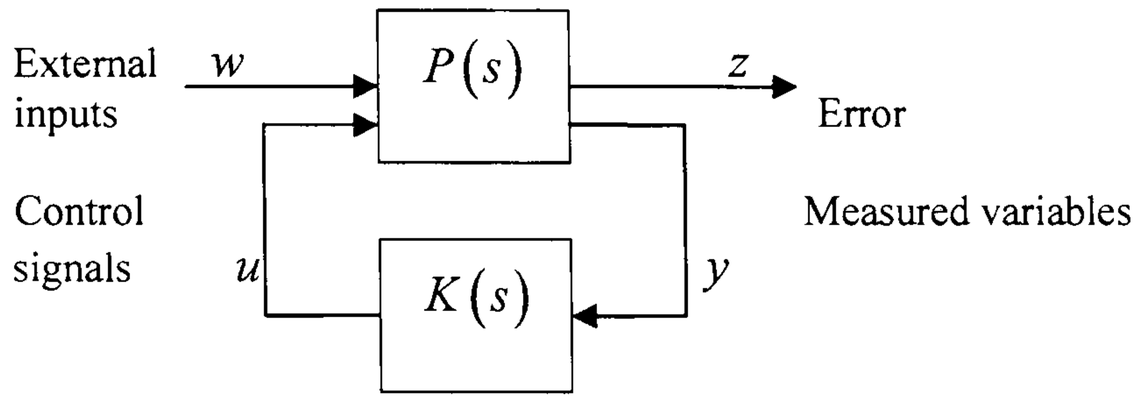

Figure 3.5 Generalised plant

Recall that the general H_∞ problem is the minimisation of an infinity norm eq. (3.42) which, via Youla's parametrisation of all stabilising controllers becomes:

$$\min_Q \left\| T_{11} + T_{12} Q T_{21} \right\|_\infty \tag{3.43}$$

where now Q is a free matrix parameter in H_∞ ("model-matching" problem). Depending on the number of rows and columns of T_{12} and T_{21} the 1-, 2- or 4-block problems arise. If T_{12} is square (or has more columns than rows) and T_{21} is square (or has more rows than columns) the problem reduces to a 1-block problem which can be solved explicitly. If T_{12} has more rows than columns or T_{21} has more columns than rows we obtain a 2-block problem or else a 4-block problem, respectively. Both 2- and 4-block problems have to be solved iteratively.

Assume without loss of generality that T_{12} and T_{21} are square and all pass (1-block problem), i.e.

$$T_{12} T_{12}^* = I \text{ and } T_{21}^* T_{21} = I$$

where $T^*(s) = T^T(-s)$ denotes the "para-hermitean conjugate" system. Then,

$$\left\|T_{11}+T_{12}QT_{21}\right\|_{\infty}=\left\|T_{12}(T_{12}^{*}T_{11}T_{21}^{*}+Q)T_{21}\right\|_{\infty}=\left\|T_{12}^{*}T_{11}T_{21}^{*}+Q\right\|_{\infty}=\left\|T_{21}T_{11}^{*}T_{12}+Q^{*}\right\|_{\infty} \quad (3.44)$$

It can be shown [Limebeer et al. 1987] that $T_{21}T_{11}^{*}T_{12}$ is a stable system, and the problem thus reduces to:

$$\min_{Q}\left\|T_{11}+T_{12}QT_{21}\right\|_{\infty}=\min_{Q}\left\|T_{21}T_{11}^{*}T_{12}+Q_{*}\right\|_{\infty}=\min_{Q}\left\|R+Q*\right\|_{\infty} \quad (3.45)$$

which is a Nehari extension problem (optimal approximation in the infinity norm of a stable system by an anti-stable system) and can be solved in closed-form, the minimum being the Hankel norm of R [Maciejowski 1989]. In the 4-block case it is possible to find transfer functions $T_{12\perp}$ and $T_{21\perp}$ such that $\begin{bmatrix}T_{12} & T_{12\perp}\end{bmatrix}$ and $\begin{bmatrix}T_{21}^{T} & T_{21\perp}^{T}\end{bmatrix}$ are stable, square and all-pass, i.e.

$$\begin{bmatrix}T_{12}^{*}\\ T_{12\perp}^{*}\end{bmatrix}\begin{bmatrix}T_{12} & T_{12\perp}\end{bmatrix}=I \text{ and } \begin{bmatrix}T_{21}\\ T_{21\perp}\end{bmatrix}\begin{bmatrix}T_{21}^{*} & T_{21\perp}^{*}\end{bmatrix}=I$$

Proceeding as above:

$$\begin{aligned}\min_{Q}\left\|T_{11}+T_{12}QT_{21}\right\|_{\infty}&=\min_{Q}\left\|\begin{bmatrix}T_{12}^{*}\\ T_{12\perp}^{*}\end{bmatrix}[T_{11}+T_{12}QT_{21}][T_{21}^{*} \quad T_{21\perp}^{*}]\right\|_{\infty}\\ &=\min_{Q}\left\|\begin{bmatrix}T_{12}^{*}\\ T_{12\perp}^{*}\end{bmatrix}T_{11}[T_{21}^{*} \quad T_{21\perp}^{*}]+\begin{bmatrix}Q & 0\\ 0 & 0\end{bmatrix}\right\|_{\infty}\\ &=\min_{Q}\left\|\begin{bmatrix}R_{11}+Q & R_{12}\\ R_{21} & R_{22}\end{bmatrix}\right\|_{\infty}\end{aligned} \quad (3.46)$$

which is the so-called general-distance problem. Here:

$$R_{11}=T_{12}^{*}T_{11}T_{21}^{*} \qquad R_{12}=T_{12}^{*}T_{11}T_{21\perp}^{*}$$

$$R_{22}=T_{12\perp}^{*}T_{11}T_{21}^{*} \qquad R_{22}=T_{12\perp}^{*}T_{11}T_{21\perp}^{*}$$

The 2-block problem with T_{12} having more rows than columns simplifies by using the same procedure to:

$$\min_Q \|T_{11} + T_{12}QT_{21}\|_\infty = \min_Q \left\| \begin{bmatrix} R_{11} + Q \\ R_{21} \end{bmatrix} \right\|_\infty \tag{3.47}$$

If T_{21} has more columns than rows then:

$$\min_Q \|T_{11} + T_{12}QT_{21}\|_\infty = \min_Q \|R_{11} + QR_{12}\|_\infty \tag{3.48}$$

The above problems have only iterative solutions [Maciejowski 1989]. Typically, a scalar γ is chosen, and a bisection algorithm is applied to discover whether a stable Q exists such that $\|T_{11} + T_{12}QT_{21}\|_\infty < \gamma$. In this way the minimising Q can be obtained (within arbitrary accuracy), from which the optimal compensator $K(s)$ can be defined by substitution. An alternative algorithm for solving the general H_∞ optimal control problem is the Glover-Doyle algorithm given below:

Glover-Doyle algorithm [Glover and Doyle 1988]

(i) A stabilising controller exists, such that $\|P_{11} + P_{12}K(I - P_{22}K)^{-1}P_{21}\|_\infty < \gamma$ if

(a) $\gamma > \max\{\bar{\sigma}[D_{1111}, D_{1111}], \bar{\sigma}[D_{1111}^T, D_{1121}^T]\}$

where D_{11} is partitioned as: $D_{11} = \begin{bmatrix} D_{1111} & D_{1112} \\ D_{1121} & D_{1122} \end{bmatrix}$

(b) there exist solutions $X_\infty \geq 0$, $Y_\infty \geq 0$ of the Riccati equations:

$$X_\infty(A - BR^{-1}D_{1*}^T C_1) + (A - BR^{-1}D_{1*}^T C_1)^T X_\infty - X_\infty BR^{-1}B^T X_\infty + C_1^T(I - D_{1*}R^{-1}D_{1*}^T)C_1 = 0 \tag{3.49}$$

and

$$Y_\infty(A - B_1 D_{*1}^T \tilde{R}^{-1}C)^T + (A - B_1 D_{*1}^T \tilde{R}^{-1}C)Y_\infty - Y_\infty C^T \tilde{R}^{-1}CY_\infty + B_1(I - D_{*1}^T \tilde{R}^{-1}D_{1*})B_1^T = 0 \tag{3.50}$$

such that:

$$\rho(X_\infty Y_\infty) < \gamma^2 \tag{3.51}$$

(ii) If (a) and (b) are satisfied, all rational stabilising controllers $K(s)$. for which

$$\left\| P_{11} + P_{12}K(I - P_{22}K)^{-1}P_{21} \right\|_{\infty} < \gamma \tag{3.52}$$

are given by $K(s) = F_l(K_a, \Phi)$, where $\|\Phi_a\|_{\infty} \leq \gamma^{-1}$ and K_a is a fixed system (for explicit formula see [Maciejowski 1989]).

The above result suggests the following method for calculating the optimal H_∞ controller: Reduce γ until one of the following three conditions fails: (i) A stabilising solution to the first Riccati equation does not exist, (ii) A stabilising solution to the second Riccati equation does not exist, or (iii) The spectral radius $\rho(X_\infty Y_\infty)$ is not strictly less that γ^2.

3.6.5. Youla parametrisation of all stabilising controllers

The Youla parametrisation is a powerful result which expresses all stabilising controllers of a given plant in terms of a linear transformation involving a free stable matrix parameter Q. In addition, all closed-loop system matrices are parametrised linearly in Q, which makes the solution of the H_∞-optimisation problem tractable [Francis 1987]. The parametrisation proceeds by defining left and right coprime factorisations of the plant.

Recall that two polynomials $f(s)$ and $g(s)$ with, say, real coefficients, are said to be coprime if their greatest common divisor is 1. It follows form Euclid's algorithm that f and g are coprime if and only if there exist polynomials $x(s)$ and $y(s)$ such that

$$fx + gy = 1$$

Consider Figure 3.5 in which the generalised plant P is partitioned as:

$$P = \begin{pmatrix} P_{11} & P_{12} \\ P_{21} & P_{22} \end{pmatrix} \tag{3.53}$$

with $P_{22} = G$ denoting the plant, assumed to be a proper real-rational matrix. Then there exist eight RH_∞, i.e. all poles in open left half plane and proper (degree of numerator ≤ degree of denominator), matrices satisfying the equations:

$$G = NM^{-1} = \tilde{M}\tilde{N} \tag{3.54}$$

and

$$\begin{bmatrix} \tilde{X} & -\tilde{Y} \\ -\tilde{N} & \tilde{M} \end{bmatrix} \begin{bmatrix} M & Y \\ N & X \end{bmatrix} = I \tag{3.55}$$

These may be defined more easily in a state-space setting. Let $G(s)$ have a state space realisation:

$$G(s) = D + C(sI - A)^{-1} B \tag{3.56}$$

with (A,B) stabilisable and (C,A) detectable. Introduce state, input and output vectors x, u and y respectively so that $y(s) = G(s)u(s)$ and

$$\dot{x}(t) = Ax + Bu$$
$$y(t) = Cx + Du$$

Next, choose a real matrix F such that $A_F = A + BF$ is stable and define the vector $v = u - Fx$ and the matrix $C_F = C + DF$. Then we get:

$$\dot{x} = A_F x + Bv$$
$$u = Fx + v \tag{3.57}$$
$$y = C_F x + Dv$$

The right coprime factors $M(s)$ and $N(s)$ may be obtained in terms of the following realisations:

$$M(s) := [A_F, B, F, I] \text{ and } N(s) := [A_F, B, C_F, D]$$

Similarly, by choosing a real matrix H so that $A_H = A + HC$ is stable and defining $B_H = B + HD$, we get the left coprime factors as:

$$\tilde{M}(s) := [A_H, H, C, I] \text{ and } \tilde{N}(s) := [A_H, B_H, C, D]$$

Formulas for the remaining four transfer functions $X, Y, \tilde{X}, \tilde{Y}$ are given as:

$$X(s) \overset{s}{=} [A_F, -H, C_F, I],\ Y(s) \overset{s}{=} [A_F, -H, F, 0],\ \tilde{X}(s) \overset{s}{=} [A_H, -B_H, F, I],\ \tilde{Y}(s) \overset{s}{=} [A_H, -H, F, 0]$$

Now one stabilising controller $K(s)$ of $G(s)$ is given by $K(s) = YX^{-1} = \tilde{X}\tilde{Y}^{-1}$. The set of all proper real rational K's stabilising G is given as:

$$K = (Y - MQ)(X - NQ)^{-1} = (\tilde{X} - Q\tilde{N})^{-1}(\tilde{Y} - Q\tilde{M}),\ Q \in RH_\infty \qquad (3.58)$$

Further, consider again the generalised regulator in Figure 3.5. It may be shown [Francis 1987] that a controller $K(s)$ stabilises $P(s)$ (internally) if and only if it stabilises $P_{22} = G(s)$ (internally). Thus, under the assumed stabilisability and detectability assumptions on (A,B) and (C,A), all stabilising controllers of $P(s)$ are given by the set K defined above. Moreover, it may be shown [Francis 1987] that all (stable) closed-loop systems between w and z in Figure 3.8 are parametrised linearly as $T_{11} - T_{12}QT_{21},\ Q \in RH_\infty$, where

$$\begin{aligned} T_{11} &= P_{11} + P_{12}\tilde{M}YP_{21} \\ T_{12} &= P_{12}M \\ T_{21} &= \tilde{M}P_{21} \end{aligned} \qquad (3.59)$$

These three matrices T_{ij} belong to RH_∞. Let P have a state space realisation:

$$P(s)\overset{s}{=}\left\{A,\begin{pmatrix}B_1 & B_2\end{pmatrix},\begin{pmatrix}C_1\\C_2\end{pmatrix},\begin{pmatrix}D_{11} & D_{12}\\D_{21} & D_{22}\end{pmatrix}\right\} \tag{3.60}$$

[Note that in this notation the realisation of the plant $G(s)$ is now re-defined as $G(s)=P_{22}(s)\overset{s}{=}(A,B_2,C_2,D_{22})$]. Then a state-space realisation of the T_{ij} is given as:

$$\begin{pmatrix}T_{11} & T_{12}\\T_{21} & 0\end{pmatrix}\overset{s}{=}\left\{\begin{pmatrix}A_F & -B_2F\\0 & A_H\end{pmatrix},\begin{pmatrix}B_1 & B_2\\B_1+HD_{21} & 0\end{pmatrix},\begin{pmatrix}C_1+D_{12}F & -D_{12}F\\0 & C_2\end{pmatrix},\begin{pmatrix}D_{11} & D_{12}\\D_{21} & 0\end{pmatrix}\right\} \tag{3.61}$$

This will be explored further in Chapter 7.

3.6.6 Systems identification

A stochastic process is a sequence of random variables with well-defined joint probability distributions. In most cases this information is too demanding for modelling purposes, and the stochastic process is described only in terms of its second-order statistics, i.e. as a collection of identically distributed random variables in which only the (common) mean and the covariance function are assumed to be known. A stochastic process can be adequately modelled as the output of a filter driven by white noise. Thus, if a disturbance entering a system can be modelled as a stochastic process, it can be assumed to be a white noise signal, the corresponding filter being augmented in the dynamics of the system. This technique allows us to model effectively disturbances of known spectral density. It is especially useful in structural control when the disturbance is an earthquake or a wind load signal whose spectral density function is approximately known. Typically the following procedure is used for modelling disturbance signals from discrete random data $\{\eta_i\}$ ([Davis and Vinter 1985]:

1. Remove any significant mean or trend components (these can be assumed to be deterministic disturbances).
2. Obtain estimates of the covariance function from the data as:

$$\hat{R}(k) = \frac{1}{N-k} \sum_{t=k+1}^{N} \eta_t \eta_{t-k} \tag{3.62}$$

for $k = 0, 1, ..., m,\ m \approx \frac{N}{4}$

3. Use Fourier transform (FFT) to obtain estimate of spectral density function:

$$\hat{\Psi}(\omega) = \hat{\Phi}_{\eta\eta}\left(e^{j\omega}\right) = \sum_{k=-m}^{m} \hat{R}(k) e^{-j\omega k} \tag{3.63}$$

4. Design a stable, minimum-phase filter

$$G\left(z^{-1}\right) = \frac{B\left(z^{-1}\right)}{A\left(z^{-1}\right)} \tag{3.64}$$

so that its frequency response $\left|G\left(e^{j\omega}\right)\right|^2$ "fits" $\hat{\Psi}(\omega)$ adequately.

The estimated model is then of the form:

$$n_t = \frac{B(z^{-1})}{A(z^{-1})} e_t + E(\eta_t) \tag{3.65}$$

as shown in figure 3.6:

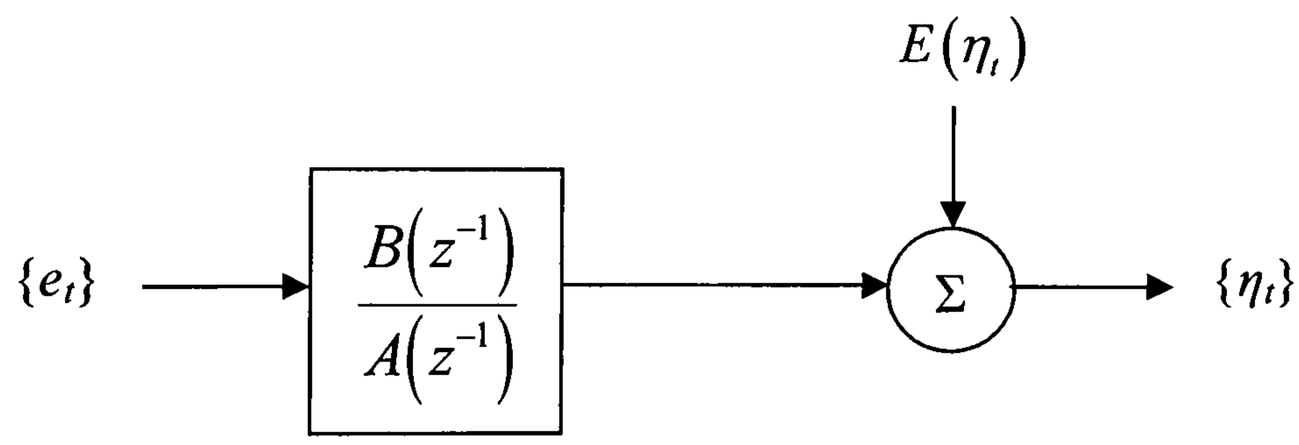

Figure 3.6. Identification filter

Here e_t is the input of the process (assumed "white"), η_t is the output of the process, and $A(z^{-1}), B(z^{-1})$ are polynomials in the unit-delay variable z^{-1}. This model type is known as Autoregressive Moving-Average (ARMA). If $B(z^{-1}) = 1$, i.e. if η_t can be written in regression form with its past values only, the model simplifies to an Autoregressive (AR) model of the form

$$A\left(z^{-1}\right)\eta_t = e_t \tag{3.66}$$

assuming for simplicity that $E(\eta_t) = 0$. Normally, the order of the polynomial $A(z^{-1})$ (order of AR model) is selected as the lowest integer for which the model fits the experimental data adequately (i.e. with the required accuracy) by using least-squares or another parameter-estimation technique.

3.7. Summary

In this chapter the background of control theory has been outlined. Fundamental ideas of system properties, control design methods have been presented, with particular emphasis to the material which will be used at the later chapters of the work related to active control design.

CHAPTER 4

STRUCTURAL DYNAMICS AND PASSIVE SYSTEM ANALYSIS OF A PENDULUM MODEL

4.1. Introduction

This chapter is divided into two parts. The first is a brief review on earthquake engineering concepts and the theory of vibrations. The second part is a detailed analysis of a pendulum-frame model. In the first part the main concepts of structural dynamics are discussed, a topic which is essential for vibration control. Buildings are modelled as LTI systems with mass, damping and stiffness. The dynamic behaviour of these models is governed by several modes. Furthermore, the period of a multi-modal system depends critically on its modal mass contribution. The effect of an earthquake on a building largely depends on the period and the modes of the building. Understanding the effect of modal frequencies and shapes is crucial because passive control is usually targeting specific modes.

The second part of the chapter examines the effect of tuned mass dampers on a frame for vibration control. A simple model consisting of a frame with a suspended mass is analysed in detail. The objective is to investigate the concept of passive control on buildings for earthquake protection. The pendulum used here is an idealisation of the most common passive control system, the tuned-mass-damper. The pendulum-frame interaction is analysed from first principles. Although the model is simple, the analysis presented is adequate to identify the main principles behind passive energy dissipation systems.

There are several approaches for explaining how a pendulum can be used for vibration control of civil engineering structures. The first is to consider the damping coefficient corresponding to the pendulum's motion. In this case, due to the pendulum-frame interaction, energy is dissipated. A second approach is to consider the reduction of the frame's amplitude due to the force applied by the pendulum on the frame. A third, more indirect, way is to consider the increase of the system's period, due to the extra

pendulum mass, which corresponds to shifting the characteristic frequency of the system outside the earthquake's bandwidth. Here is examined which of the above mechanisms, and to what extend, can help reduce the vibrations of a structure. If this type of vibration control proves to be efficient, it can be the most economic way of protecting structures.

The final part of this chapter introduces an area that has received very little attention in structural control. It investigates a building's behaviour when the material yields (reaches its elastic limit) and behaves inelastically. Although conventional ways of seismic design are based on inelastic concepts, these are rarely taken into account in structural control. It is normally assumed that the controller's action will be effective enough to ensure that the controlled structure will not enter the inelastic region, an assumption which cannot be guaranteed in general (e.g. if the earthquake signal is sufficiently strong). Here, the frame pendulum model is simulated by taking into account its inelastic behaviour i.e. change of the stiffness and consequently the characteristic frequency of the frame. This analysis is not carried out in depth, as the main objective is simply to investigate the efficiency of the pendulum in reducing the amplitude of vibrations when the stiffness is altered.

4.2.1. Earthquake engineering design

Earthquakes are probably the worst natural hazards in terms of economic loss and death toll. Due to the nature of this type of loading it is typically difficult to design against earthquakes. Seismic design was first introduced into the codes during the 1920's in the USA. The code assumed that the earthquake loading was a horizontal load of about 10% the weight of the structure. In the 1960's due to technological advances and the emergence of accelerogramms, the actual seismic force could be estimated more reliably. By observing damaged or destroyed buildings from earthquakes, it was noticed that buildings that allowed for high elastic deformations survived large earthquakes with damage but without collapse.

This observation led to a new era of earthquake design. Ductile structures were able to withstand much higher loadings than others of equal strength but no deformation

capacity. Since then, buildings were designed in the inelastic range rather than in the elastic. The force that a structure needs to resist is much lower than the actual earthquake force. This leads to economic and safe structures that have to be carefully designed to meet the requirements of inelasticity and the capacity design procedures [Elnashai 2001].

Modern codes are based on concepts of inelasticity and deformation capacity. As the stress on a member during earthquake loading increases, it reaches the yield point (elastic limit), after which the member enters the inelastic region. At even larger loads the member starts elongating without collapsing until the ultimate member strength is reached. By having members with high ductility (ratio of ultimate to yield deformation) structures can keep deforming without failing. This allows the member to be able to withstand only a portion of the total load but without collapsing. As a consequence, at large earthquakes the building does not fail but at moderate earthquakes there is damage due to the members exceeding the yield point. Hence, construction is economic and collapse may be avoided (thus reducing human deaths and injuries), although there can be a high economic loss due to repairs needed after earthquakes.

Figure 4.1 shows an idealised force-displacement graph of steel. From this figure, we can define the stiffness and ductility of the material as follows: Stiffness is the tangent of the force displacement graph and ductility the ratio of maximum elongation before collapse over elongation at yield point, i.e.

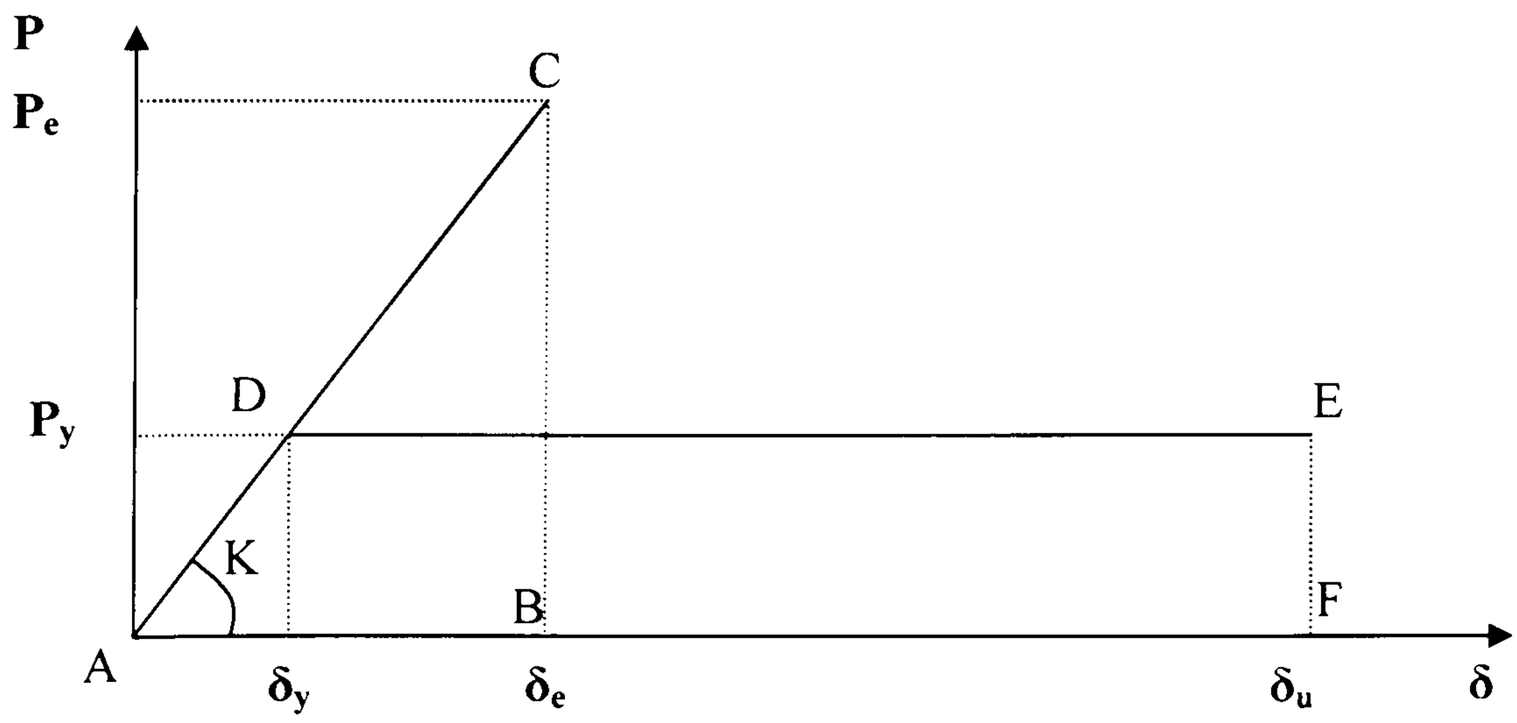

Figure 4.1 Idealised elastic and inelastic force-displacement graph

$$K_e = \frac{P_e}{\delta_e} \qquad \mu = \frac{\delta_u}{\delta_y}$$

A strong and stiff structure having maximum force P_d and deformation δ_e has total stress capacity equal to the area ABC. A structure with low strength, yielding at P_y, low stiffness ($K = \frac{P_y}{\delta_u}$) but large ductility (δ_u / δ_y), has larger stress deformation capacity equal to area ADEF. This is the concept upon which current seismic codes are based.

The earthquake force is assumed as a horizontal load applied at the top of the building. This can be deduced from the Acceleration Response Spectrum (ARS), which is a graph that gives the maximum response of a Single-Degree-Of-Freedom (SDOF) system with respect to natural frequency. The idealised shape of such an ARS is shown in the graph below. Several countries use their own ARS and there exists also one used by Eurocode 8 (figure 4.2). The exact values depend mainly on the soil, the seismicity of the region and damping of the material used. The elastic response spectrum is divided by the force modification factor q, to obtain the inelastic spectrum response. The force modification factor is mainly a function of ductility. Once the period of the building is known, the acceleration experienced by the building as a result of an earthquake is obtained from the inelastic acceleration response spectrum.

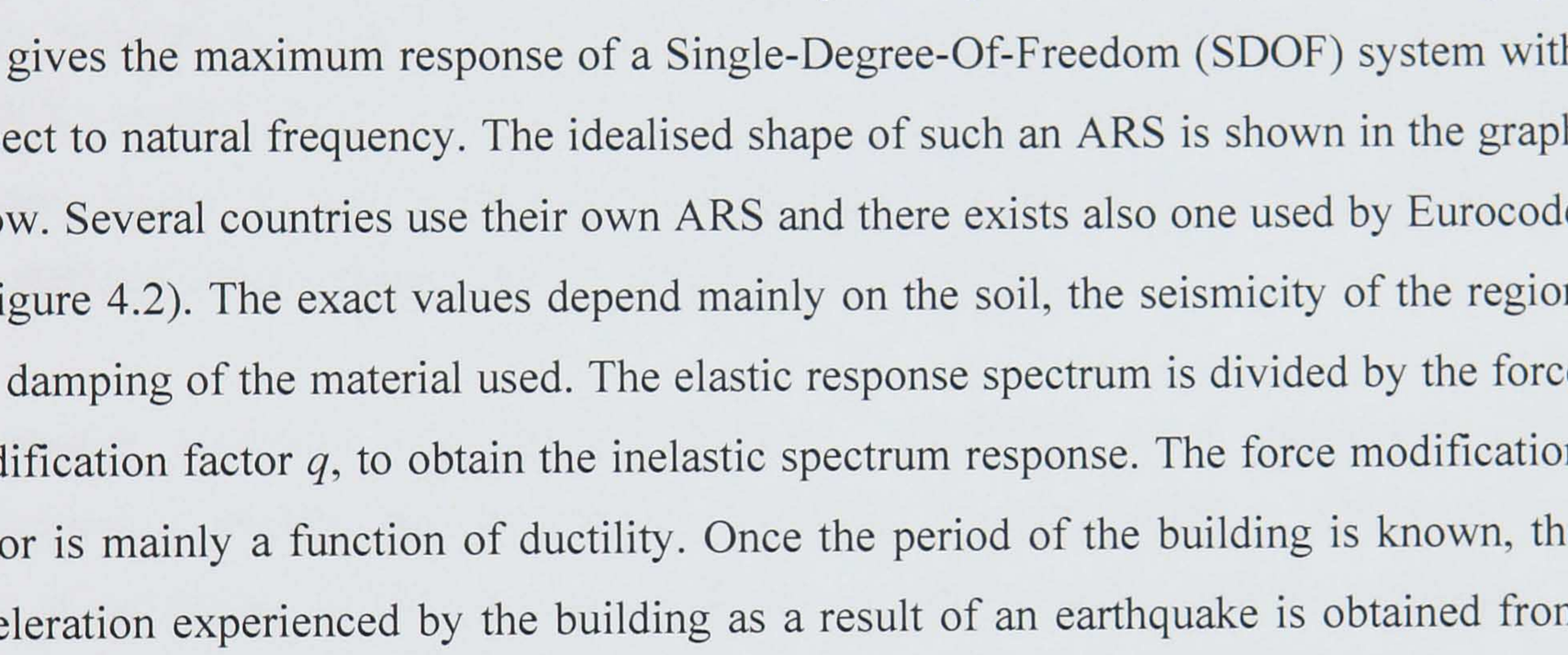

Figure 4.2 Idealised elastic and inelastic acceleration response spectrum

Structural Modelling In Civil Engineering buildings are represented by lumped mass parameters. This approach is valid when a large part of the mass is concentrated at a few locations and assumes that the mass is located at a discrete point, or is uniformly distributed at a specific part of a structure. This approach is valid for buildings where most of the mass is at floor levels. The column mass is negligible compared to the rest of the building and is therefore assumed to be weightless.

The lumped parameter method simplifies the mathematical derivations related to vibration analysis problems. Differential equations govern the behaviour of such systems. An advantage of using lumped mass parameters is the underlying assumption that the degrees of freedom of a structure are as many as the number of masses, e.g. a 3-storey building has 3 degrees of freedom. The behaviour of a multi-degree-of-freedom (MDOF) system can be significantly different from SDOF systems. Typically there are as many modes of vibration as degrees of freedom. Each degree of freedom corresponds to a different mode of vibration and characteristic frequency.

A second structural representation involves distributed mass parameters. This description is usually used for bridges where the mass distribution is similar at most parts of the bridge. In this case, partial derivatives are normally used for modelling. A third representation which is much more powerful is the finite element method. In this method, piecewise polynomial interpolation is used to describe a field quantity between nodes. A structure is divided into several elements, typically hundreds in number and its structural behaviour analysed. Elements are reconnected at nodes and thus the structure is modelled as a lumped parameter system whose order depends on the required accuracy. The method relies on the solution of hundreds or thousands of equations, depending on the number of elements used, which depends on a matrix inversion of order twice as high as the number of elements. The finite element method was only theoretical until the introduction of computers, which were able to handle large number of equations. Finite element problems are especially useful when dealing with irregular structures or shapes, non-linearities and non-uniform materials. These days, most realistic design problem involving structural analysis are modelled with finite elements.

Modal analysis The governing dynamic equation of a lamped parameter model in structural dynamics is:

$$M\ddot{x}(t) + C\dot{x}(t) + Kx(t) = P(t) \tag{4.1}$$

where M is the mass matrix, C is the damping matrix and K the stiffness matrix. All three matrices are typically positive definite and sparse. Usually, the stiffness and damping matrices are tri-diagonal while the mass matrix is diagonal, and the (i,i)-th entry represents the mass at the i-th floor.

Eigenvalue analysis The equation of motion for an undamped freely vibrating system is:

$$M\ddot{x} + Kx = 0 \tag{4.2}$$

where x represents the vector of displacements of each DOF. Assume that the free vibration motion is simple harmonic,

$$x(t) = \hat{x}\sin(\omega t + \theta) \tag{4.3}$$

In this expression $\hat{x}$ represents the shape of the system and θ is the phase angle. The second derivative of the above expression is:

$$\ddot{x}(t) = -\omega^2\hat{x}\sin(\omega t + \theta) = -\omega^2 x \tag{4.4}$$

Substituting (4.3) and (4.4) into (4.2) gives:

$$-\omega^2 M\hat{x}\sin(\omega t + \theta) + K\hat{x}\sin(\omega t + \theta) = 0 \tag{4.5}$$

or,

$$\left[K - \omega^2 M\right]\hat{x} = 0 \tag{4.6}$$

For a non-trivial solution $(\hat{x} = 0)$, the matrix $K - \omega^2 M$ must be singular and hence

$$\det(K - \omega^2 M) = 0 \tag{4.7}$$

This is an eigenvalue problem, where the square of the angular frequency variable. ω^2 corresponds to the eigenvalues of the pencil. There are as many eigenvalues as degrees of freedom and each one corresponds to a mode of vibration. Eigenvalues provide important information about systems, as discussed in the previous chapter. The eigenvectors $\hat{x}$ in equation (4.6) define the corresponding mode shapes. The smallest ω is the fundamental mode corresponding to the first mode of vibration, the second smallest corresponds to the 2nd mode and so on.

Mode shape analysis: Once the N frequencies are obtained, the mode shapes for each frequency can be derived by solving equation (4.6) in terms of $\hat{x}$. The actual amplitude of vibration cannot be determined because the problem is indeterminate, but the relative displacement of each floor can be obtained. The solution is normalised by making one of the displacements equal to 1 (top floor usually) as in example 4.1. The procedure is repeated for all the frequencies and an N by N matrix is obtained where each column represents the mode shape at each frequency. All elements of the first mode shape have the same sign, the elements of the second mode change sign once, the elements of the third change sign twice and so on, until the last mode shape changes sign every other element (figure 4.3). In mathematical terms each eigenvector defines the mode shape at the frequency corresponding to each eigenvalue. The above argument can be expressed mathematically in the following example.

Example 4.1.

$$\left[K-\omega^2 M\right]\hat{x}=0 \Rightarrow$$

$$\left[K-\omega_i^2 M\right]\cdot\left[\Phi_i\right]=\begin{bmatrix}0\\ \vdots\\ 0\end{bmatrix}$$

where $\Phi_{1i}=1$

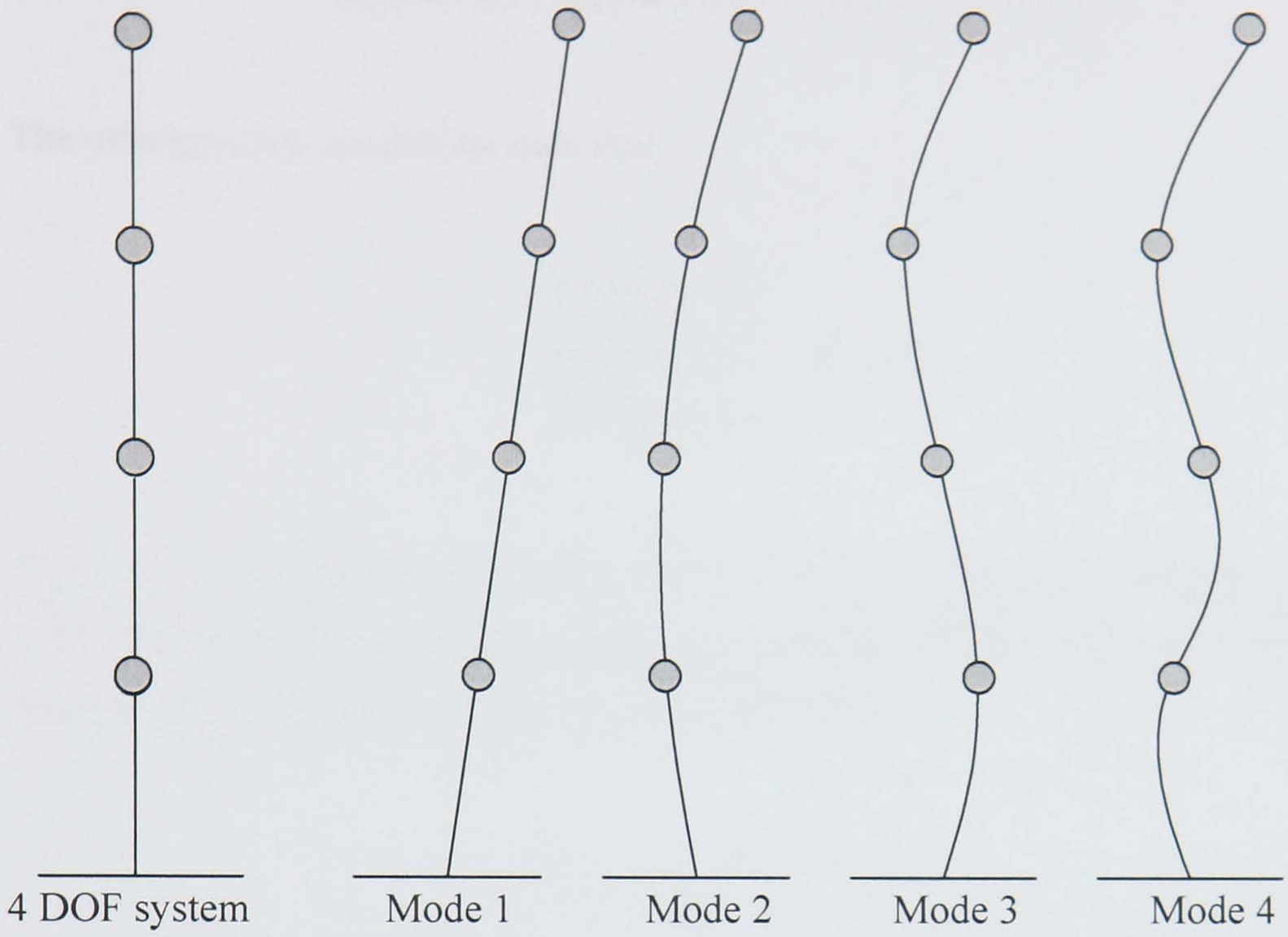

Figure 4.3 Mode shape of a 4 DOF system.

Modal mass contribution: This section outlines the analytical derivations of the dynamic equations needed for modal analysis [Clough and Penzien 1993].

Recall equation (4.1) where, the dynamic equation of motion for a damped systems is:

$$M\ddot{x} + C\dot{x} + Kx = P(t)$$

In order to proceed to modal analysis, the above system of coupled equations needs to be de-coupled. The displacement vector x, in matrix notation is given as:

$$x = \Phi Y = \Phi_1 y_1 + \Phi_2 y_2 + \ldots + \Phi_N y_N = \sum_{n=1}^{N} \Phi_n y_n \qquad (4.8)$$

where Φ is the $N \times N$ mode shape matrix, Y is the vector of generalised displacements, and y_n is the n^{th} modal amplitude. By substituting (4.8) into (4.1) and multiplying by the transpose of the n^{th} mode shape vector Φ_n^T we have:

$$\Phi_n^T M\Phi\ddot{Y}(t)+\Phi_n^T C\Phi\dot{Y}(t)+\Phi_n^T K\Phi Y(t)=\Phi_n^T P(t) \tag{4.9}$$

The orthogonality conditions state that:

$$\begin{aligned}&\Phi_m^T M\Phi_n=0\\&\Phi_m^T K\Phi_n=0 \qquad m\neq n\\&\Phi_m^T C\Phi_n=0\end{aligned} \tag{4.10}$$

The first two conditions for stiffness and mass are derived in [Clough and Penzien 1993] while the third one for damping can be derived similarly. By substituting the orthogonality conditions, equation (4.9) is simplified to:

$$m_n\ddot{y}_n+c_n\dot{y}_n+k_n y_n=p_n(t) \tag{4.11}$$

where m_n, k_n and p_n are the normal coordinates generalised mass, stiffness and load defined and derived in [Clough and Penzien 1993]. c_n is the generalised viscous damping coefficient defined accordingly. The formal definition of these variables is given in the following equation:

$$\begin{aligned}m_n&\equiv\Phi_n^T M\Phi_n\\k_n&\equiv\Phi_n^T K\Phi_n\\c_n&\equiv\Phi_n^T C\Phi_n\\p_n(t)&\equiv\Phi_n^T P(t)\end{aligned} \tag{4.12}$$

Finally, by dividing (4.11) with the generalised mass m_n, the modal equation of motion is expressed as:

$$\ddot{y}_n+2\xi_n\omega_n\dot{y}_n+\omega^2 y_n=\frac{p_n(t)}{m_n} \tag{4.13}$$

where the stiffness and damping terms have been replaced by:

$$k_n = \omega_n^2 m_n \quad \xi_n = \frac{c_n}{2\omega_n m_n} \tag{4.14}$$

The modal viscous damping ratio ξ_n can be determined experimentally. It is convenient to define the damping of a MDOF system using the damping ratio, as is commonly used in civil engineering. In control engineering when state space models are used expressing all terms as matrices, it is more convenient to express the damping in terms of the coefficients of the damping matrix C.

Equation (4.13) is the final dynamic equation of motion which requires the following parameters in order to be solved: m_n, c_n, ω_n, and p_n.

The load vector P is the external load applied on the MDOF system. It can vary with time in amplitude and spatial distribution. In the case of earthquake loading the load distribution varies with time but is assumed to have the same load distribution per DOF. The general form of the load vector can be expressed as:

$$P(t) = Rf(t) \tag{4.15}$$

where R is the load distribution vector, and f is the amplitude function. In the specific case of earthquakes the effective loading vector is taken as:

$$P_{eff} = Mr\ddot{u}_g(t) \tag{4.16}$$

where M is the structure mass matrix, $\ddot{u}_g(t)$ is the earthquake acceleration history applied at the structure's support, and r is a displacement transformation vector that expresses the displacement of each structural degree of freedom due to static application of a unit support displacement.

It is common practice in earthquake engineering to express the seismic input as a fraction of the acceleration of gravity, g:

$$f(t) = \frac{1}{g}\ddot{u}_g(t) \tag{4.17}$$

By substituting equations (4.16) and (4.17) into (4.15) and solving for R, the load distribution factor becomes:

$$R = Mrg \tag{4.18}$$

The displacement transformation vector r for lumped mass models subject to earthquakes is a unit column vector. If equation (4.16) is substituted for the normal coordinate generalised load and mass into equation (4.13), the earthquake loading equation of motion takes its final form:

$$\ddot{y}_n + 2\xi_n\omega_n\dot{y}_n + \omega^2 y_n = \frac{\Phi_n^T Mr}{\Phi_n^T M\Phi_n}\ddot{u}_g(t) \tag{4.19}$$

The coefficient of $\ddot{u}_g(t)$ at the right hand side of the above expression is the modal Participation factor (MPF), i.e.

$$\text{MPF} = \frac{\Phi_n^T Mr}{\Phi_n^T M\Phi_n} \tag{4.20}$$

This function shows the importance of each mode of a lumped mass with N degrees of freedom as a percentage. Thus the sum of all mode contribution factors is equal to one. Most structures are regular, which means that they have similar mass distribution per floor, equal distance per floor and are rigid. In these cases the first mode has a large participation factor compared to the other modes and contributes for most of the earthquake load. Thus, it is acceptable in the preliminary design stage to assume that the building has one mode only as in simplified static analysis. In structural control dampers are normally used to suppress vibration of the fundamental mode since only this contributes for most of the loading. This is not the case for irregular and flexible structures, where the participation factor of the higher modes has a large contribution and all modes need to be taken into account, as can be seen from the solution of equation (4.20).

From the modal mass contribution the "overall" period of the building can be obtained. From the ARS the acceleration (and hence force) for each mode is obtained by multiplying the spectral acceleration corresponding to each period by its modal mass contribution. Finally, the total force on the building is obtained by combining the modes: Several equations can be used for this purpose, the most common being the square root of the sum of squares (SRSS) given by:

$$F = \sqrt{\sum_{i=1}^{N} F_i^2} \tag{4.21}$$

Equivalent lateral force method: This is a simpler design method referred to also as the fundamental mode analysis. Here only the fundamental mode is taken into account and the others are ignored. This is valid only if the modal contribution of the fundamental mode is significantly large. The method is conservative if the spectral acceleration of the fundamental mode is larger than that of the other modes, i.e., the fundament mode period is in the ascending part of the ARS. If the structure has a low period, then the higher modes have a lower period and thus a lower spectral acceleration making the design conservative. If on the other hand the structure has a large fundamental period, larger than the ascending part of the ARS, the higher modes of lower period correspond to larger accelerations. Thus, the spectral accelerations are larger than the designed ones.

4.3 Frame-Pendulum Model Analysis

The simplest form of vibration control is achieved with a tuned mass damper. In its idealised form this consists of a hanging mass from the roof of a building, like a suspended pendulum. The aim of this section is to derive the governing differential equations that describe the motion of the system and also to simulate the model and investigate the response of such a system to earthquake signals. There are generally three possible ways that could help mitigate the earthquake response of such a system. The first one is to increase the energy dissipation by making the pendulum to have a large damping factor which dissipates energy from the system. The second is to minimise the amplitude of the frame vibration due to the pendulum's motion being opposite to the frames. The third method is to move the frequency of the frame (which increases due to the added mass of the pendulum) away from the critical frequency range excited by the earthquake signal. The objective here is to determine if any of the methods can be useful in vibration control problems and, in general, how energy dissipation mechanisms work.

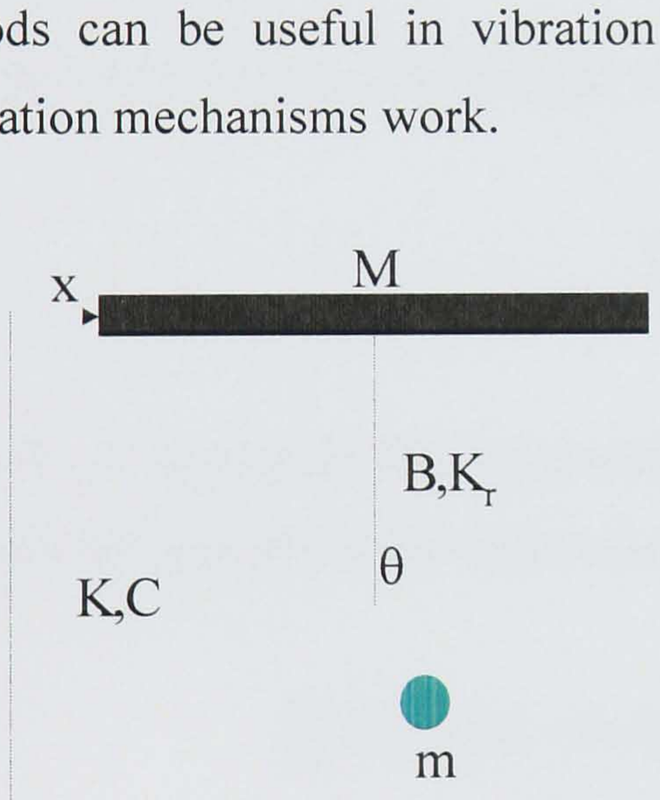

Figure 4.4 Pendulum model

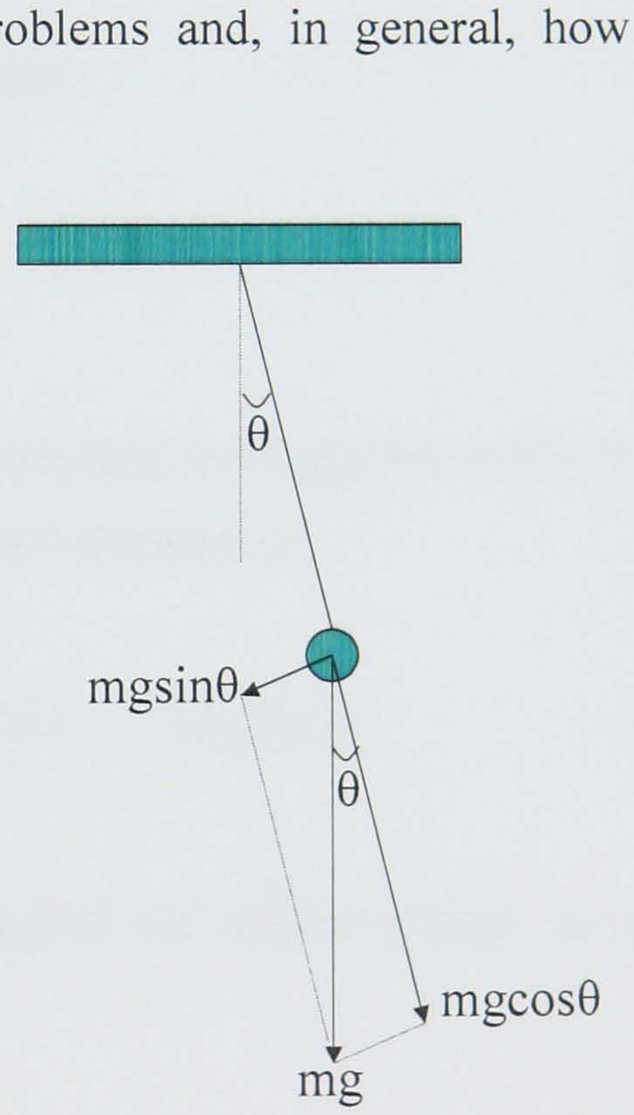

Figure 4.5 Forces on suspended mass

Model: The model consists of a frame with massless columns of horizontal stiffness K and damping C. The frame has mass M, uniformly distributed as a beam on top of the columns. At its centre hangs a massless member of rotational stiffness K_r and frictional damping B, with a mass m attached to it. The beam of mass M moves horizontally,

while the suspended mass m rotates in the plane of the frame and is restricted of any horizontal or vertical movement apart from rotating. The frame is fully fixed to the ground.

4.3.1. Modelling

The system will be modelled in order to find the governing differential equations and then analysed. The variational method will be used [Wellstead 1979]. The modelling steps are as follows:

1. Obtain generalised co-ordinates:

The generalised co-ordinates are chosen as the beam horizontal movement x, and the hanging member rotation θ.

2. Forces in direction of generalised co-ordinates.

$$\sum F_x = F_{EQ} \tag{4.22}$$

where F_{EQ} is any horizontal component of the earthquake force applied on the frame. The moment applied on the suspended mass in the θ direction is:

$$\sum M_\vartheta = M = F \times d = -mg \sin \vartheta \times l = -mgl \sin \vartheta \tag{4.23}$$

Next, the dependence of the kinetic and potential (or strain) energy on the two generalised coordinates needs to be established:

3. Energies: In standard notation these are summarised as:

$$KE_x = \frac{1}{2} M \dot{x}^2$$

$$KE_\theta = \frac{1}{2} m \left(\dot{x}^2 + l^2 \dot{\vartheta}^2 + 2 l \dot{x} \dot{\vartheta} \cos \vartheta \right)$$

$$PE_x = \frac{1}{2}Kx^2$$

$$PE_\vartheta = \frac{1}{2}K_r\vartheta^2$$

4. Total Energy:

$$\begin{aligned} L &= U - T \\ &= KE_x + KE_\theta - PE_x - PE_\theta \\ &= \frac{1}{2}M\dot{x}^2 + \frac{1}{2}m\left(\dot{x}^2 + l^2\dot{\vartheta}^2 + 2l\dot{x}\dot{\vartheta}\cos\vartheta\right) - \frac{1}{2}Kx^2 + \frac{1}{2}K_r\vartheta^2 \end{aligned} \quad (4.24)$$

5. Dissipative energy is:

$$J = \frac{1}{2}C\dot{x}^2 + \frac{1}{2}B\dot{\theta}^2 \quad (4.25)$$

6. Solve the Lagrangians:

$$\begin{aligned} \frac{d}{dt}\left(\frac{\partial L}{\partial \dot{x}}\right) - \frac{\partial L}{\partial x} + \frac{\partial J}{\partial \dot{x}} &= \sum F_x \\ \frac{d}{dt}\left(\frac{\partial L}{\partial \dot{\vartheta}}\right) - \frac{\partial L}{\partial \theta} + \frac{\partial J}{\partial \dot{\theta}} &= \sum M_\theta \end{aligned} \quad (4.26)$$

Here,

$$\frac{\partial J}{\partial \dot{x}} = C\dot{x}$$

$$\frac{\partial L}{\partial x} = -Kx$$

$$\frac{\partial L}{\partial \dot{x}} = M\dot{x} + m\dot{x} + ml\dot{\vartheta}\cos\vartheta$$

$$\frac{d}{dt}\left(\frac{\partial L}{\partial \dot{x}}\right) = M\dot{x} + m\ddot{x} + ml\ddot{\vartheta}\cos\vartheta - ml\dot{\vartheta}^2\sin\vartheta$$

$$\frac{d}{dt}\left(\frac{\partial L}{\partial \dot{x}}\right) - \frac{\partial L}{\partial x} + \frac{\partial J}{\partial \dot{x}} = \sum F_x \Rightarrow M\ddot{x} + m\ddot{x} + ml\ddot{\vartheta}\cos\vartheta - ml\dot{\vartheta}^2\sin\vartheta + Kx + C\dot{x} = F_{EQ} \quad (4.27)$$

$$\frac{\partial J}{\partial \dot{\theta}} = B\dot{\vartheta}$$

$$\frac{\partial L}{\partial \theta} = -ml\dot{x}\dot{\vartheta}\sin\vartheta$$

$$\frac{\partial L}{\partial \dot{\vartheta}} = ml^2\dot{\theta} + 2l\dot{x}\cos\vartheta$$

$$\frac{d}{dt}\left(\frac{\partial L}{\partial \dot{\vartheta}}\right) = ml^2\ddot{\vartheta} + ml\ddot{x}\cos\vartheta - ml\dot{x}\dot{\vartheta}\sin\vartheta$$

$$\frac{d}{dt}\left(\frac{\partial L}{\partial \dot{\vartheta}}\right) - \frac{\partial L}{\partial \theta} + \frac{\partial J}{\partial \dot{\theta}} = \sum M_\theta \Rightarrow ml^2\ddot{\vartheta} + ml\ddot{x}\cos\vartheta + B\dot{\vartheta} + K_r\vartheta = -mgl\sin\vartheta \quad (4.28)$$

From the Lagrangians two coupled equations are obtained. In order to find the state – space model of the system the state variables need to be decided, which are the generalised co-ordinates (x,θ) and their derivatives ($\dot{x}, \dot{\theta}$). The next part is to solve for the second derivative of the generalised co-ordinates ($\ddot{x}, \ddot{\theta}$), from equation (4.27) and (4.28) to obtain:

$$f_1 : \ddot{x} = \frac{ml\cos\theta\left(B\dot{\theta} + K_r\theta + m\lg\sin\theta\right) - ml^2(Kx + C\dot{x} - ml\dot{\theta}\ \sin\theta)}{\left(M+m\right)ml^2 - m^2l^2\cos\theta} + F_{EQ} \quad (4.29)$$

$$f_2 : \ddot{\theta} = \frac{ml\cos\theta(Kx + C\dot{x} - ml\dot{\theta}^2\sin\theta) - (M+m)\left(B\dot{\theta} + K_r\theta + m\lg\sin\theta\right)}{\left(M+m\right)ml^2 - m^2l^2\cos\theta} \quad (4.30)$$

The equations have many non-linear terms and therefore non-linear simulations should be performed. Alternatively the equations can be linearised around an equilibrium point, and linear simulations performed which, however, will be valid only for small amplitude motion around the equilibrium point.

Non-linear simulations

A large class of second-order systems, including spring mass damper models, can be described by differential equations off the form [Slotine and Li 1991]

$$\ddot{x} + f\left(x, \dot{x}\right) = 0 \quad (4.31)$$

Their dynamics in state-space form are represented as:

$$\dot{x}_1 = x_2$$
$$\dot{x}_2 = -f(x_1, x_2)$$

Such a system is non-linear. All physical systems are to a certain extend non-linear and time varying, but for small range motions they can be approximated with their linearised counterpart. For autonomous systems, i.e. time invariant systems, the dynamics can be expanded using Taylor series (Slotine and Li 1991) which in the scalar case is given by:

$$f(a+h) = f(a) + h\left(\frac{\partial f}{\partial x}\right)_{x=a} + \frac{h^2}{2!}\left(\frac{\partial^2 f}{\partial x^2}\right)_{x=a} + \ldots \qquad (4.32)$$

under the assumption that $f(x)$ is continuously differentiable. For a function $f(x)$ depending on vector parameters a and h the Taylor series expansion is of the form:

$$f(a+h) = f(a) + h^T \nabla f(a) + \frac{1}{2!} h^T \nabla^2 f(a) h + \cdots$$

where

$$\nabla f(a) = \left[\frac{\partial f(x)}{\partial x_j}\right]$$

denotes the gradient of $f(x)$ evaluated at $x = a$ and

$$\nabla^2 f(a) = \left[\frac{\partial^2 f(a)}{\partial x_i \partial x_j}\right]$$

is the Hessian matrix of $f(x)$ evaluated at $x = a$.

If a is an equilibrium point then $f(a) = 0$, and by neglecting second order and higher terms, the dynamics matrix at an equilibrium point is given by:

$$A = \left(\frac{\partial f_i}{\partial x_j}\right)_{x=0} \qquad (4.33)$$

In this case, the state–space model having as states the 4 generalised coordinates $x, \dot{x}, \theta, \dot{\theta}$ is:

$$\begin{bmatrix} \dot{x} \\ \ddot{x} \\ \dot{\theta} \\ \ddot{\theta} \end{bmatrix} = \begin{bmatrix} 0 & 1 & 0 & 0 \\ \frac{\partial f_1}{\partial x} & \frac{\partial f_1}{\partial \dot{x}} & \frac{\partial f_1}{\partial \theta} & \frac{\partial f_1}{\partial \dot{\theta}} \\ 0 & 0 & 0 & 1 \\ \frac{\partial f_2}{\partial x} & \frac{\partial f_2}{\partial \dot{x}} & \frac{\partial f_2}{\partial \theta} & \frac{\partial f_2}{\partial \dot{\theta}} \end{bmatrix} \begin{bmatrix} x \\ \dot{x} \\ \theta \\ \dot{\theta} \end{bmatrix} \tag{4.34}$$

where u is zero since no control is needed to maintain the system at its equilibrium position (in the absence of any external interference). Here the origin is an equilibrium point at which the system is at rest. Therefore, calculating all partial derivatives and substituting $(x, \theta, \dot{x}, \dot{\theta})$ with zero, the state-space A matrix is reduced to:

$$A = \begin{bmatrix} 0 & 1 & 0 & 0 \\ -\frac{K}{M} & -\frac{C}{M} & \frac{K_r + m\lg}{Ml} & \frac{B}{Ml} \\ 0 & 0 & 0 & 1 \\ \frac{K}{Ml} & \frac{C}{Ml} & -\frac{(M+m)(K_r + m\lg)}{Mml^2} & -\frac{B}{Mml^2} \end{bmatrix}$$

4.3.2. Frequency analysis

The characteristic frequencies of the two subsystems (frame and pendulum) can be obtained from the eigenvalues of the A matrix. In order to simplify the calculations the rotational stiffness K_r was set to zero, effectively assuming that the pendulum is hanging from a rope, which is a more realistic approach. Note, that even in this simple model the symbolic Matlab toolbox has difficulties to obtain the exact natural frequencies expressions. Here:

$$\omega^2 = -\frac{1}{2}\left(\frac{(m+M)g + Kl \pm \sqrt{[Kl - g(M+m)]^2 + 4Klmg}}{Ml} \right) \tag{4.35}$$

The above expression gives four solutions in pairs, each pair having opposite signs. The two positive solutions correspond to the two natural frequencies of the system. In order for the two subsystems to have the same period, the square root must be zero. Now,

$$\left[Kl - g(M+m)\right]^2 + 4Klmg > 0 \qquad (4.36)$$

since all parameters are positive. Therefore the two subsystems can never have the same period and the two modes of the system are always different. The period of the pendulum is always larger than that of the frame. To investigate numerically the behaviour of the two modes, the following choice of parameters was made so as to make the two frequencies similar (of the same order of magnitude):

Frame parameters		**Pendulum parameters**	
K	$125\ KN$	Kr	0
M	$10\ Kg$	M	$1\ Kg$
C	0	B	$0.5\ Ns/m$
$T_1 = 1.6s$	$T_2 = 2.2s$	L	$1\ m$

Table 4.1

The period of the building as a function of the pendulum mass and length is shown below:

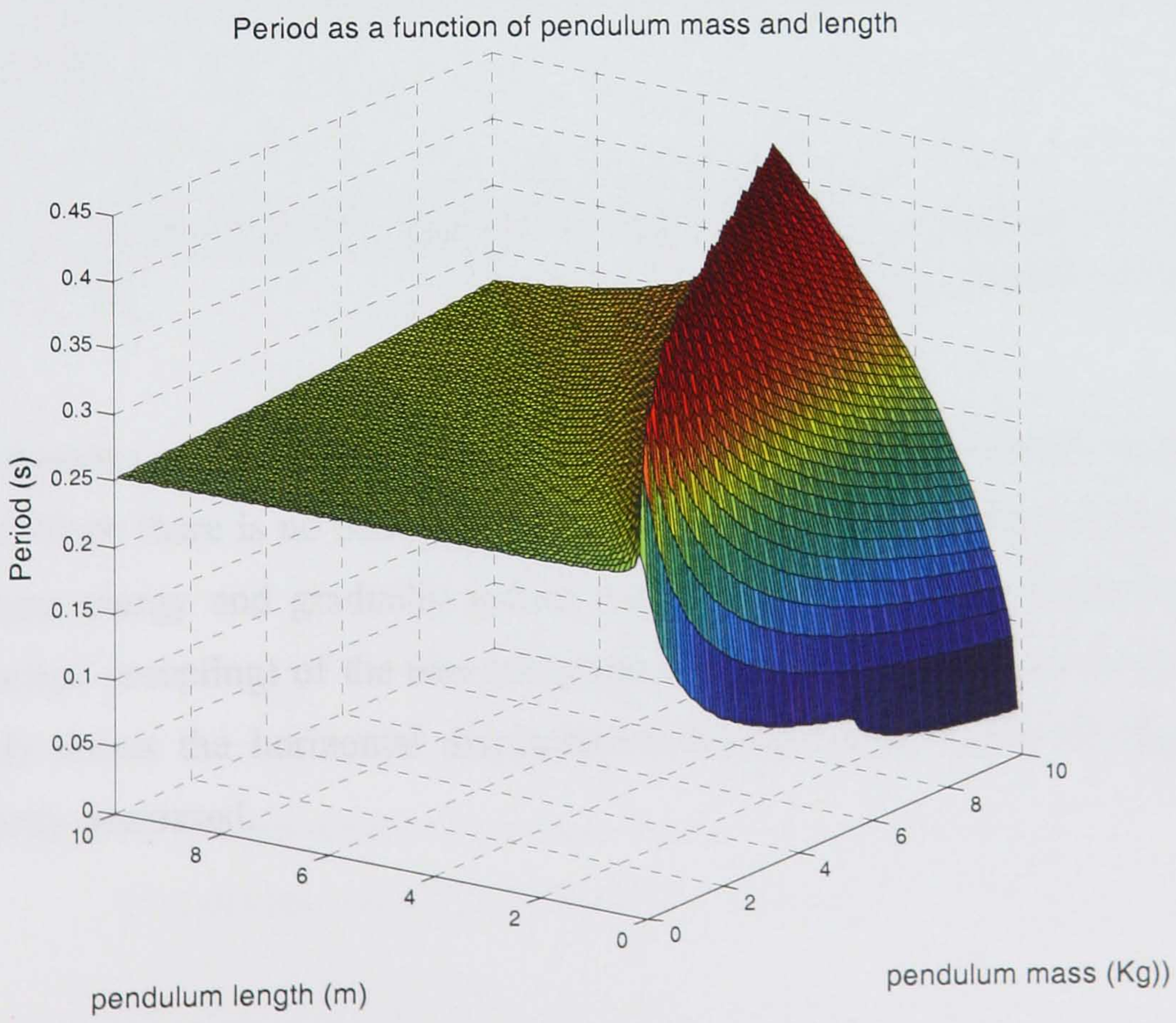

Figure 4.6.a) Period (of frame) as a function of m and l

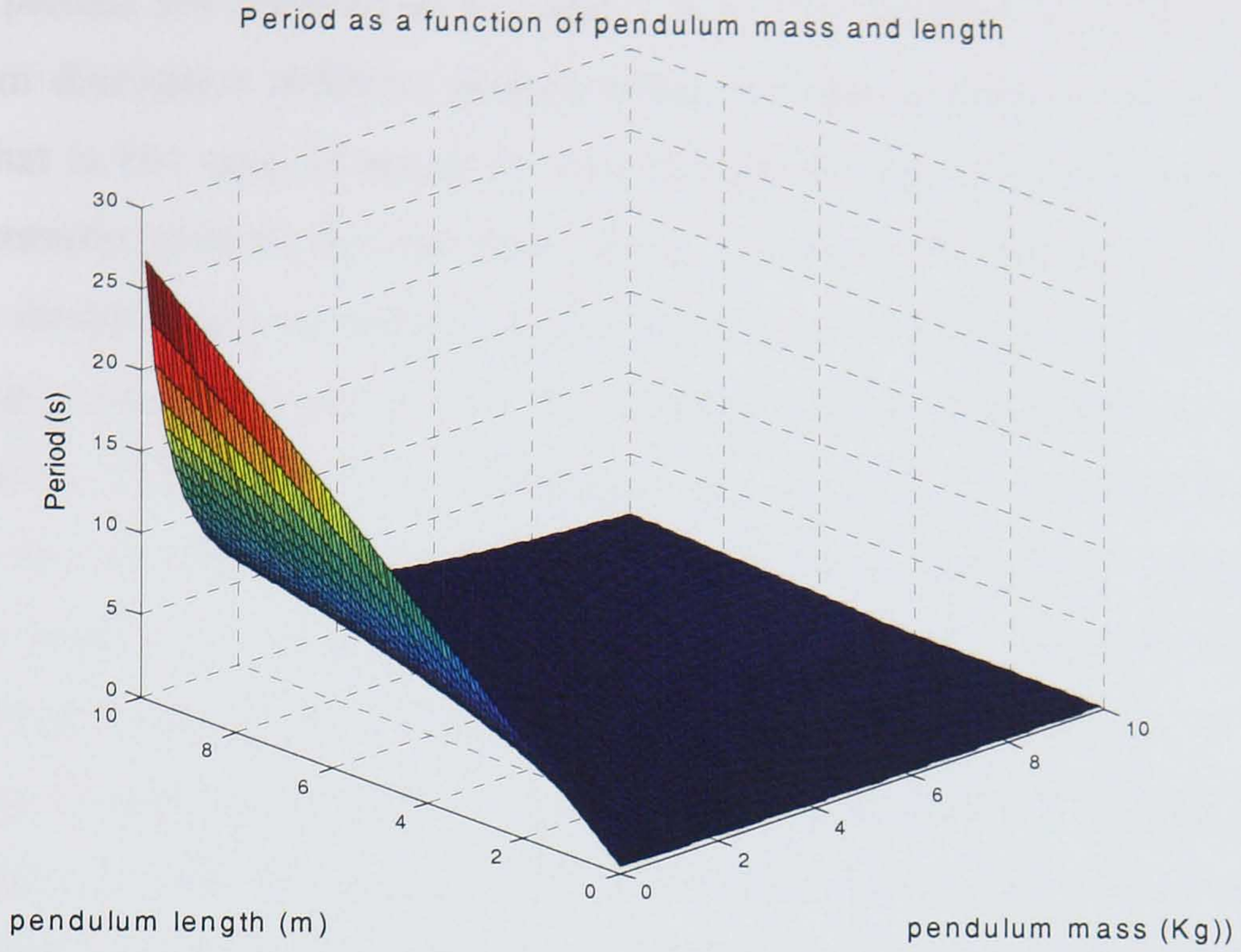

Figure 4.6.b) Period (of pendulum) as a function of m and l

4.3.3. Effect of pendulum's parameters to system damping

To simulate the system's behaviour the periods are chosen to be as close as possible, by choosing the following structural parameters. The period of the frame-pendulum system depends on

$$\omega^2 = \frac{1}{2}\left(\frac{(m+M)g + Kl \pm \sqrt{[Kl - g(M+m)]^2 + 4Klmg}}{Ml}\right) \Rightarrow \begin{matrix} \omega_1 = 3.9 rad/s \Rightarrow T_1 = 1.6s \\ \omega_2 = 2.9 rad/s \Rightarrow T_2 = 2.2s \end{matrix}$$

The response of the system is calculated after a unit displacement is applied to the frame. Since there is no damping from the frame the system relies on the pendulum to dissipate energy and gradually reduce the displacements. This is achieved from the interaction (coupling) of the two subsystems. Figure 4.7 (pendulum dissipation similar period) shows the horizontal displacement of the frame where the displacement is gradually decreased.

Next, the period of the two modes is examined. The pendulum length was set to 10 m and the periods are obtained as 4 *s*. and 1.26 *s*. The response is shown in figure (4.7-pendulum dissipation different period) where the displacement is almost steady. This means that in this case (in which the two periods are very different) there is very little energy transfer between the two sub-systems, and thus very limited energy dissipation. When a similar value of damping-factor coefficient is assumed for the frame and the pendulum's damping is set to zero, the amplitude of the displacement is reduced even more slowly (figure 4.7-frame dissipation similar period) indicating that it is more efficient in this case to add damping by means of the pendulum rather than to the structure itself as the coupling between the two systems is asymmetric. Also, damping on the frame is not related to the period of the two subsystems. Figure (4.8) shows the Bode plots (magnitude frequency responses) for the four cases (dissipation on the frame with similar periods, dissipation on the frame with different periods, on the pendulum with similar mode periods and on the pendulum with different mode periods). The main conclusions of the previous analysis are supported from these four frequency responses.

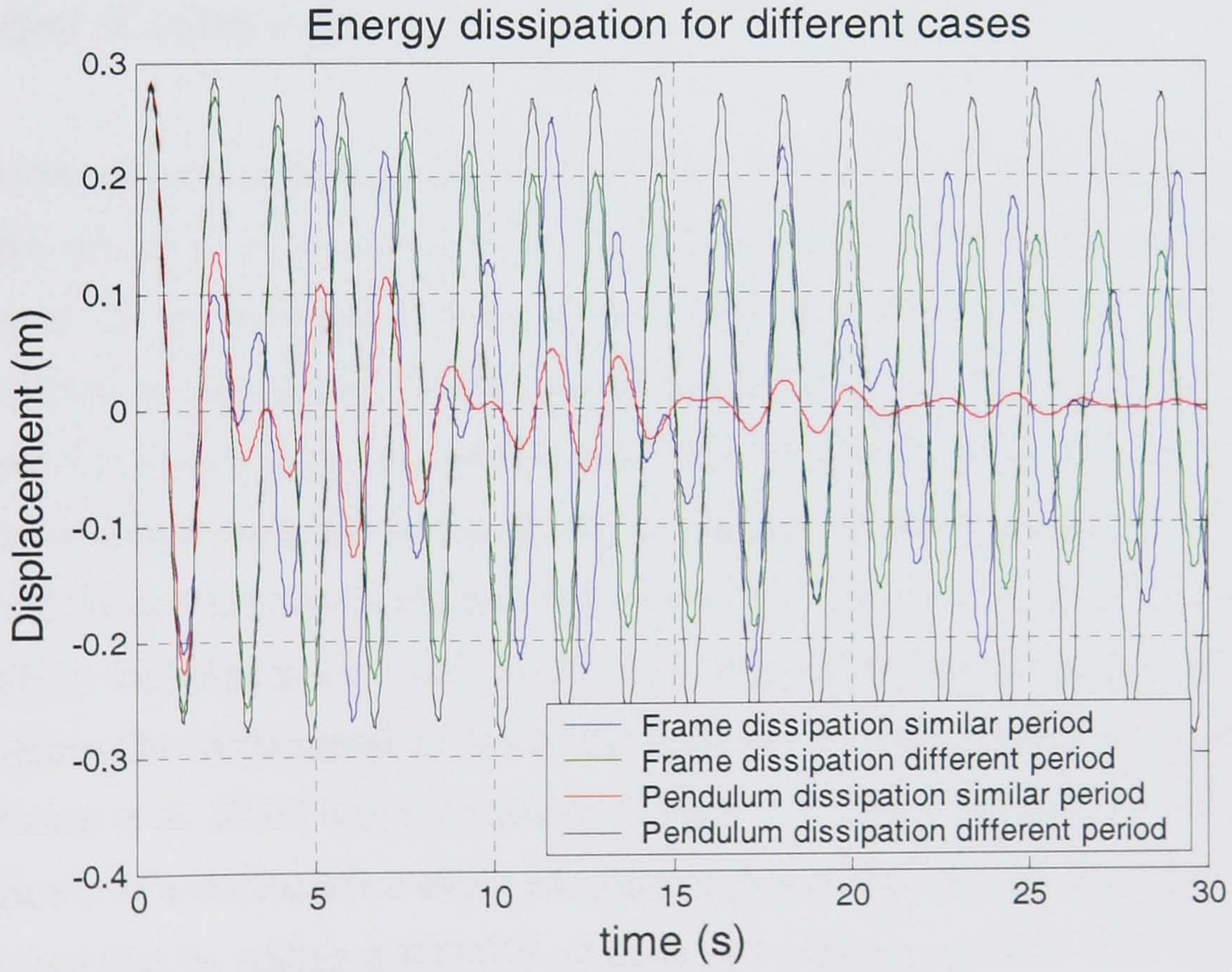

Figure 4.7 Displacement when frame and pendulum have similar and different frequencies, when damping occurs in the frame or the pendulum

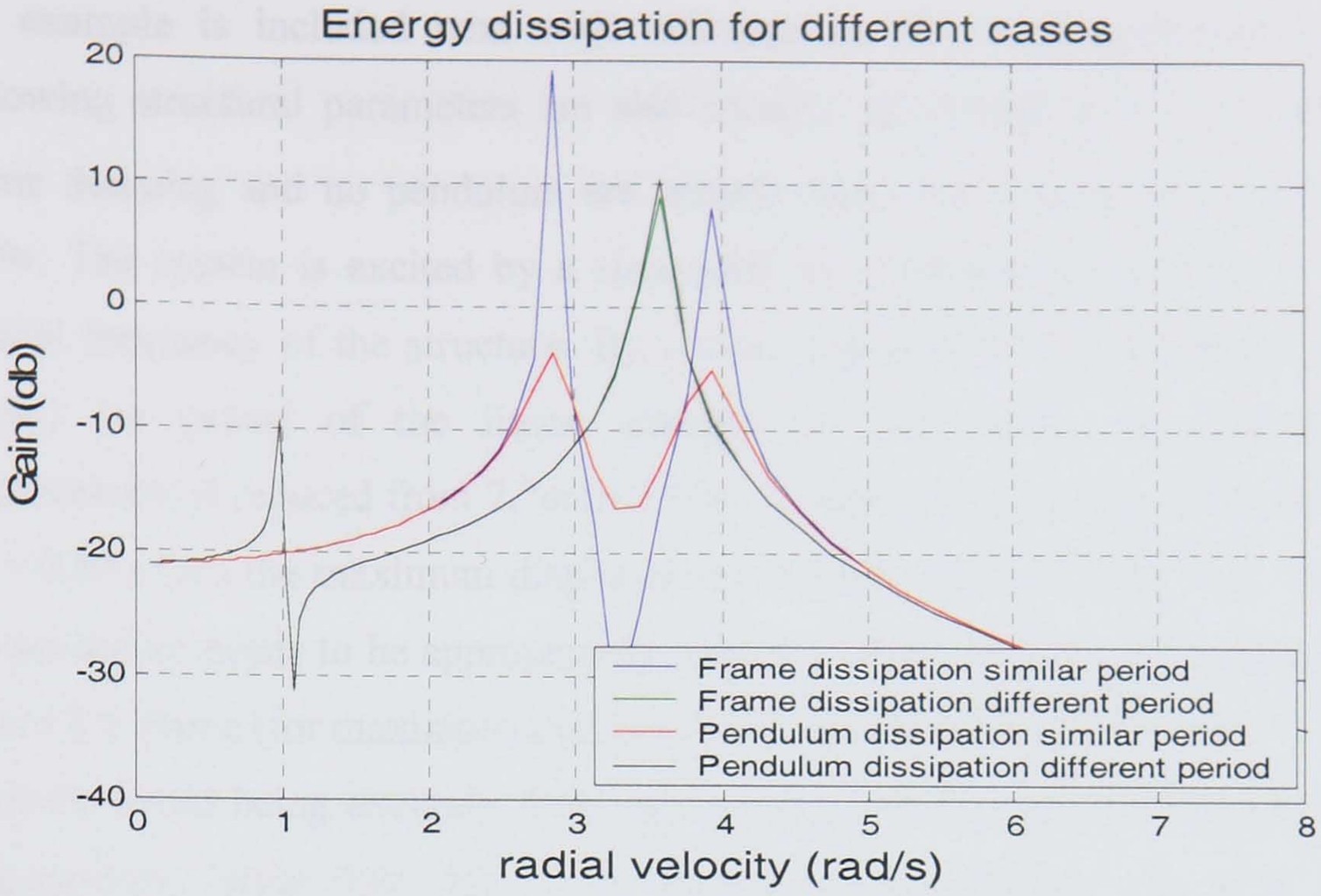

Figure 4.8. Frequency responses when frame and pendulum have similar and different frequencies, when damping occurs in the frame or the pendulum

4.3.4. Effect of pendulum's parameters in shifting the structure's period of oscillation.

Another effect of using a pendulum or a tuned mass damper is to increase the total mass which results in an increase of the period of the system. Depending on the frequency content of the earthquake acceleration signal, this may result in lower levels of excitation of the system's modes and hence lower amplitudes of displacement. The shape of a typical earthquake spectrum or ARS is shown in figure 4.2. If a structure has a period longer than that corresponding to the peak of the spectrum, by increasing the period the acceleration on the building is reduced. This is common practise when base-isolation techniques are used. Apart from minimising accelerations, base isolation increases the fundamental period of the building. A similar study was undertaken by [Johnson et al. 2003] where the use of rooftop tuned mass dampers, i.e. a TMD placed at the top of a structure was explored, without considering the effects of damping. It was reported that by adding a RTMDF of mass and stiffness equal to $1/20^{th}$ of that of the building, the period is increased by approximately 12%.

An example is included next with reference to the frame-pendulum system. The following structural parameters are also chosen: $M = 10Kg$ and $K = 125N/m$. Zero frame damping and no pendulum are initially assumed. The period of this system is $1.79s$. The system is excited by a sinusoidal input having a frequency similar to the natural frequency of the structure. By adding a pendulum of mass $1Kg$ ($1/10^{th}$ of the frame) the period of the frame changes to $1.59s$ while the maximum output displacement is reduced from $7.7m$ to $0.37m$. If some damping is added to the pendulum ($C = 0.5Ns/m$) the maximum displacement is further reduced to $0.33m$. The length of the pendulum needs to be appropriately chosen so that the pendulum's mode is close to that of the frame (for maximum energy dissipation) and different to the frequency of the input (to avoid being excited). This method is valid only for structures with relatively long periods, larger than that of the excitation, for otherwise the opposite result is achieved (see section 4.2.4 about Equivalent lateral force method). This is not a problem in practice because usually passive control systems are added to tall flexible structures that normally have long periods. With the addition of the pendulum, the angular frequency of the system changes from 3.5 to 3.9 *rads/s* which is an increase of 11%, while the total mass increases by 10%. It is difficult to calculate the exact period change, because equation (4.35) is non-linear and hence the steady-state response is not a sinusoid at the input frequency (as in the linear case), although linearisation techniques applicable to small amplitude oscillations can be used.

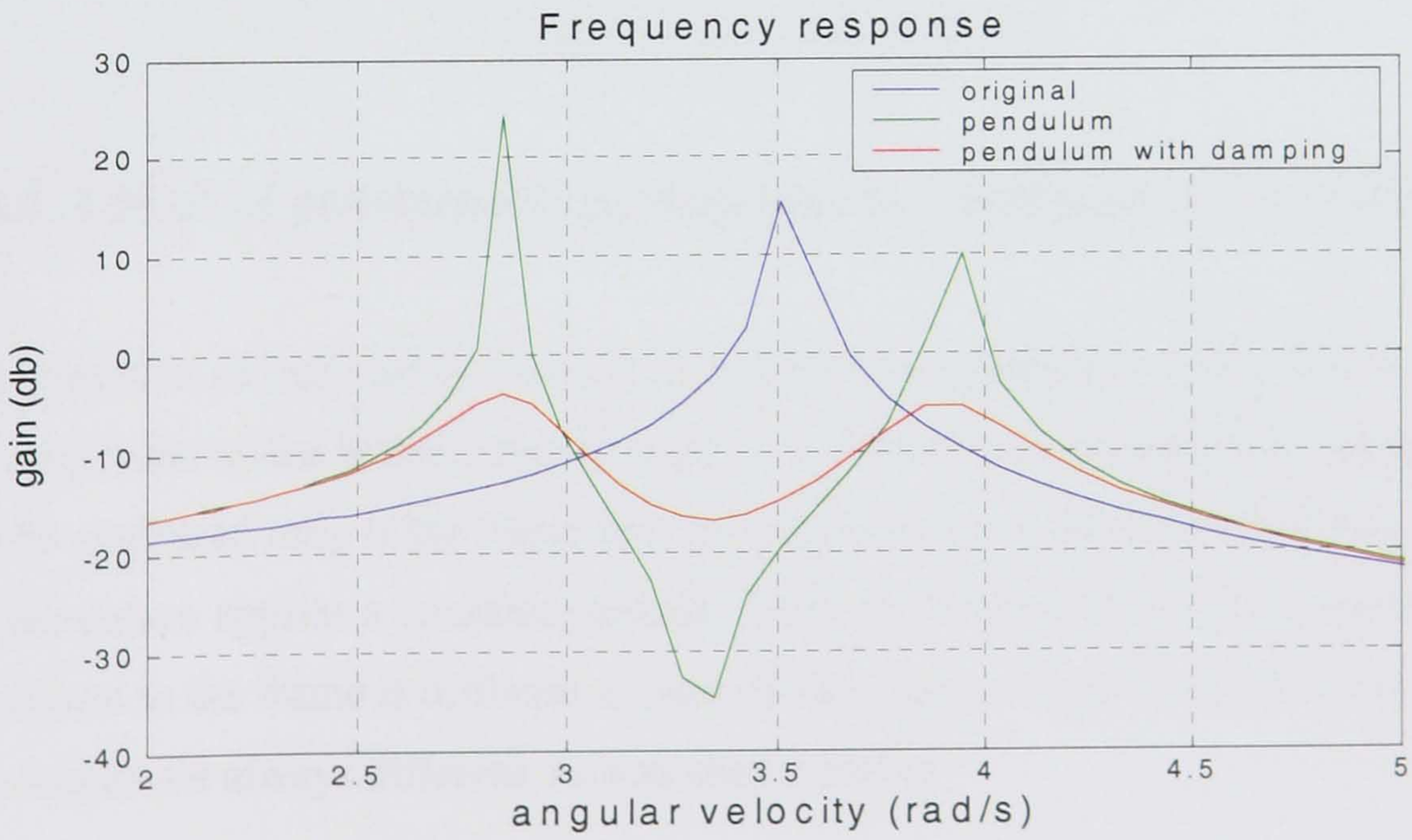

Figure 4.9 Frequency responses for system: frame, frame with pendulum and frame with pendulum and damping.

Maximum response for different arrangements	
Method	Maximum displacement
Frame, no pendulum	7.7 *m*
Pendulum, no damping	0.37 *m*
Pendulum and damping	0.33 *m*

Table 4.2

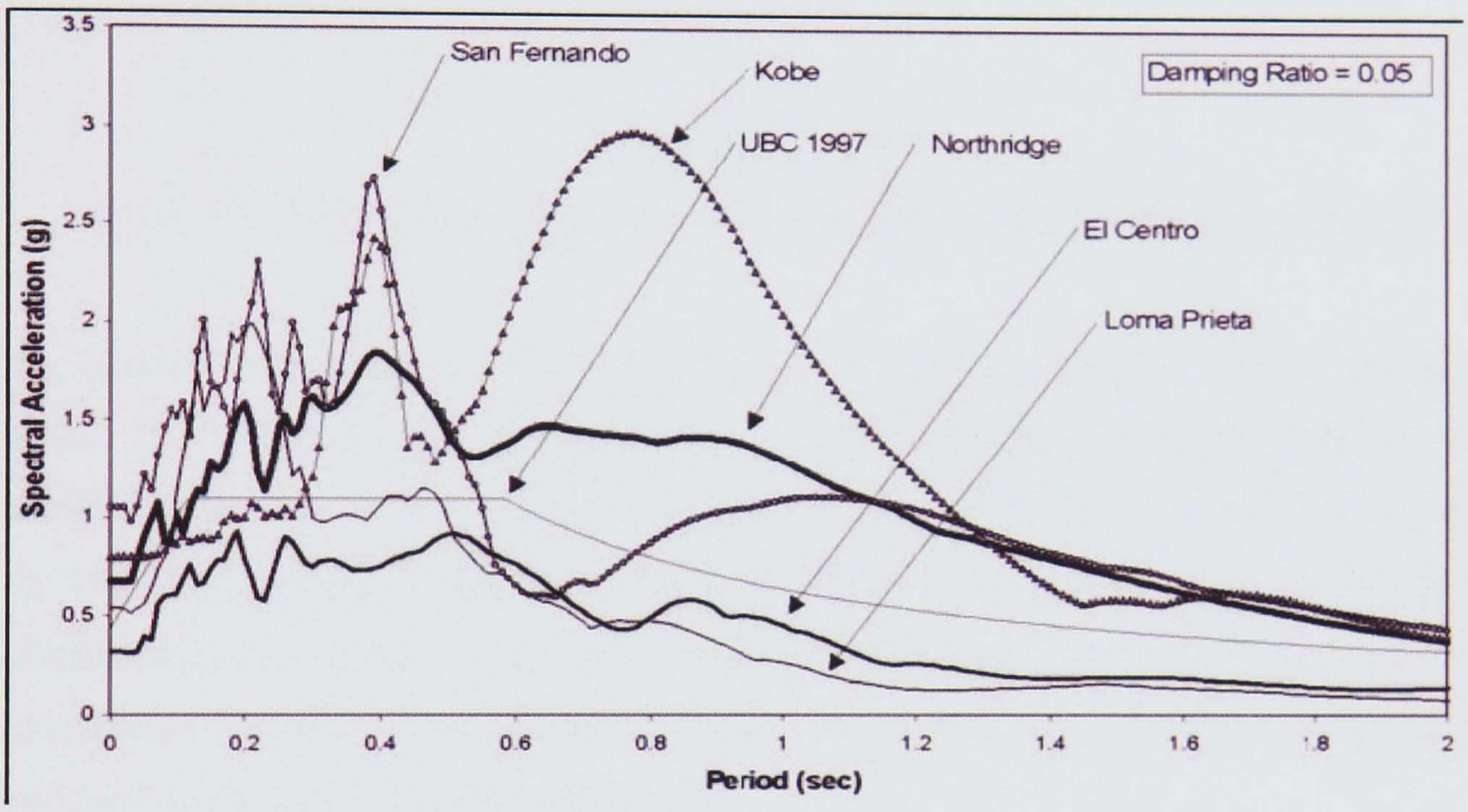

Figure 4.10 Acceleration response spectra of various earthquakes

Source:[_Johnson et al. 2003]

4.3.5. Effect of pendulum's parameters to amplitude of oscillations

The objective of this part is to establish whether the pendulum motion has an effect on the amplitude of the frame's displacements, in the absence of pendulum damping. This can be evaluated only if the frame and the pendulum have the same frequency such that the pendulum applies a constant opposite force (for otherwise the force exerted by the pendulum to the frame is different at each cycle). However this is not possible, since the two modes are always different, as was shown earlier.

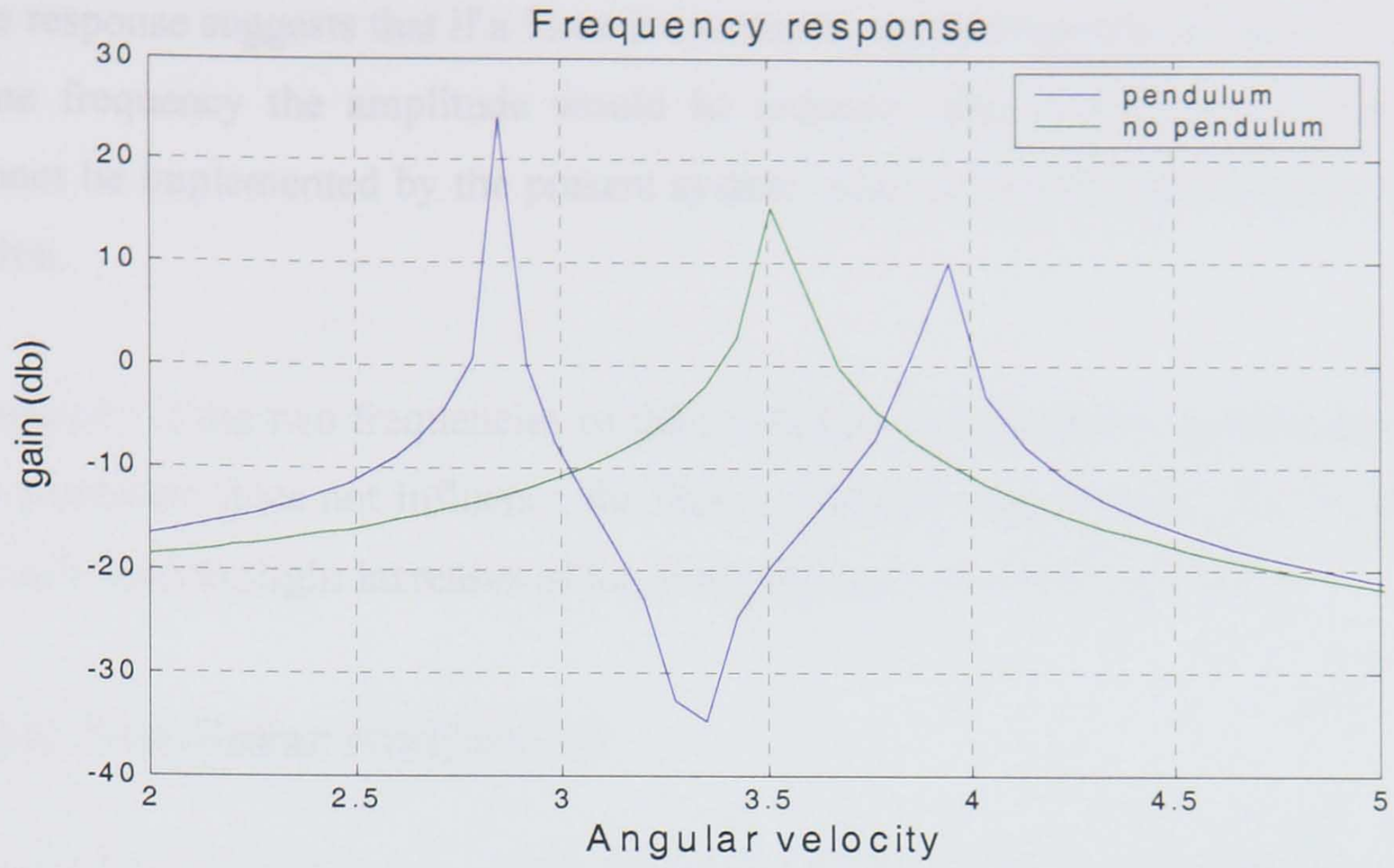

Figure 4.11 Frequency responses frame with and without undamped pendulum

By adding the pendulum to the system a new mode is produced at lower frequency, while the frame's frequency is increased due to the added mass. From this graph it is not clear if the pendulum has a positive effect or not. Its main effect is to change the modes by keeping the gain at similar levels. If the input is an impulse then the maximum displacement is exactly the same as without the pendulum (figure 4.12). However, the amplitude of the frame's displacement is not constant and thus the RMS displacement is reduced by the presence of the pendulum.

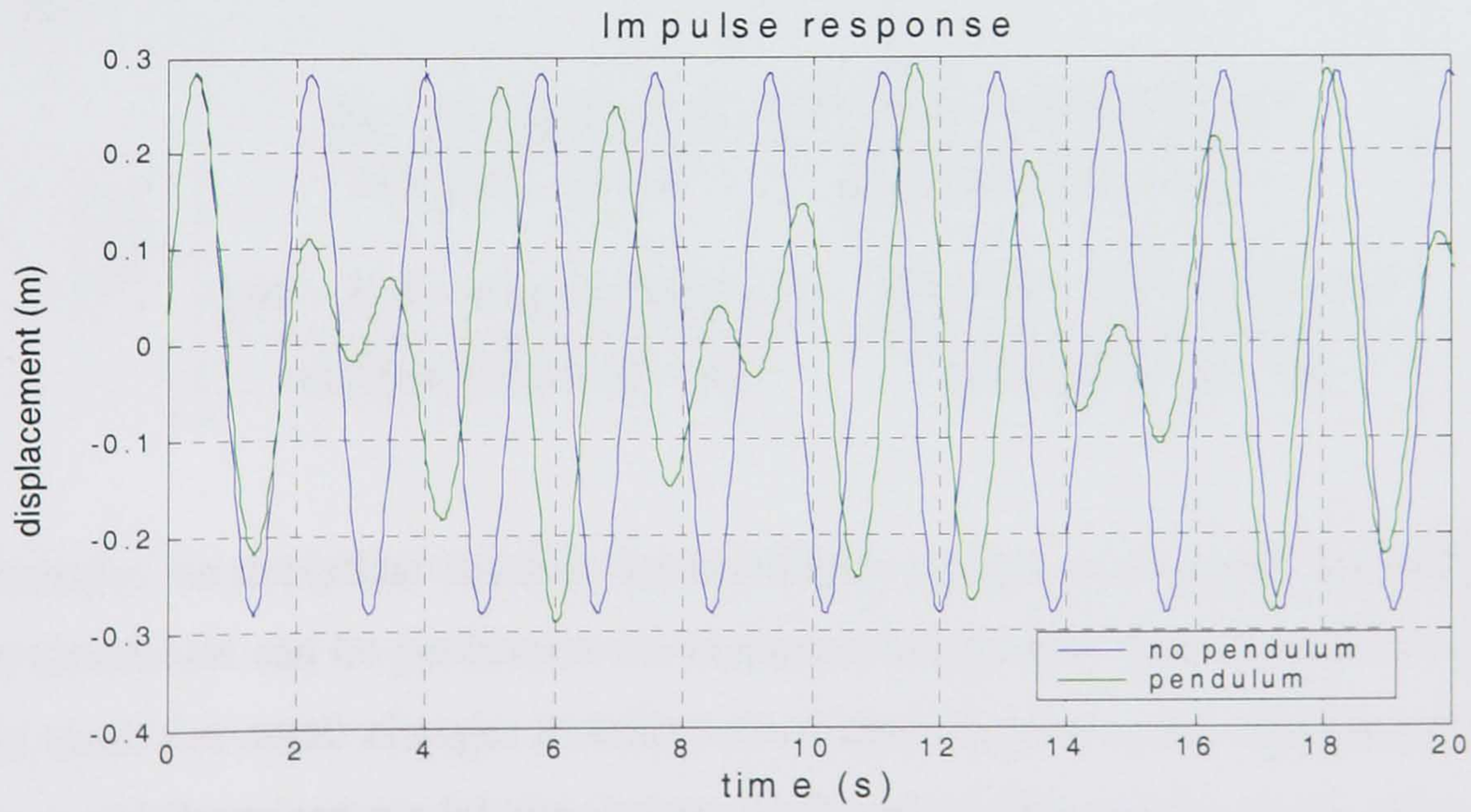

Figure 4.12 Displacement of frame with and without undamped pendulum

The response suggests that if a force is constantly applied opposite to the structure at the same frequency the amplitude would be reduced. This is a forced vibration which cannot be implemented by the present system. Such a control system would need to be active.

Obviously if the two frequencies of the pendulum and frame are significantly different the pendulum does not influence the frame amplitude significantly, and in fact it may actually lead to slight increases of the peak displacements at some times.

4.3.6. Non-linear simulations

For the frame-pendulum system the non-linear state space model is of the form:

$$M(\theta)\begin{bmatrix}\ddot{x}\\ \ddot{\theta}\end{bmatrix}+K(x,\dot{x},\theta,\dot{\theta})=0$$

where

$$M(\theta)=\begin{bmatrix}M+m & ml\cos\theta\\ ml\cos\theta & ml^2\end{bmatrix}$$

and

$$K(x,\dot{x},\theta,\dot{\theta})=\begin{bmatrix}Kx+C\dot{x}-ml\dot{\theta}^2\sin\theta\\ B\dot{\theta}+K_r\theta+ml\,\mathrm{g}\sin\theta\end{bmatrix}$$

So that

$$\begin{bmatrix}\ddot{x}\\ \ddot{\theta}\end{bmatrix}=\begin{bmatrix}\dfrac{Kx+C\dot{x}-ml\dot{\theta}^2\sin\theta}{m\cos^2\theta-M-m}-\dfrac{\left(B\dot{\theta}+K_r\theta+m\lg\sin\theta\right)\cos\theta}{L\left(m\cos^2\theta-M-m\right)}\\ \dfrac{\left(B\dot{\theta}+K_r\theta+m\lg\sin\theta\right)(M+m)}{mL^2\left(m\cos^2\theta-M-m\right)}-\dfrac{\left(Kx+C\dot{x}-ml\dot{\theta}^2\sin\theta\right)\cos\theta}{L\left(m\cos^2\theta-M-m\right)}\end{bmatrix}$$

Normally, no analytical solution for non-linear models exists (apart for simple cases) but simulation can be performed via numerical integration. Here Simulink's *s-function* was used. For small changes in initial conditions (relative to the equilibrium) the non-linear and linearised-model simulations produced similar results, which shows that the linearisation method is accurate, even for relatively large angles (figures 4.13 and 4.14).

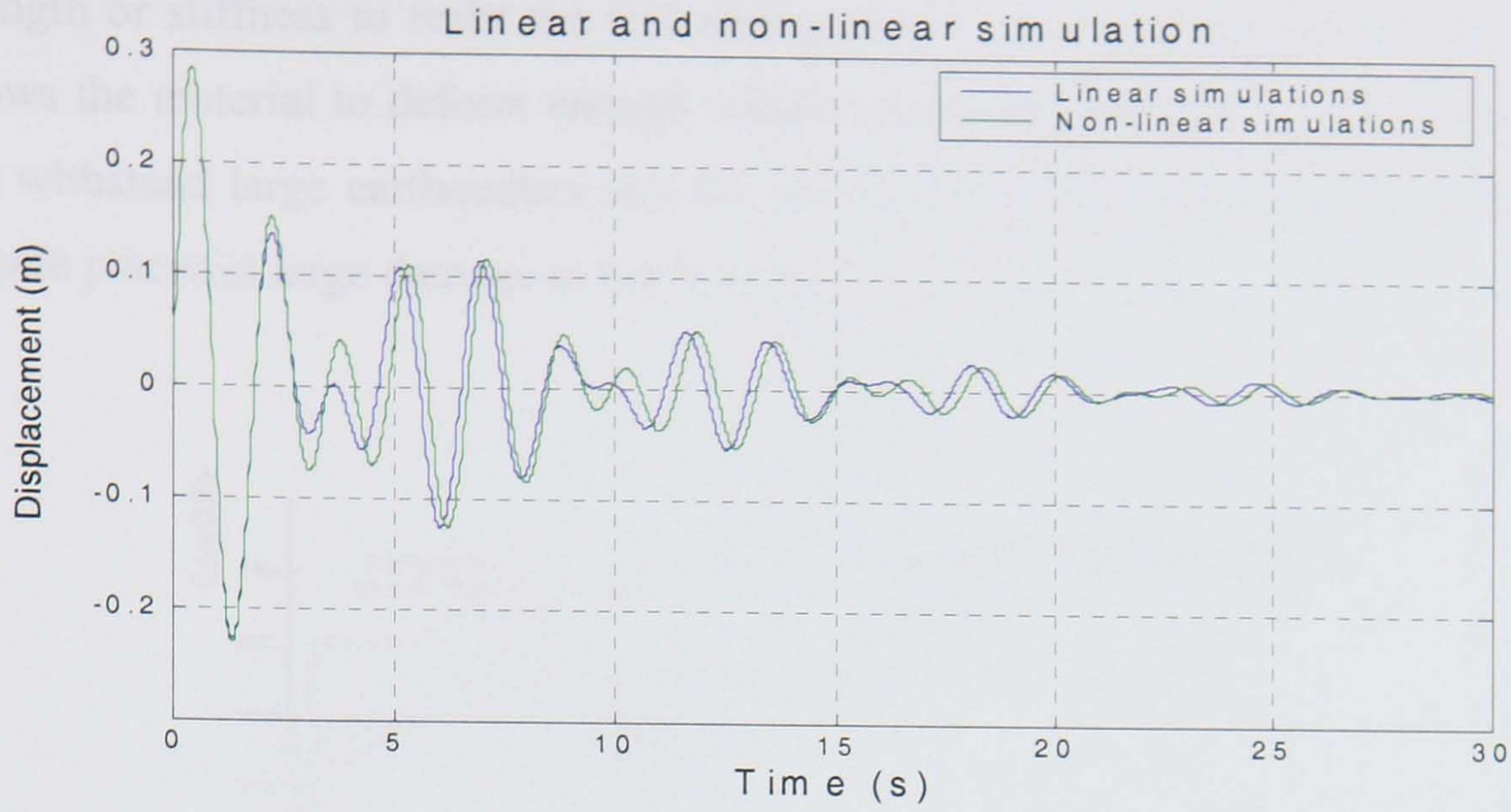

Figure 4.13. Frame displacement, linear and non-linear simulations

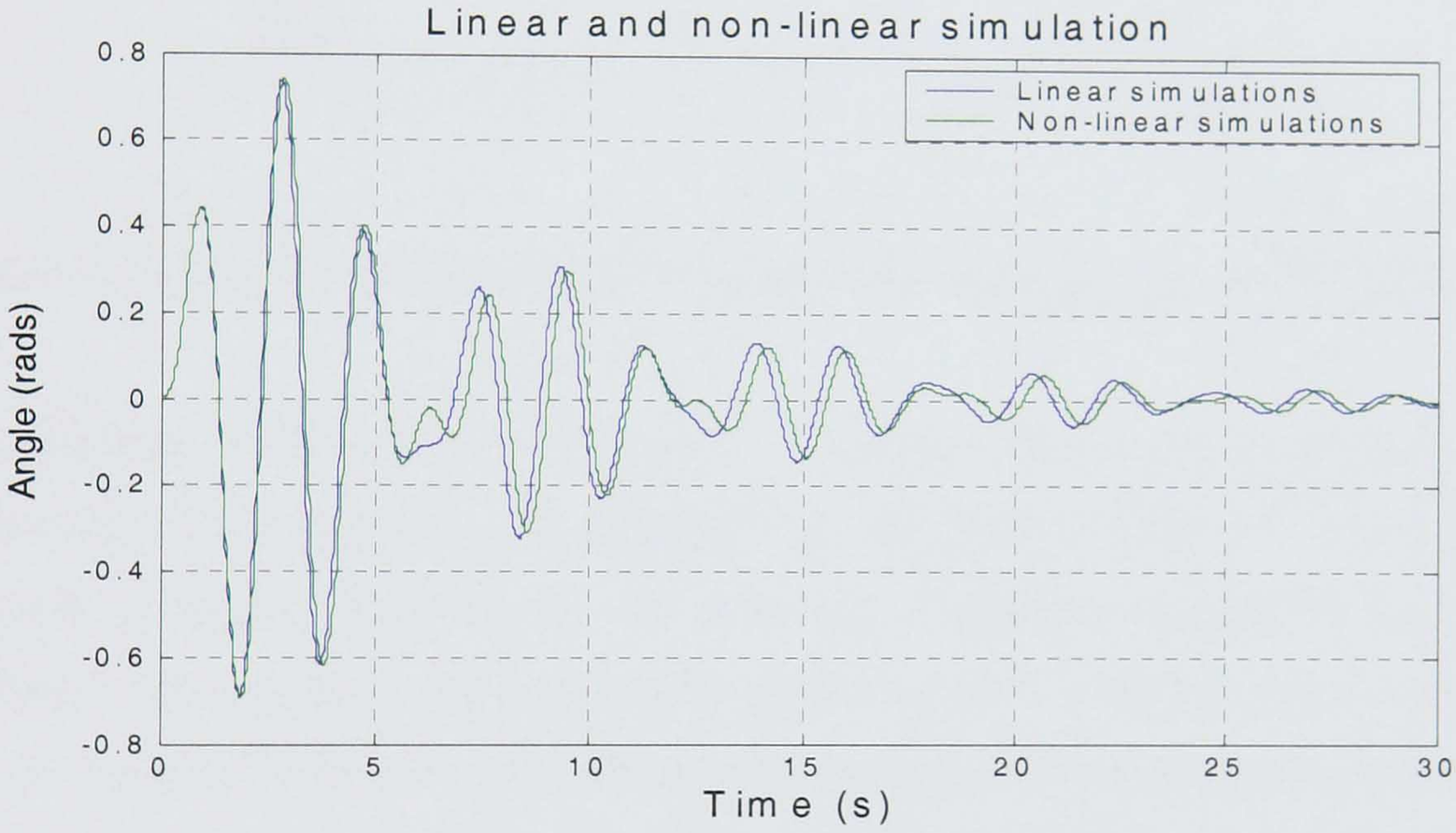

Figure 4.14. Pendulum angle, linear and non-linear simulations

4.4. Inelastic behaviour

During strong earthquakes structures experience large inelastic deformations. The behaviour of materials during these inelastic deformations is non-linear. Current seismic design relies on this behaviour to protect structures against collapse. The materials used have a large deformation capacity to allow for effective energy dissipation and to absorb the majority of the earthquake load (figure 4.1). This is the main philosophy behind current methods of design against earthquakes. A building may not have enough

strength or stiffness to resist the full earthquake but can have enough ductility, which allows the material to deform enough without breaking. The result is that the structure can withstand large earthquakes and the building's function and integrity is preserved despite potential large damage to the structure.

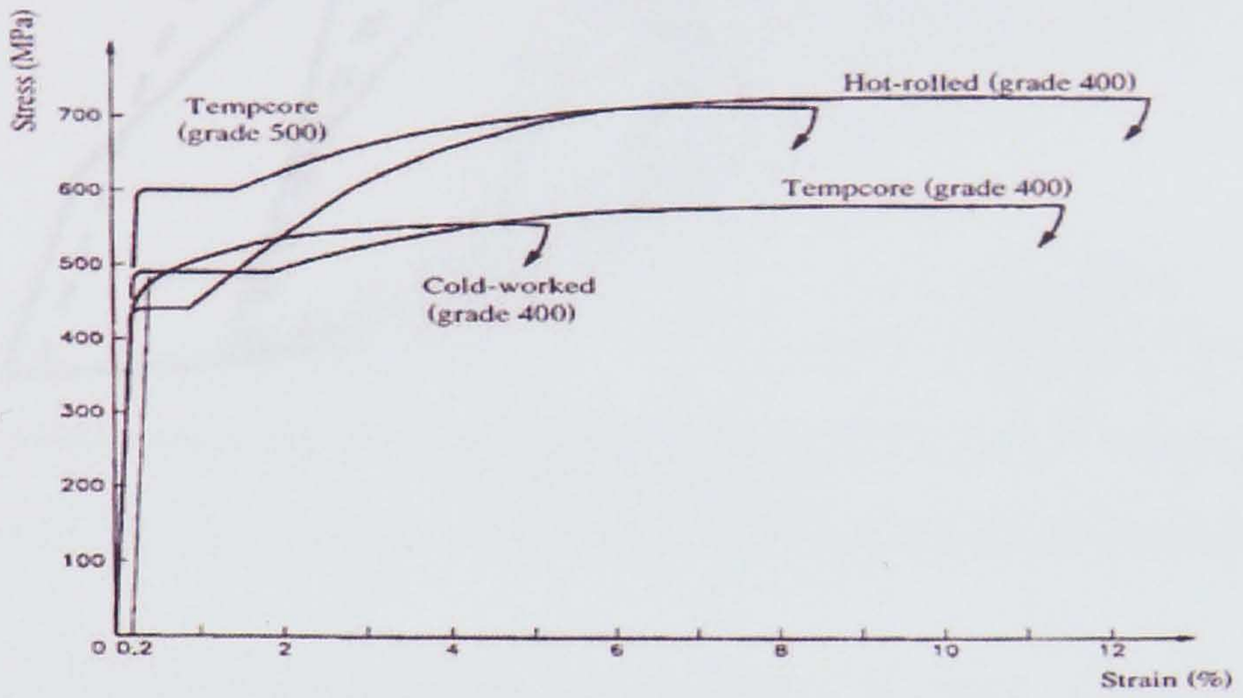

Figure 4.15 Typical diagrams of high-strength reinforcement bars: Source [Pinho 2001]

The response of elastic structures is linear. This is not the case when structures behave inelastically. The behaviour of structures in the inelastic region is non-linear and difficult to model. Entering the inelastic region changes significant the effective stiffness of the structure, and thus also its period and its overall response to earthquakes. This is usual in the favour of the structure since longer period structures tend to have a lower spectral acceleration (figures 4.10 and 4.2). Furthermore, during an earthquake there is cyclic loading (figure 4.16), i.e. loading of the structure on one side and immediate unloading and re-loading on the opposite side. This is of insignificant when a material is in the elastic range. During inelastic behaviour there is gradual strength and stiffness degradation. This results in further structural period change and makes the material even weaker and more susceptible to the earthquake load.

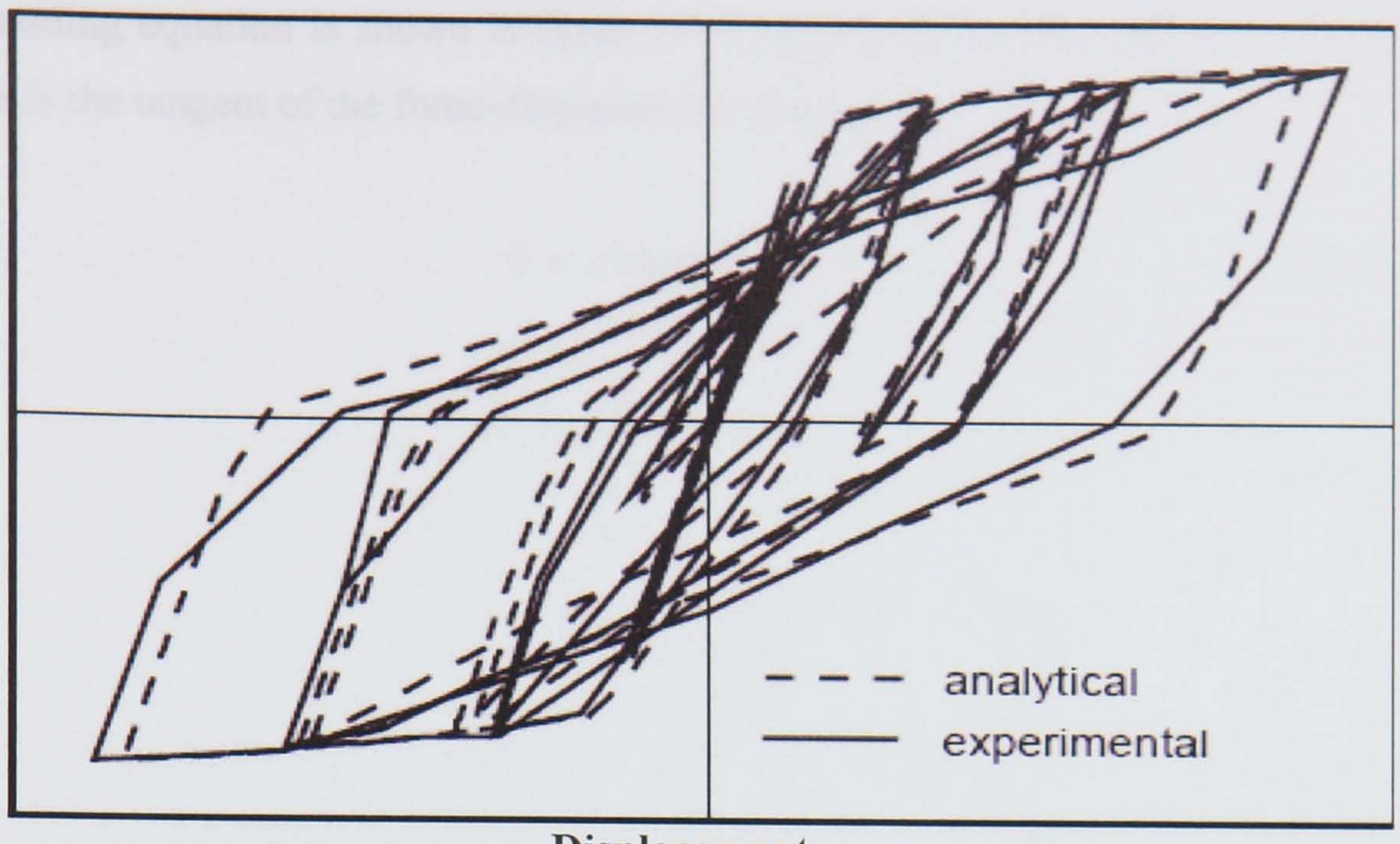

Figure 4.16 Force-displacement hysteretic graph under cyclic loading

In structural control the effects of cyclic loading and inelastic behaviour play an even more important role since specific modes are being targeted. If the period of these modes changes the (modal) controller will be less effective. This effect has been neglected so far in structural control literature. This may be because during moderate earthquakes and large winds structures are not supposed to enter the inelastic range. In active control the controllers are prevented from functioning during large earthquakes, in order not to have a negative effect and destabilise the system [Koshika et al. 1996]. This choice of not turning the controller on is usually not possible especially in passive systems where the controller is a part of the structure. Here the behaviour of the frame-pendulum system when the material follows a non-linear force-displacement pattern is investigated.

Choice of P-δ graph: Previous work in this area was presented by Yang in papers including [Wong and Yang 2003] where an active controller using the instantaneous optimal control algorithm was designed. The force analogy method was used where there is inelastic deformation but no stiffness degradation. Here the effect of stiffness change is included but not the effect of cyclic loading and stiffness degradation. There is no unique acceptable shape of an inelastic force displacement graph. An idealised graph was given by [Erberik and Sucuoglou 2004] shown in figure 4.17. Here, a simpler shape is assumed where the stiffness is a function of the displacement, and the force is always zero when the displacement is zero (and vice versa). The shape and

corresponding equation is shown is figure (4.18) and is given by equation (4.37). The stiffness is the tangent of the force-displacement graph:

$$F = A\tanh(Bx) \tag{4.37}$$

where

$$A \cdot B = K = 125N/m$$

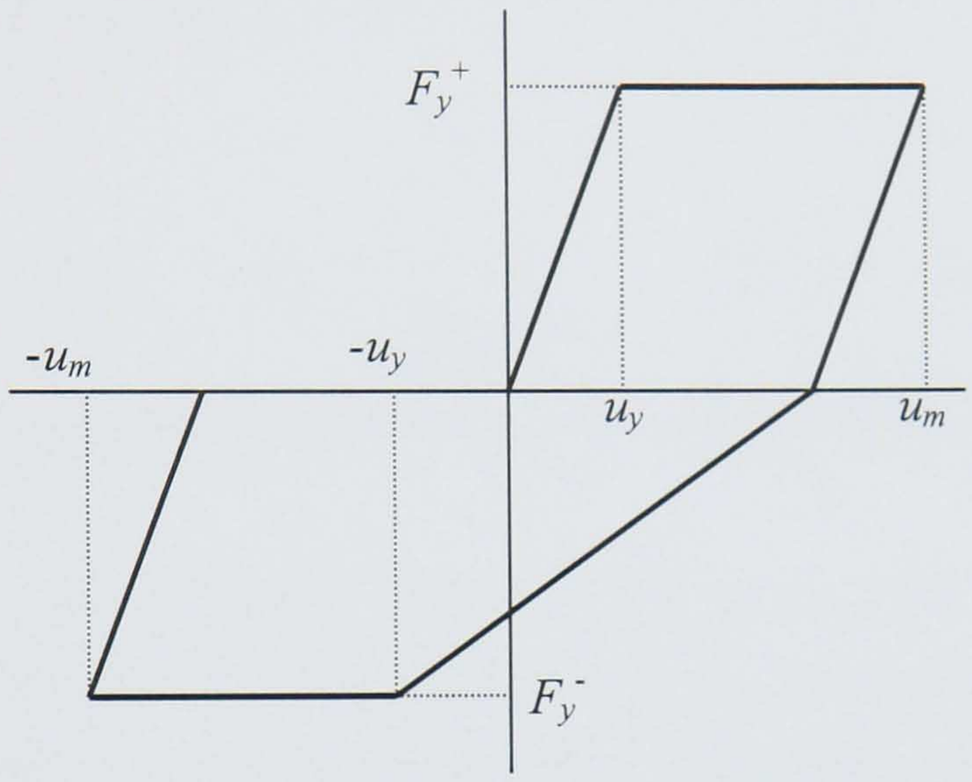

Figure 4.17 Geometric description of the idealised first cycle by Erberik and Sucuoglou (2004)

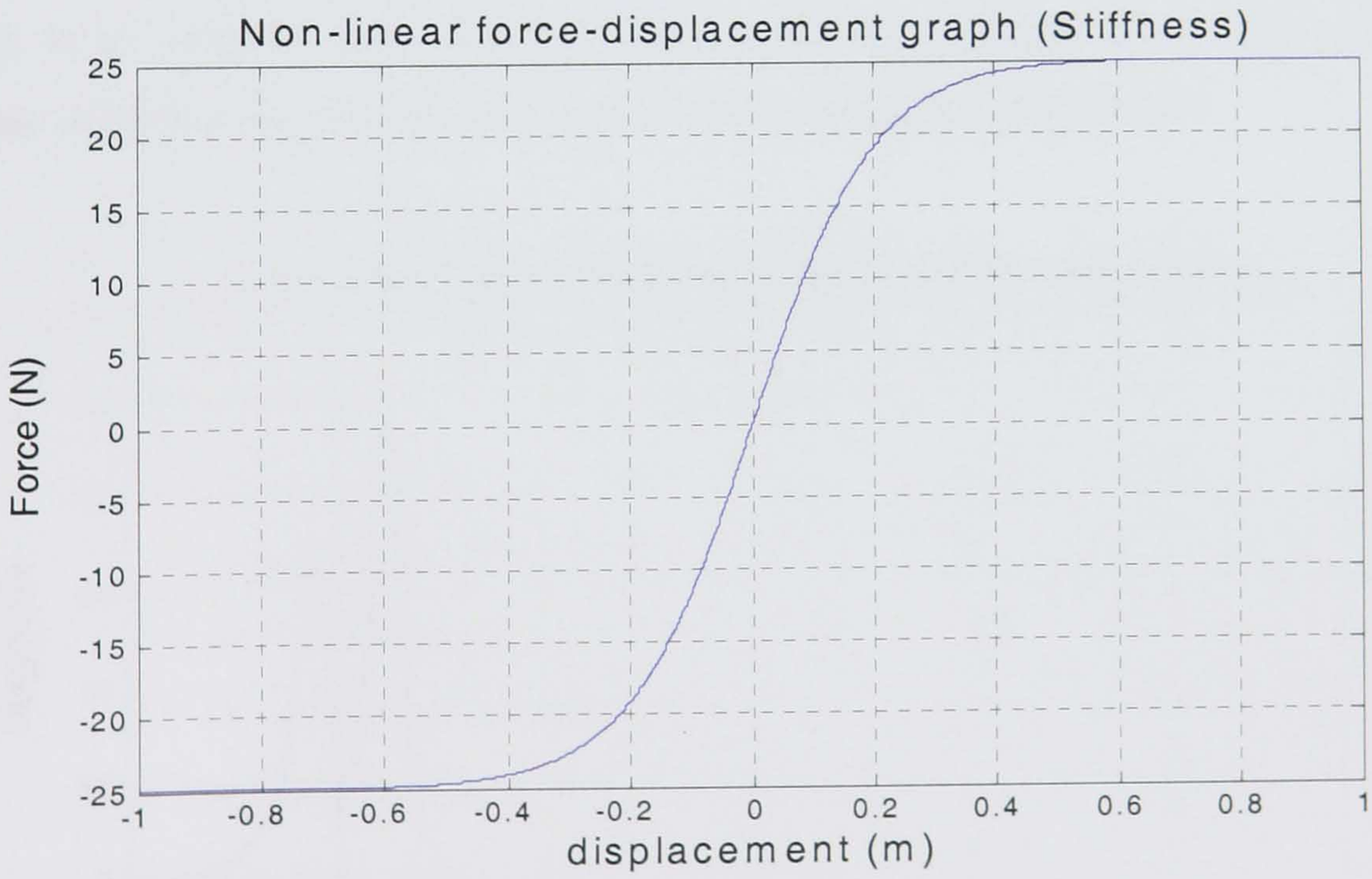

Figure 4.18 Stiffness as a function of force and displacement

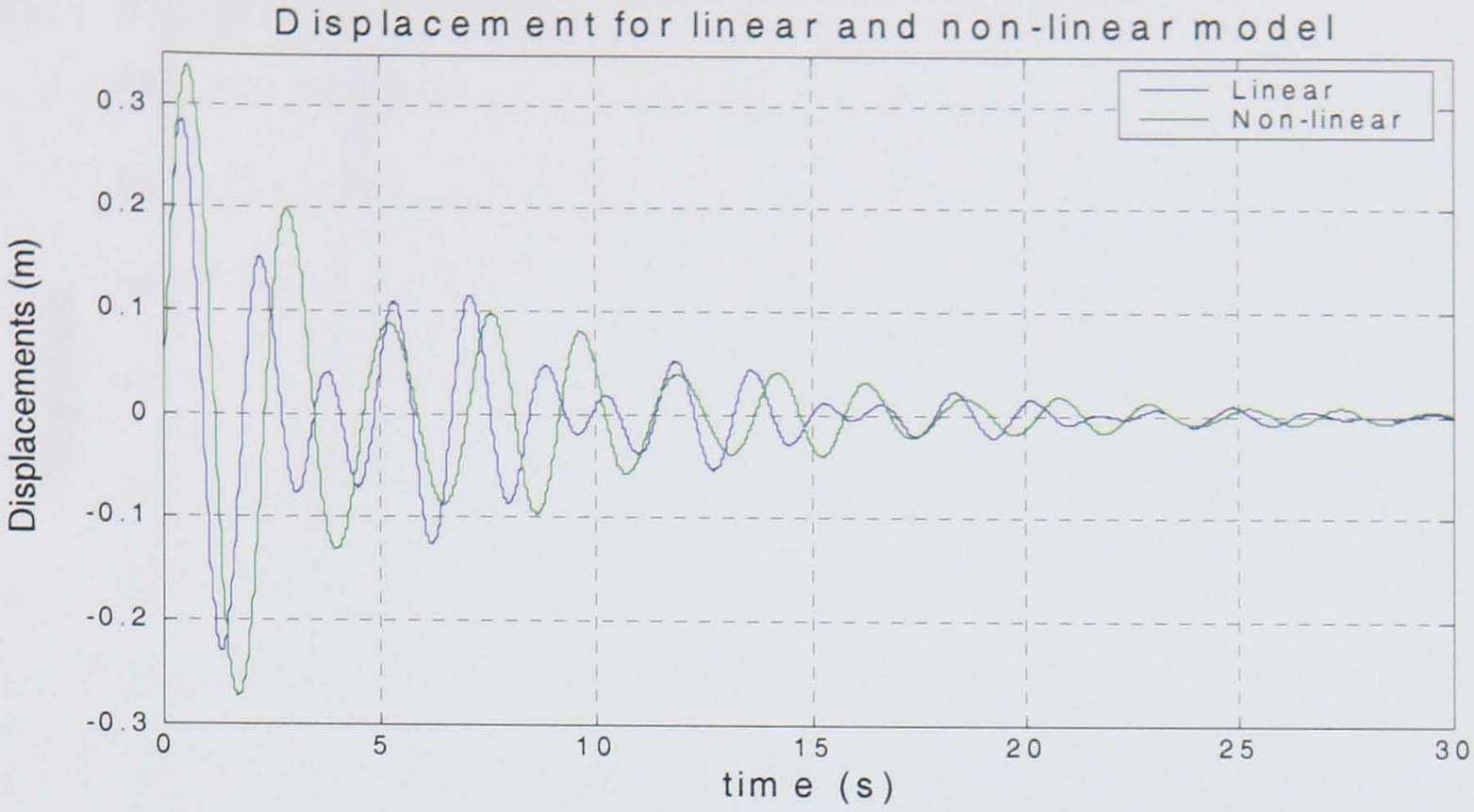

Figure 4.19 Displacement response for linear and non-linear stiffness model

The displacement of the non-linear model is larger, as expected. After the first two peaks where the displacement is larger due to the stiffness reduction, the displacements are reduced again but are marginally larger than the non-linear ones. There is a period increase visible in the first few peaks (but it reduces back to its original value), which remains for the rest of the time despite the system gaining its original stiffness. In a real example where there would be permanent stiffness degradation, the period would not return to its original value and the TMD would be targeting the wrong period. The change of period can also be seen in the Fourier transform plots below.

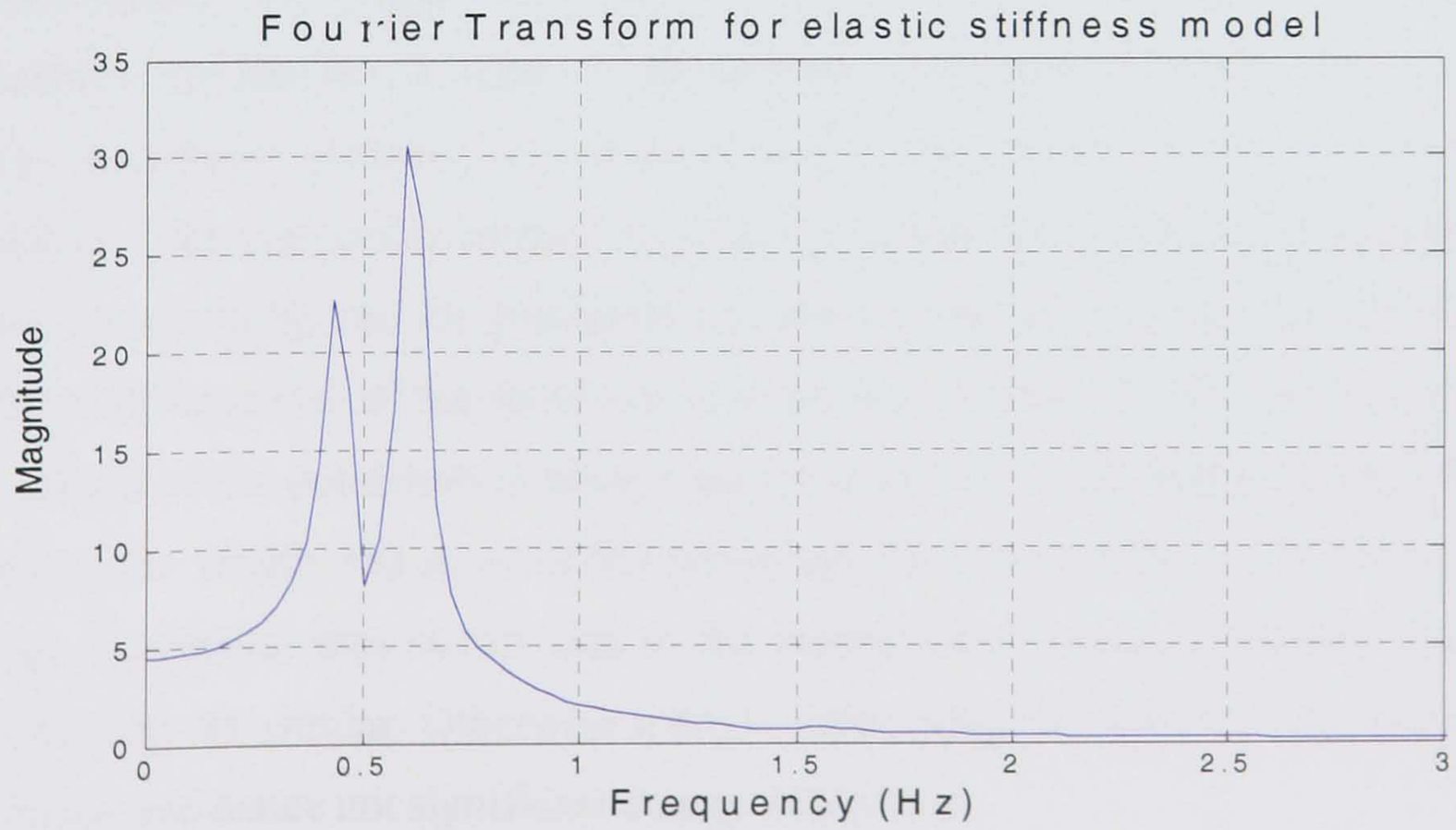

Figure 4.20 Power spectrum of elastic stiffness model

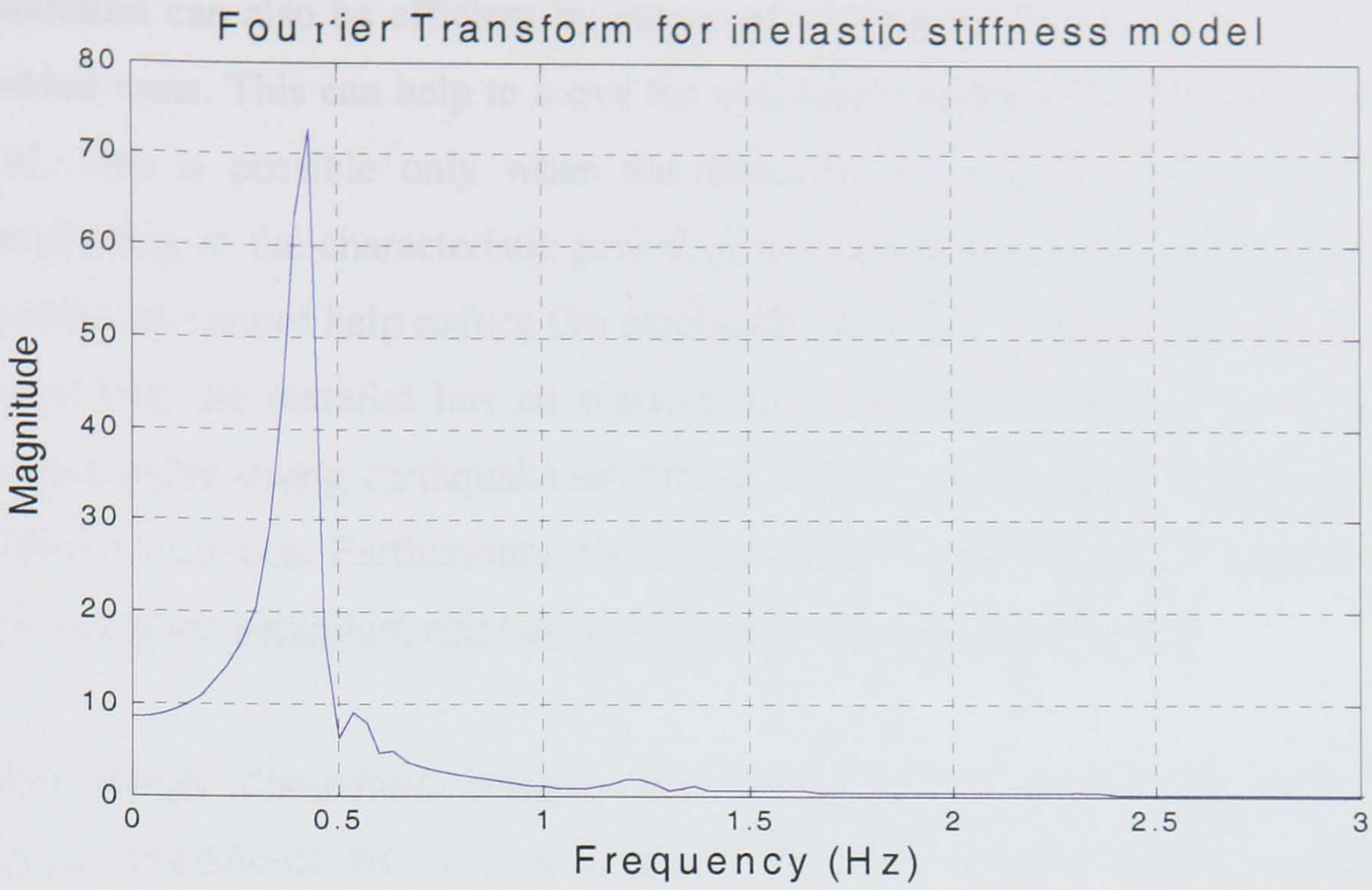

Figure 4.21 Power spectrum of inelastic stiffness model

The Fourier Transform of the elastic model has two sharp peaks at the two modes and then rapidly reduces to zero. The inelastic model has one large peak, corresponding to the pendulum mode, but has a wider spectrum with a few additional minor peaks due to the stiffness change.

4.5. Summary

In this chapter the simplest form of a structural system was designed with an energy dissipation mechanism in order to demonstrate from first principles the concepts of energy dissipation systems. The structure was a frame with a suspended mass like a pendulum. The variational method was used to model the system which is highly non-linear. By assuming that the pendulum can provide damping, energy dissipation can be achieved if the period of the pendulum is as close as possible to the period of the frame. The period of the pendulum is always higher than that of the frame but by effectively choosing the length and mass of the pendulum the two periods can be made similar. Energy dissipation thus occurs due to the interaction of the two-systems, but only if their periods are similar. Otherwise there is little energy transfer from the frame to the pendulum and hence not significant energy dissipation.

A pendulum can also be efficient by means of altering the period of the frame, due to the added mass. This can help to move the structure's period away from the earthquake period. This is possible only when the structure has a period larger than the one corresponding to the characteristic period of the earthquake. Finally, the movement of the pendulum cannot help reduce the amplitude of motion. The last part of the chapter assumed that the material has an elasto-plastic behaviour which is the case in real structures under strong earthquake excitation. This results in higher displacements and in stiffness reduction. Furthermore, the period of the frame changes, moving away from the period of the pendulum and hence the energy dissipated is reduced.

Passive energy dissipation systems are very effective because they can increase damping. Pendulums are natural systems, "internal" to the structure without any external interference. The period can be tuned to be similar to that of the frame by simply altering the length (or mass) of the pendulum. The limitation of this system is that it cannot reduce displacements. The amplitude of motion can only be reduced by active control where external forces are applied. Furthermore, at large earthquakes passive systems are not effective because the period of the system changes and dissipation is no longer possible. This problem can be solved by using active control where the forces are stronger and can ensure that the structure will not move to the inelastic region. Even if this occurs, active control can alter the period of the controller and be effective even when the structural period changes. The remaining parts of the thesis investigate various active control methods.

CHAPTER 5

LQG CONTROL

5.1. Introduction

In the previous chapter the concept of passive control via damping was introduced in a simple example involving a frame. It was shown how damping can dissipate energy and hence strengthen a structure subject to dynamic loading. Here, the concept of active control is explained. In active control an actuator applies forces and counteracts the disturbing forces. This is typically more efficient than passive control but requires large forces and accurate control design including sensors, actuators and a mathematical dynamic model of the system. In active control if forces are applied at the wrong time or place the structure may become unstable and the controller can therefore have the opposite than the desired effect. Feedback control is used in this chapter to illustrate the concept of active control.

The objective of the present (and the next) chapter is to examine two control design methods in depth, which are the Linear Quadratic Regulator (LQR) and H_∞ optimal control. The main aspects of these design methods are considered and many different design scenarios are analysed. The overall aim is to examine different control algorithms and compare their results with those expected by theory, and also to compare the methods between themselves in order to determine their relative advantages and limitations. Finally, several other issues of control applicable to specific problems are investigated. The main limitations of each control scheme are described and the main conclusions about their effectiveness are drawn.

The theory of LQR has been outlined in chapter 3 and here it is examined with extensive Matlab simulations. LQG is an optimal control design methodology, which aims to minimise the RMS values of the regulated signals subject to the presence of white disturbance and sensor-noise processes. A quadratic optimisation index is

formulated involving the energy of the state and control variables which is minimised via the solution of Riccatti equations. The Kalman filter may be used to estimate the states from noisy measurements if these are not directly measurable. Also, penalty terms can be added in the scalar performance index to shift the emphasis between different design objectives. Frequency weights can also be used to penalise the energy of the regulated signal in different frequency bands or to reflect more accurately the energy distribution of the disturbance and noise signals.

A regular three-storey structure has been chosen where all designs will be tested and simulated. Several design inputs are examined including an impulse, the simplest form of loading, a sinusoidal input and finally a real earthquake signal. The structure employs an active tendon control system and also includes a passive energy dissipation element.

5.2 Structural model

5.2.1 Description of structure

The structure chosen employs active tendon control, which is reported in the literature to achieve the best results disregarding cost and power supply considerations [Soong 1990]. An existing structure investigated by other researchers is considered [Nishimura and Kojima 1991]. This represents a simple and regular 3-storey structure, so that the effect of the higher order modes is minimal. A schematic of the structure is shown in figure 5.1 and its parameters are summarised in table 5.1.

Structural parameters				
Floor	$M\,(kg)$	$C(Ns/m)$	$K\,(N/m)$	Actuator
Base	5	100	16000	$K_f = 2\ N/A$
1st	1.72	0.078	2600	$K_e = 2\ V \cdot s/m$
2nd	1.48	0.078	2600	$R = 1.5\ \Omega$
3rd	2.34	0.078	2600	

Table 5.1

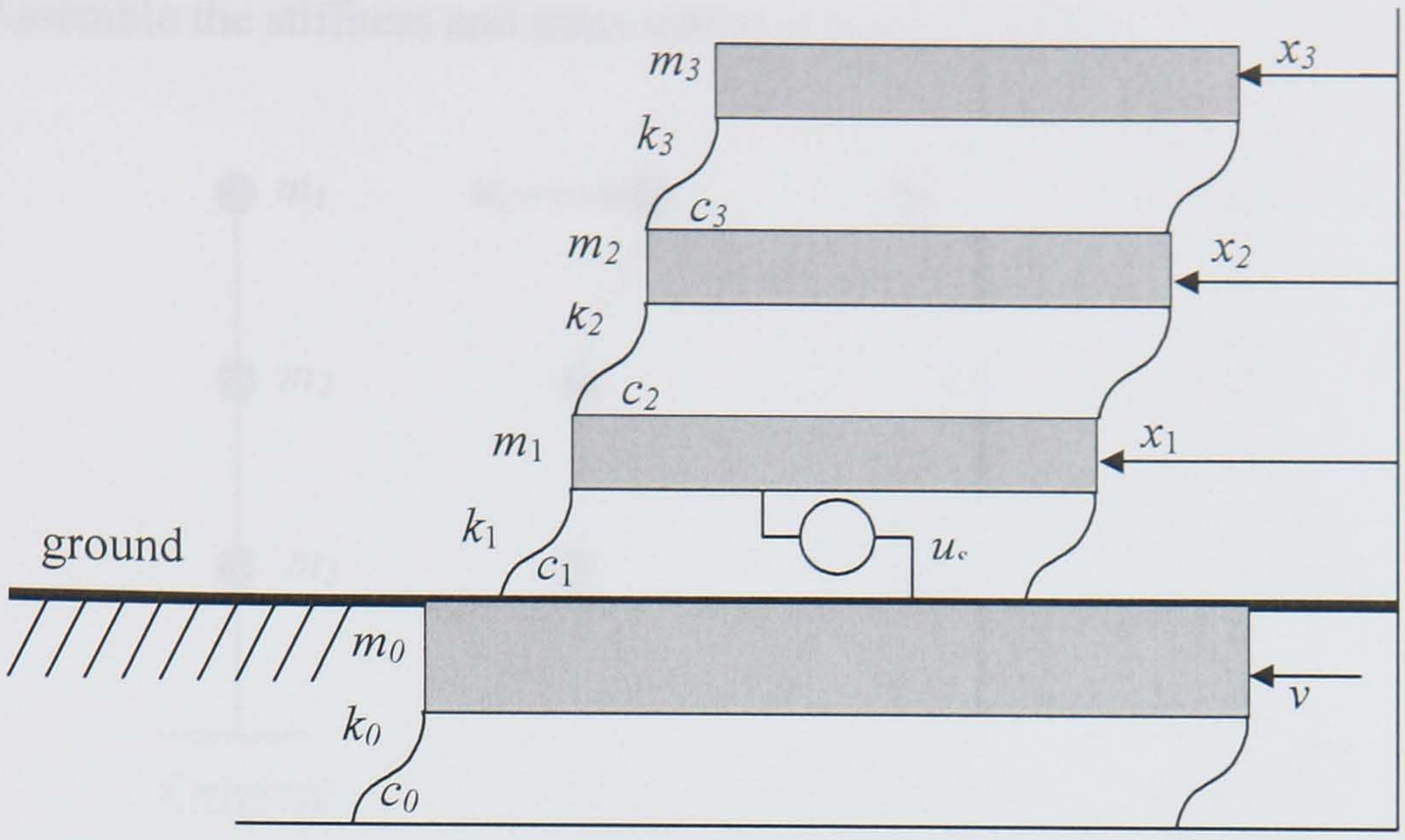

Figure 5.1 Representation of 3-storey building as a mass-spring-damper model

The tendons are connected between the ground and first floor and produce an equal and opposite force, which means that even when the maximum possible force is applied by the actuator the displacements of the building's floors cannot be made zero. The structure is a test model and has small masses and dimensions. A large stiffness value is assumed for the base to account for the stiffness between the base and the surrounding ground. The objectives of the controller are to minimise the ground floor acceleration and the inter-storey drift between first and second floor.

The structure is idealised as a large mass-spring-damper system as shown in figure (5.1). In this diagram, u_s is the actuator force and v is the disturbance (earthquake) force signal assumed to act on m_0. The tendons add damping to the structure, therefore even if no force is applied by the actuator there is some resistance from the tendons.

5.2.2 Modal analysis

Modal analysis needs to be performed to identify the natural period of each mode and the modal mass contribution. Since the structure is a three-storey building, three distinct modes are expected. By including the ground floor a fourth mode can be observed, but due to the high damping value ($C = 100\ Ns/m$) this does not contribute significantly to the mode shapes. The procedure for carrying out modal analysis, as outlined in section 4.2.1 (page 72) and by Eurocode 8 (1998) is as follows:

i) Assemble the stiffness and mass matrices for the building:

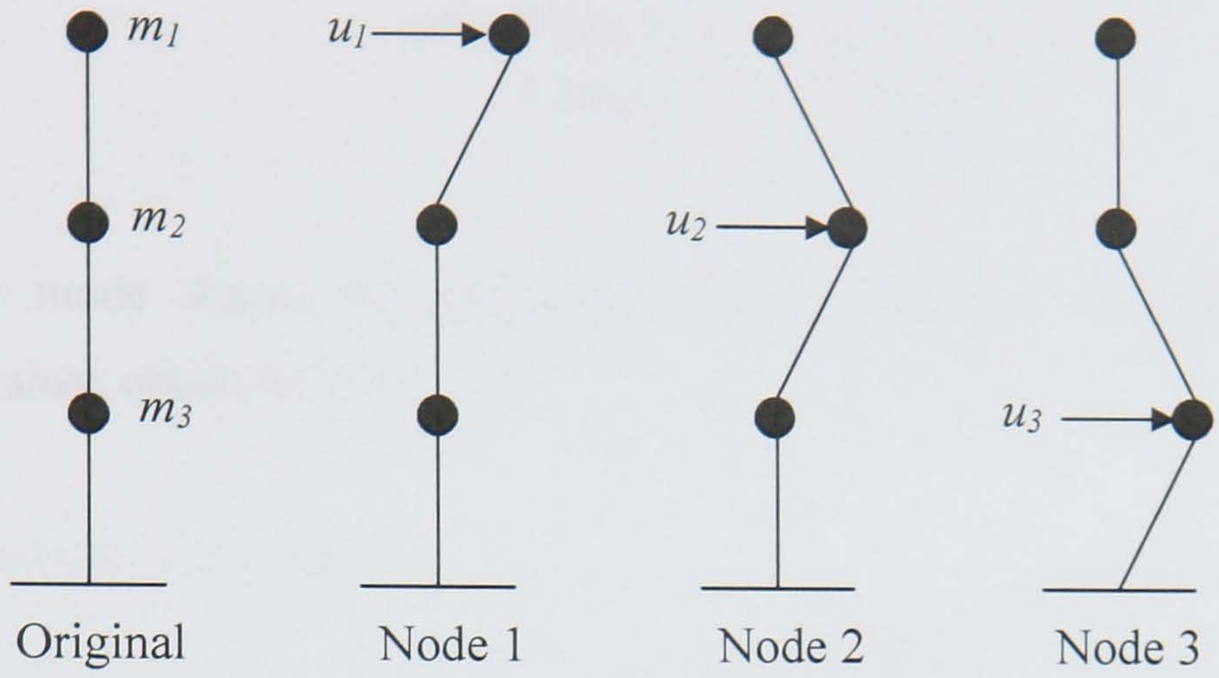

Figure 5.2 Assembly of stiffness matrix for a 3 DOF system

Here, $K_1 = \begin{bmatrix} k_1 \\ -k_1 \\ 0 \end{bmatrix}$ $K_2 = \begin{bmatrix} -k_1 \\ k_1 + k_2 \\ -k_2 \end{bmatrix}$ $K_3 = \begin{bmatrix} 0 \\ -k_2 \\ k_2 + k_3 \end{bmatrix}$

where, K_{ij} is the force corresponding to coordinate i, due to a unit displacement of coordinate j [Clough and Penzien 1993]. Here, a unit displacement is applied at each node and the corresponding force at each node is determined. The three vectors are combined to give the stiffness matrix. Also, all element have the same stiffness $\left(k_1 = k_2 = k_3\right)$. Hence, the overall stiffness and mass matrices are:

$$K = \begin{bmatrix} 1 & -1 & 0 \\ -1 & 2 & -1 \\ 0 & -1 & 2 \end{bmatrix} \times 2600\ N/m$$

and

$$M = \begin{bmatrix} 1.72 & 0 & 0 \\ 0 & 1.48 & 0 \\ 0 & 0 & 2.35 \end{bmatrix} Kg$$

respectively.

ii) Solve the corresponding eigenvalue equation; Each eigenvalue represents physically the angular frequency of each mode.

$$\left|K - \omega^2 M\right| = 0 \Rightarrow \left|KM^{-1} - \omega^2 I\right| = 0$$

Hence,

$$\omega^2 = \begin{bmatrix} 301.7 \\ 1955.2 \\ 4981 \end{bmatrix} \Rightarrow \omega = \begin{bmatrix} 17.37 \\ 44.21 \\ 70.58 \end{bmatrix} rad/s$$

iii) Obtain mode shapes by calculating the eigenvectors corresponding to the eigenvalues obtained in step ii)

For example, for mode 1:

$$\left[K - \omega_1^2 M\right]\Phi_1] = \begin{bmatrix} 0 \\ 0 \\ 0 \end{bmatrix}$$

or,

$$\begin{bmatrix} 2600 - 301.7 \times 1.72 & -2600 & 0 \\ -2600 & 5200 - 1955 \times 1.48 & -2600 \\ 0 & -2600 & 5200 - 4982 \times 2.34 \end{bmatrix} \begin{bmatrix} \Phi_{1,1} \\ \Phi_{2,1} \\ \Phi_{3,1} \end{bmatrix} = \begin{bmatrix} 0 \\ 0 \\ 0 \end{bmatrix}$$

where Φ_1 is the first eigenvector. The same procedure is followed for the remaining mode shapes. Every mode shape is normalised to have its first element equal to 1. In this case the mode shapes are given below and shown in figure 3.

$$\Phi = \begin{bmatrix} 1 & 1 & 1 \\ 0.68 & -0.25 & -1.97 \\ 0.63 & -1.72 & 1.25 \end{bmatrix}$$

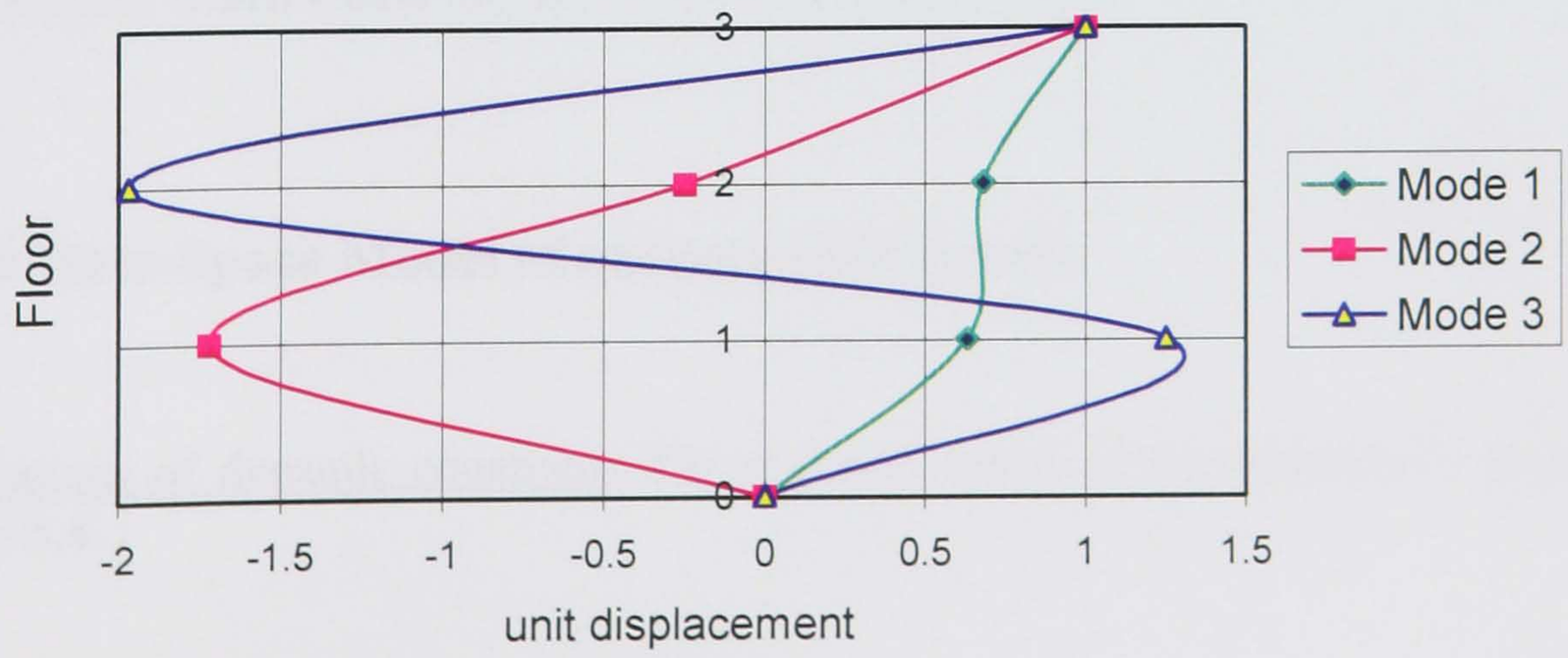

Figure 5.3. Building mode shapes

iv) Determine modal mass contribution: this is achieved by solving equation (4.20):

$$m^i = \frac{L^{i2}}{GM^i}$$

where L and GM is given by:

$$GM^i = \Phi^{iT} M \Phi_1$$

$$L^i = \Phi^{iT} M \begin{bmatrix} 1 \\ 1 \\ 1 \end{bmatrix}$$

Hence, in this case:

$$m = [83\% \quad 13\% \quad 4\%]$$

where the percentages represent the modal mass contribution of each mode.

v) Determine the natural periods of vibration. Here,

$$T = \frac{2\pi}{\omega} \Rightarrow T = \begin{bmatrix} 0.36 \\ 0.14 \\ 0.09 \end{bmatrix} \text{ seconds}$$

Note that the fundamental mode has 83% modal contribution, which is significantly large, as expected for a regular structure.

The majority of buildings possessing active control schemes, place the controller on the roof. The disadvantage of this scheme is that the controller is only able to suppress one mode. In the structure under consideration such a controller would be powerful, but for taller and more flexible buildings the fundamental mode has a lower modal contribution, which would make the controller less efficient.

5.2.3 State-Space Model of uncontrolled system

Derivations of dynamic equations: The dynamic model of the structure is shown in figure 5.4. :

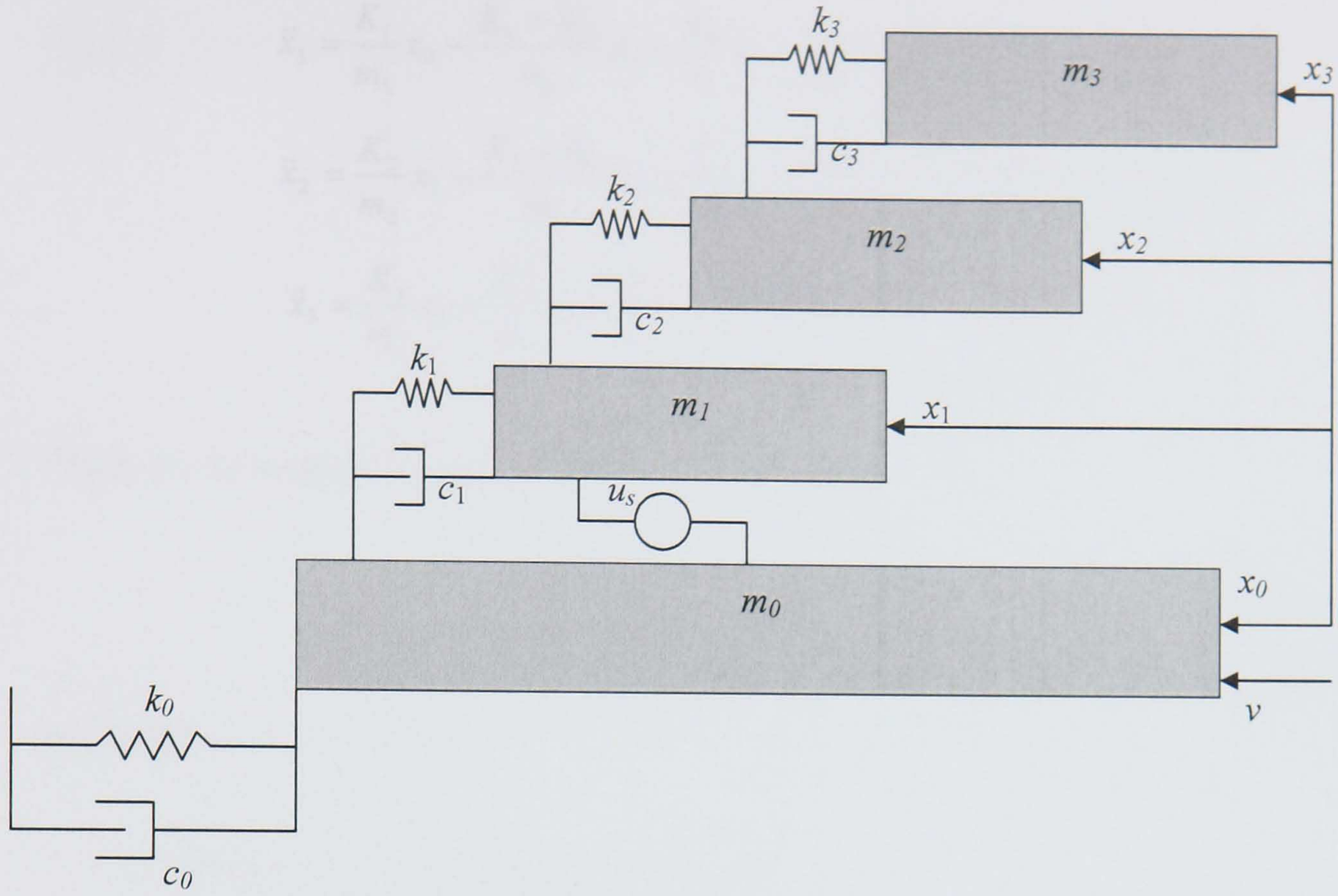

Figure 5.4. Building idealisation as a Mass-spring-damper model

By setting the inertial force for each mass m_i $(i = 0,1,2,3)$ to zero, we obtain:

$$m_0\ddot{x}_0 + C_0\dot{x}_0 + K_0x_0 - C_1\left(\dot{x}_1 - \dot{x}_0\right) - K_1\left(x_1 - x_0\right) = v - u$$

$$m_1\ddot{x}_1 + C_1(\dot{x}_1 - \dot{x}_0) + K_1(x_1 - x_0) - C_2\left(\dot{x}_2 - \dot{x}_1\right) - K_2\left(x_2 - x_1\right) = u$$

$$m_2\ddot{x}_2 + C_2(\dot{x}_2 - \dot{x}_1) + K_2(x_2 - x_1) - C_3\left(\dot{x}_3 - \dot{x}_2\right) - K_3\left(x_3 - x_2\right) = 0$$

$$m_3\ddot{x}_3 + C_3(\dot{x}_3 - \dot{x}_2) + K_3\left(x_3 - x_2\right) = 0$$

where u is the control force produced by the actuator and v is the disturbance force. Note, that the actuator produces a force u acting in equal and opposite directions between the ground and first floor (masses m_0 and m_1).

By solving for $\ddot{x}_i$, the above equations can be written as:

$$\ddot{x}_0 = -\frac{K_0 + K_1}{m_0}x_0 + \frac{K_1}{m_0}x_1 - \frac{C_0 + C_1}{m_0}\dot{x}_0 + \frac{C_1}{m_0}\dot{x}_1 - \frac{u}{m_0} + v$$

$$\ddot{x}_1 = \frac{K_1}{m_1}x_0 - \frac{K_1 + K_2}{m_1}x_1 + \frac{K_2}{m_1}x_2 + \frac{C_1}{m_1}\dot{x}_0 - \frac{C_1 + C_2}{m_1}\dot{x}_1 + \frac{C_2}{m_1}\dot{x}_2 + \frac{u}{m_1}$$

$$\ddot{x}_2 = \frac{K_2}{m_2}x_1 - \frac{K_2 + K_3}{m_2}x_2 + \frac{K_3}{m_2}x_3 + \frac{C_2}{m_2}\dot{x}_1 - \frac{C_2 + C_3}{m_2}\dot{x}_2 + \frac{C_3}{m_2}\dot{x}_3$$

$$\ddot{x}_3 = \frac{K_3}{m_3}x_2 - \frac{K_3}{m_3}x_3 + \frac{C_3}{m_3}\dot{x}_2 - \frac{C_3}{m_3}\dot{x}_3$$

These can be written in compact form as:

$$\dot{x} = Ax + Fv + Bu \tag{5.1}$$

$$y = Cx + Du \tag{5.2}$$

In equation (5.1) and (5.2),

A represents the dynamics of the structure

F is the disturbance input matrix

B is the control input matrix

C is the output (measurement) matrix

D is the direct feed-through matrix

$x = \begin{bmatrix} x_0 & x_1 & x_2 & x_3 & \dot{x}_0 & \dot{x}_1 & \dot{x}_2 & \dot{x}_3 \end{bmatrix}^T$ is the state, all floor displacements and accelerations.

In full,

$$A = \begin{pmatrix} 0 & 0 & 0 & 0 & 1 & 0 & 0 & 0 \\ 0 & 0 & 0 & 0 & 0 & 1 & 0 & 0 \\ 0 & 0 & 0 & 0 & 0 & 0 & 1 & 0 \\ 0 & 0 & 0 & 0 & 0 & 0 & 0 & 1 \\ -\frac{k_0 + k_1}{m_0} & \frac{k_1}{m_0} & 0 & 0 & -\frac{c_0 + c_1}{m_0} & \frac{c_1}{m_0} & 0 & 0 \\ \frac{k_1}{m_1} & -\frac{k_1 + k_2}{m_1} & \frac{k_2}{m_1} & 0 & \frac{c_1}{m_1} & -\frac{c_1 + c_2}{m_1} & \frac{c_2}{m_1} & 0 \\ 0 & \frac{k_2}{m_2} & -\frac{k_2 + k_3}{m_2} & \frac{k_3}{m_2} & 0 & \frac{c_2}{m_2} & -\frac{c_2 + c_3}{m_2} & \frac{c_3}{m_2} \\ 0 & 0 & \frac{k_3}{m_3} & -\frac{k_3}{m_3} & 0 & 0 & \frac{c_3}{m_3} & -\frac{c_3}{m_3} \end{pmatrix}$$

$$B = \begin{pmatrix} 0 & 0 & 0 & 0 & -\frac{1}{m_0} & \frac{1}{m_0} & 0 & 0 \end{pmatrix}^T$$

$$F = \begin{pmatrix} 0 & 0 & 0 & 0 & 1 & 0 & 0 & 0 \end{pmatrix}^T$$

$$C = \begin{pmatrix} \frac{K_1}{m_1} & -\frac{K_1 + K_2}{m_1} & \frac{K_2}{m_1} & 0 & \frac{C_1}{m_1} & -\frac{C_1 + C_2}{m_1} & \frac{C_2}{m_1} & 0 \\ 0 & -1 & 1 & 0 & 0 & 0 & 0 & 0 \end{pmatrix}$$

$$D = \begin{pmatrix} \frac{1}{m_1} \\ 0 \end{pmatrix}$$

Since the controller is not present the control signal u is set to zero.

5.2.4. State-Space model including actuator dynamics

Typically, the control force is produced by an electromechanical actuator. The actuator is a dynamic system of a finite bandwidth and hence cannot produce its force instantaneously (after a certain input voltage command). The dynamic model of a typical linear actuator is described below. Note that this resembles the dynamics of a DC motor, except that the angular speed ω is now replaced by linear velocity v_0. As the actuator is connected between m_0 and m_1,

$$v_0 = \dot{x}_1 - \dot{x}_0 \tag{5.3}$$

which is the relative velocity between the two masses. The electromechanical equation describing the system is:

$$F = K_f I \tag{5.4}$$

where F represents actuator force, I is the armature current and K_f is the "force constant" of the actuator. Kirchoff's law for the circuit in Figure 5.5 gives:

$$V = IR + e = IR + K_e(\dot{x}_1 - \dot{x}_0) \tag{5.5}$$

Here V is the applied armature voltage and $K_e\nu_0$ represents the "back-emf" e of the actuator, where K_e is the actuator's back-emf constant. For an ideal actuator (no losses) the input electrical power (ignoring the power dissipated in the armature resistance R) must be equal to the output mechanical power and thus:

$$eI = Fv_0, \quad or \quad \frac{k_e v_0 F}{k_f} = Fv_0 \Rightarrow k_e = k_f \tag{5.6}$$

In order to obtain the overall closed-loop system the actuator dynamics need to be added:

$$F = k_f I \tag{5.7}$$

$$V - IR = k_e(\dot{x}_1 - \dot{x}_0) \tag{5.8}$$

From equations (5.7) and (5.8),

$$F = k_f \frac{V - k_e(\dot{x}_1 - \dot{x}_0)}{R} \tag{5.9}$$

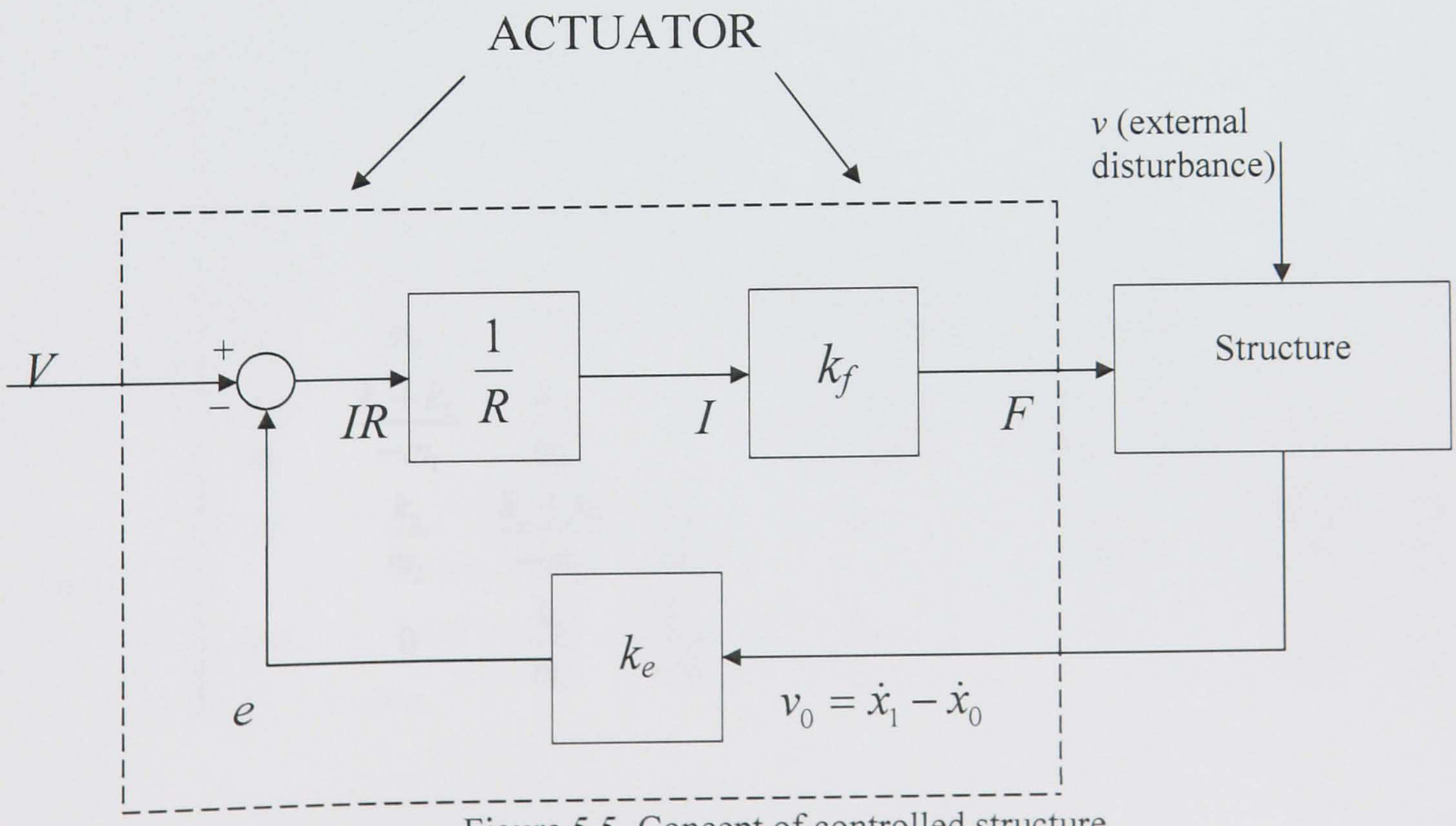

Figure 5.5. Concept of controlled structure

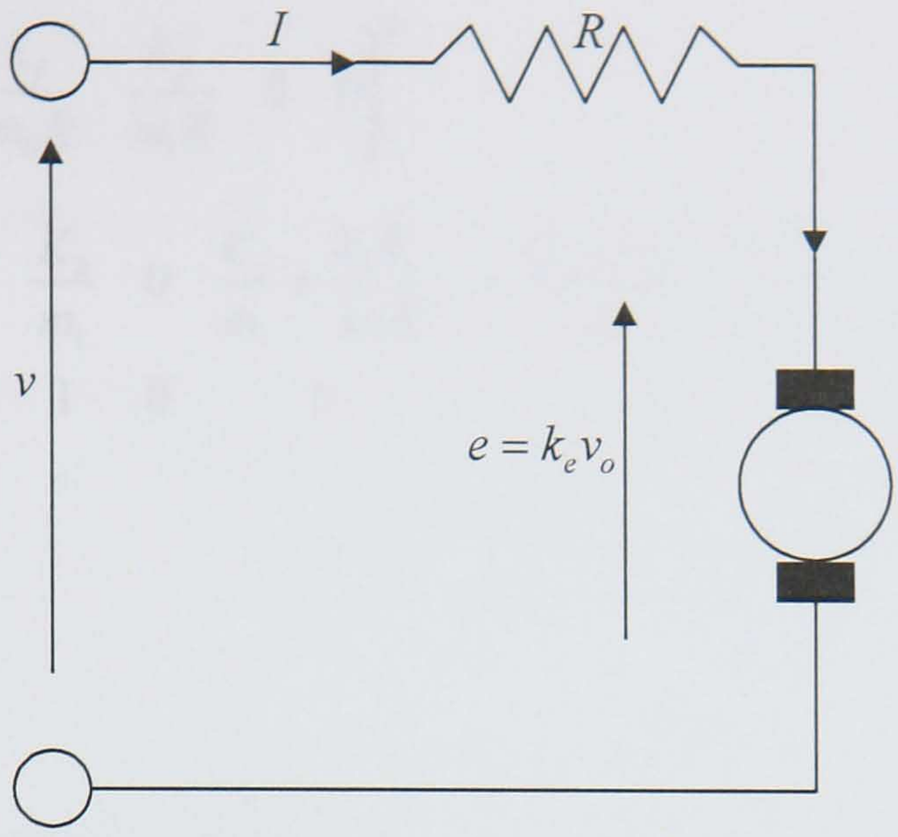

Figure 5.6 Representation of DC motor

or,

$$F = \frac{K_f V}{R} - \frac{K_f K_e}{R} x_1 + \frac{K_f K_e}{R} x_0 \qquad (5.10)$$

By substituting F from (5.10) into equation (5.1) and rearranging in order to remove all state variables from the control input, we get the following augmented state space system which now includes the linear actuator's dynamics, where the control force F is denoted by u in the state space matrix:

$$A_1 = \begin{pmatrix} 0 & 0 & 0 & 0 & 1 & 0 & 0 & 0 \\ 0 & 0 & 0 & 0 & 0 & 1 & 0 & 0 \\ 0 & 0 & 0 & 0 & 0 & 0 & 1 & 0 \\ 0 & 0 & 0 & 0 & 0 & 0 & 0 & 1 \\ \frac{k_0 + k_1}{-m_0} & \frac{k_1}{m_0} & 0 & 0 & \frac{c_0 + c_1}{-m_0} + \frac{k_f k_e}{m_0 R} & \frac{c_1}{m_0} - \frac{k_f k_e}{m_0 R} & 0 & 0 \\ \frac{k_1}{m_1} & \frac{k_1 + k_2}{-m_1} & \frac{k_2}{m_1} & 0 & \frac{c_1}{m_1} + \frac{k_f k_e}{m_1 R} & \frac{c_1 + c_2}{-m_1} - \frac{k_f k_e}{m_1 R} & \frac{c_2}{m_1} & 0 \\ 0 & \frac{k_2}{m_2} & \frac{k_2 + k_3}{-m_2} & \frac{k_3}{m_2} & 0 & \frac{c_2}{m_2} & \frac{c_2 + c_3}{-m_2} & \frac{c_3}{m_2} \\ 0 & 0 & \frac{k_3}{m_3} & \frac{k_3}{-m_3} & 0 & 0 & \frac{c_3}{m_3} & \frac{c_3}{-m_3} \end{pmatrix}$$

$$B_1 = \begin{pmatrix} 0 & 0 & 0 & 0 & -\dfrac{k_f}{m_0 R} & \dfrac{k_f}{m_1 R} & 0 & 0 \end{pmatrix}^T$$

$$C_1 = \begin{pmatrix} \dfrac{K}{m_1} & -\dfrac{K_1+K_2}{m_1} & \dfrac{K_2}{m_1} & 0 & \dfrac{C_1}{m_1}+\dfrac{k_f k_e}{m_1 R} & -\dfrac{C_1+C_2}{m_1}-\dfrac{k_f k_e}{m_1 R} & \dfrac{C_2}{m_1} & 0 \\ 0 & -1 & 1 & 0 & 0 & 0 & 0 & 0 \end{pmatrix}$$

$$D_1 = \begin{pmatrix} \dfrac{1}{m_0 R} \\ 0 \end{pmatrix}$$

This may be written more compactly as:

$$\begin{aligned} \dot{x} &= Ax + \begin{bmatrix} B & F \end{bmatrix} \begin{bmatrix} u \\ v \end{bmatrix} \\ y &= Cx + Du \end{aligned} \tag{5.11}$$

where now u represents the actuator voltage.

5.3. Controller Analysis and Design

5.3.1. Uncontrolled response

There are three different types of simulations, specifically uncontrolled, passive and closed loop. In passive simulations an actuator is included but without applying any forces, hence the ATC works only as a passive system adding damping. This is only added for completeness because the uncontrolled responses are different to the closed-loop responses when there in no control input. In closed loop simulations the active control is fully employed.

The first simulation is for the uncontrolled system. First an impulsive load was applied as an input, then a sinusoid and finally a real earthquake signal (appropriately scaled). The peak levels, RMS values and frequency responses were obtained to evaluate the structure`s response.

The next section shows the natural response of the building due to the three different inputs, i.e. impulse, sinusoidal and earthquake. These help identify the building's dynamic behaviour in order to design an effective active controller.

5.3.1. Impulsive loading: The observed displacement of all masses was sinusoidal, with a very low damping, in agreement to the low damping characteristics of the structure. The floors were at all times out of phase to each other, behaving almost randomly. Raising all stiffnesses by a factor of 10 or higher results in greater synchronism between the motion of each mass, i.e. they are out of phase by 10-20° only. Clearly, the building is very flexible which gives rise to high modes with significant amplitudes; thus a passive device targeting only one mode would be inefficient for such a building, as has been confirmed from the modal mass contribution. The displacements of each floor x_i $(i = 0,1,2,3)$ are shown in the figure below:

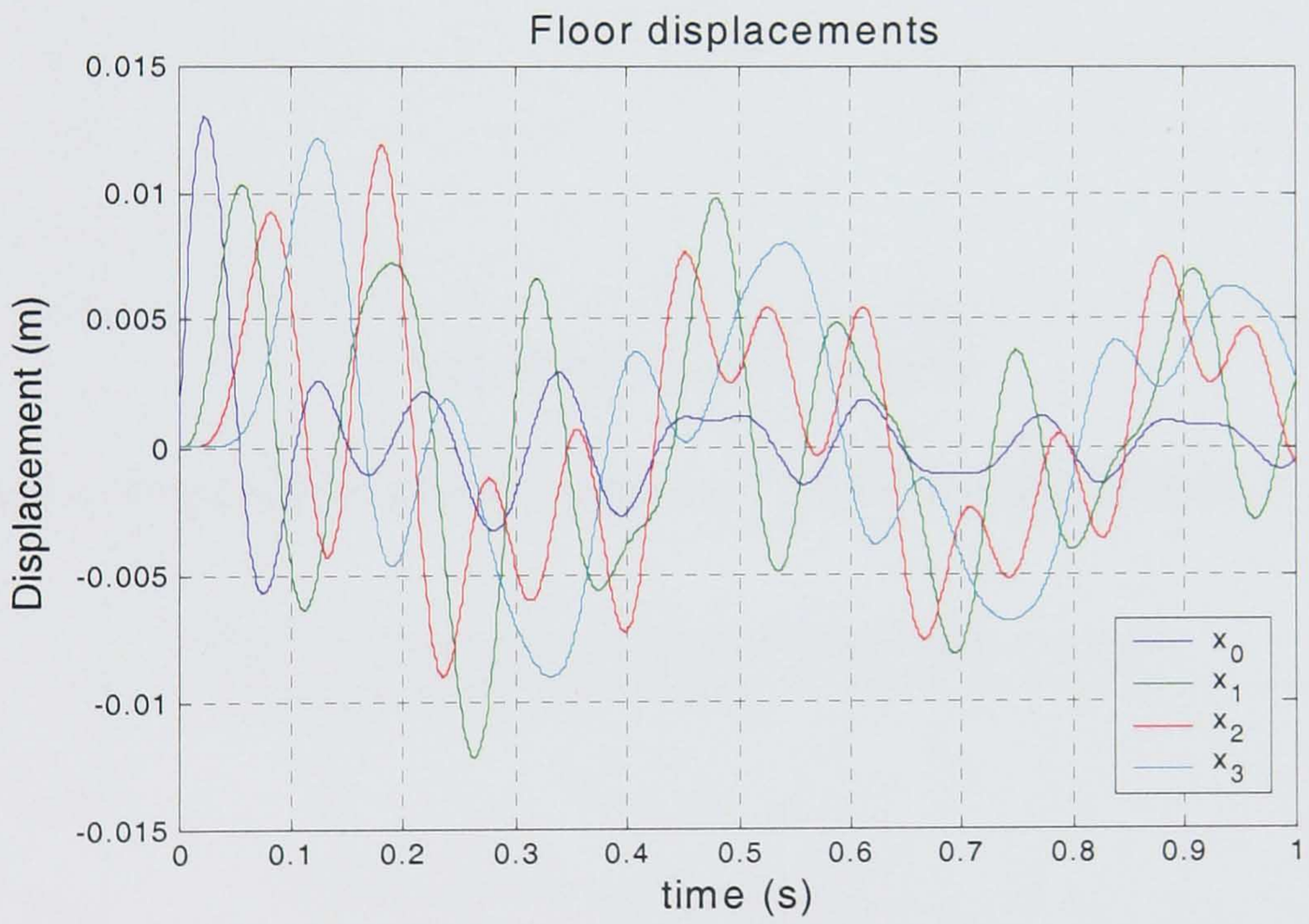

Figure 5.7 Uncontrolled displacements for impulsive input

Sinusoidal response: The same experiment was conducted with a sinusoidal wave as the disturbance input. The behaviour of the building was as expected (steady-state output is sinusoidal at input frequency after an initial transient). The three modes of vibration have the following periods, also shown in the Bode diagram as sharp resonance peaks. As expected, the steady-state amplification is related to the magnitude frequency response at the input frequency.

Modes of vibration			
	Period T (s)	ω (rads/s)	Frequency ν (Hz)
1st mode	0.4	15.52	2.5
2nd mode	0.143	43.95	6.99
3rd mode	0.086	73.28	11.63

Table 5.2

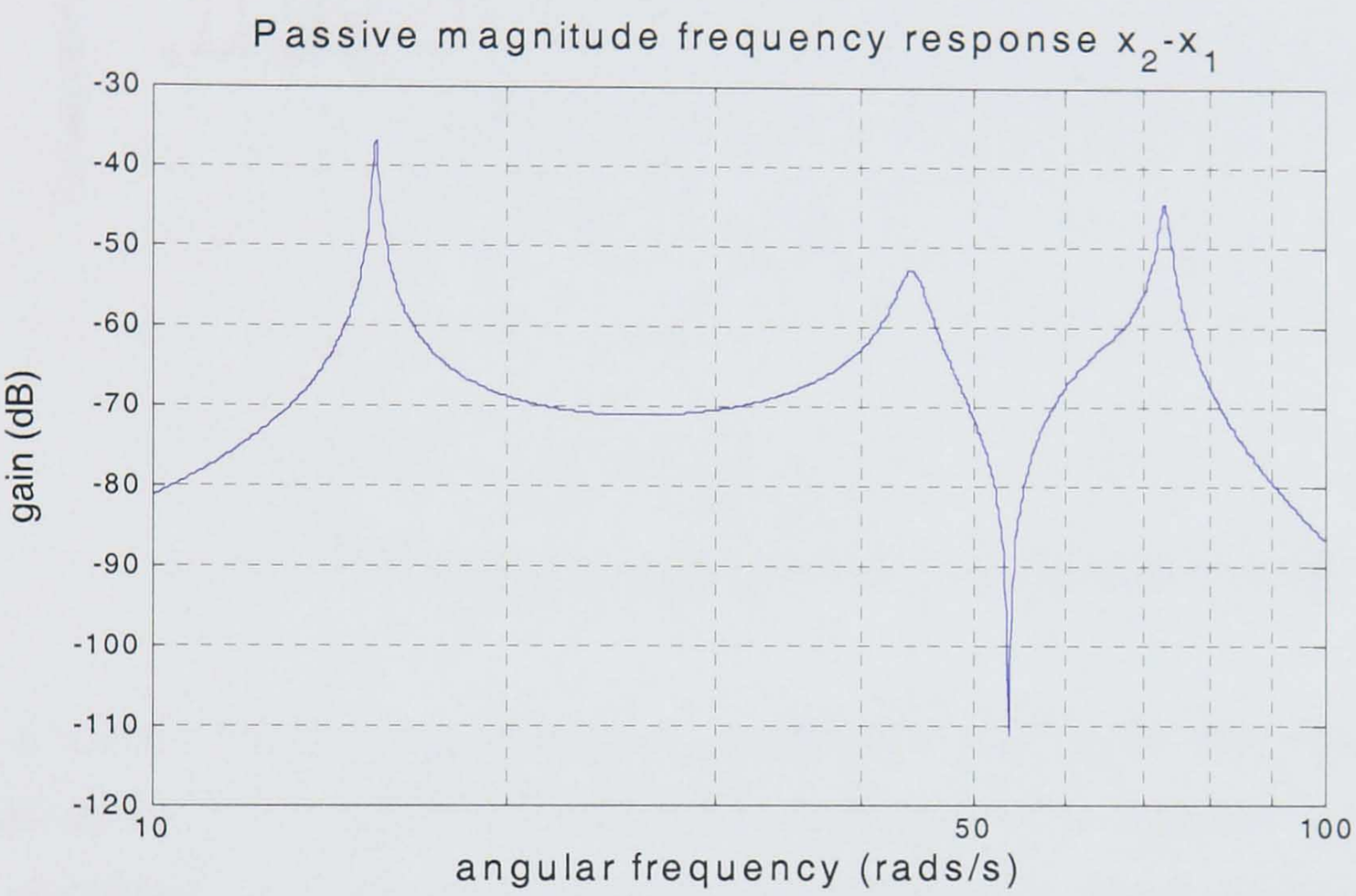

Figure 5.8 Magnitude frequency responses of inter-floor displacement $x_2 - x_1$

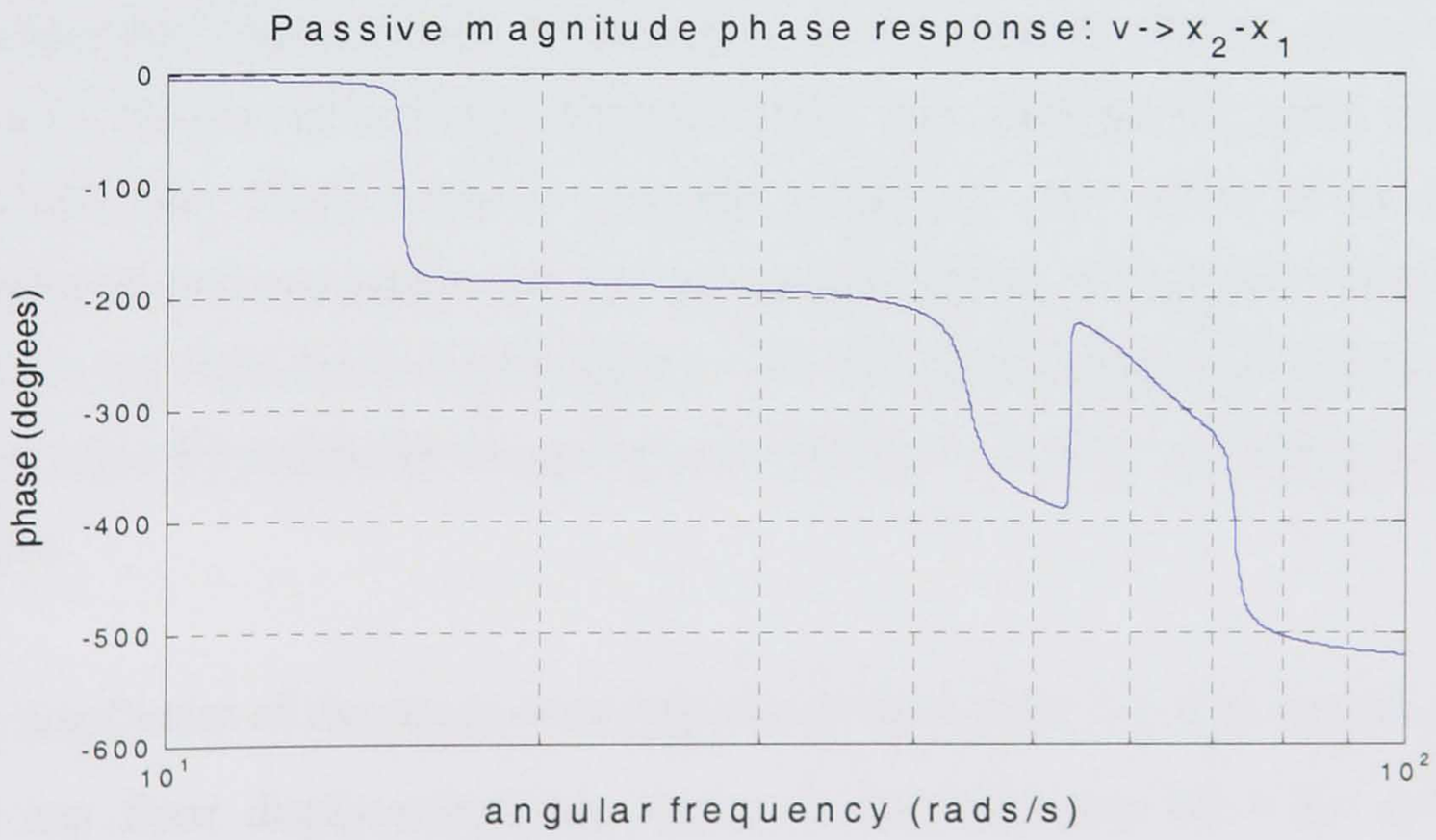

Figure 5.9 Phase frequency response of inter-floor displacement $x_2 - x_1$

The first disturbance input applied was a sine-wave of angular frequency $\omega = 10$ rad/s. The response of the system (each floor) is shown in figure 5.10.

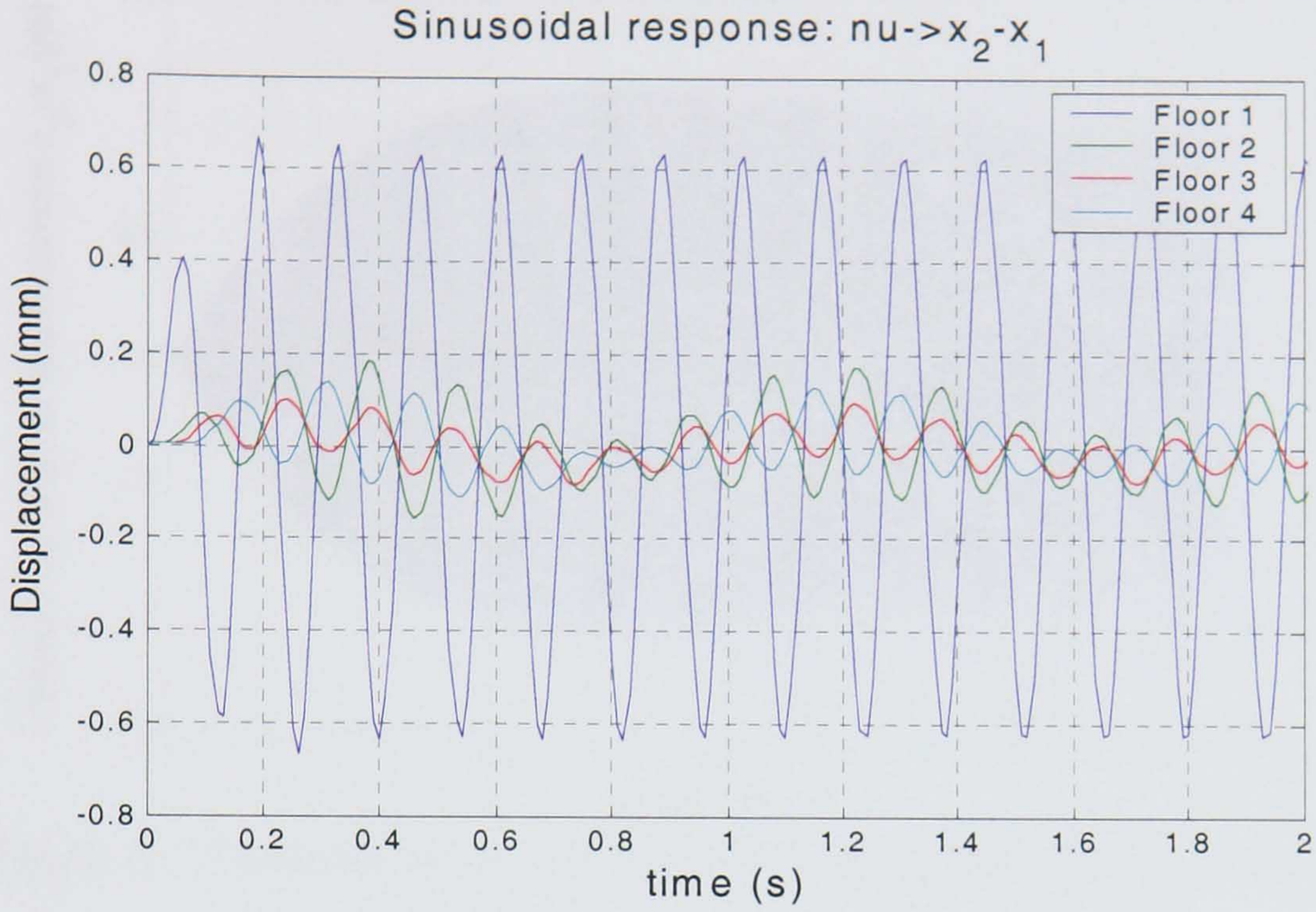

Figure 5.10 Uncontrolled displacements after sinusoidal loading

The response of each mass tends to a sinusoidal oscillation at the input frequency, after a brief transient. In contrast to the impulsive-loading case the amplitude of oscillation is not diminishing, but stays at constant levels throughout the period of simulation, since the load is constantly applied. The behaviour is different when the input frequency coincides with one of the building's natural frequencies. The acceleration and displacement response keep increasing for a few seconds which is considered a long time for such a short period structure. Next, they fluctuate for some time (transient response) and finally settle to a steady oscillation, after about 50 seconds, a huge amount of time compared with the 0.4 seconds period. The diagram below shows the inter-storey drifts for the input signal $\nu = \sin 70t$ (third mode frequency). In this case, it takes about 9 seconds for the response to stabilize to a value much higher than the first output.

The amplitudes of the steady-state response of the system (1st floor acceleration, $x_2 - x_1$ and top floor displacement) are shown in the following table for different input frequencies:

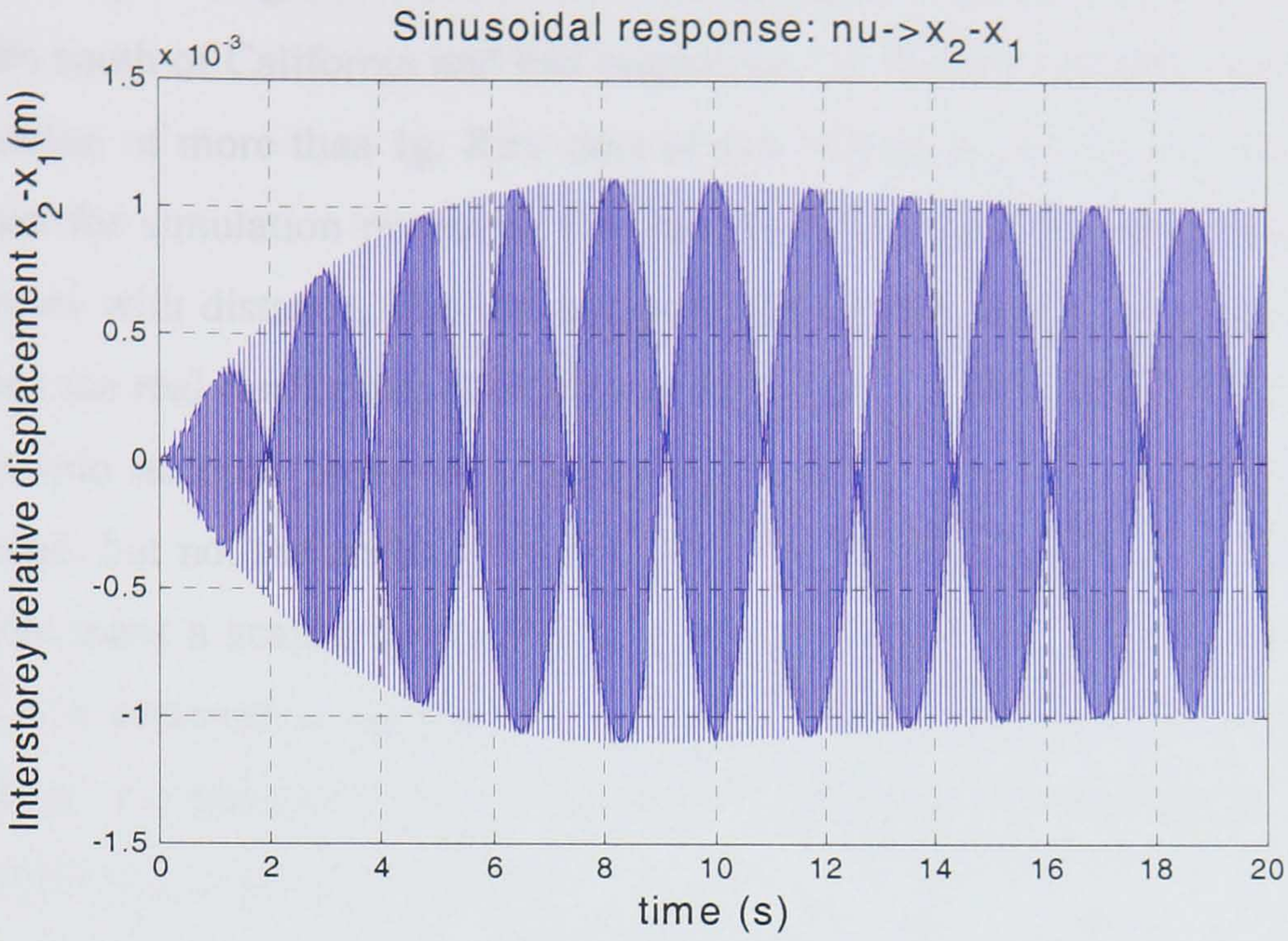

Figure 5.11 Uncontrolled displacement for a sinusoidal loading $\nu = \sin 45t$

Response as a function of radial frequency									
ω (rads/s)	10	15	20	30	40	45	50	60	70
x_2-x_1 (mm)	0.23	2.81	0.61	0.49	1	2.1	0.6	0.6	2
$\ddot{x}_1\left(m/s^2\right)$	0.6	0.737	0.845	0.747	2.122	7.385	3.652	1.904	4.085
x_3 (mm)	0.99	8.98	1.40	0.61	1	2.3	0.9	0.5	0.4

Table 5.3

It can be seen that as the angular frequency increases, the response of the building slightly increases but when the frequency of the input is similar to a natural frequency of the building $\omega = (15, 45, 70)$ rad/s the amplification factor is very high. The first floor acceleration is similar in all cases and shows small fluctuations, a problem also encountered in the impulsive load case. Hence, a controller should target the frequencies that coincide with the building's natural frequencies. These are the frequencies that would make the building unstable, as opposed to all other input frequencies.

5.3.1. Real Earthquake signal: Here the response of the system was modelled for a "real" earthquake signal. The Loma Prieta earthquake, occurred on October 17th 1989, 60 miles south of California and had magnitude 7.1 Richter and maximum peak ground acceleration of more than 1g. Real data of this earthquake were extracted from Matlab and used for simulation purposes. The acceleration caused by an earthquake typically diminishes with distance. The test structure used in this study is a 1-meter model, and therefore the real earthquake acceleration would have a devastating effect on it. In order to take into account these two factors, the amplitude of the acceleration data were attenuated, but not the period. Since the mass of the building is about 1/100th of a real buildings mass a scaling factor of 100 was applied to the model. Note that since the structure is assumed to operate in the elastic region, scaling the input force results in scaling of all responses. Here, the east-west acceleration is shown which is used throughout this section as an input.

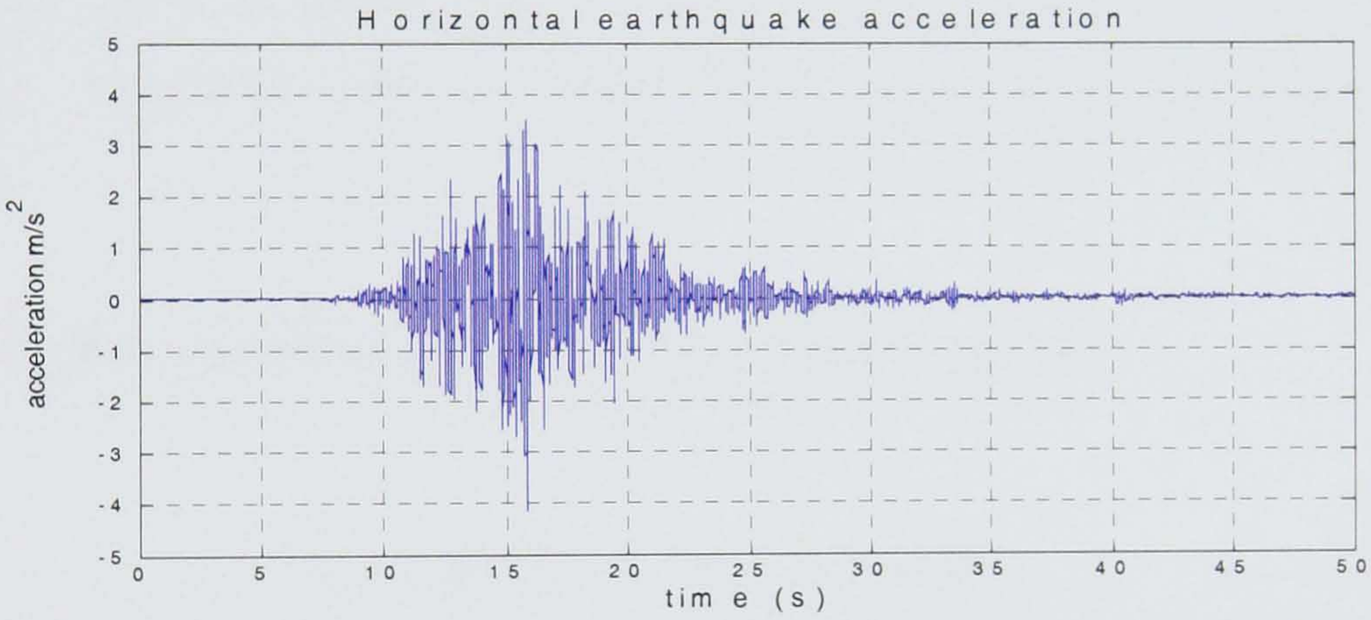

Figure 5.12 Normalised east-west acceleration of earthquake signal

The response of the building to the earthquake was also calculated and the interstorey drifts are shown (figure 5.13).

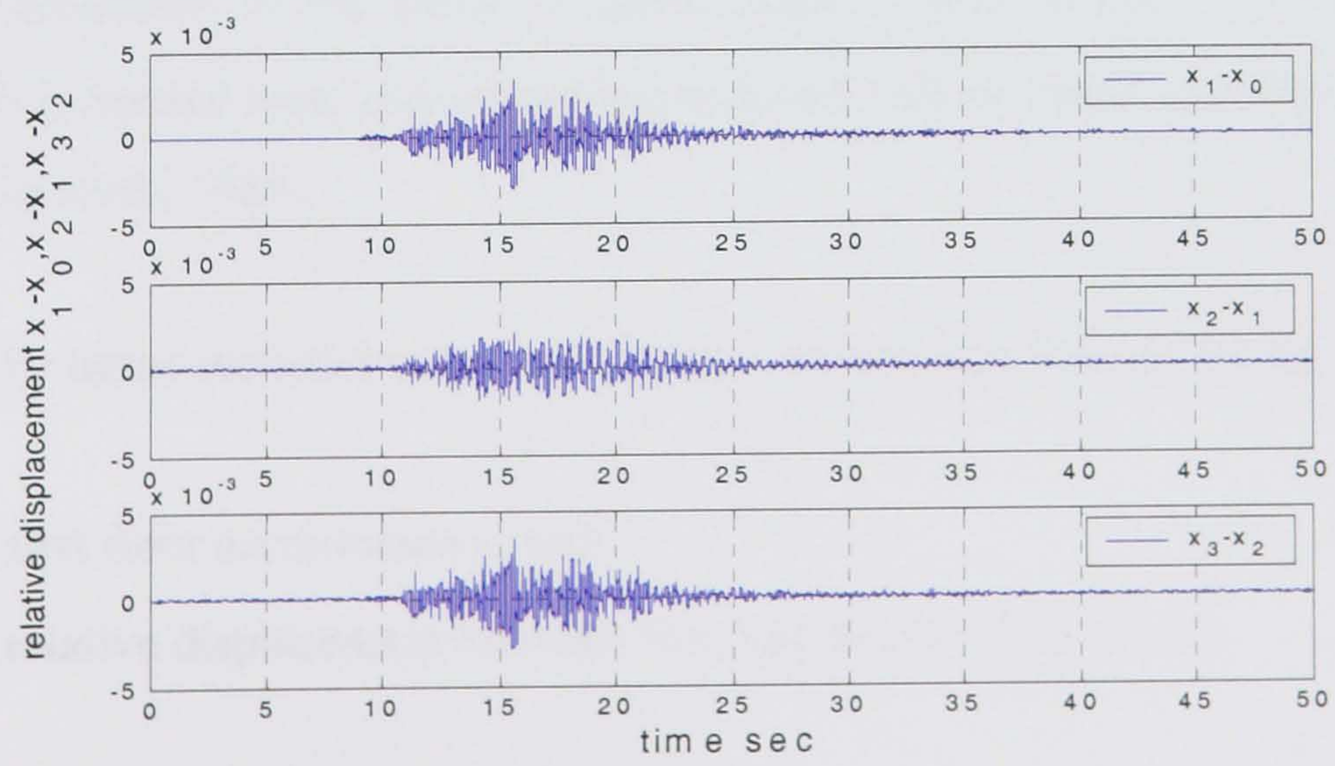

Figure 5.13 Interstorey drifts ($x_2 - x_3$, $x_1 - x_2$, $x_0 - x_1$)

The three different inputs represent different requirements for the controller. The impulsive load shows the effectiveness of the controller to target maximum peak responses, how quickly it can respond to large loads and how long it requires to reach the steady state (zero) and hence stabilise the structure. It can be assessed in the time domain. The sinusoidal input shows the effectiveness of controller to target loads at specific frequencies and the earthquake shows the effectiveness of the controller at all levels, minimising peaks, RMS, and targeting specific frequencies.

5.3.2 LQR Closed-loop responses

LQR design: After the response of the designed building under different kind of loadings was studied, a controller was designed. The LQR method was used first since it is the most widely accepted design method in structural control. It has a simple mathematical formulation that has resulted in good designs for many diverse applications.

The goal of LQR is to minimise the following performance index:

$$\hat{J}(u) = \int_0^\infty \left(x^T Q x + u^T R u + 2 x^T N u \right) dt \qquad (5.12)$$

subject to plant dynamic constraints $\dot{x} = Ax + Bu$. Note that the performance index is slightly more general then the one presented in an earlier section (equation 3.30) where the general exposition of the theory is given, since it also includes the "cross-term" $2x^T Nu$. This is needed here, and can be incorporated with minimal modifications to the theory [Maciejowski 1989].

In this case the terms included in the cost function (apart from the control signal u) are:

- the first floor acceleration $\ddot{x}_1$ and
- the relative displacement between first and second floor $x_2 - x_1$

as described by the problem specifications. Minimising each of the two terms indirectly minimises the other, but both will be included in the performance index. The aim is to choose matrices Q, R and N so that the given control problem can be formulated in the standard LQR problem formulation. Specifically, we wish to select matrices Q, R and N so that:

$$\hat{J}(u) = J(u) \tag{5.13}$$

where:

$$\hat{J}(u) = \left[\int_0^\infty \ddot{x}_1^2 + \rho_1 |x_2 - x_1|^2 + \rho_2 u^2 \right] dt \tag{5.14}$$

Here $\ddot{x}_1$ represents acceleration of mass m_1, $|x_2 - x_1|$ is the absolute relative displacement of m_1 and m_2, u is the control input effort (actuator voltage). Parameters ρ_1, ρ_2 are penalty coefficients on $|x_2 - x_1|$ and u respectively. The penalty coefficient for x_1 is taken as 1 (note that only the relative weighting between the three variables included in the cost function is important).

The terms involved in the integrand can be written as: (i) $\ddot{x}_1 = C_1^T x + Du$ where:

$$C_1^T = \left[\frac{K_1}{m_1} \quad -\frac{K_1 + K_2}{m_1} \quad \frac{K_2}{m_1} \quad 0 \quad \frac{C_1}{m_1} \quad -\frac{C_1 + C_2}{m_1} \quad \frac{C_2}{m_1} \quad 0\right]$$

and $D_1 = 1/m_1$, and thus

$$\ddot{x}_1^2 = (x^T C_1 + Du)(C_1^T x + Du) = x^T C_1 C_1^T x + 2x^T C_1 Du + D^2 u^2 \tag{5.15}$$

Further, (ii) $x_2 - x_1 = C_2^T x$, where

$$C_2^T = [0 \ -1 \ \ 1 \ 0 \ \ 0 \ 0 \ 0 \ 0]$$

and thus

$$\rho_1 (x_2 - x_1)^2 = \rho_1 x^T C_2 C_2^T x \tag{5.16}$$

Hence:

$$\ddot{x}_1^2 + \rho_1(x_2 - x_1)^2 + \rho_2 u^2 = x^T(C_1C_1^T + \rho_1 C_2 C_2^T)x + 2x^T C_1 D u + (\rho_2 + D^2)u^2 \quad (5.17)$$

which is in the standard form $x^T Q x + 2x^T N u + u^T R u$ by setting

$$Q = C_1C_1^T + \rho_1 C_2 C_2^T; \quad N = C_1 D; \quad R = \rho_2 + D^2 \quad (5.18)$$

Also, the standard assumptions of LQR theory must be satisfied [Maciejowski 1989]

- The pair (A, B) is stabilisable
- $R > 0$ and $Q - NR^{-1}N^T \geq 0$
- $(Q - NR^{-1}N^T, A - BR^{-1}N^T)$ has no unobservable modes on the imaginary axis

It may be easily seen that all the assumptions are satisfied for $\rho_1 > 0, \rho_2 > 0$, for example,

$$Q - NR^{-1}N^T = \left(1 - \frac{D^2}{\rho_2 + D^2}\right) C_1C_1^T + \rho_1 C_2 C_2^T \geq 0 \quad (5.19)$$

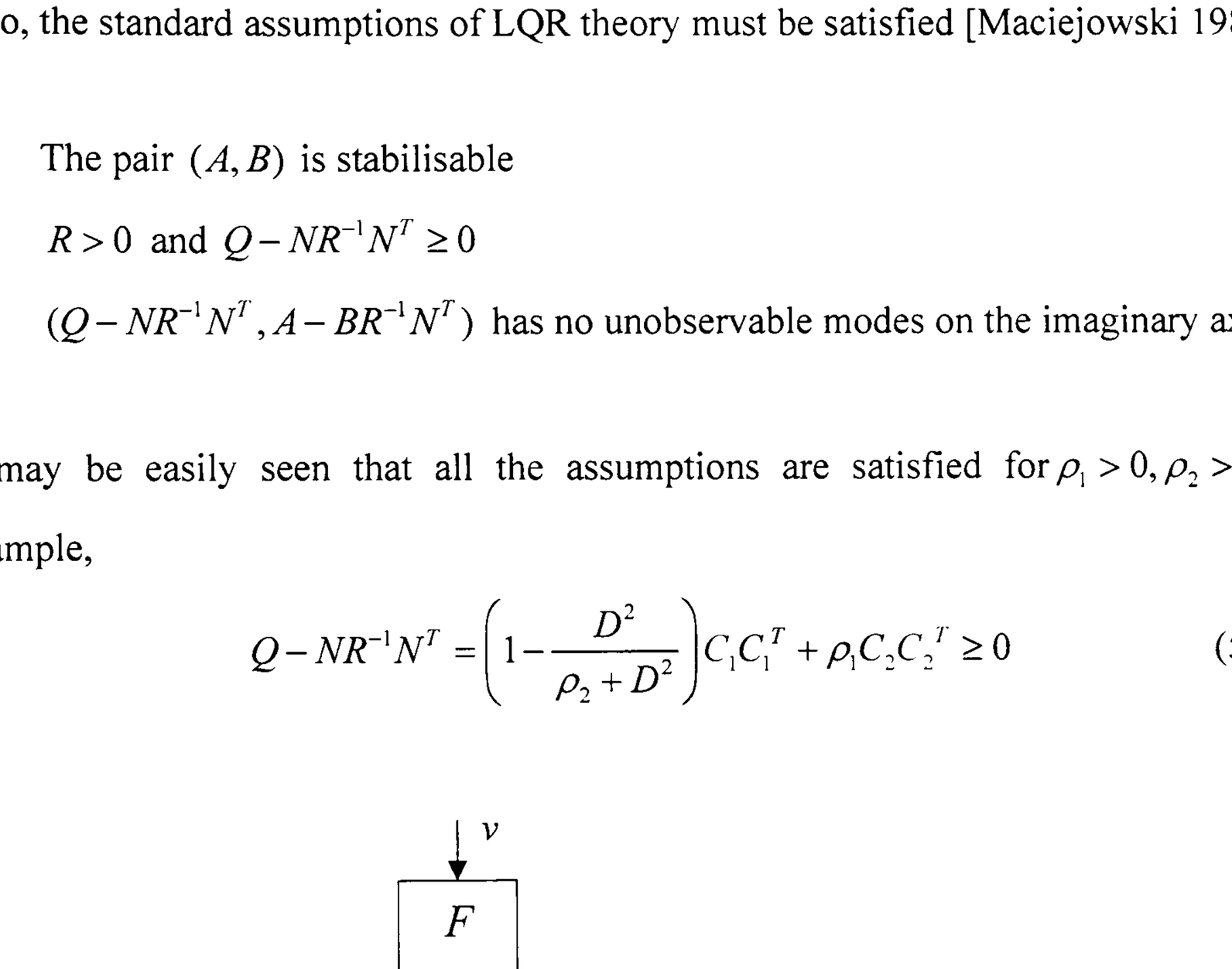

Figure 5.14 Block diagram of LQR

The penalty terms $\rho_1 = \rho_2 = 1$ were initially assumed for the design, placing equal emphasis to all three objectives. In the simulations, closed-loop responses are compared with the responses of the passive system.

Impulse response: The uncontrolled peak acceleration is $29.3\,m/s^2$ and the closed loop peak acceleration is $8.4\,m/s^2$. The LQR controller reduces the response by about 15 times after 4 cycles (or 0.47 seconds) only, which means that the controller has good transient response characteristics. The passive response, where the actuator is included but without injecting any forces, is very similar to the uncontrolled response but has larger damping, therefore after two seconds its response is almost half that of the uncontrolled response. The maximum is $27.3\,m/s^2$.

Note that the first peak is almost identical in both the closed- and uncontrolled responses. This is because the controller does not have enough time to respond to the impulsive loading under the actuator's bandwidth constraints. Similar results can be obtained from the relative displacement graph. The maximum closed-loop response is reduced to 3.3 *mm* from 12.6 *mm* for the passive system. In this case it takes longer for the displacement to decay to zero because the two floors vibrate with a small phase difference. But after 2 seconds the relative displacement is still significant (0.5 *mm*) as opposed to the accelerations which are almost zero.

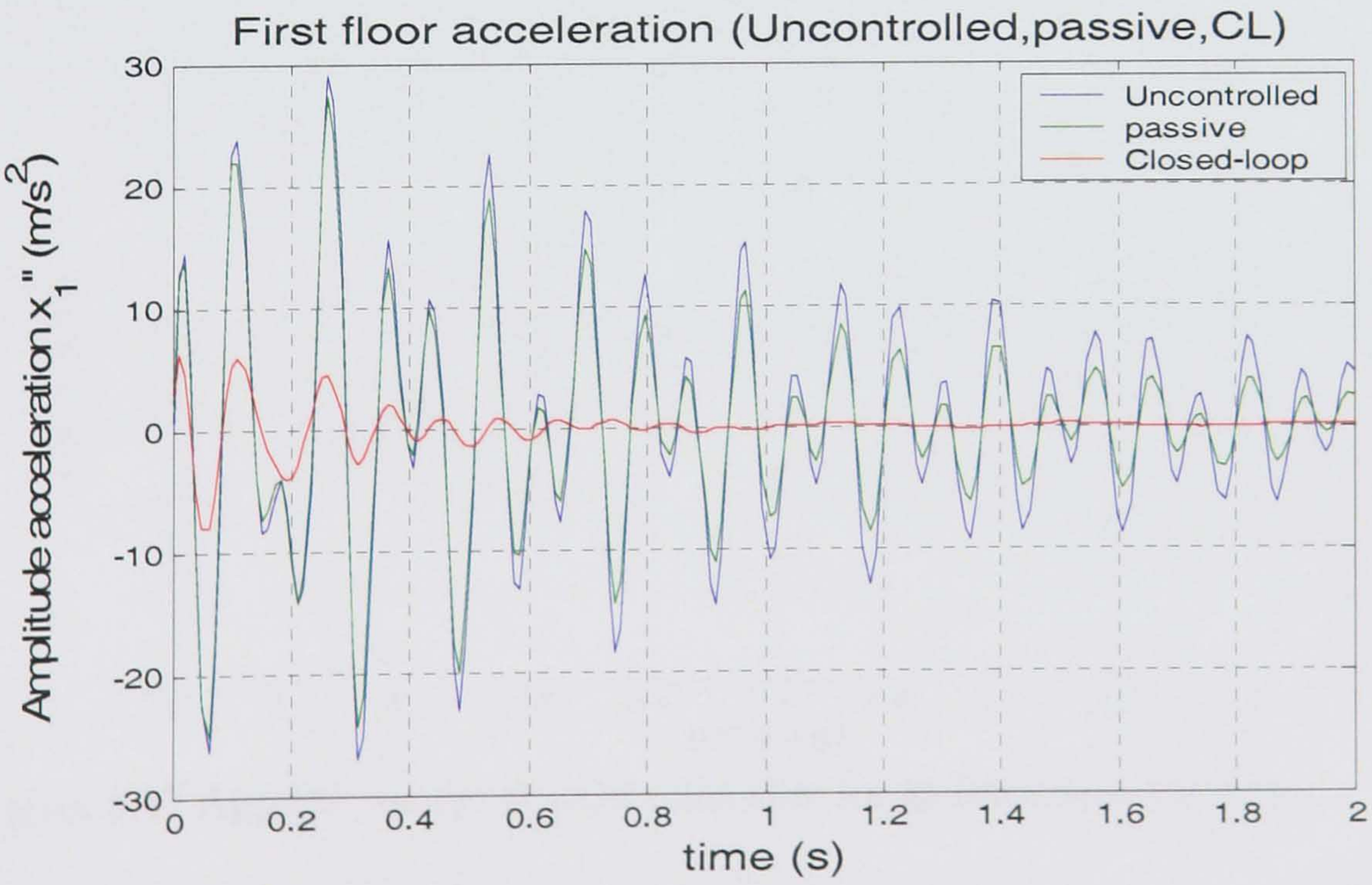

Figure 5.15 Passive and closed loop acceleration responses of impulsive loading

The main disadvantage of simulations having an impulse as the disturbance is that the maximum response usually occurs at the first peak because the disturbance force is applied only at time $t = 0$ and the controller does not have time to respond. Even a powerful controller will not be able to reduce this peak and will thus give a conservative indication about the controller's capabilities in more realistic situations where the disturbance signal is applied more gradually.

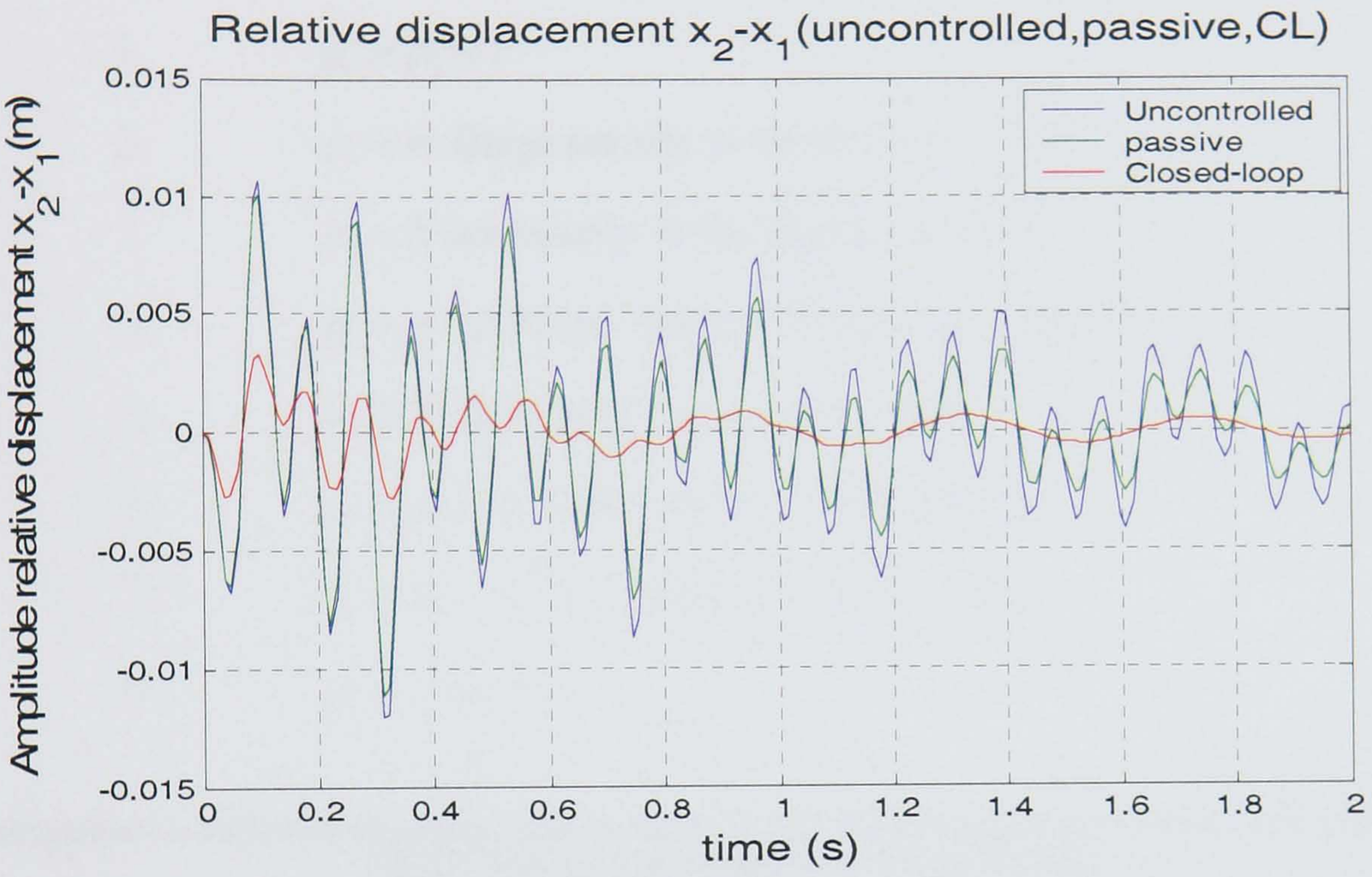

Figure 5.15 Passive and closed loop acceleration responses of impulsive loading

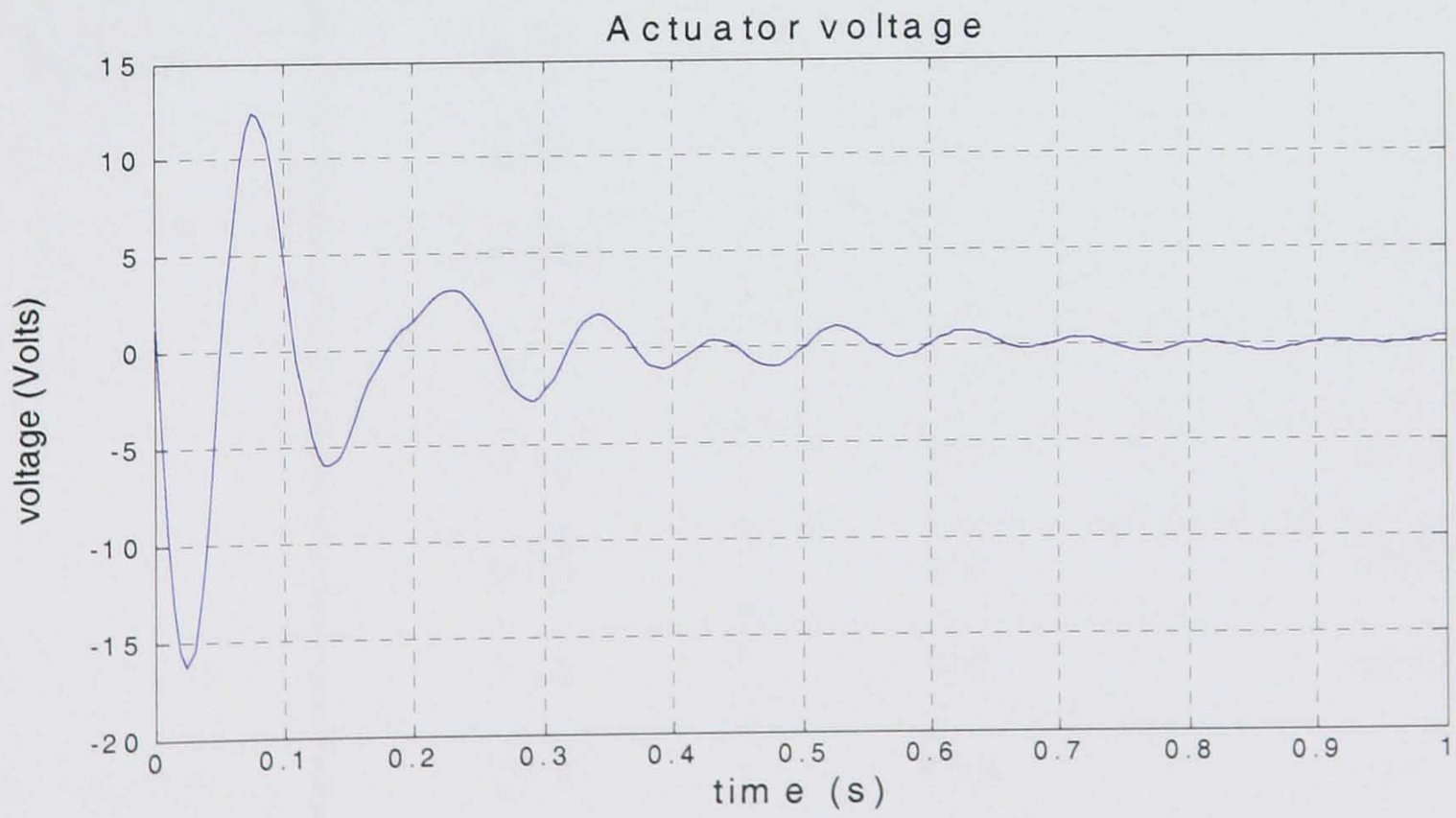

Figure 5.17 Applied voltage of LQR controller for an Impulsive loading

The simulation of the control signal reveals that a maximum voltage of 16.28 volts has been applied at around 0.03 seconds. The voltage gradually decreases and after 1 second the system control input is almost zero. Different values for the penalty coefficients have been used in order to reduce the peak voltage, e.g. by setting $\rho_1 = \infty$ thus assuming that the magnitude of the actuator force is unconstrained. A summary of results is included for eight distinct cases:

1. $\rho_1 = \rho_2 = 1$
2. $\rho_1 = \infty$ (large penalty in the interstorey drift)
3. $\rho_1 = 0$ (no penalty in the interstorey drift)
4. $\rho_2 = \infty$ (minimal amount of input force present)
5. $\rho_2 = 0$ (no penalty on actuator signal)
6. $\rho_1 = \rho_2 = 0$ (large penalty on acceleration)
7. $\rho_1 = \rho_2 = \infty$ (no penalty on acceleration)
8. $\rho_1 = \infty, \rho_2 = 0$

LQR Output comparison (peak values)			
	$\ddot{x}\left(m/s^2\right)$	$x_2 - x_1\left(mm\right)$	Voltage(Volts)
Uncontrolled	27.3	11.5	-
Passive	29.32	12.6	-
$\rho_1 = \rho_2 = 1$	8.36	3.3	16.28
$\rho_1 = \infty$	0.00061	$\cong 0$	26.83
$\rho_2 = \infty$	27.3	11.5	$\cong 0$
$\rho_1 = 0$	8.36	3.3	16.28
$\rho_2 = 0$	0.36	$\cong 0$	26.83
$\rho_1 = \rho_2 = 0$	0.36	$\cong 0$	26.83
$\rho_1 = \rho_2 = \infty$	27.3	11.5	$\cong 0$
$\rho_1 = \infty, \rho_2 = 0$	$\cong 0$	$\cong 0$	26.83

Table 5.4

In the case when there is no input constraint $(\rho_1 = \infty)$, both the interstory drift $x_2 - x_1$ and the acceleration are reduced to zero. The peak voltage is 26.83 volts. This is the control effort needed by the actuator, in order to make the response zero

From table 5.4 it is clear that the response is governed by the penalty on the control rather than that on displacement. There are three different cases: When the controller penalty is ∞, the accelerations and displacements are similar to those in the uncontrolled case, irrespective of the penalty on the displacement. When the control penalty is zero, which means that the control signal is unconstrained, the inter-storey drift is almost zero, although small fluctuations exist. In this case the controller tries to stop the higher floors from moving and therefore keeps the drifts to zero, but is unable to minimise the first floor acceleration because it is placed below the actuator. Finally, when the control effort penalty is set to one there is some change in the interstorey drift, which ranges from 0.45 *mm* to 3.3 *mm*, a significant difference. Obviously by increasing the inter-storey drift acceleration levels also increase.

In a realistic problem the maximum force applied by the system would be set by the type of actuator used (in terms of a constraint) and the system would have to minimise the objective function without exceeding this maximum force. This is not directly possible in the formulation of the LQR problem which penalises energy rather than peak levels, although, by adjusting the penalty factor this can be achieved indirectly via an iterative design-simulation procedure.

5.3.1. Sinusoidal input As stated earlier in the case where the input is a sine wave the steady-state response is governed by the frequency of the sine wave. The following two Bode plots show the gain of the open and closed loop systems with respect to the angular frequency ω, for the relative displacement $x_2 - x_1$ and the acceleration signal $\ddot{x}_1$. The horizontal axis is logarithmically spaced and the gain is given in *dB's*.

The gain drop at the frequencies corresponding to the three modes of vibration in the displacement graph are 18 *dB's* for the first two modes and 24 *dB's* where gain in $dB's = 20\log_{10}(\text{linear gain})$ for the third mode. In all other frequencies in the range displayed, the gain is about 5 *dB's*, while for very high frequencies, e.g.

above 100 *rads/s*, the gain rolls-off at a rate of 20 *dB's* /decade, a typical characteristic of LQR designs.

For the input $v = \sin 20t$ the controller stabilises the system and reduces the peak 3rd floor displacement from 0.597 to 0.31 *mm*. Since the force is now constantly acting, the response remains at constant levels for all time. In the case where the period of the input is the same as the natural period of the building $v = \sin 15.52t$ the closed-loop response is reduced to 1.1 *mm* and the response is stable.

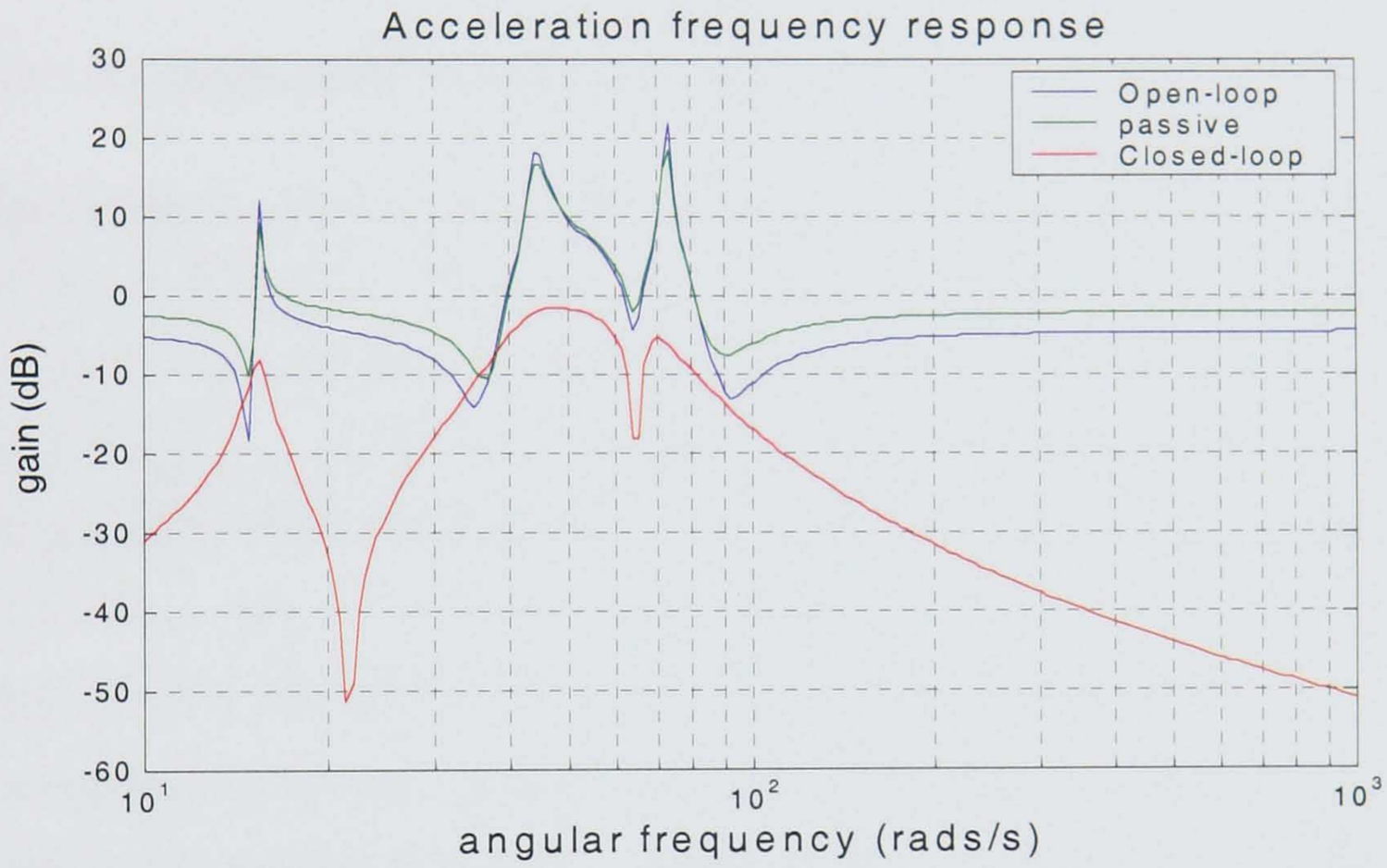

Figure 5.18 Frequency responses of acceleration

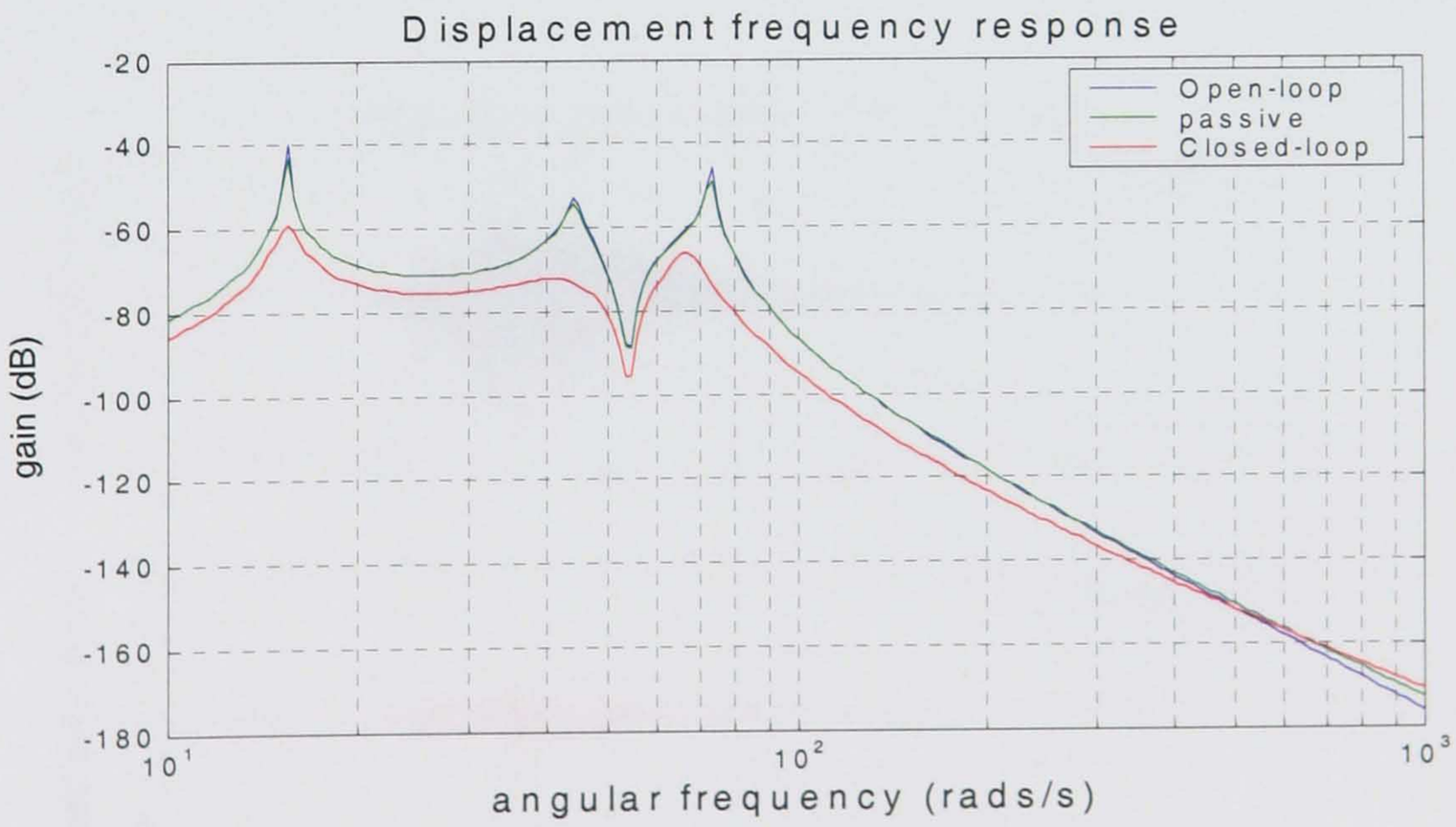

Figure 5.19 Frequency responses of displacement

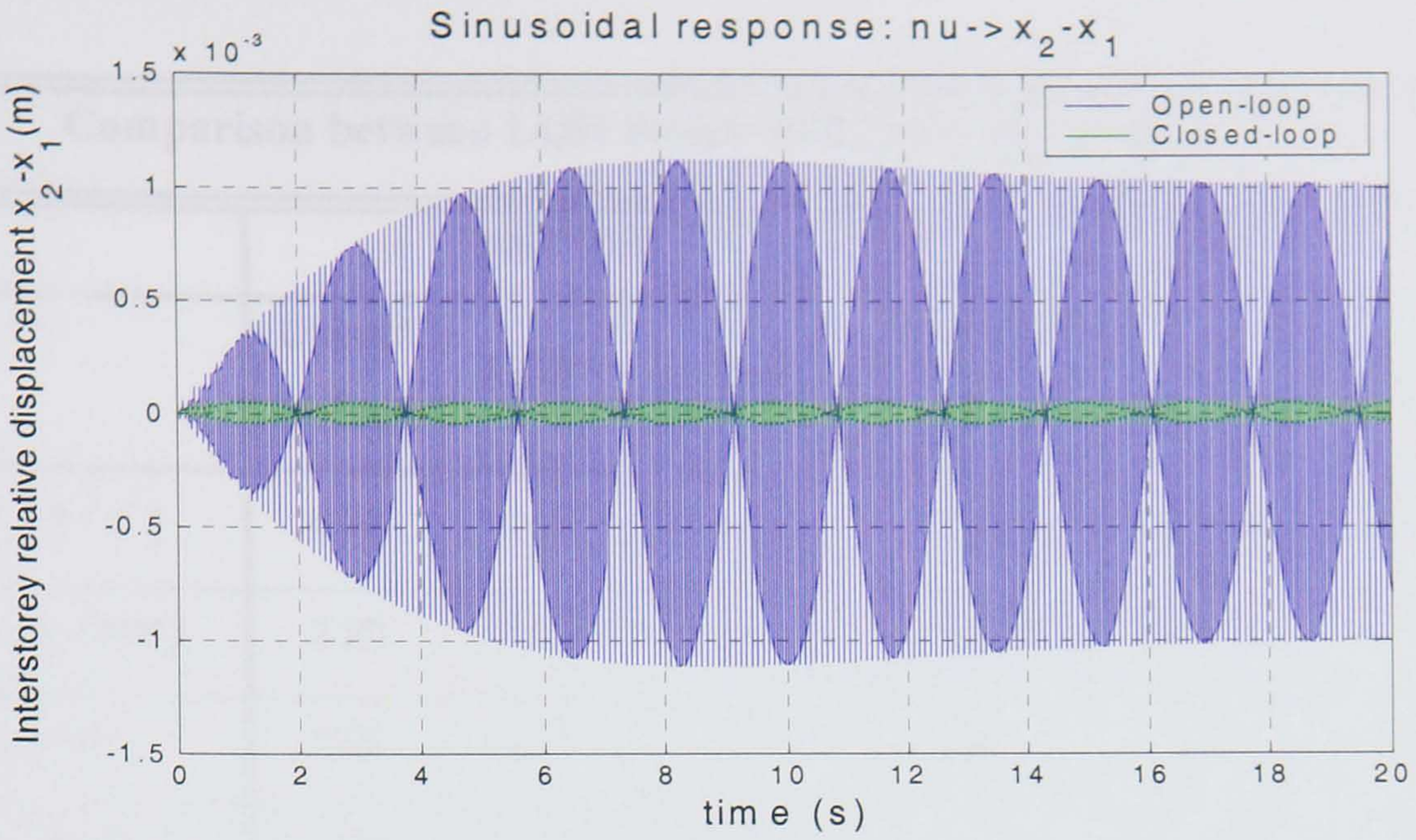

Figure 5.20 Displacement responses for sinusoidal input $\nu = \sin 70t$ (mode 3)

Earthquake signal: Figure 5.12 shows the normalised east-west acceleration applied at the base of the building, m_0. The disadvantages of the impulse and sine-input case are no longer present because the earthquake starts slowly before building up to its maximum amplitude and therefore the controller has more time to respond; in addition the signal contains several frequencies so the natural frequencies are excited by a reduced amount of energy. The maximum inter-storey drift x_2-x_1 is reduced from 2 *mm* to 0.83 *mm*, whereas the acceleration $\ddot{x}_1$ remains at similar levels (as noticed in the previous examples). Apart from the maximum values the root-mean-square values of all variables have been calculated to gain a further insight into the system. The controller minimises the RMS closed loop inter-storey drift from 0.46 *mm* to 0.11 *mm* and the

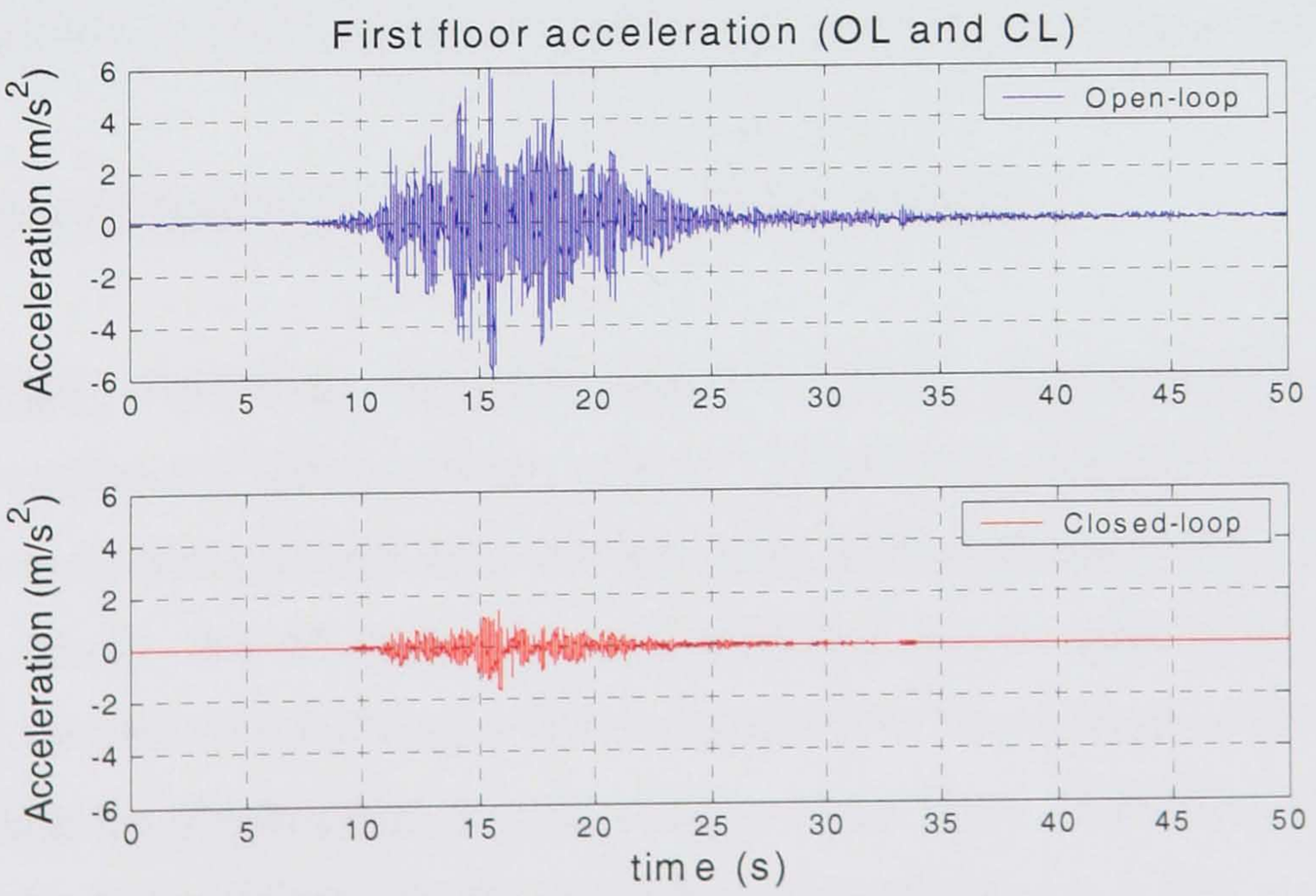

Figure 5.21 First floor uncontrolled and closed loop accelerations

Comparison between LQR design with and without filter $\rho_1 = \rho_2 = 1$						
	Peak value			RMS		
	Uncontrolled	LQR	% change	Uncontrolled	LQR	% change
$\ddot{x}_1 \left(m/s^2\right)$	6.38	1.65	74.2	0.90	0.182	79.7
x_2-$x_1 \left(mm\right)$	2.20	0.83	62.6	0.438	0.107	75.6
$x_0 \left(mm\right)$	1.93	1.79	7.5	0.233	0.213	8.4
$x_1 \left(mm\right)$	1.59	0.89	43.9	0.565	0.132	76.6
$x_2 \left(mm\right)$	3.62	1.09	69.9	0.743	0.169	77.3
$x_3 \left(mm\right)$	3.89	1.33	65.9	0.931	0.21	77
Voltage (V)		2.78			0.3	
Force (N)		3.58			0.38	

Table 5.5

acceleration from 6.38 to $1.65\,m/s^2$. The LQR controller succeeds in its goal to minimise the RMS value of the regulated variables and indirectly reduces the peak value as well to a smaller degree. The peak acceleration in the closed loop is 74% lower whereas the RMS values are 80% lower. Also the inter-storey drift peak is reduced by 63% and the RMS by 76%. These results indicate that there is scope in developing control algorithms that can directly minimise the peak levels of the regulated variables.

5.3.3 Linear Quadratic Gaussian (LQG) Control:

Kalman filter: The linear Quadratic Gaussian (LQG) control scheme is a linear quadratic regulator (LQR) combined with an optimal state estimator. Linear quadratic control is a powerful design tool, but has some restrictive assumptions for real case problems, mainly that all states are measurable and can be used directly for control action. In the case of a building it is too expensive to have sensors at every floor that measure both the displacement and the velocity of the floor. Therefore a filter is added to the system that estimates the states and uses the estimates as if they were the "true"

measured variables. There are several methods and algorithms for state estimation, the most commonly used method being the Kalman-Bucy filter [Davis and Vinter 1985].

The Kalman filter is an exact replica of the system. Since information is not known about all the states, the information from the known measurements together with the replicated dynamics helps to estimate all states. The estimated and measured outputs are compared and the Kalman filter iterates until the estimated state $\hat{x}$ matches the real state x. The aim of the Kalman filter is to minimise the error

$$e(t) = \hat{x}(t) - x(t) \tag{5.20}$$

in the mean squared sense. The full structure of the Kalman filter is shown in Figure 5.22. The state space equations are assumed to be of the form:

$$\dot{x} = Ax + Bu + \Gamma\omega \tag{5.21}$$

$$u = Cx + Du + \nu \tag{5.22}$$

where ω and ν are unknown disturbance signals modelled as white noise signals (zero-mean, stochastic processes uncorrelated in time), i.e.

$$E[\omega(t)] = 0 \quad \forall t \tag{5.23}$$

$$E[\nu(t)] = 0 \quad \forall t \tag{5.24}$$

$$E(\omega\omega^T) = W\delta(t-s) \geq 0 \tag{5.25}$$

$$E(\nu\nu^T) = V\delta(t-s) > 0 \tag{5.26}$$

$$E(\omega\nu^T) = N\delta(t-s) \tag{5.27}$$

where

$$\begin{aligned} \delta(t-s) &= 1 \quad t = s \\ \delta(t-s) &= 0 \quad t \neq s \end{aligned} \tag{5.28}$$

The Kalman filter constructs a state estimate $\hat{x}$ that minimises the steady-state error covariance:

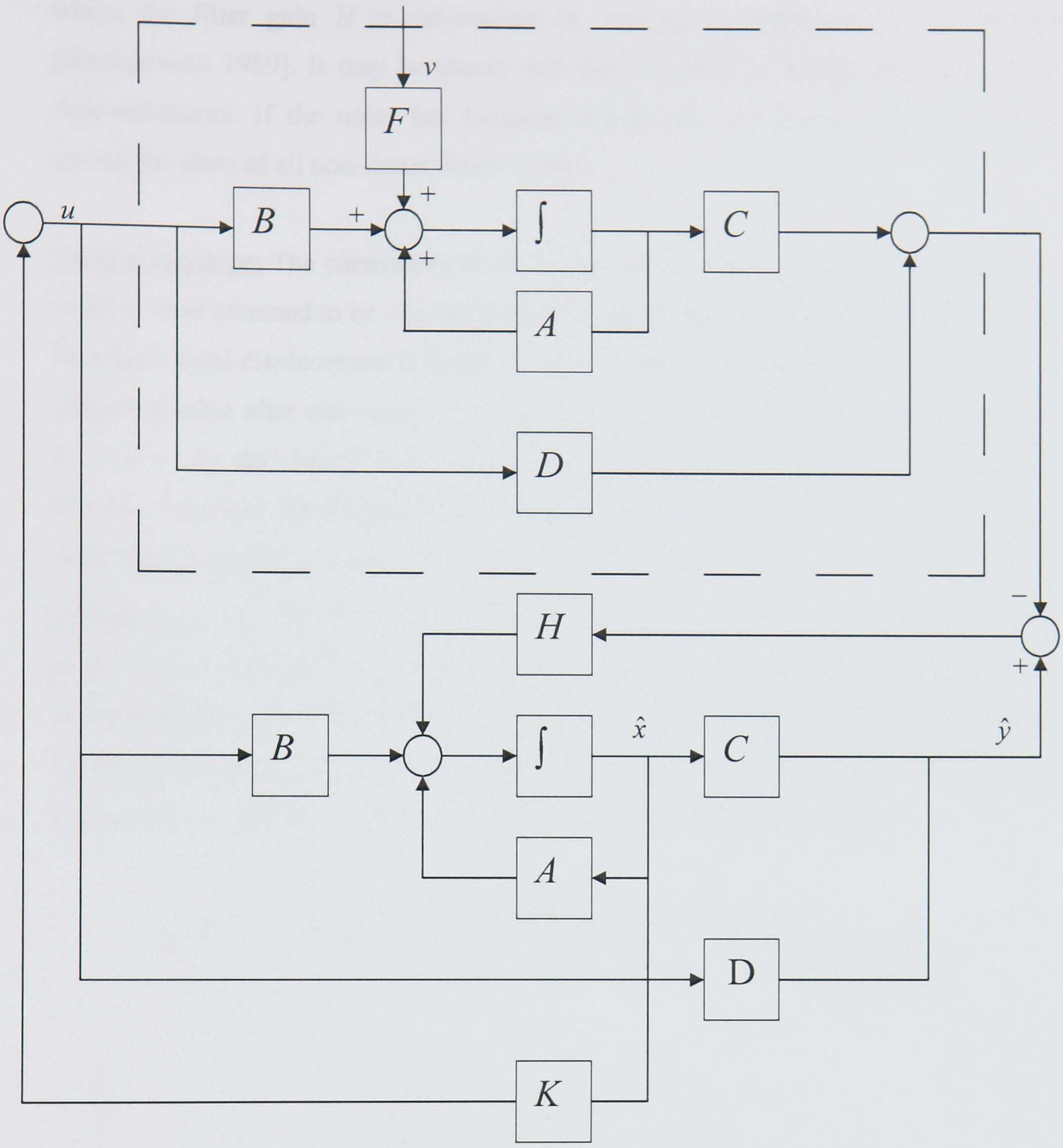

Figure 5.22 Block diagram of Kalman filter

$$P = \lim_{t \to \infty} E(\{x - \hat{x}\}\{x - \hat{x}\}^T) \tag{5.29}$$

The optimal solution to this problem is the Kalman filter with state equations

$$\dot{\hat{x}} = A\hat{x} + Bu + H(C\hat{x} - Cx) \tag{5.30}$$

$$\hat{y} = C\hat{x} + Du \tag{5.31}$$

where the filter gain H is determined by solving an algebraic Riccati equation [Maciejowski 1989]. It may be shown that Kalman filter is optimal among all linear state-estimators. If the noise has Gaussian distribution the Kalman filter is optimal among the class of all non-linear filters as well.

Impulse response: The parameters W, V, N where chosen as W=2, V=0.01 and N=0, i.e. v and ω were assumed to be uncorrelated with each other. The estimated value of the 3rd floor horizontal displacement is larger in the first peak but then is almost identical to the measured value after one cycle, i.e. the estimate converges to the true state in the limit as $t \to \infty$. In the second case where inter-storey drift is measured, the difference between LQR and the estimated LQG is less in the first peak but converges slower to zero. This is because the inter-storey drift is a function of two states (x_2, x_1) as opposed to one state in the third floor displacement. The speed of convergence depends on the parameters W, V representing process and measurement noise covariances, respectively. In real applications the appropriate values of both W and V values can easily be obtained by experimentation and manufacturers data for the sensors used. Thus, LQG design is very similar to LQR and in our simulations produces very similar results

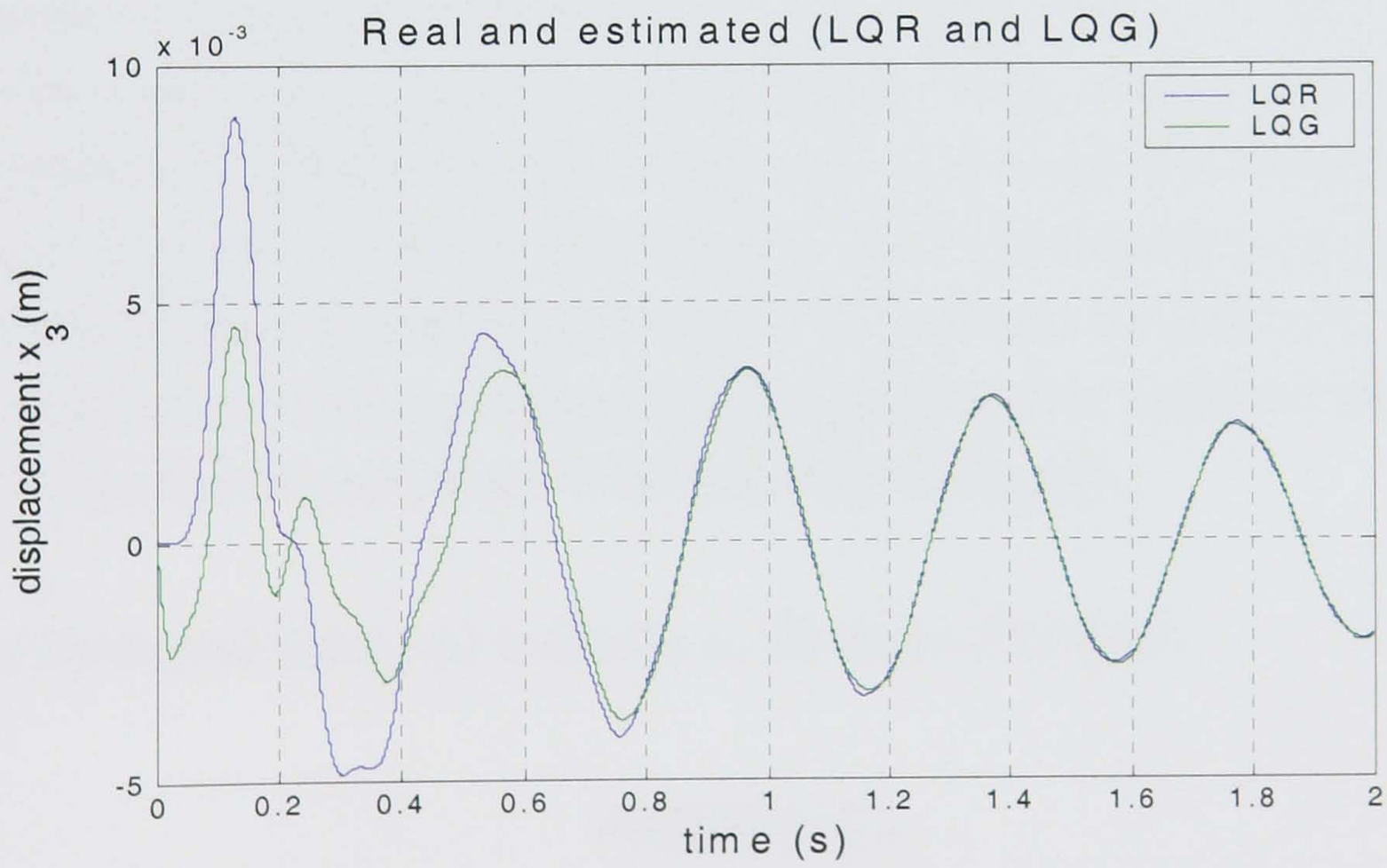

Figure 5.23 Comparison between real (LQR) and estimated (LQG)

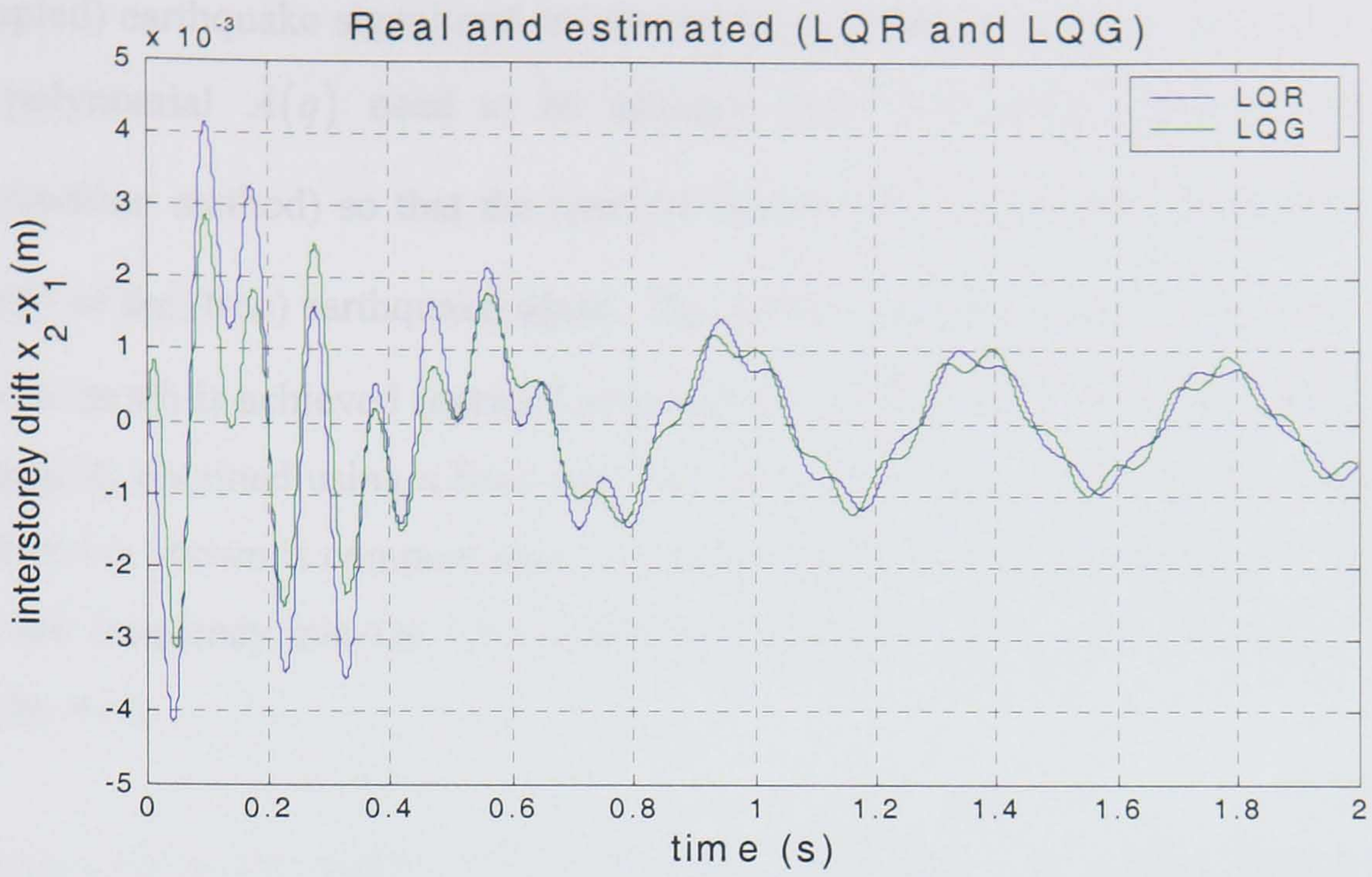

Figure 5.24 Comparison between real (LQR) and estimated (LQG) $x_2 - x_1$

5.3.4. LQR with identification filter

5.3.4. Identification filter design: The next design is an LQR controller with the addition of a shaping filter. The filter forces the controller to place more emphasis to the frequencies of the input. When the input is the earthquake signal, its Fourier transform can be calculated from which the distribution of the signal's energy with frequency can be obtained. An identification filter is designed by approximating the spectral plot of the signal, by placing emphasis in those frequency ranges where the energy is concentrated and less emphasis at other frequency ranges. By increasing the order of the filter the accuracy is increased, but so is the order and complexity of the controller. Diagram 5.25 shows the Fourier transform plot of the Loma Prieta Earthquake.

The (discretised) signal $y(t)$ is fitted by an AR-model of the form:

$$A(q)y(t) = e(t) \tag{5.32}$$

using Matlab's Identification Toolbox. The white noise signal $e(t)$ is filtered through the discrete filter $1/A(q)$ and produces an output, say $n(t)$ which corresponds to the

(sampled) earthquake signal and is interpreted as a random process. The coefficients of the polynomial $A(q)$ need to be selected (e.g. by a least squares fit or another optimisation method) so that the spectral density of $n(t)$ matches closely the spectral density of the (true) earthquake signal. The order of the polynomial $A(q)$ can vary until a close match is achieved (optimal order selection techniques can also be applied). The optimal fit obtained using a first- and second-order filter is shown below. This spectral distribution shown is common among earthquakes but has a strong energy concentration in a low frequency interval. The fit obtained using the second-order filter was judged to be adequate.

To make use of the spectral information of the real earthquake signal (captured by the filter) the following procedure is used. First the filter was transformed to continuous time (using a bilinear transform) and its transfer function was obtained in the form $F(s) = (sI - A)^{-1} B$. Next the dynamics of the filter were absorbed to the dynamics of the plant, as shown in Figure 5.26. Denoting by $\nu(t)$ the state (and output) of the filter, the combined state-space realisation of the structure and filter can be written as:

$$\begin{bmatrix} \dot{x} \\ \dot{\nu} \end{bmatrix} = \begin{bmatrix} A & F \\ 0 & A_f \end{bmatrix} \begin{bmatrix} x \\ \nu \end{bmatrix} + \begin{bmatrix} B \\ 0 \end{bmatrix} u + \begin{bmatrix} 0 \\ B_f \end{bmatrix} e \tag{5.33}$$

$$[y] = [C \quad 0] \begin{bmatrix} x \\ \nu \end{bmatrix} + [D] u \tag{5.34}$$

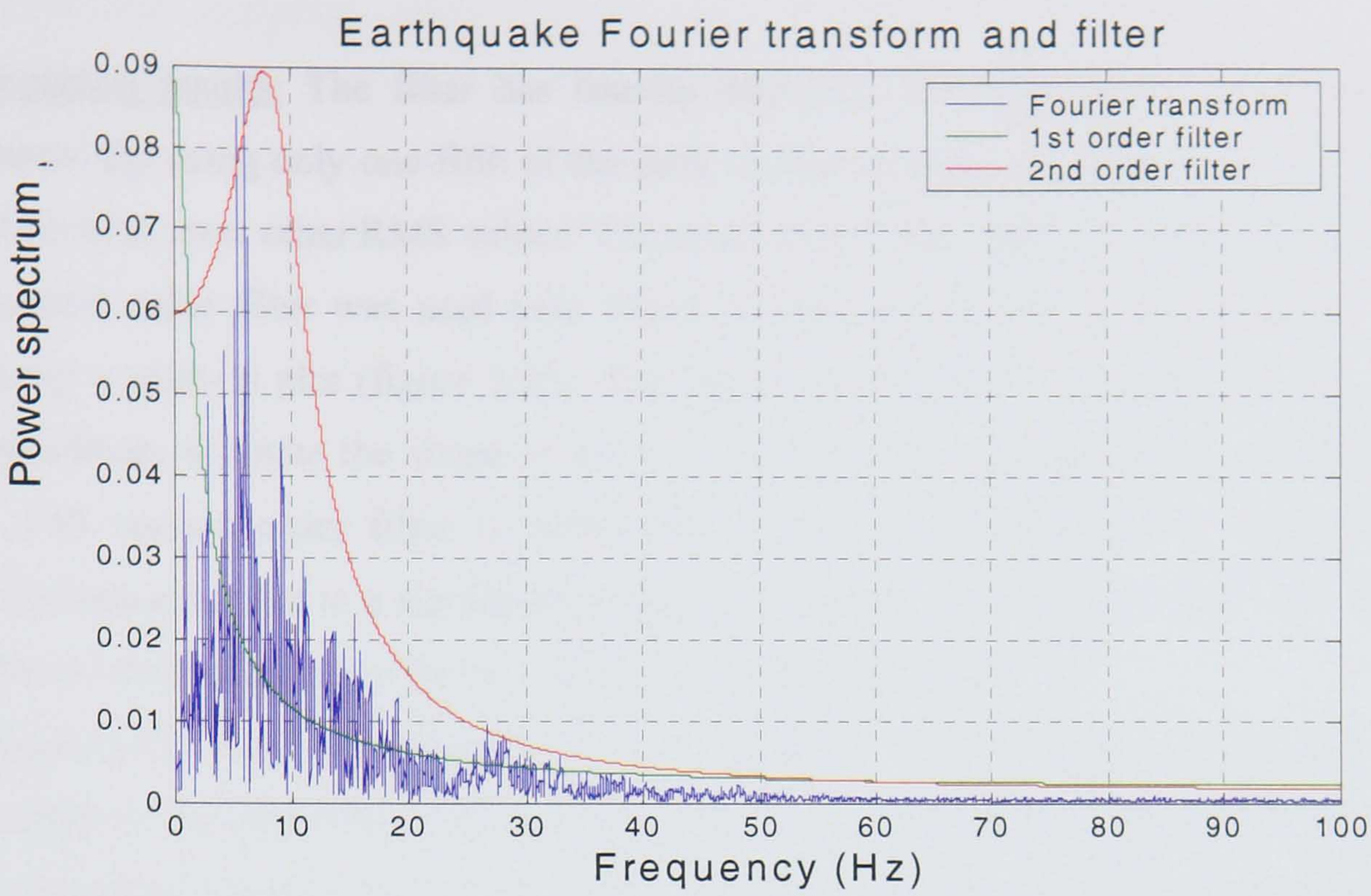

Figure 5.25 Fourier transform of earthquake frequencies and filter idealisation

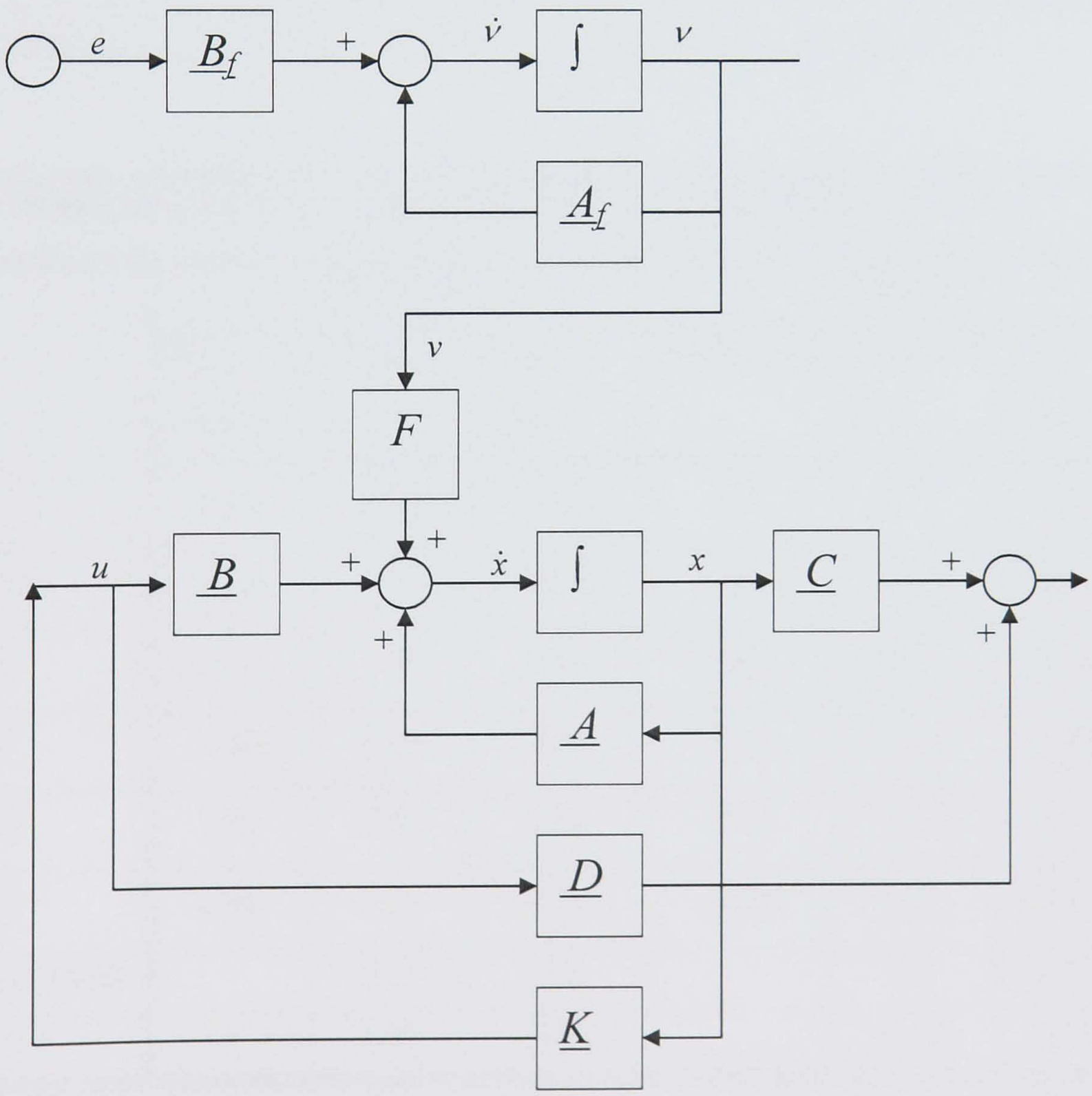

Figure 5.26 Block diagram of identification filter

Simulation results: The filter has heavily improved the performance of the control scheme. By using only one-fifth of the peak voltage the acceleration was 5 times lower and so were most other RMS values. The peaks were of the order of 4 times lower. Only a second order filter was used here which is sufficient as can be seen from the Fast Fourier transform plot (figure 5.25). The 1st order filter is not adequate as it does not approximate accurate the shape of the signal's spectrum, whereas the improvement of fit with second order filter is significant. A higher order filter still improves the performance but not to a significant extent. By using the second order filter, the degree of the controller increases by two additional poles – and zeros.

Designing for such an earthquake is a very idealistic scenario because it assumes that the input is the known EQ. Different EQ would have a different FFR response therefore the controller designed from a filter obtained from a particular earthquake signal may be less optimal or even inadequate. If several "standard" earthquake signals are analysed then an average FFR can be obtained, typical of earthquakes in a certain geographical region. This would result in the best LQR design for this class of inputs.

Comparison between LQR design with and without filter $\rho_1 = \rho_2 = 1$

	Peak value			RMS		
	No control	Closed loop	Filter LQR	No control	Closed loop	Filter LQR
$\ddot{x}_1\left(m/s^2\right)$	6.38	1.65	0.42	0.9	0.18	0.042
x_2-$x_1\left(mm\right)$	2.20	0.83	0.14	0.44	0.11	0.019
$x_0\left(mm\right)$	1.93	1.79	0.43	0.23	0.21	0.049
$x_1\left(mm\right)$	1.59	0.89	0.18	0.56	0.13	0.02
$x_2\left(mm\right)$	3.62	1.09	0.16	0.74	0.17	0.021
$x_3\left(mm\right)$	3.89	1.33	0.16	0.93	0.21	0.021
Voltage (Volts)		2.78	0.6		0.3	0.069
Force (N)		3.58	0.77		0.38	0.088

Table 5.6

Acceleration response spectra have been developed, appropriate for specific geographical regions. The use of this information is very important in designing controllers. As has been shown by the previous example, the use of any possible information about the input is vital.

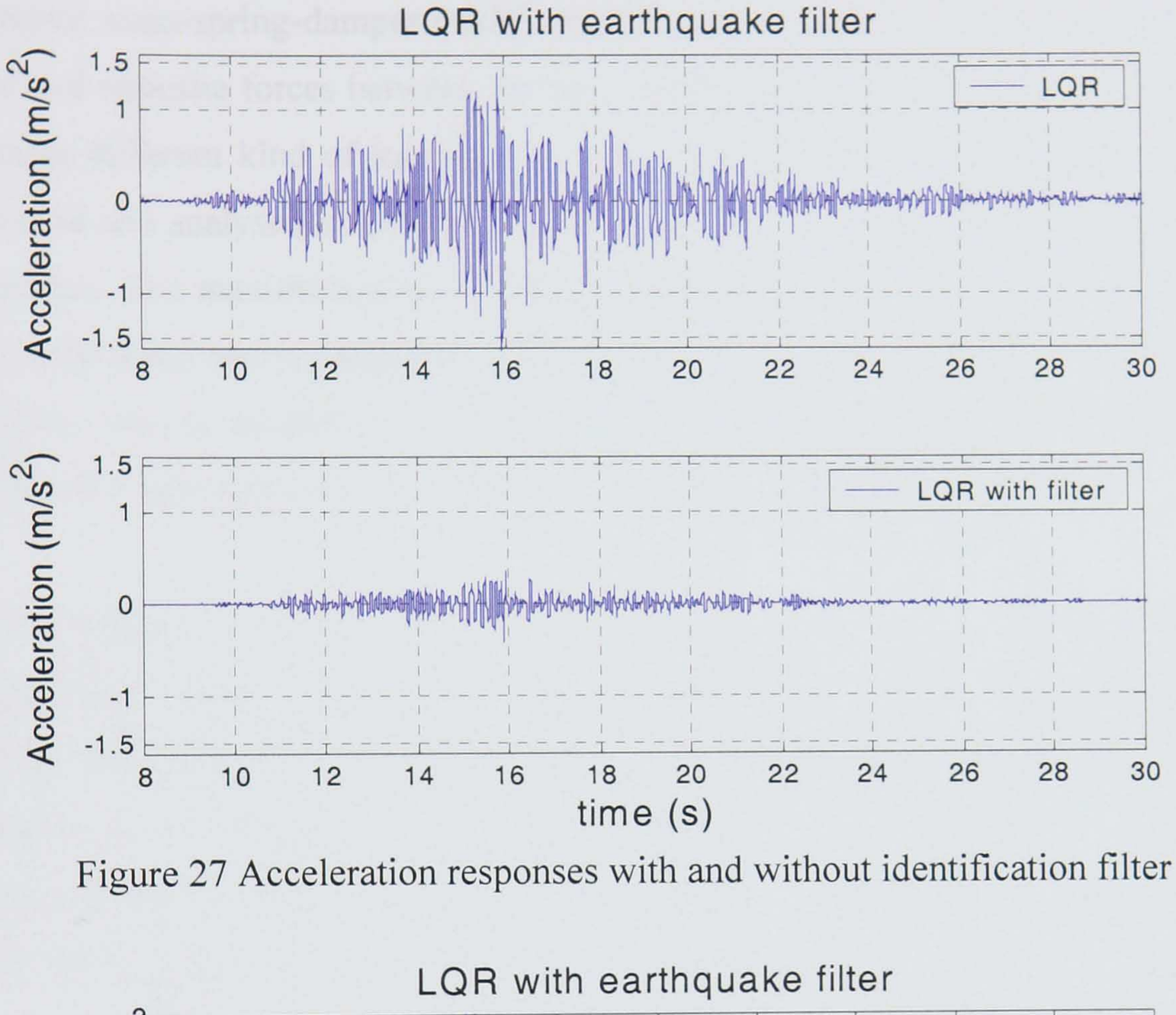

Figure 27 Acceleration responses with and without identification filter

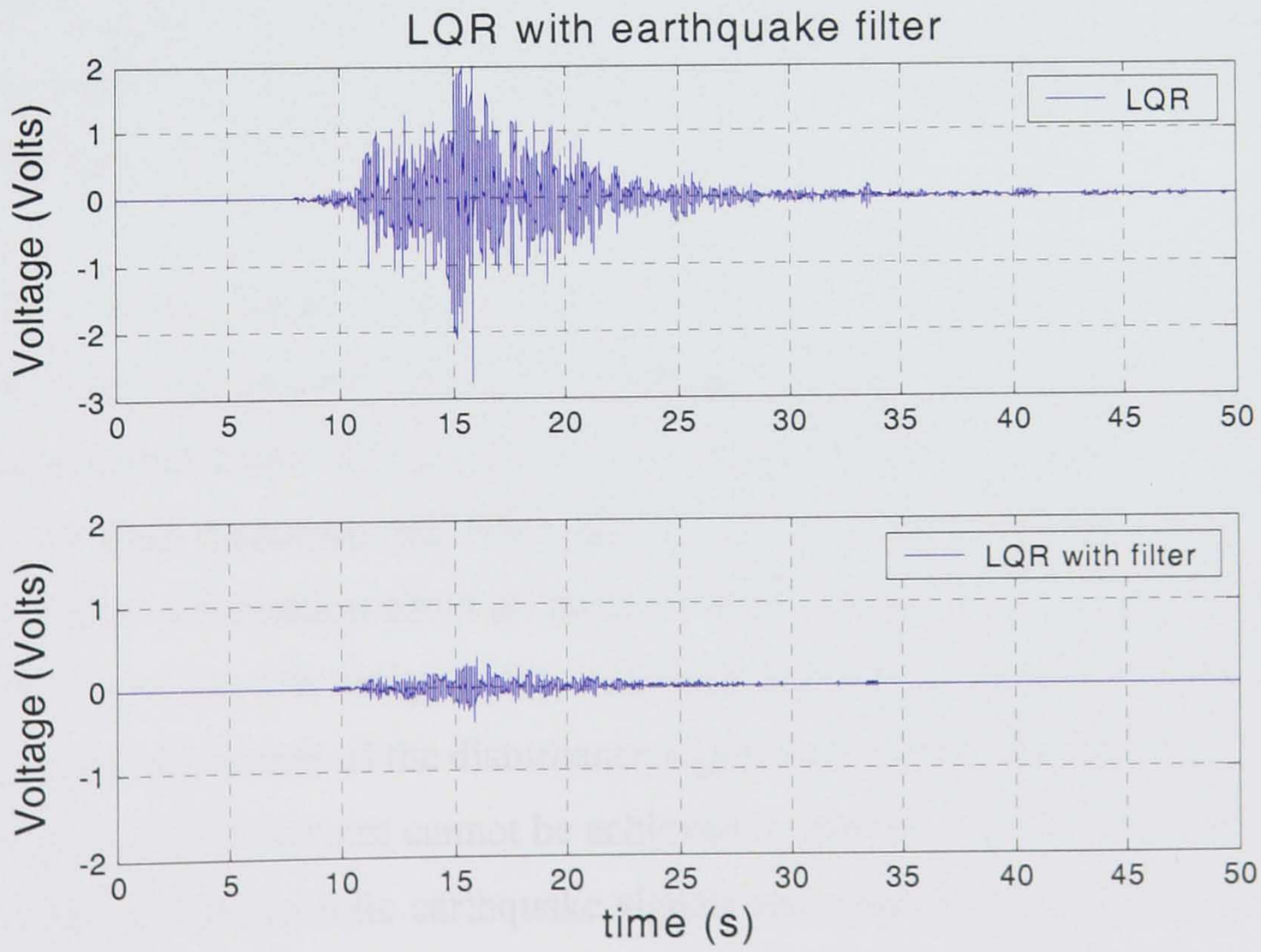

Figure 28 Control input with and without identification filter

5.4. Summary

In this chapter a building was modelled employing active control. This is a 3 storey regular building which includes base dynamics. The structure was modelled as a lumped parameter mass-spring-damper model. An active tendon control was chosen, producing equal and opposite forces between the base and first floor. The response of the building for three different kind of loadings impulse, sinusoidal and an earthquake signal was simulated and analysed extensively. Several metrics were used to validate the designed controllers, like maximum peak response, RMS values, settling time (i.e. time to reach the steady state) and resistance to inputs of several harmful frequencies. The controller objective was to minimise the first floor acceleration and the relative displacement between the first and second floor subject to realistic control effort levels.

All the designs obtained were stable and by tuning the performance penalties the response was further optimised. When a Kalman filter was used the design was still optimal and matched the initial LQR design with acceptable accuracy. The only limitation of the method is its inability to minimise the first peak for impulsive loads. This is because the controller does not have enough time to respond to this sudden load. Furthermore, the penalty coefficients used in the formulation of the performance index which is optimised can not impose direct constraints on the maximum control signal magnitude allowable for the specific actuator used.

The last part of the design incorporated an identification filter which was augmented to the model. Here the spectral content of an earthquake signal was obtained from recorded data and assumed fixed. The controller used around 5 times less effort to achieve a 5 times lower peak responses and RMS values. This is a large improvement and shows that any known information about an input is heavily improving the performance of the controller. However, this design is too ambitious since in real cases it is not possible to know the spectral content of the disturbance signal with this accuracy and thus this level of performance improvement cannot be achieved in practice. In the case of earthquakes, if a multiple of characteristic earthquake signals are recorded in a certain geographical region, then an average frequency content characteristic of the region can be obtained

with some accuracy. Using this information for control design could then prove useful for additional protection of a building in this geographical region.

Overall, LQG is effective, stable and flexible design method. One slight drawback is the inability of the method to reduce directly peak levels. From the definition of the problem, LQR is penalising energy levels, not peak responses. In structural engineering failure occurs when maximum deformation or force level is exceeded and thus tuning of the method or alternative optimisation techniques may be appropriate.

CHAPTER 6

H_∞ ROBUST CONTROL

6.1. Introduction

This chapter is a continuation of the work presented in the previous one. The same structure is designed and evaluated, this time using H_∞ control methods. H_∞ controllers are less common than their LQG counterparts but are also widely used in control design. As opposed to LQG, H_∞ is considered a "robust control" method. Robust control aims primarily at designing controllers that keep the system stable despite the presence of model uncertainty and external disturbances. H_∞ control is a strong tool when various types of uncertainties, unknown external perturbations and errors in the system exist. The control design follows a "worst-case" methodology and can result in conservative designs if the set of uncertainty is too large. This is however, closer to real life applications because physical systems can never be exactly modelled, especially as LTI models. In structures model uncertainties are common in terms of stiffness and damping parameters or high- frequency unmodelled dynamics. In this chapter no uncertainties are considered explicitly and H_∞ controllers are assessed in terms of their nominal performance, mainly in comparison to LQG-based design.

The Euclidean norm of a vector denotes the square root of the sum of squares of all its elements, i.e. $\|x\| = \sqrt{\sum_i x_i^{\,2}}$. The largest singular value of a matrix A is an induced norm defined as:

$$\bar{\sigma}(A) = \max_{x \neq 0} \frac{\|Ax\|}{\|x\|}$$

and thus defines the largest "gain" between the input and output space. In the dynamic case when $A(s)$ is a function of the complex variable s, the infinity-norm of $A(s)$ is defined as:

$$\|A(s)\| = \max_{\omega \in \Re} \bar{\sigma}[A(j\omega)]$$

and thus denotes the maximum energy transfer between the input and output spaces along all frequencies and directions. The aim of H_∞ control is to minimise the maximum singular value of an appropriate closed-loop transfer function over all frequencies, while making the closed-loop transfer function stable (all poles in the left half plane). A large mathematical background is involved in the theory of H_∞ control relative to the simpler theory involved in the solution of the LQG problem. Here, only those aspects needed for the design of H_∞ controllers are considered.

6.2. H_∞ Control design

The H_∞ design problem is extensively described in chapter 3.6.4. The main points are summarised below. The problem is often posed in the framework of a generalised plant in feedback connection with the controller, as shown in figure 6.1. The plant is connected to a controller K whose aim is to stabilise the closed loop system and minimise the infinity norm of the transfer function from the disturbance v to the regulated output z. The generalised plant is partitioned into P_{11}, P_{12}, P_{21}, P_{22}, where P_{22} is the true plant and the other three transfer functions are defined by the type of optimisation problem which is formulated. First define the generalised plant:

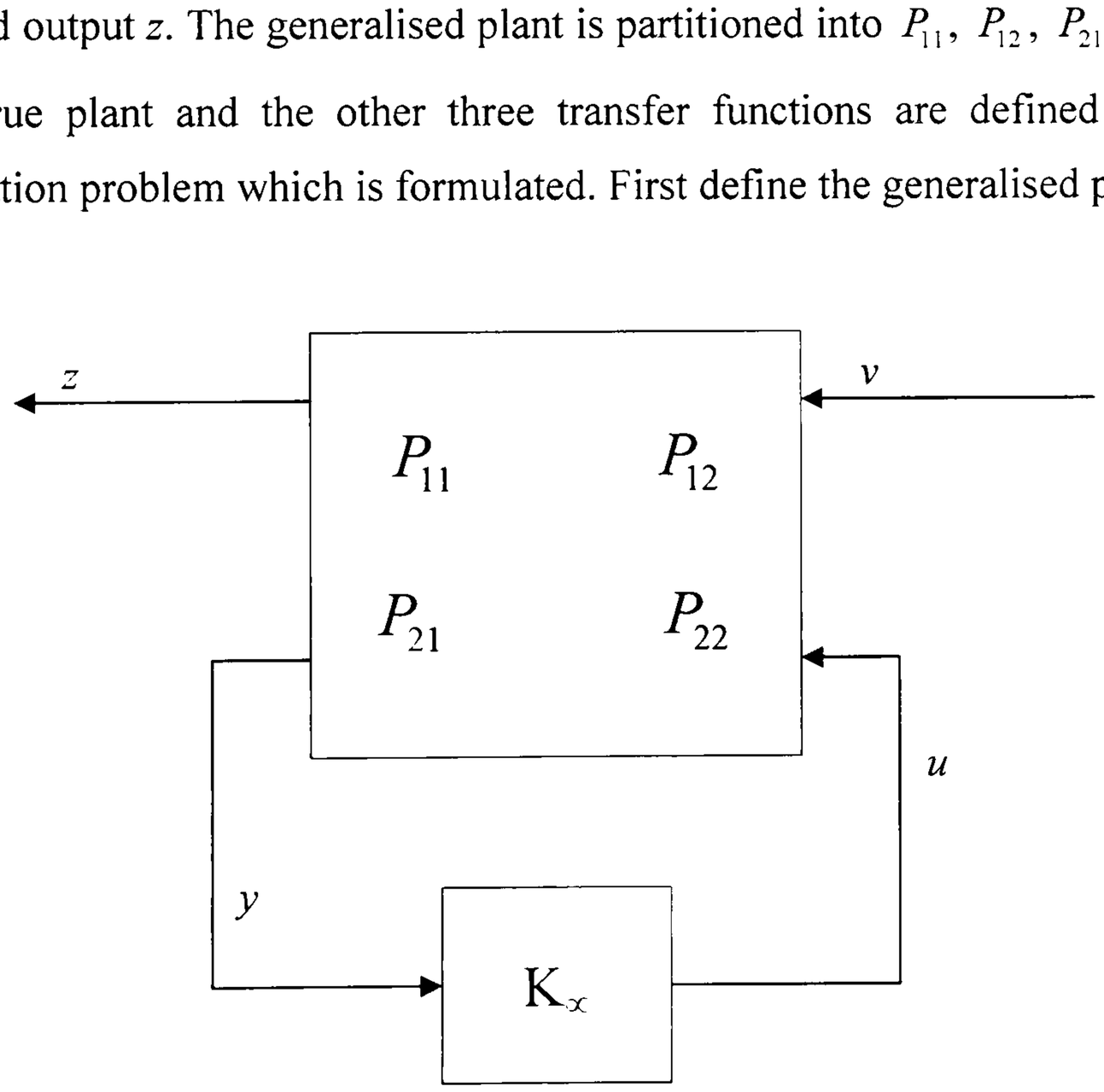

Figure 6.1 Generalised Plant

The four signals in figure 6.1 are v, z, y and u where.

v is the external disturbance

z is the regulated output

y is the measurement, and

u is the control input.

For our purposes we define v to be the earthquake signal force acting on m_0. The regulated signals are defined as:

$$[z] = \begin{bmatrix} \ddot{x}_1 \\ \rho_1(x_2 - x_1) \\ \rho_2 u \end{bmatrix} \tag{6.1}$$

where ρ_1 and ρ_2 are weighting (penalty) terms, initially taken to be frequency independent. These terms have a similar meaning as in LQR, and emphasise each objective against the others. Both were initially set to one, for direct comparison with the LQR design.

The generalised regulator $P(s)$ has a state space realisation:

$$\dot{x} = Ax + Bu + Fv,$$

$$\begin{bmatrix} z_1 \\ z_2 \\ z_3 \end{bmatrix} = \begin{bmatrix} \ddot{x}_1 \\ \rho_1(x_1 - x_2) \\ \rho_2 u \end{bmatrix} = \begin{bmatrix} C_1 \\ C_2 \\ 0 \end{bmatrix} \underline{x} + \begin{bmatrix} D_1 \\ 0 \\ \rho_2 \end{bmatrix} u + \begin{bmatrix} 0 \\ 0 \\ 0 \end{bmatrix} v \tag{6.2}$$

where

$$C_1 = \begin{bmatrix} \frac{k_1}{m_1} & -\frac{k_1 + k_2}{m_1} & \frac{k_2}{m_1} & 0 & \frac{c_1}{m_1} + \frac{k_f k_e}{m_1 R} & -\frac{c_1 + c_2}{m_1} + \frac{k_f k_e}{m_1 R} & \frac{c_2}{m_1} & 0 \end{bmatrix}$$

$$C_2 = \begin{bmatrix} 0 & -1 & 1 & 0 & 0 & 0 & 0 & 0 \end{bmatrix}$$

and

$$D_1 = \begin{bmatrix} 0 & \frac{k_f}{m_1 R} \end{bmatrix} \rho_1$$

The measured output is:

$$\begin{bmatrix} y_1 \\ y_2 \end{bmatrix} = \begin{bmatrix} C_1 \\ C_2 \end{bmatrix} [\underline{x}] + \begin{bmatrix} D_1 \\ 0 \end{bmatrix} u \tag{6.3}$$

the two measurements y_1, y_2 being the first floor acceleration $\ddot{x}_1$, and the inter-storey drift x_2-x_1, respectively. The generalised plant is represented in state-space form in figure 6.2 as:

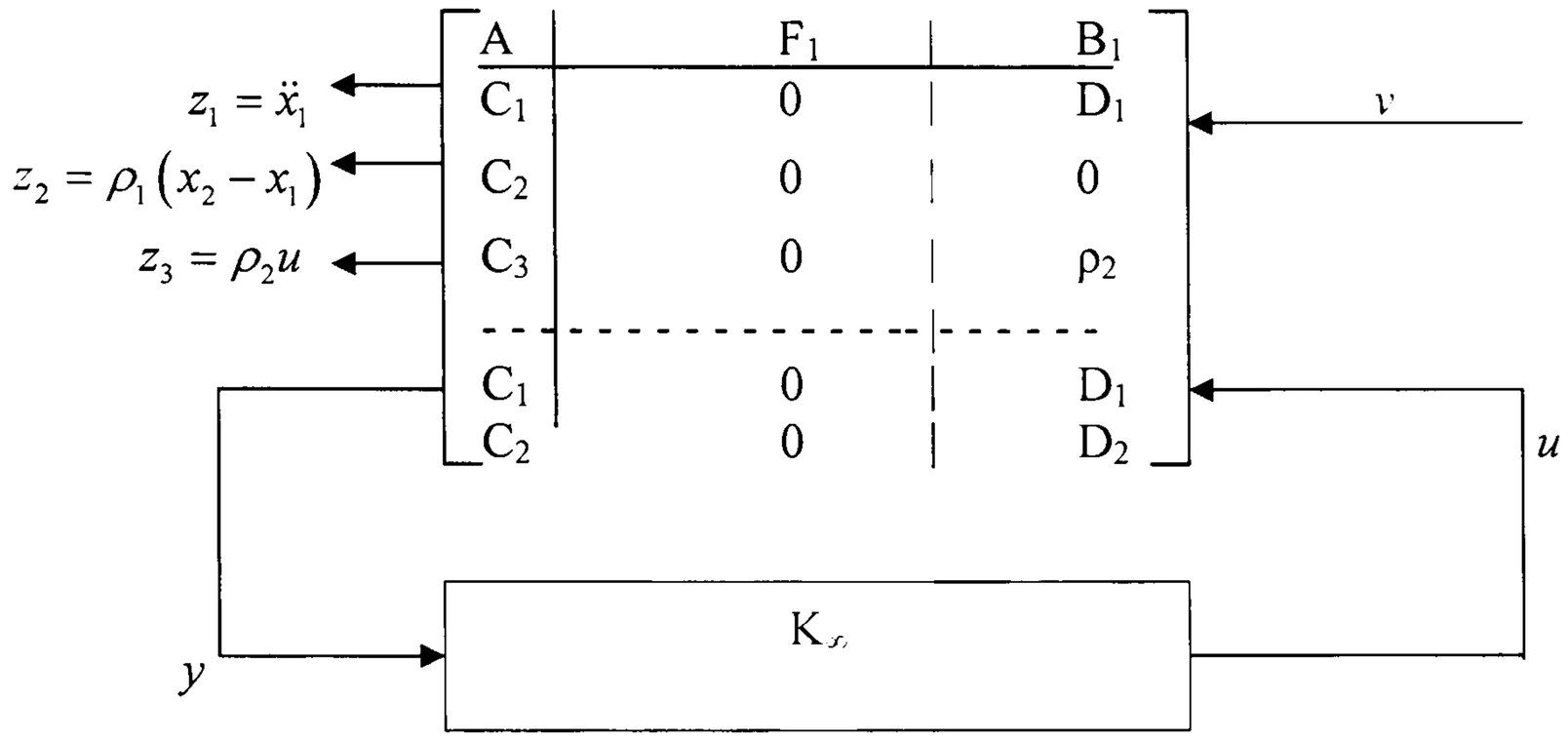

Figure 6.2 System partitioning

Here,

y : measured output

z_1 : regulated output $\left(z_1 = \ddot{x}_1 \quad z_2 = \rho_1 (x_2 - x_1) \quad z_3 = \rho_2 u\right)$

u : control signals

v : disturbance

K_∞ : H_∞-controller

The objective is to design a controller $K(s)$ that stabilises the system and minimises the infinity norm of the transfer function between v and the regulated output vector, i.e:

$$\min_{K \in S} \left\| \begin{bmatrix} T_{\ddot{x}_1 v} \\ T_{\rho_1 (x_1 - x_1), v} \\ T_{\rho_2 u, v} \end{bmatrix} \right\|_\infty = \min_{K \in S} \max_{\omega \in \Re} \sqrt{\left|T_{\ddot{x}_1 v}(j\omega)\right|^2 + \left|T_{\rho_1 (x_2 - x_1), v}(j\omega)\right|^2 + \left|T_{\rho_2 u, v}(j\omega)\right|^2} \quad (6.4)$$

where S is the set of all (internally) stabilising controllers, or equivalently

$$\min_{K\in S}\max_{\omega\in\Re}\left\{\left|T_{\ddot{x}_1\nu}(j\omega)\right|^2+\rho_1^2\left|T_{(x_2-x_1),\nu}(j\omega)\right|^2+\rho_2^2\left|T_{\rho_2 u,\nu}(j\omega)\right|^2\right\}^{1/2} \tag{6.5}$$

which represents the weighted sum of the energy of the three regulated signals. Note that the H_∞ is a dynamic output feedback controller and not state-feedback based, as in LQR. Thus it is more directly comparable to LQG designs and can be thought to consist of two parts, a dynamic estimator (similar to the Kalman filter) and a state-feedback gain vector operating on the state-estimate.

Simulation results: The method used in Matlab to design the controller was based on the Glover-Doyle algorithm [Glover and Doyle 1988] involving the solution of two Riccati equations (see chapter 3.5.4, page 24). The peak inter-storey drift was reduced from 12.6*mm* in the uncontrolled response to 5*mm* and the peak acceleration was also reduced from 29.3m/s^2 to 7.5m/s^2. The response was similar to the LQR case with the acceleration being suppressed more with H_∞ control than with LQR control. However, it takes longer for the response to settle to its steady-state (zero). A sine wave and an earthquake signal were also tested as external disturbances. The responses were similar to the LQR case and therefore are not included here. The uncontrolled and H_∞ responses for an impulsive disturbance input are shown in the figure below:

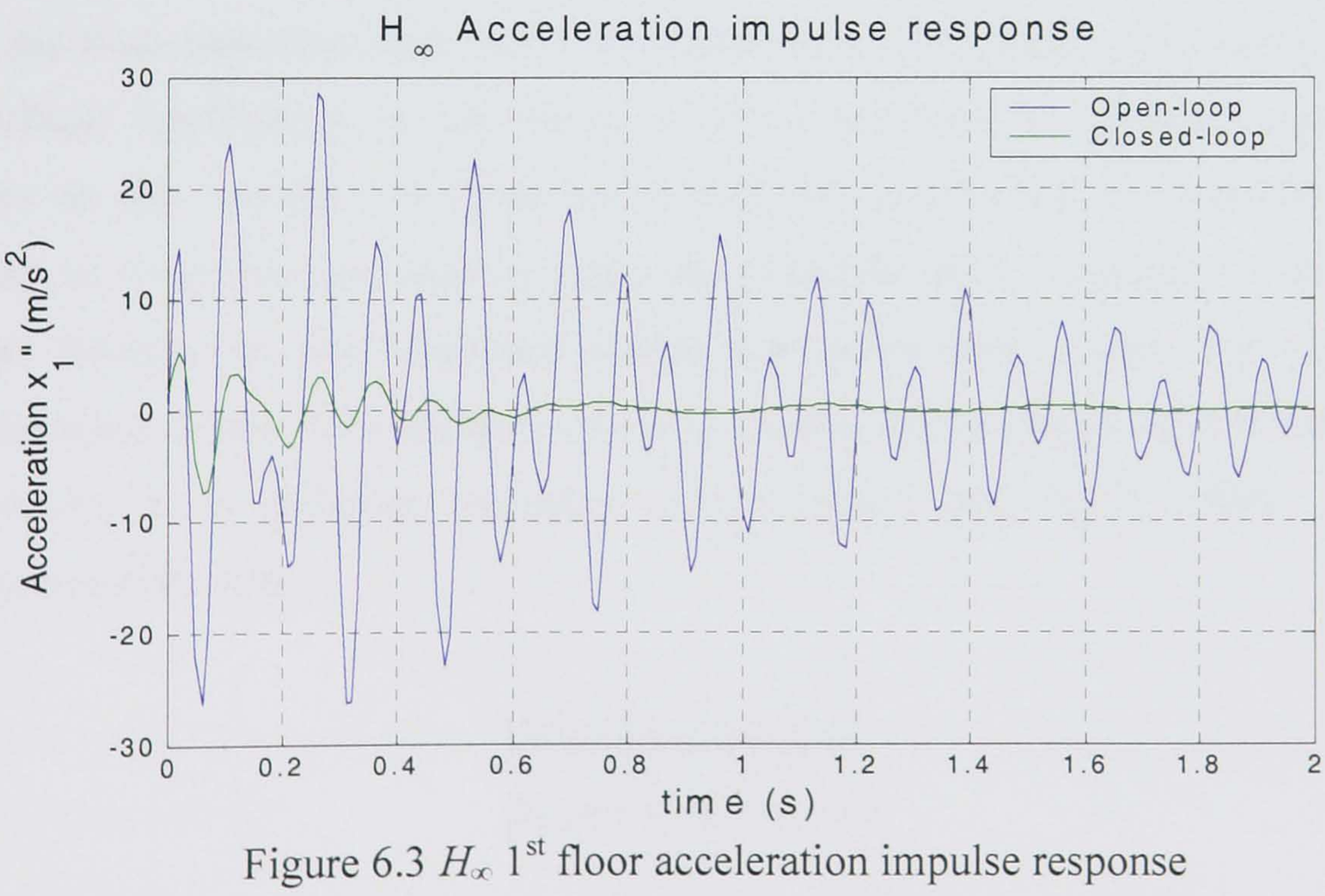

Figure 6.3 H_∞ 1st floor acceleration impulse response

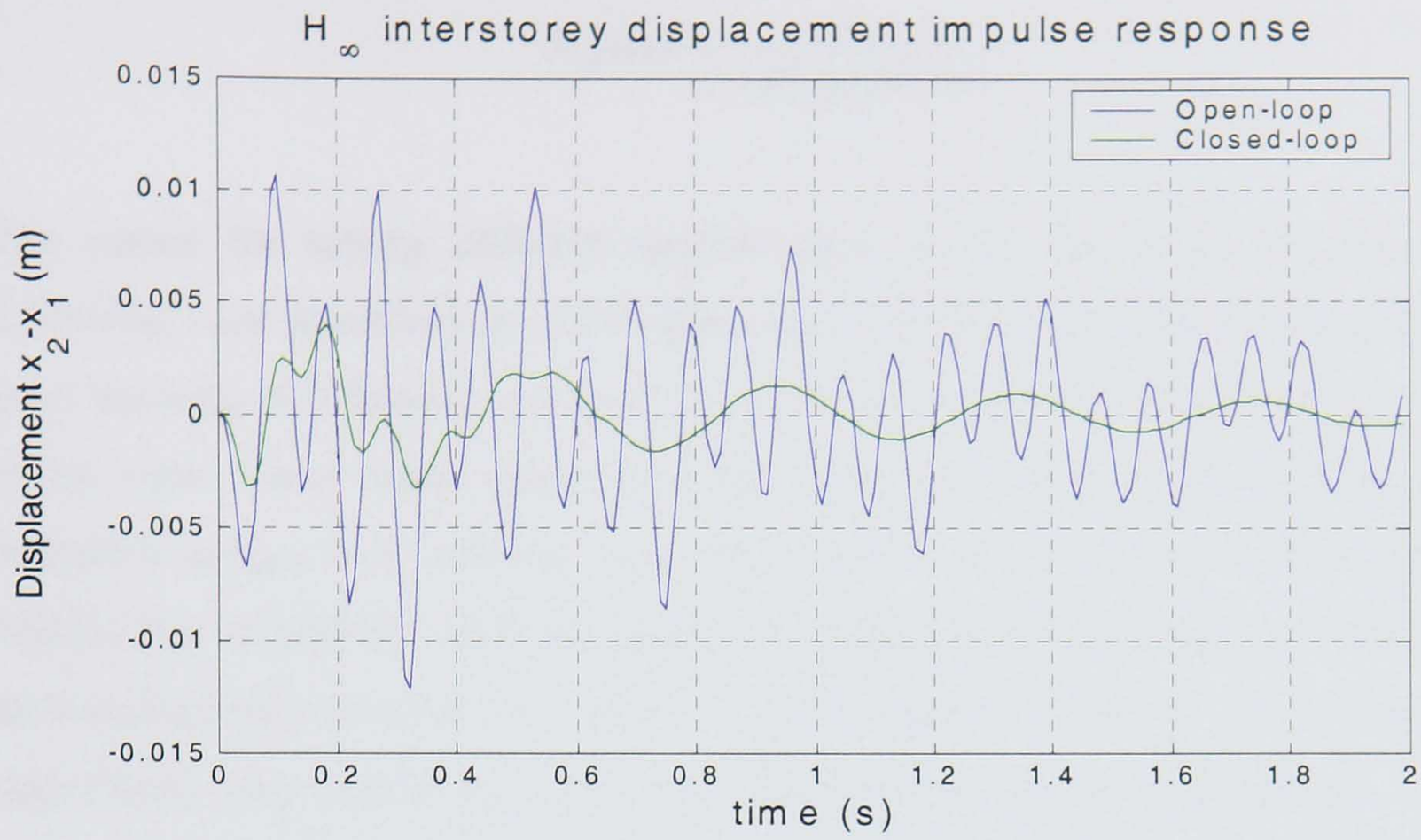

Figure 6.4 H_∞ Relative displacement ($x_2 - x_1$) impulse response

6.3 H_∞-control design with frequency weights

In optimal H_∞ design, weighting functions are typically used to improve performance. The main reason is to emphasise components of regulated signals in frequency ranges that are more important than others. In simple terms, this means that some frequencies contribute significantly to the energy of the disturbance or regulated signals while others do not. Usually it is either low or high frequencies that are important for each signal, so weightings are used to make the controller more "sensitive" in the relevant range. Weights are also important if there are uncertainties present. For example the performance criteria for a scalar system may be specified by requiring different levels of sensitivity S in different frequency ranges [Zhou and Doyle 1998]. A typical requirement for S is:

$$\begin{aligned} |S(j\omega)| &\le \varepsilon, \forall\, \omega \le \omega_0 \\ |S(j\omega)| &\le M, \forall\, \omega > \omega_0 \end{aligned} \tag{6.6}$$

where

$$S(j\omega) = \frac{1}{1 + P(j\omega)K(j\omega)} \tag{6.7}$$

The reason for setting different specifications at low and high frequencies is the following. Low sensitivity at low frequencies is related to the system's performance, i.e. good tracking of reference inputs or the rejection of disturbances entering at the output of the plant. Since these signals typically have their energy concentrated in the low frequency range, it is typically required to keep sensitivity low at low frequencies. Making the sensitivity small at frequencies larger than those actually required by the performance specifications may result in over-design of the system, i.e. an unnecessarily high closed-loop bandwidth, which may have adverse effects on the design, e.g. sensor noise amplification, loss of stability due to unmodelled fast dynamics, etc. In addition, for certain types of systems (non-minimum phase) it is simply impossible to make the sensitivity small over all frequencies [Zhou and Doyle 1998]. At high frequencies, however, although it is not required to make the sensitivity of the system small, its magnitude should be bounded in order for the design to have good stability margins (high values of sensitivity means that the Nyquist plot of the system is near to the -1 point).

This objective can be imposed using frequency-weighting terms as [Zhou and Doyle 1998]:

$$|W_e(j\omega)| \le 1, \forall \omega$$

$$|W_e(j\omega)| = \begin{cases} \frac{1}{\varepsilon}, \forall \omega \le \omega_o \\ \frac{1}{M}, \forall \omega > \omega_0 \end{cases} \tag{6.8}$$

In the structure examined here there are three distinct modes with three corresponding natural frequencies, which must not be excited excessively by the controller. After a few iterations, the following three weighting functions were chosen for the three regulated signals, respectively:

$$w_1(s) = 0.5\left(1 + \frac{1 + s/z_1}{1 + s/p_1}\right) \tag{6.9}$$

$$w_2(s) = 0.0001\left(\frac{1 + s/z_2}{1 + s/p_2}\right) \tag{6.10}$$

$$w_3(s) = 0.1\left(\frac{1 + s/z_3}{1 + s/p_3}\right) \tag{6.11}$$

where $z_1 = z_2 = p_3 = 10000$, $p_1 = p_2 = z_3 = 0.01$. The weighting functions were obtained iteratively. The diagram below shows the magnitude frequency response of the three weighting functions and the acceleration Bode plots.

Note that the control effort weight does not need to emphasise any particular frequency and is set at a low level. The other two functions emphasise the frequencies in the region between 10 to 100 *rads/s* and essentially correspond to first-order low-pass and high-pass filters.

The first function, corresponding to first-floor acceleration emphasises the frequencies in the interval between 10 and 100 *rads/*s which contains the building's natural frequencies. The gain of the control frequency weight is progressively diminishing, crossing the acceleration weight at about 70 *rads/s* which is roughly the frequency of the third and last mode, after which the natural modes of the structure are no longer in danger of being excessively excited. Hence, the control input weight increases because the remaining frequencies are no longer important. These two weighting functions essentially correspond to a low pass and high pass filter respectively. The third weight does not need to emphasise any particular frequency and is set at a low level and is therefore practically inactive. Since the two objectives (inter-storey drift and acceleration) are of the same importance and are both excited by the same frequencies, it is irrelevant which of the two is set at a low level.

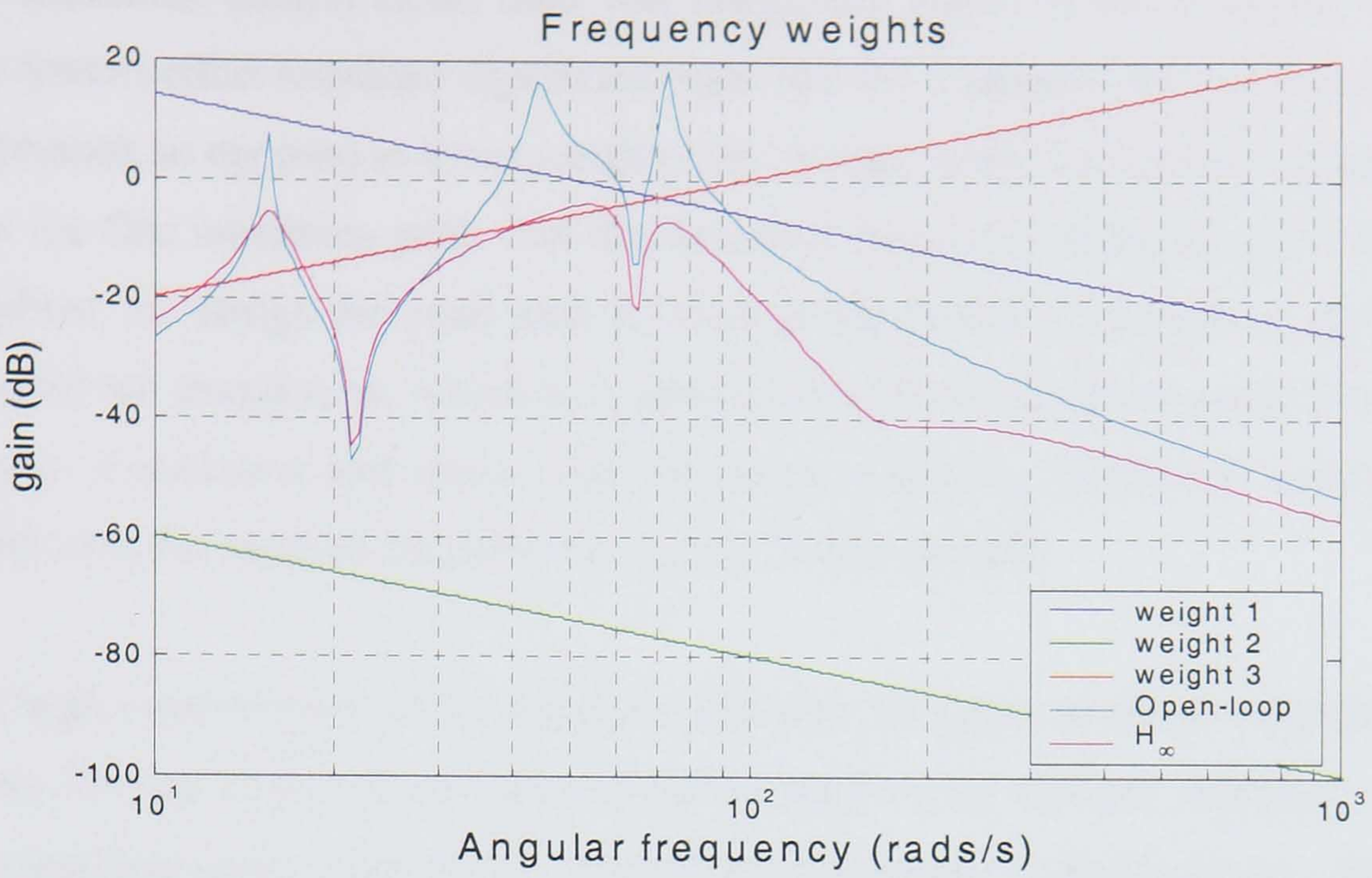

Figure 6.5 H_∞ Bode frequency responses and frequency weights

<u>H_∞ design with weights:</u> By introducing the three weights the performance of the design is significantly improved. The maximum acceleration is reduced from 7.5 to 5.9 m/s^2 relative to the unweighted design and the maximum inter-storey drift reduces from 5 *mm* to 3.6 *mm*. The main difference is that apart from the first maximum, which is always high, the system is stabilised very quickly. After three cycles (0.7 seconds) the displacement is lower than the one achieved after 3 seconds for the unweighted case, and a similar characteristic is observed in the acceleration response. When considering the 3rd floor displacement, the maximum peak is almost the same with both methods but the weighted H_∞ design reaches its steady state almost immediately after that. Note that it is difficult to draw any firm conclusion on maximum signal reduction from the impulse response because the first oscillatory peak of the response is the highest, since the controller does not have time to respond fast enough.

A drawback of the method is that although the weighting functions significantly improve the performance, they cannot directly affect the peak value of the applied control (voltage). For example in the LQG design the peak of the control signal is quite sensitive to the control penalty term, which is not the case for the H_∞ design, even by adjusting the frequency weights $w(s)$. The reason for this behaviour needs further examination.

The maximum control effort used was marginally higher in the weighted H_∞ design. The control effort remained significant high until the vibrations were almost completely suppressed, as opposed to the unweighted H_∞ design, where the applied voltage was low after the first maximum peak. The displacement frequency responses show that for the weighted H_∞ design the peak gain is lower at the resonant frequencies and higher at intermediate frequencies, which is in agreement with the results obtained from the time domain simulations and shows that frequency weighting makes the controller more effective at the required frequencies where it is most needed.

The large improvement of the weighted response compared to the unweighted response shows that any known information about the input or the required frequency content of the regulated signal, appropriately reflected in the choice of the frequency weights, can have a significant impact on the system's responses.

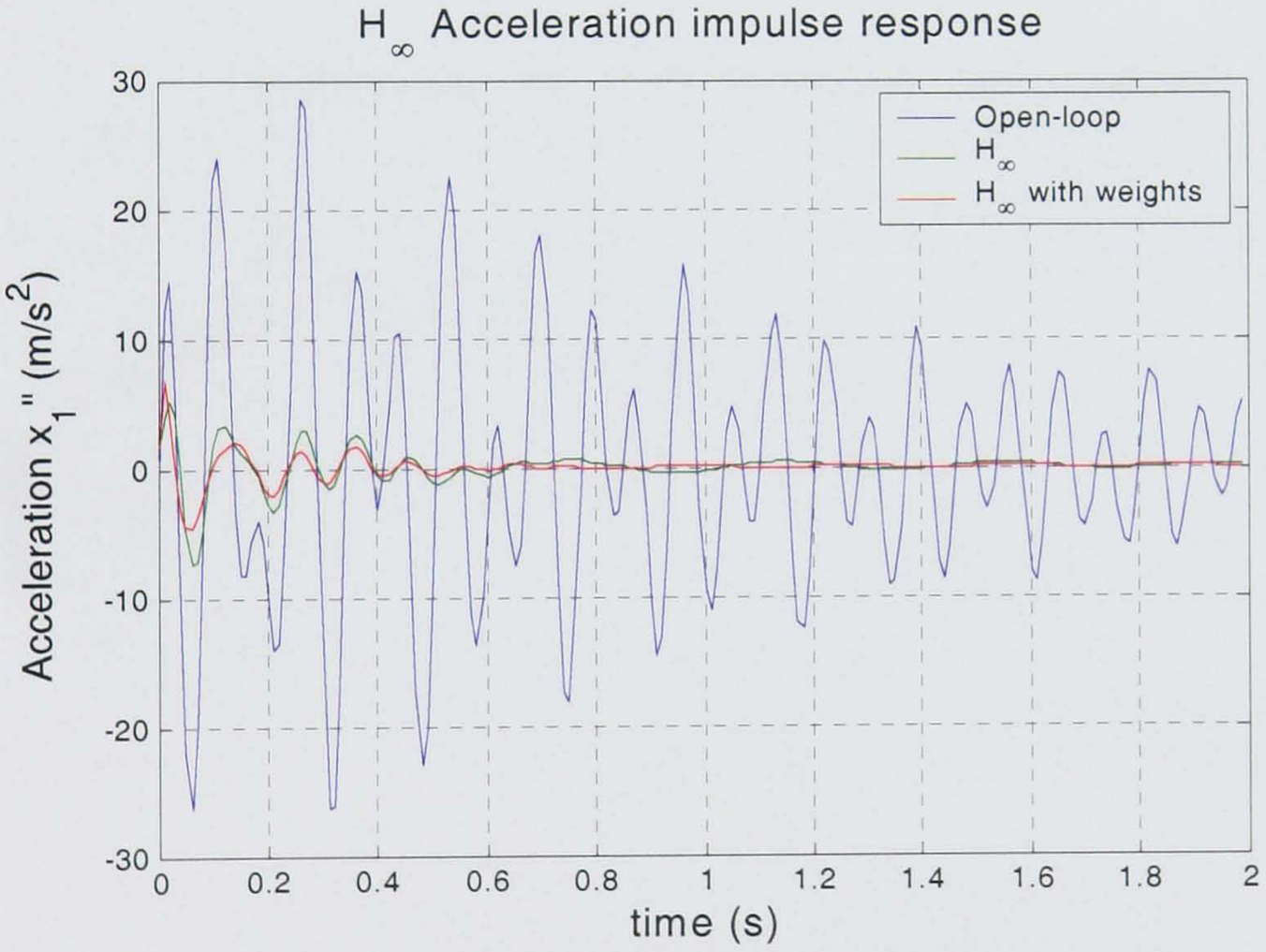

Figure 6.6 H_∞ with frequency weights 1st floor acceleration impulse response

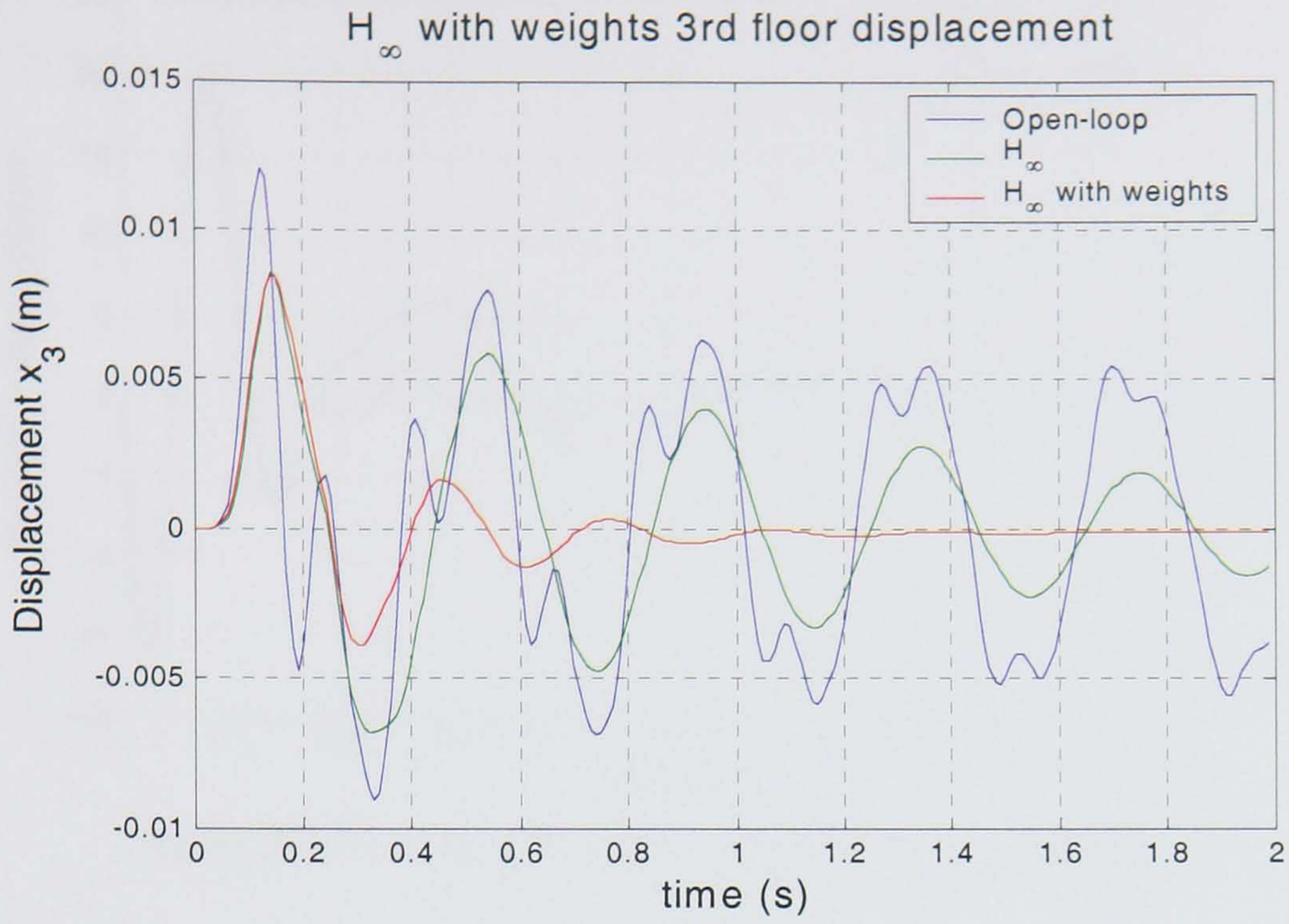

Figure 6.7. H_∞ with frequency weights 3rd floor displacement impulse response

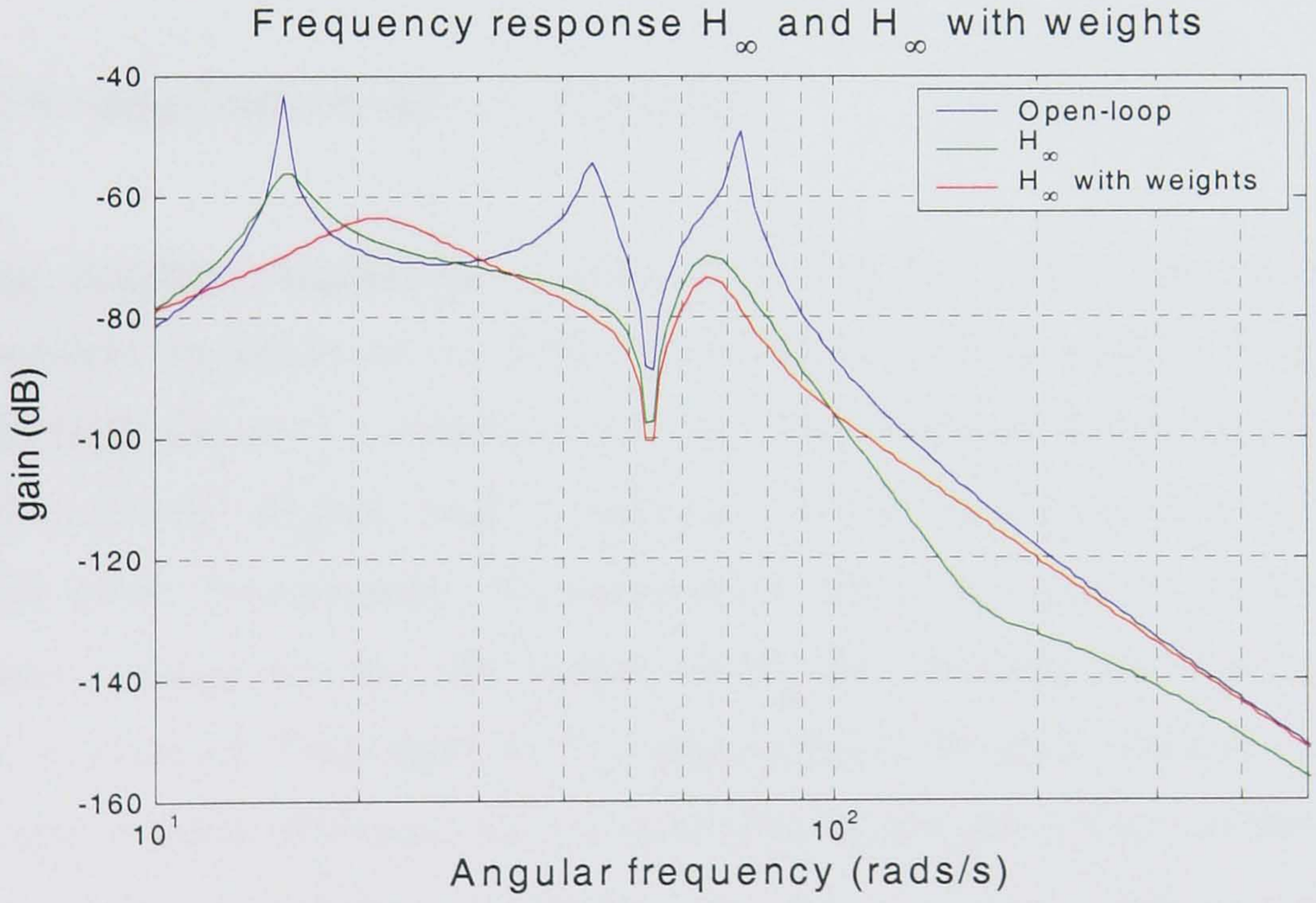

Figure 6.8 H_∞ with frequency weights Bode frequency response

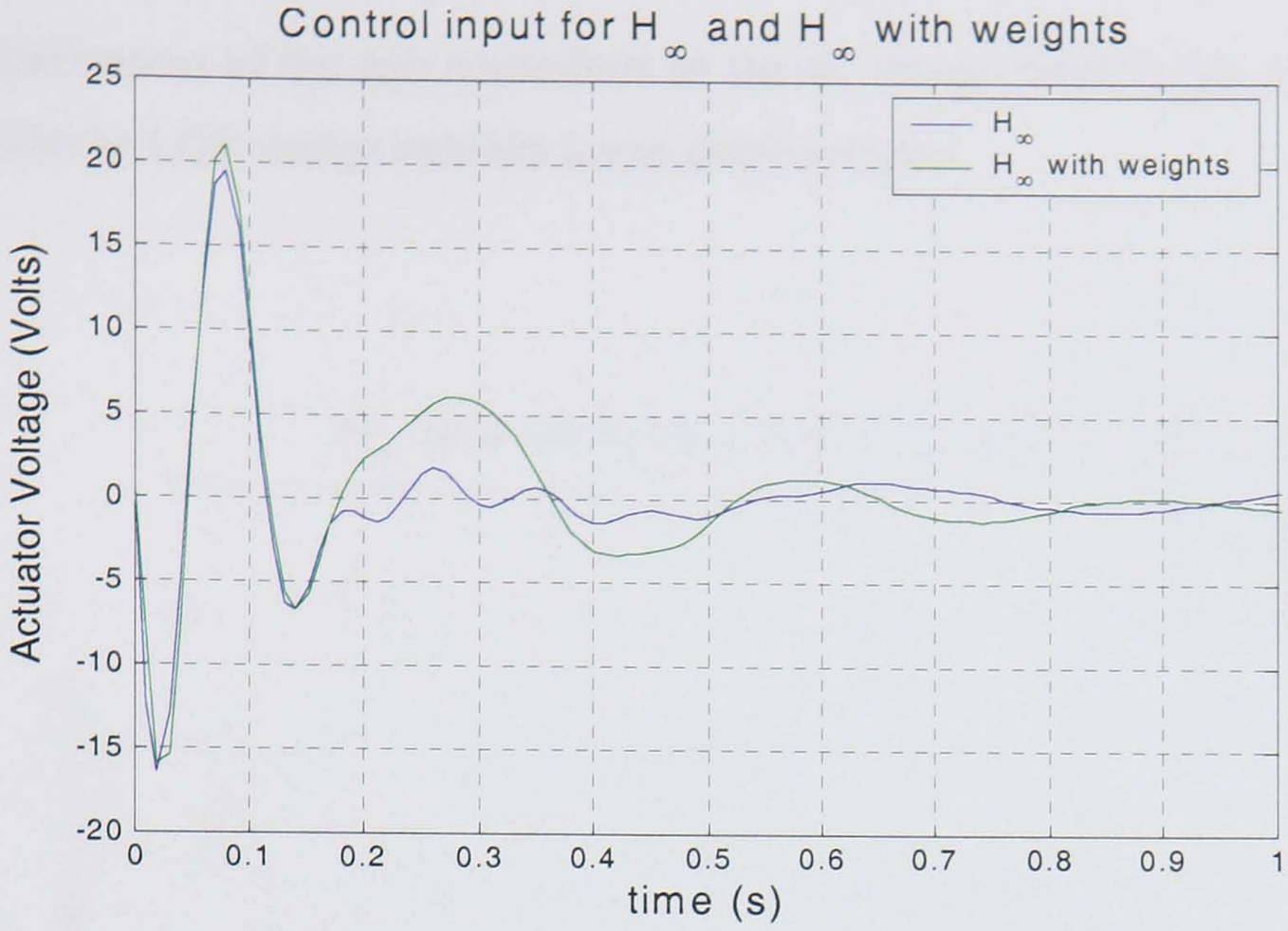

Figure 6.9 H_∞ with and without weights control voltage

6.4. Simulation results

6.4.1. Comparison LQR- H_∞ Control

Impulse response simulations: Figures 6.10 and 6.11 show the acceleration and displacement responses of the three-storey structure for an impulsive input when an optimal LQR and an H_∞ controller were used. The responses are similar, with the LQR design exhibiting slightly smaller amplitude in the inter-storey drift (x_2-x_1) and the absolute floors displacements. The acceleration responses appear to be less linear. The first peak is larger for the LQR design, but for the remaining time the H_∞ response is larger, as expected. Once again the first peak in the acceleration response is larger in the LQR case. Another difference for the displacement and acceleration responses between the two designs is that the response from the two controllers is almost constant for all times in the inter-storey drift, whereas for the acceleration signal the response is out of phase and more oscillatory. This is another sign that the inter-storey drift is a better indicator for the controller evaluation than the first floor absolute acceleration response. The input (voltage) signal of the controller was almost identical for the two control designs, which makes the comparison meaningful. It is difficult to compare directly the

effectiveness of the two controllers as the H_∞ design exhibits lower acceleration levels while the LQR design exhibits lower displacements.

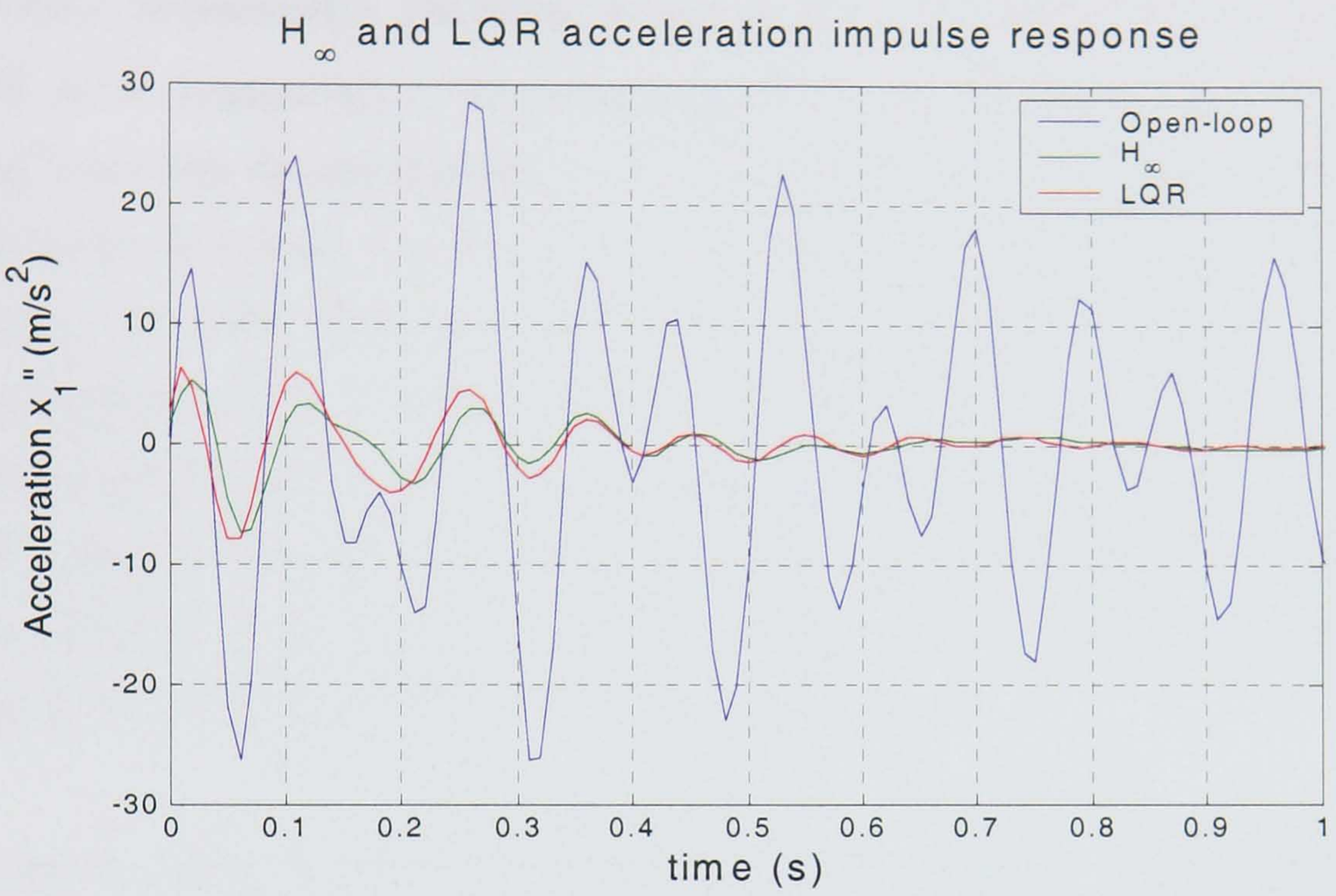

Figure 6.10 H_∞ 1st floor acceleration impulse response (LQR and H_∞)

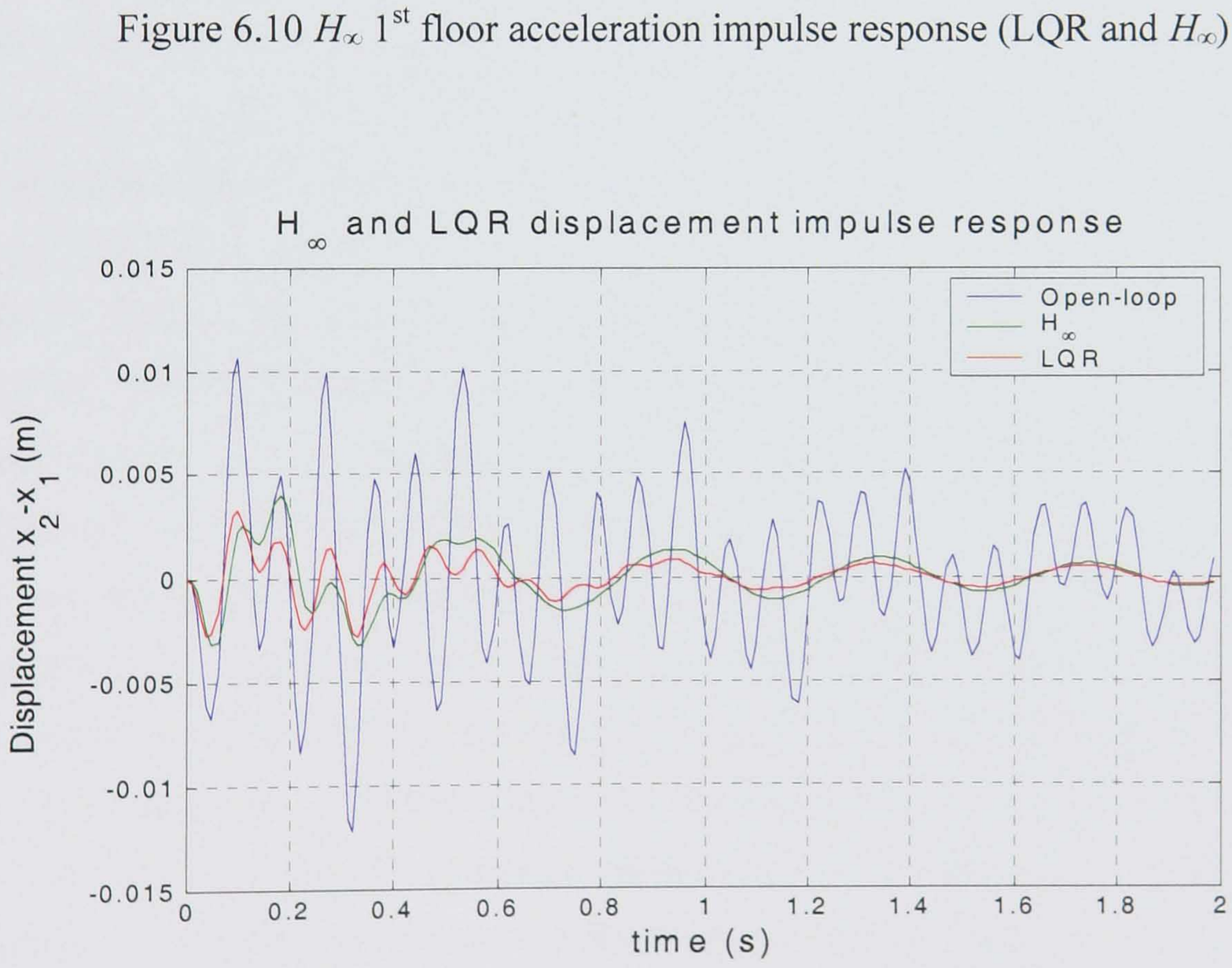

Figure 6.11 H_∞ relative displacement impulse response (LQR and H_∞)

Earthquake signal responses: The two control design methods were also tested with the Loma Prieta earthquake signal, and the corresponding peak and root-mean-square values were compared. As mentioned earlier, the peak acceleration with LQR was higher than for the uncontrolled case, whereas the peak H_∞ value was lower (1.65 and 1.56 m/s^2 respectively). The RMS values were lower in the H_∞ case as well (0.182 and 0.148 m/s^2 respectively.). The inter-storey drifts were different, the LQR response being lower than the one obtained by the H_∞ design. The H_∞ controller reduced the peak inter-storey drift from 2 *mm* to 1.05 *mm*, whereas the LQR controller reduced it to 0.83*mm*. The RMS values were almost the same with either controller. The absolute displacements of each floor were also calculated, the second and third floor displacements being lower in the LQR design, both in terms of maximum peak and RMS values. Finally, the LQR peak levels were always lower than the corresponding RMS values. The controller input peak and RMS value (measured in volts) was higher in the H_∞ case than in the LQR case (about 50% higher).

The above results indicate that LQR design produced better overall results than H_∞ since it managed to reduce absolute displacements in excess to the reduction achieved by the H_∞ controller by using less energy (with the exception of first floor acceleration). Such a significant difference between acceleration and displacement was not expected and is difficult to explain. The reason for the difference could be attributed to the fact that the highest floor exhibits much smaller displacements (x_3) with LQR control than with H_∞, whereas the lower floors have similar responses for the two methods. Overall, LQR control tends to minimise the higher floors displacements by a larger factor relative to the displacements of lower floors.

By comparing the theory underlying the two methods, it is expected that LQR would produce better results in terms of the time-domain responses than H_∞ control. LQR minimises the RMS value of the regulated signals rather than the peak value of their frequency response. In addition, impulsive simulations clearly favour LQR designs, as the spectrum of an impulse is equally spread-out over all frequencies, which is in tune with the white-noise assumptions on disturbances made by this theory. H_∞ control is a powerful design method when uncertainties are present in the plant model. In this design, the model was assumed "perfect" with no perturbations or uncertain parameters. The responses obtained from the H_∞ controller exhibited higher damping, which

indicates that establishing good stability margins is an important aspect of this design method. In contrast, the LQR formulation of the problem does not necessarily cause fast decays in the system's response, since by keeping the regulated signals oscillating at small amplitude over a longer time may not contribute significantly to its minimisation index.

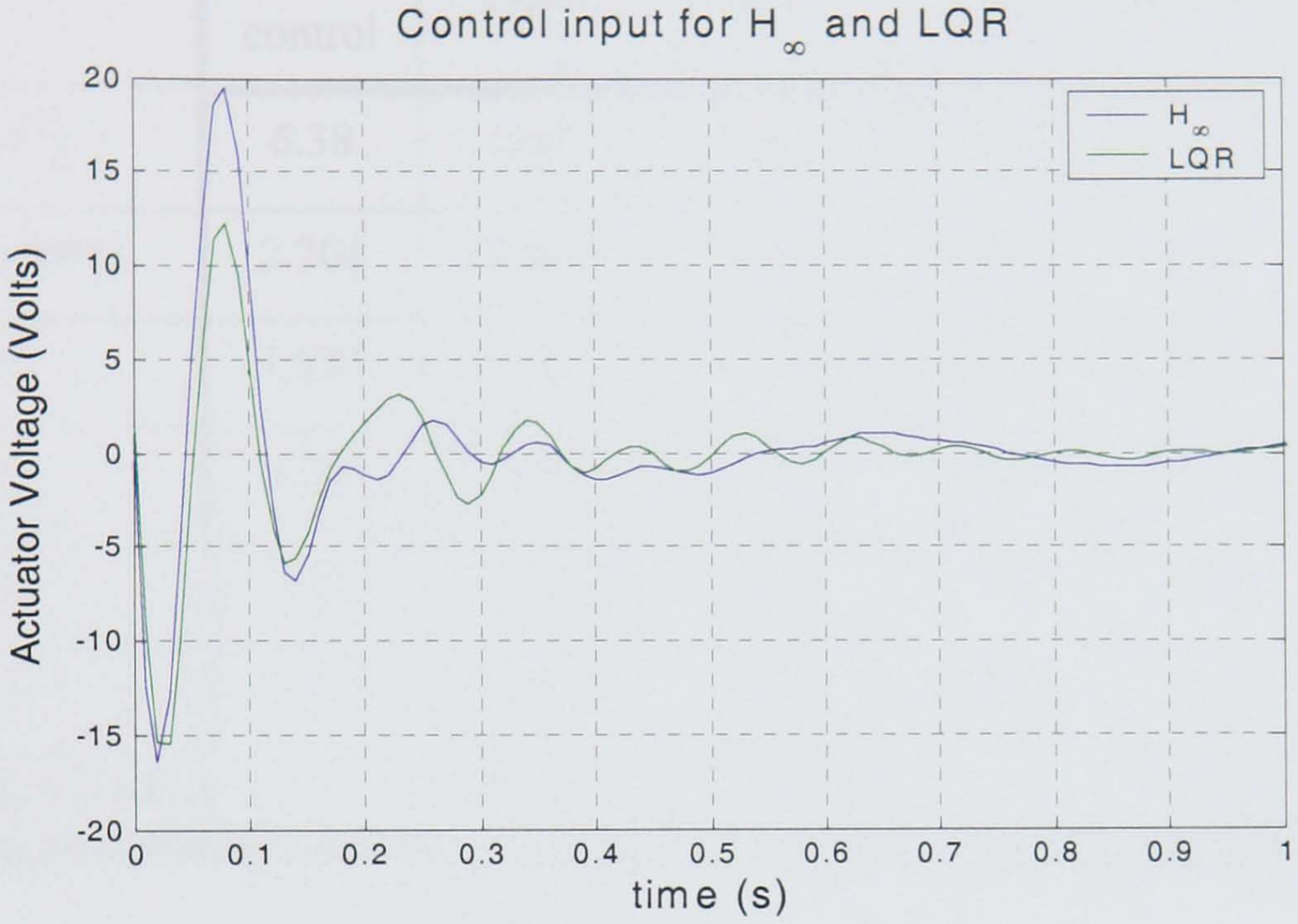

Figure 6.12 H_∞ and LQRVoltage

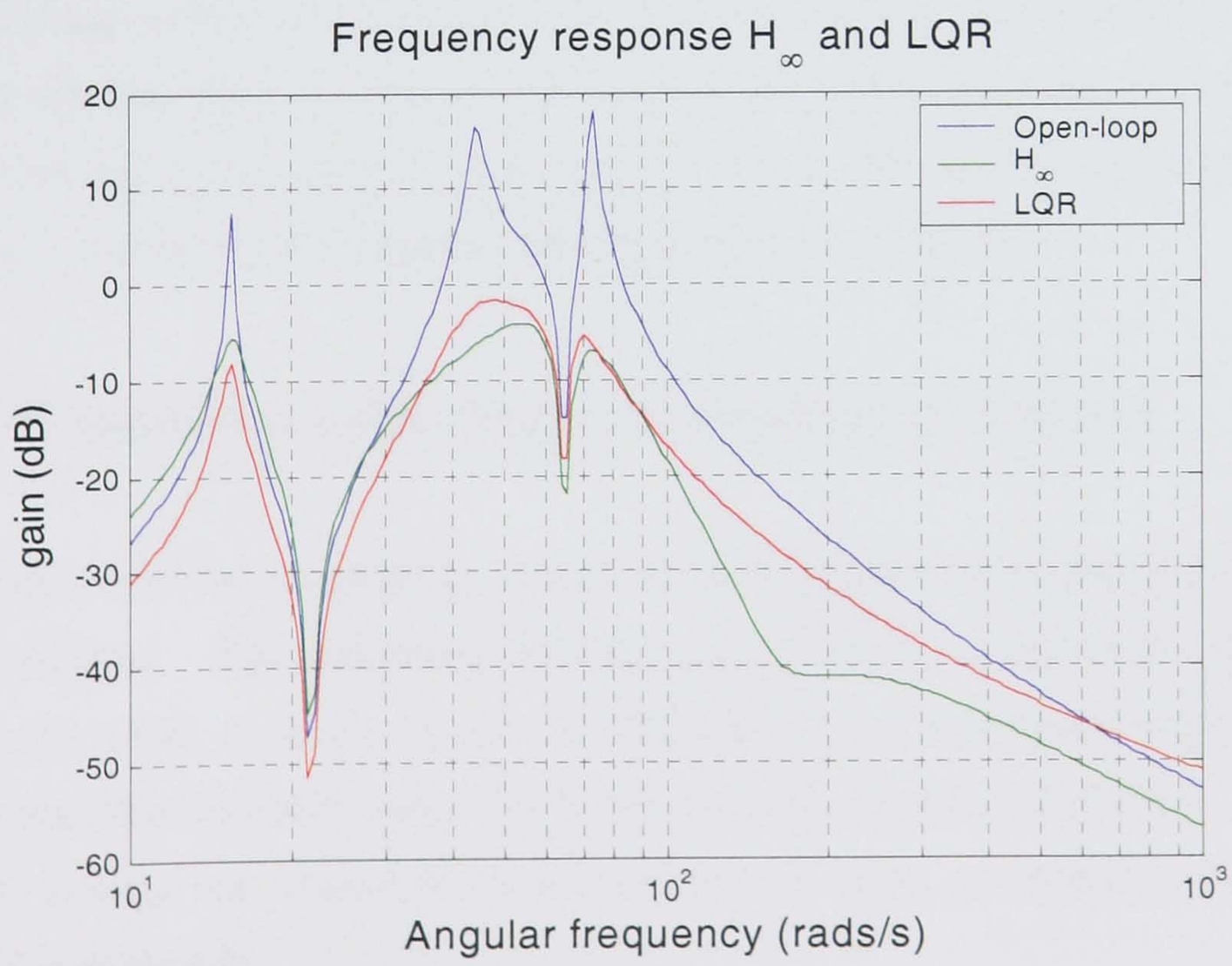

Figure 6.13 Bode frequency plots 1st floor acceleration (LQR and H_∞)

Comparison between Open- and closed-loop Peak and RMS values (for $\rho_1 = \rho_2 = 1$)

	Peak value			RMS		
	No control	LQR	H_∞	No control	LQR	H_∞
$\ddot{x}_1 \left(m/s^2\right)$	6.38	1.65	1.56	0.897	0.182	0.148
$x_2 - x_1 \left(mm\right)$	2.204	0.83	1.05	0.438	0.107	0.106
$x_0 \left(mm\right)$	1.933	1.79	1.93	0.233	0.213	0.22
$x_1 \left(mm\right)$	1.59	0.89	1.28	0.565	0.132	0.132
$x_2 \left(mm\right)$	3.62	1.09	1.72	0.743	0.169	0.273
$x_3 \left(mm\right)$	3.89	1.33	2.2	0.931	0.214	0.356
Voltage (Volts)		2.78	3.72		0.296	0.423

Table 6.1

Developing the systematic procedures for comparing the responses resulting from two different optimal design methods is an important issue for which no standard methodology exists. One possible way for achieving this is to choose the appropriate penalty coefficients ρ_1 and ρ_2 and iterate until the voltage resulting by both methods is approximately equal (either in peak or RMS value). This method however, is not exact because "optimality" is defined differently for the two methods.

6.4.2. Comparison LQR- frequency weighted H_∞ Control

The response of the weighted H_∞ design for an impulsive input was still worse than the LQR response. The maximum inter-storey drift (x_2-x_1) was 3.6mm as opposed to 3.3mm for LQR. A similar result was obtained for the acceleration signal, with LQR producing superior results since this is below the H_∞ response at all times. This time the applied voltage was almost the same for the two cases, and therefore the results are directly comparable.

In the case of an earthquake signal the weighted H_∞ method produced better results compared to the unweighted H_∞ design, as shown in table 6.1. The RMS values were lower for the H_∞ controller than the LQR controller, but the peak inter-storey drift was lower in the LQR design relative to the H_∞ design. The reason for this difference is that from definition the LQR minimises the total (weighted) power of the response, to which the peak contributes significantly. Surprisingly, LQG also exhibited improved performance in terms of peak response attenuation compared to H_∞. This was not expected since by definition, LQR penalises total power and hence indirectly RMS values. This result may be explained by the fact that as H_∞ is a more robust methodology it tends to produce smoother control signals and thus cannot generate sharp voltage peaks, which would tend to increase the control bandwidth and may thus reduce the stability margins. LQG control has also reduced the 2nd and 3rd floor displacements significantly compared to H_∞ despite the fact that this was not included directly in the optimisation index, which means that the overall design is good. The voltage used by both controllers had different waveforms, which makes the direct comparison between the two designs difficult to assess. The maximum weighted H_∞ voltage was 5.15 volts, almost double the one obtained from LQR (2.78 volts).

Uncontrolled and closed-loop Peak and RMS values (for $\rho_1 = \rho_2 = 1$)

	Peak value				RMS			
	No control	LQR	H_∞	Fw H_∞	No control	LQR	H_∞	Fw H_∞
$\ddot{x}_1\left(m/s^2\right)$	6.38	1.65	1.56	1.23	0.897	0.182	0.148	0.11295
$x_2 - x_1\left(mm\right)$	2.204	0.83	1.05	0.972	0.438	0.107	0.106	0.073
$x_0\left(mm\right)$	1.933	1.79	1.93	2	0.233	0.213	0.21	0.218
$x_1\left(mm\right)$	1.59	0.89	1.28	0.99	0.565	0.132	0.132	0.0817
$x_2\left(mm\right)$	3.62	1.09	1.72	0.98	0.743	0.169	0.273	0.139
$x_3\left(mm\right)$	3.89	1.33	2.2	1.63	0.931	0.214	0.356	0.196
Voltage (Volts)		2.78	3.72	5.15		0.296	0.423	0.466

Table 6.2

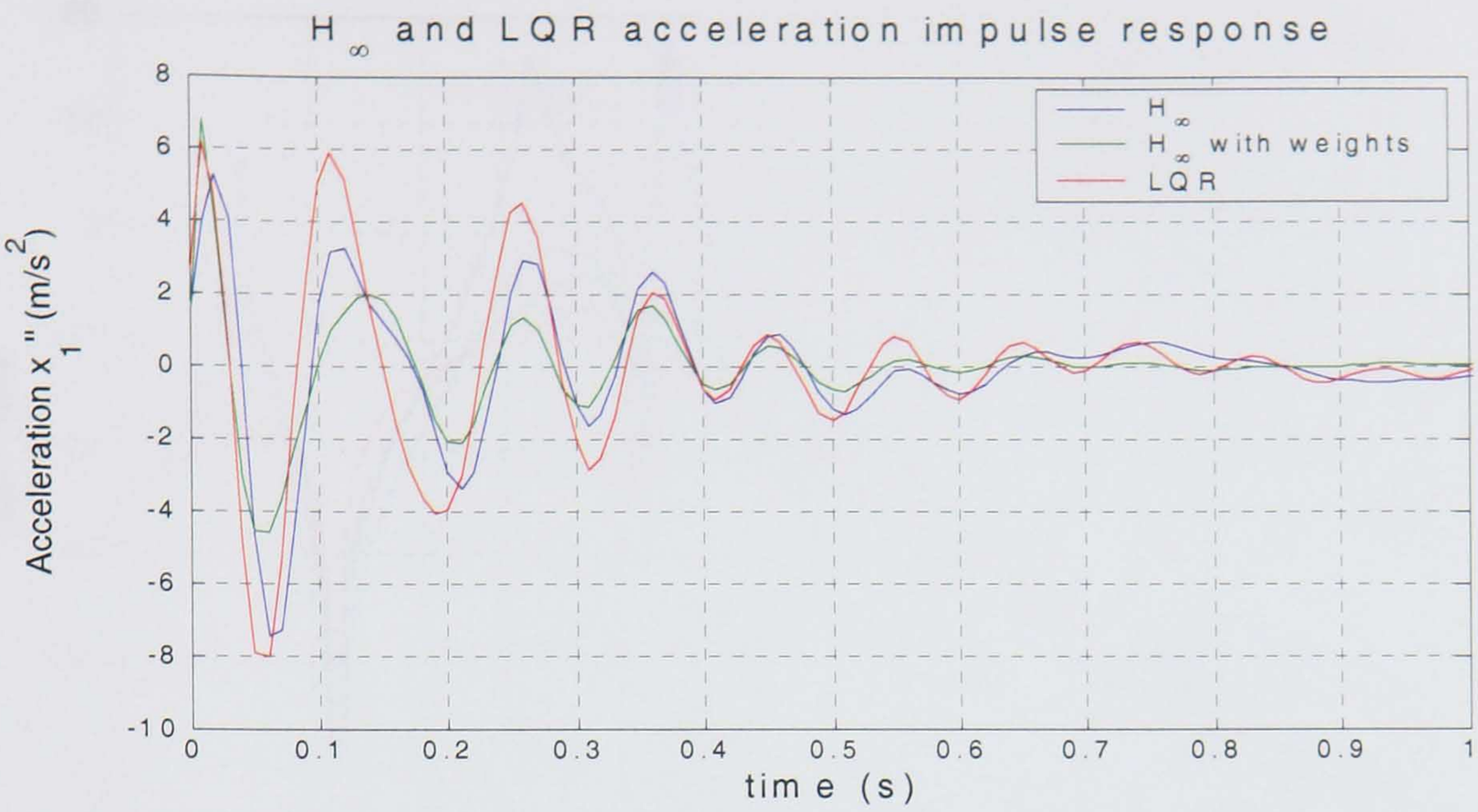

Figure 6.14 1st floor acceleration impulse responses (LQR, H_∞ and weighted H_∞)

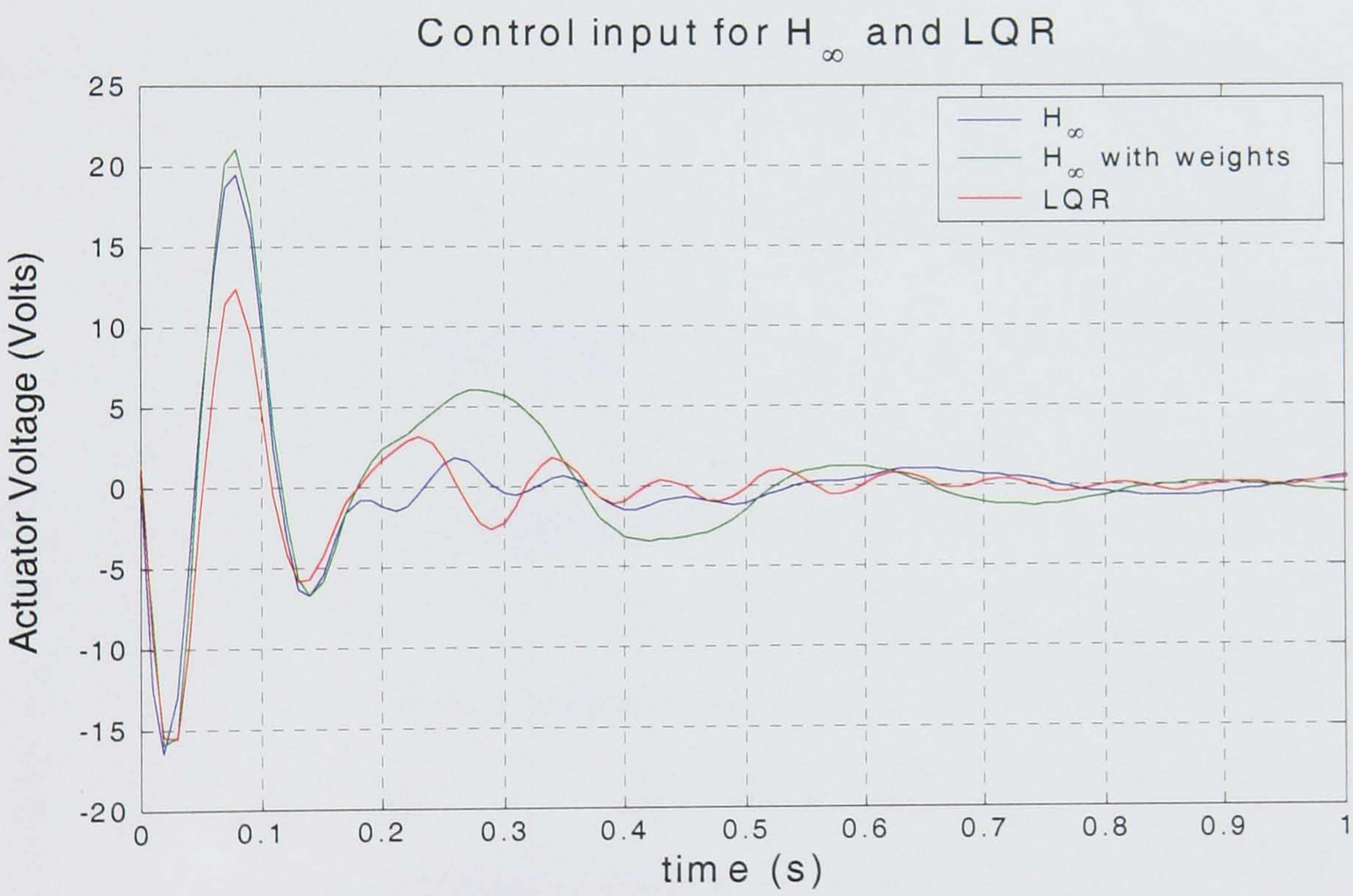

Figure 6.15 Control voltage (LQR, H_∞ and weighted H_∞)

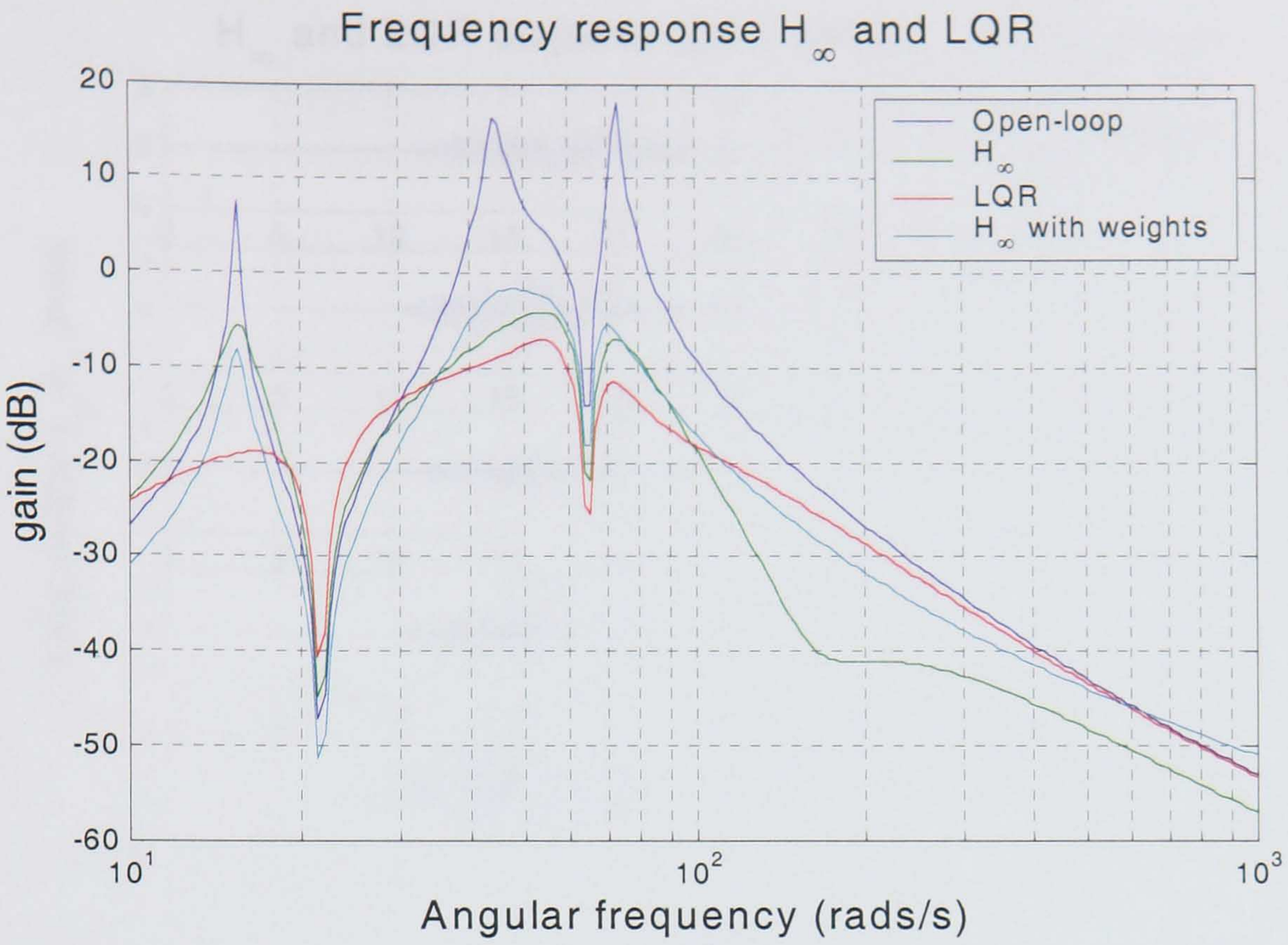

Figure 6.16 1st floor acceleration Bode frequency plots (LQR, H_∞ and weighted H_∞)

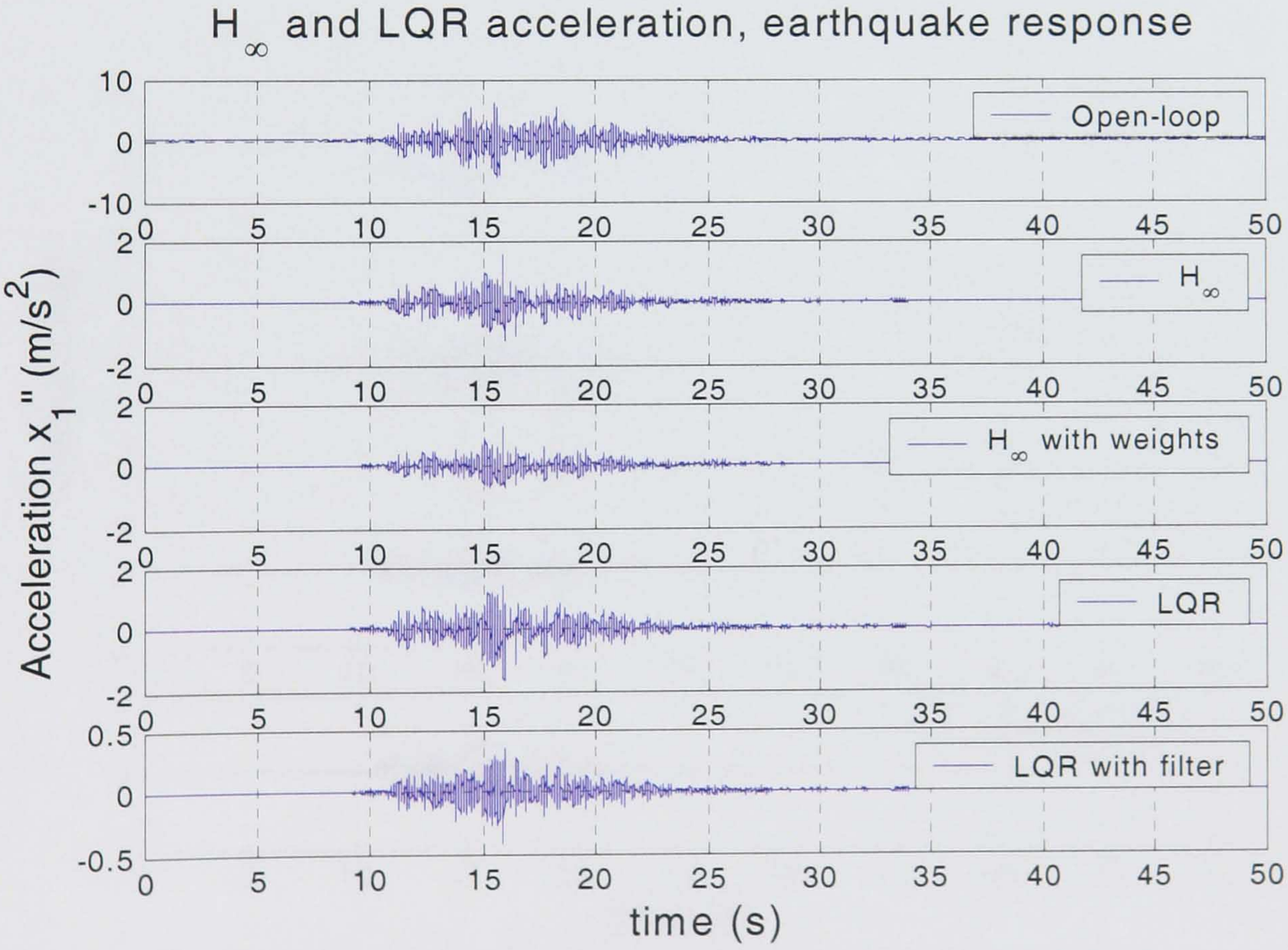

Figure 6.17 Earthquake signal 1st floor acceleration responses

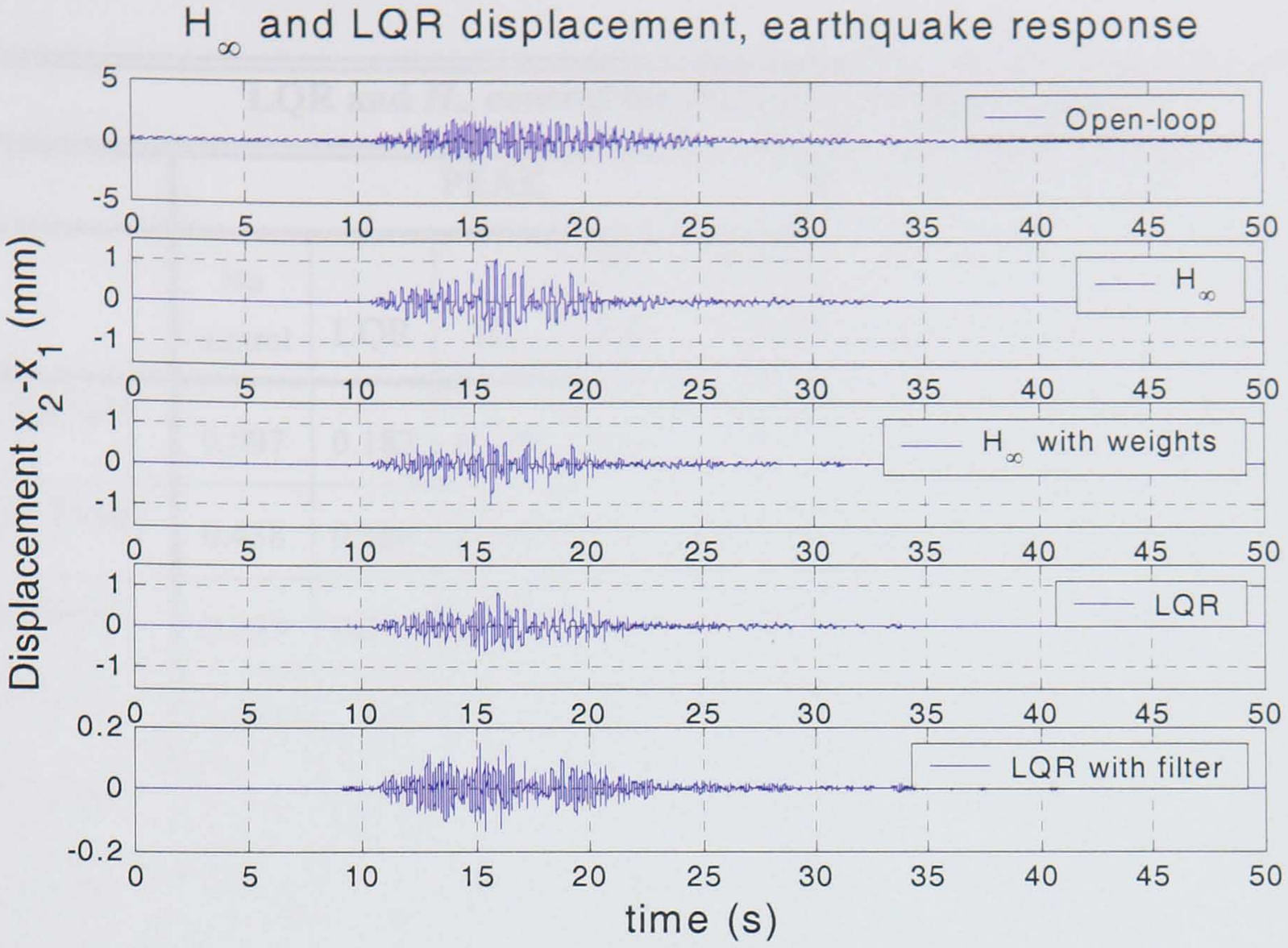

Figure 6.18 Earthquake signal relative displacement ($x_2 - x_1$) responses

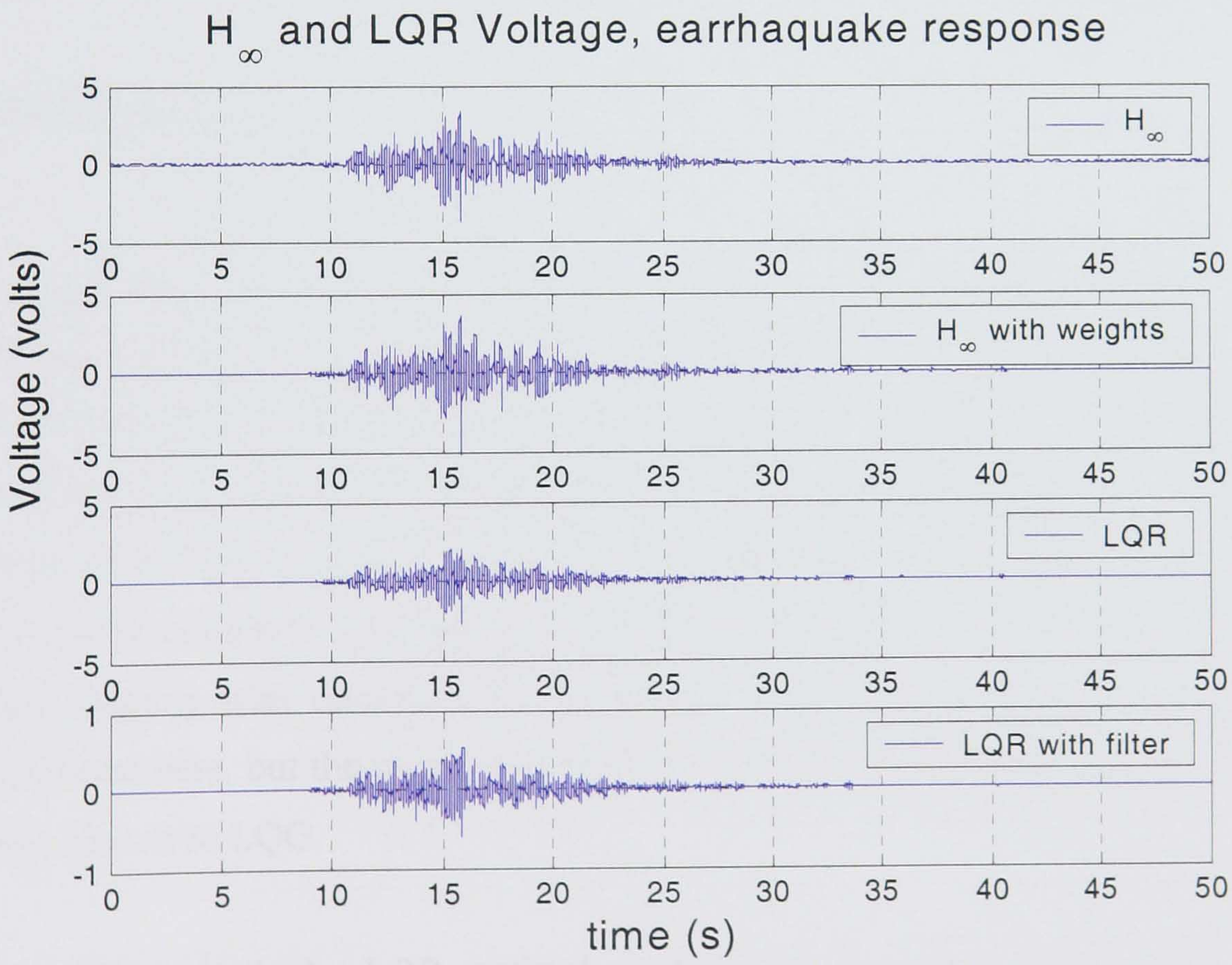

Figure 6.19 Earthquake signal control effort (voltage)

LQR and H_∞ control for earthquake signal response

	PEAK					RMS				
	No control	LQR	H_∞	H_∞ FW	LQR -IF	No control	LQR	H_∞	H_∞ FW	LQR -IF
$\ddot{x}_1\left(m/s^2\right)$	0.897	0.182	0.148	0.113	0.42	6.38	1.64	1.56	1.23	0.412
$x_2\text{-}x_1\left(mm\right)$	0.438	0.107	0.144	0.105	0.02	2.204	0.84	1.047	0.973	0.144
$x_0\left(mm\right)$	0.233	0.213	0.22	0.219	0.048	1.933	1.79	1.93	2	0.434
$x_1\left(mm\right)$	0.565	0.133	0.175	0.111	0.02	1.59	0.89	1.28	0.99	0.178
$x_2\left(mm\right)$	0.743	0.169	0.273	0.134	0.021	3.62	1.09	1.716	0.986	0.156
$x_3\left(mm\right)$	0.931	0.214	0.356	0.195	0.021	3.89	1.33	2.2	1.63	0.16
Voltage (Volts)		2.783	3.724	5.154	0.599		0.296	0.423	0.466	0.069

Table 6.3

6.5 Summary

In this chapter the structure modelled in Chapter 5 was designed with an H_∞ active vibration controller. The design was simulated for three separate loading cases, an impulsive load, a sinusoidal load and a real earthquake signal. The design included the introduction of frequency weights to emphasise important frequency ranges for the design objectives. A generalised regulator was used to formulate the problem, resulting in a stable controller with good performance. Primarily H_∞ controllers are effective when dealing with uncertainties, perturbations and model errors, which were not considered here, but the results showed good nominal performance, perhaps inferior in some aspects to LQG.

Two design methods, LQR optimal control and H_∞ robust control were directly compared and many features were included to improve the performance of the designs. The main simulation results show that although both designs produced effective control schemes, the LQR controller had marginally better performance. This is expected from

theory because LQR is designed to improve performance for the type of excitation considered, whereas H_∞ is more concerned with robust stability and may thus be more conservative. Nevertheless, H_∞ has shown improved acceleration responses than LQG and in certain cases equally good RMS values as LQG.

Several ways were used to improve the overall design performance, such as the introduction of penalty terms and frequency weights. Also the designer has a choice of adding estimators for unknown states to finally get a robust design which can be implemented in practice. The best design by far was the one where the frequencies of the input disturbance were assumed known and were reflected in the design of a filter augmented to the generalised plant.

The control schemes employed were based on Linear Quadratic Regulator (LQR) theory, Linear Quadratic Gaussian (LQG) theory and H_∞ optimal control. The most powerful controller in terms of minimising the response for the given specifications was LQR, as expected from the problem formulation and the choice of loading. Direct comparison between the different methods was difficult, due to the nature of the problem. Overall, the weighted H_∞ controller performed better compared to the un-weighted LQR design, but it is expected that a weighted LQR will be even more powerful, especially for typical seismic signals whose energy is concentrated in the low-frequency range. The main conclusion that can be drawn from the simulations is that all the examined methods cannot directly minimise the time-domain peak response (displacement or acceleration). H_∞ control typically results in higher damping and LQR emphasises RMS response minimisation; in the case of active control of buildings, however, the most important objective is to minimise the peak response, to prevent the structure from entering the inelastic region. In the case of an impulsive loading, the controller was not able to act on time, as expected due to bandwidth constraints, and the first peak has similar magnitude for both the uncontrolled and active control case, which means that the controller cannot provide protection in this case. Clearly, an impulse is the most severe type of loading, but also in the case of real earthquake data it was noticed that the controllers could reduce the peak response by only a limited amount. Therefore it is of primary importance to develop a design method and algorithms which directly address this issue.

CHAPTER 7

7. LINEAR PROGRAMMING OPTIMISATION-BASED CONTROL (LPOC)

7.1. Introduction

The most important consideration when dealing with structural failure is not exceeding the maximum deformation capacity. Structural members fail when a maximum displacement (or force) is exceeded. A constant load below the yield strength is not harmful to a structure. Only if the yield point of a member has been reached, then a large constant load, like a cyclic load present in earthquakes, is slowly degrading the structure. Therefore, reducing peak responses is the most crucial aspect in structural control.

Current control algorithms do not address this issue since most of them have been developed for purposes other than civil engineering. LQR minimises the power (RMS value) of the signals selected for regulation, not their peak levels. In the example of the previous chapter where the structure is excited with an impulse, a very large peak was observed followed by a much lower one and very soon the steady state was reached. This maximum level of the first peak could be diminished by control action, but as a consequence the subsequent peaks would need to increase, although at levels not exceeding the first. As consequence the total energy of the response would be larger, but the maximum peak would be reduced. Hence, in this case LQR is not equipped to minimise peak responses, although from inspecting the impulse responses it is clear that there is plenty of room for improvement.

Other control methods rely on more sophisticated background theory and thus their behaviour cannot be explained in simple terms like in the example mentioned above. Some directly minimise maximum peaks to some extend and some do not. Most modern control methods involve the minimisation of a norm like the H_2 or H_∞ norm of a closed–loop transfer function between an input (typically disturbance) signal and a regulated

output. The H_2 norm measures the expected power energy of the output signal (mean-square value). Normally the input signal is assumed to be a random white-noise signal (flat spectrum).

Alternative control design methods aiming to minimise the peak response of the regulated signal have recently been reported both in the area of active vibration control [Lim et al. 2003] and also in general control literature [Sznaier et al. 2003], [Sznaier 1995], [Dahleh and Bobill 1995]. [Lim et al. 2003] is based on an adaptive bang-bang methodology, which clearly offers advantages when the disturbance-signal is uncertain, but is also difficult to apply in practice and could easily cause instability. A systematic general approach is the l_1 optimal control theory, which attempts to minimise the peak amplification gain between disturbance input and regulated output, assuming bounded inputs [Dahleh and Bobill 1995] [Pearson n.d.]. Interestingly, the method results in a Linear Programming optimisation framework also used here. However, as l_1 is an induced norm, all bounded disturbance signals are taken into account in the formulation of the optimisation problem. As a result, the design may be excessively conservative, unless the method can be restricted to specific models of disturbances that are likely to arise in practice, i.e. signal classes whose spectral content is similar to those observed in typical seismic acceleration signals.

In this section a design method is proposed that directly minimises the maximum peak response of an actively controlled structure. It involves the use of linear programming, a strong optimisation tool with a wide range of applicability. All closed-loop controllers are parametrised in terms of a free stable parameter Q that is subsequently optimised for a discrete impulse acting as an input. After imposing some appropriate constraints on the maximum control signal applied and its maximum rate of change, an optimal controller is designed that directly minimises the maximum peak acceleration of the controlled structure.

Overview of control design methods

Consider the diagram in figure 1 where $\eta(t)$ represents a zero-mean white noise vector signal and $e(t)$ is the system's output.

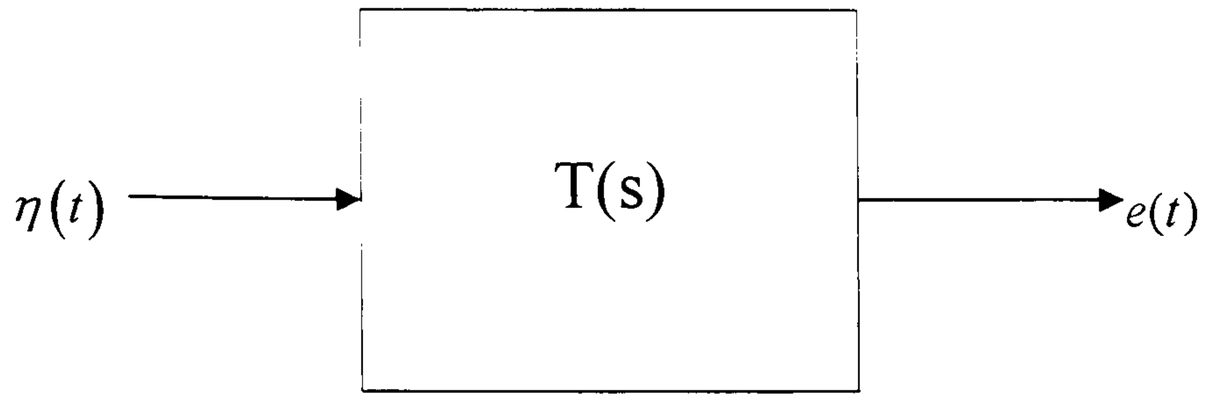

Figure 7.1. System with white noise input and output

Assuming that $T(s)$ is stable with $T(\infty)=0$, its H_2 norm can be defined as:

$$\|T\|_2 = \sqrt{E\left\{\int_0^\infty \|e(t)\|^2\, dt\right\}} \tag{7.1}$$

(see section 5.3.3.a) where $\|\cdot\|$ denotes the Euclidean-norm of $e(t)$, i.e.

$$\|\underline{e}\| = \sqrt{\sum_{i=1}^{n} e_i^{\,2}} \tag{7.2}$$

Normally $T(s)$ is an implicit function of a controller and the H_2 optimal control problem is to choose a controller so that $T(s)$ is stable and minimises (7.1). The regulated (vector) signal typically includes the control input as one of its components. Thus the H_2-problem involves the minimisation of

$$E\left\{\|z\|_2^2 + \rho\|u\|^2\right\} \tag{7.3}$$

where z is a linear function of the state vector $\underline{x}$. This can be expressed equivalently in the more familiar Linear Quadratic Gaussian (LQG) form involving matrix weighting terms Q and R, written as:

$$\text{Minimise } J(u) = E\left\{\int_0^\infty \left\{x^T Q x + u^T R u\right\}\right\} \tag{7.4}$$

It is well known [Maciejowski 1989] that the above minimisation can be split into two sub-problems. The first is to optimally estimate the state-vector (in the means-square sense), whose solution is provided by Kalman-filtering theory. The second sub-problem is to find the control signal which minimises the deterministic version of the cost function of (7.4), subject to constraints of the systems dynamics, $\dot{x} = Ax + Bu$.

The solution is to let the control signal *u(t)* be a linear function of the state:

$$u(t) = -K_c x(t) \tag{7.5}$$

where K_c is the optimal state-feedback matrix that minimises $J(u)$ (with the expectation operator removed and assuming that all state variables are accessible). Then the so-called separation principle (or certainty equivalence principle) guarantees that the overall optimal solution of (7.4) is still obtained when the optimal state-feedback is applied on the state estimates, rather than the states themselves.

The H_∞ problem assumes bounded-energy for both input and output signals and minimises the maximum input-output energy transfer, which is given by the infinity-norm of their transfer function, i.e.,

$$\min\|T\|_\infty = \min \max_{\omega \in \Re} \bar{\sigma}[T(j\omega)] \tag{7.6}$$

where the minimisation is again carried out over the set of all stabilising controllers. H_∞ control models systems in the frequency domain and is especially powerful in dealing with uncertainties in the model's inputs or parameters. It is more robust than H_2-control but could be conservative if the disturbances are modelled naturally as white-noise signals. In this section, we are interested to minimise the peak value of the regulated signal over the class of bounded input disturbances, which, as was concluded in the previous chapter, is more relevant for active vibration control of civil engineering structures. This leads to a minimisation of the l_∞-norm of the impulse response of the system between the disturbance input and the regulated output. A novel approach is developed for solving this problem in discrete time (subject to peak magnitude and rate

constraints on the control signal), using a dead-beat parametrisation of all discrete-time stabilising controllers, which leads to a linear-programming optimisation framework.

7. 2. Design of 1-storey model

As explained in earlier chapters, the main objective of active vibration control for civil engineering structures is to minimise the peak-magnitude of displacements during earthquake excitation, so that, if possibly, the structure does not enter into the inelastic region.

The structure described in chapter 5.2.1 will be examined here, but in order to simplify the analysis only the base and first floor are taken into account as shown in diagram 7.2. This allows the analysis by means of single-input single-output (scalar) techniques. Extensions to the multivariable case are more complex and will be investigated at a later point.

Specifications of Structure			
Floor	M (kg)	C (N.s/m)	K (N/m)
Base	5	100	16000
1st	1.72	0.078	2600

Table 7.1

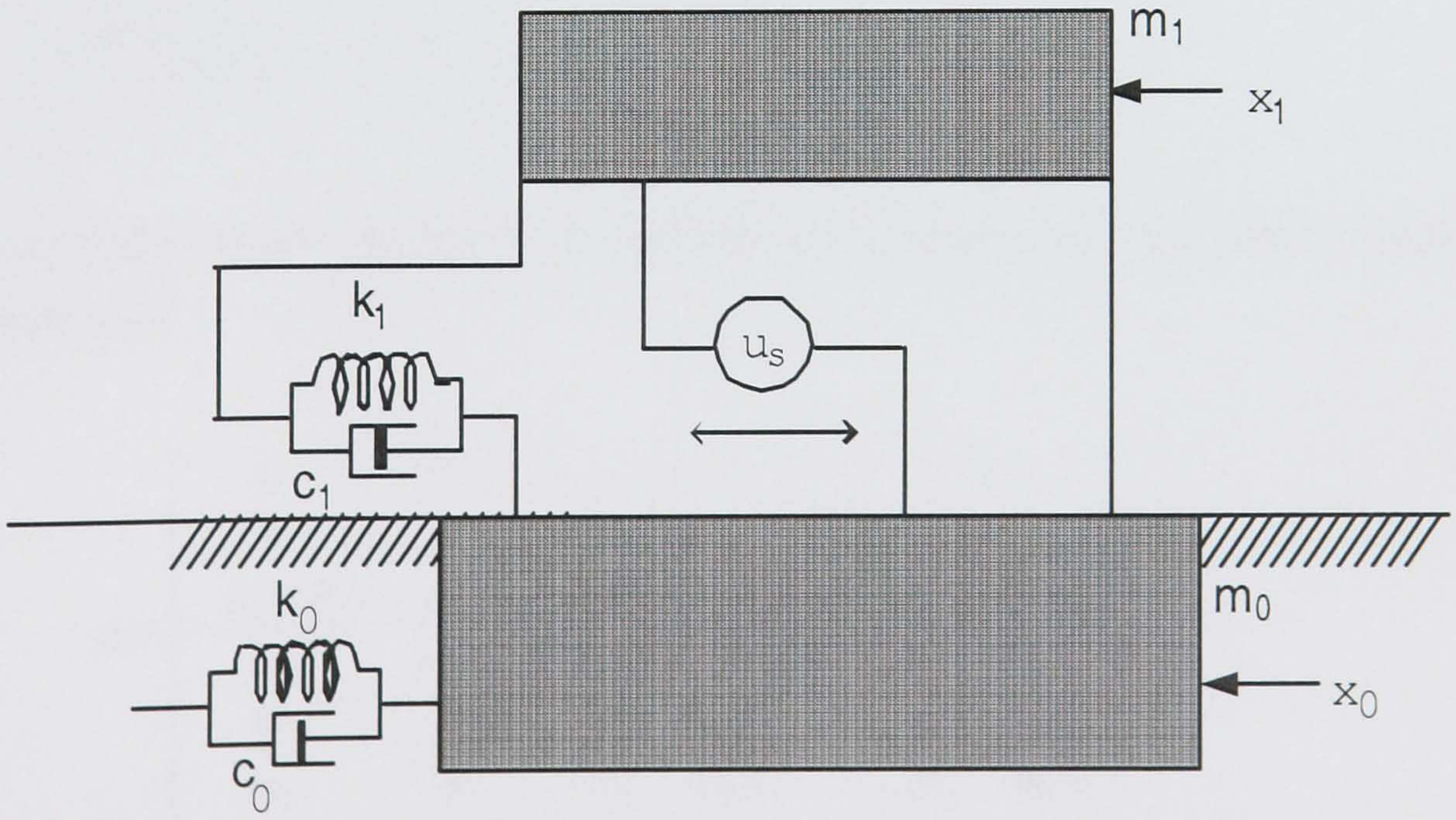

Figure 7.2. Idealisation of a 2 storey building as a spring mass damper model

By following the same procedure as in chapter 4.2, the following state space equations are obtained for the passive system:

$$\dot{x} = Ax + F\nu + Bu$$

$$y = Cx + Du$$

The passive state-space matrices are:

$$A = \begin{bmatrix} 0 & 0 & 1 & 0 \\ 0 & 0 & 0 & 1 \\ -\frac{k_0 + k_1}{m_0} & \frac{k_1}{m_0} & -\frac{c_1 + c_0}{m_0} & \frac{c_1}{m_0} \\ \frac{k_1}{m_1} & -\frac{k_1}{m_1} & \frac{c_1}{m_1} & -\frac{c_1}{m_1} \end{bmatrix}$$

$$B = \begin{bmatrix} 0 & 0 & -\frac{1}{m_0} & \frac{1}{m_0} \end{bmatrix}^T$$

$$F = \begin{bmatrix} 0 & 0 & 1 & 0 \end{bmatrix}^T$$

$$C = \begin{bmatrix} -\frac{k_0 + k_1}{m_0} & \frac{k_1}{m_0} & \frac{c_1 + c_0}{m_0} & \frac{c_1}{m_0} \end{bmatrix}$$

and

$$D = \begin{bmatrix} \frac{1}{m_1} \end{bmatrix}$$

When linear actuator dynamics are included in the model, the state-space matrices are modified as:

$$A = \begin{bmatrix} 0 & 0 & 1 & 0 \\ 0 & 0 & 0 & 1 \\ -\frac{k_0 + k_1}{m_0} & \frac{k_1}{m_0} & -\frac{c_1 + c_0}{m_0} + \frac{k_f k_e}{m_0 R} & \frac{c_1}{m_0} + \frac{k_f k_e}{m_0 R} \\ \frac{k_1}{m_1} & -\frac{k_1}{m_1} & \frac{c_1}{m_1} + \frac{k_f k_e}{m_1 R} & -\frac{c_1}{m_1} + \frac{k_f k_e}{m_1 R} \end{bmatrix}$$

$$B_1 = \begin{bmatrix} 0 & 0 & -\dfrac{k_f}{m_0 R} & \dfrac{k_f}{m_1 R} \end{bmatrix}^T$$

$$F = \begin{bmatrix} 0 & 0 & 1 & 0 \end{bmatrix}^T$$

$$C_1 = \begin{bmatrix} -\dfrac{k_0 + k_1}{m_0} & \dfrac{k_1}{m_0} & -\dfrac{c_1 + c_0}{m_0} + \dfrac{k_f k_e}{m_0 R} & -\dfrac{c_1 + c_0}{m_0} + \dfrac{k_f k_e}{m_0 R} \end{bmatrix}$$

and

$$D_1 = \begin{bmatrix} \dfrac{k_f}{m_1 R} \end{bmatrix}$$

Note that the only measured output in this case is the acceleration signal $\ddot{x}_1$.

7.3. LPOC control design algorithm

An optimisation method is developed here, whose aim is to minimise the maximum peak output of one regulated signal (subject to magnitude and rate constraints of a second regulated signal) for a particular class of disturbances (to be specified later). The method is called Linear Programming Optimal Controller (LPOC) throughout this thesis. The procedure for solving the problem is as follows:

STEP 1: Define the generalised plant

The generalised plant is depicted in Figure 7.3.

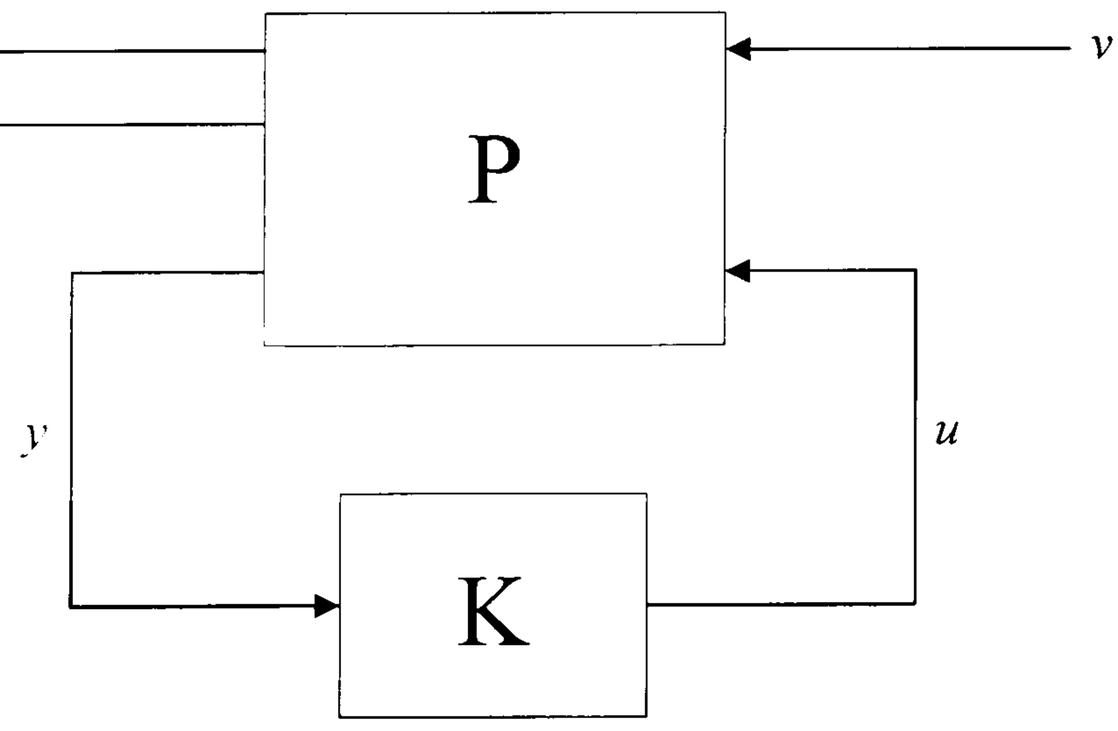

Figure 7.3. Generalised plant

where,

u is the control input

y is the measured output (first floor acceleration)

v is the external disturbance

z is the regulated output vector

In our case, we take the two regulated signals to be the first-floor acceleration and the control signal. It is required that the controller should stabilise the system and

$$\min \max_{t \geq 0} \left| \ddot{x}_1(t) \right| \text{ subject to } \left| u(t) \right| \leq u_{\max} \text{ for all } t \geq 0$$

Additionally, to avoid highly discontinuous signals we may impose constraints of the derivative of the control, e.g.

$$\left| \dot{u}(t) \right| \leq \dot{u}_{\max} \text{ for all } t \geq 0$$

Choosing $z = \begin{pmatrix} \ddot{x}_1 & u \end{pmatrix}^T$ where $\ddot{x}_1$ is first-floor acceleration and u is the actuator voltage, the generalised plant has a state-space description.

$$\begin{aligned} \dot{x} &= Ax + Fv + Bu \\ \begin{pmatrix} z \\ y \end{pmatrix} &= \begin{bmatrix} C_1 \\ C_2 \end{bmatrix} x + \begin{bmatrix} D_1 \\ D_2 \end{bmatrix} u + \begin{bmatrix} 0 \\ 0 \end{bmatrix} v \end{aligned} \tag{7.7}$$

where A,B,C,D are as defined above. Note that there is no direct feedthrough term from the disturbance v to z or y. The systems state-space realisation can be partitioned as shown below:

$$P(s) = \left[\begin{array}{c|cc} A & B_1 & B_2 \\ \hline C_2 & 0 & D_{12} \\ 0 & 0 & 1 \\ \hline C_2 & 0 & D_{22} \end{array}\right]$$

Rows 1 and 2 of the C matrix correspond to the two regulated outputs, in this case the first floor acceleration $\ddot{x}_1$ and the control input effort u. The last row defines the measured output, in this case also $\ddot{x}_1$.

STEP 2: System discretisation.

The solution to the problem will be obtained in discrete-time. This means that we need to discretise the system using an appropriate sampling interval of T seconds. The zero-order hold discrete-time equivalent of the system can be employed using the standard procedure for transforming between continuous and discrete times [Antsaklis and Mitchell 1998]: At time t_k, the ZOH maintains the value of its input analog signal $u(t)$ constant until the next sampling time t_{k+1}. Discrete-time systems are described by the z-transform. In the z-domain a system is stable if all its poles are inside the unit circle (within a distance of one from the origin). The period of the system is chosen as $T = 0.01ms$. The corresponding sampling frequency $f_s = 100Hz$ is significantly larger than the highest frequency of interest (frequency of the first mode).

STEP 3: Youla parametrisation of all stabilising controllers.

The procedure is outlined in section 3.6.5 but the main results are summarised below: The controller and closed-loop systems are defined in terms of two matrices F and H (state-feedback and output injection). F and H can be any two matrices such that $A + B_2F$ and $A + HC_2$ are asymptotically stable (all eigenvalues inside unit circle). The aim of Youla parametrisation is to obtain a parametrisation of all stabilising controllers and the corresponding closed-loop systems between the disturbance and the regulated signals. The parametrisation proceeds by first expressing the plant $G(z)$ as the ratio of two stable, relatively prime transfer functions. The procedure is identical in continuous and discrete domains, with the exception that "stability" is defined appropriately in each domain. In addition, we have complete freedom in the choice of state-feedback (F) and output injection (H) matrices, as long as $A + B_2F$ and $A + HC_2$ are asymptotically stable; here F and H will be chosen so that all eigenvalues of $A + B_2F$ and $A + HC_2$ are placed at the origin; this is always possible under appropriate controllability and observability assumptions (which are satisfied in this case).

The set of stabilising controllers is parametrised in bilinear (linear-fractional) form, while the set of closed-loop systems in linear (more precisely affine) form, i.e.

$$T(z) = T_1(z) - T_2(z)Q(z)T_3(z) \tag{7.8}$$

where $Q(z)$ is a free stable matrix parameter; the functions $T_1(z)$, $T_2(z)$ and $T_3(z)$ have been defined in an earlier chapter and depend solely on the state space matrices A, F, C, D and the choice of F and H. We will also make use of the slightly different parametrisation

$$T(z^{-1}) = T_1(z^{-1}) - T_2(z^{-1})Q(z^{-1})T_3(z^{-1}) \tag{7.9}$$

in which all terms have been redefined as functions of z^{-1} rather than z. This will be useful in describing recursive relations between the input and output discretised signals used later.

STEP 4: Pole placement at the origin

The problem here is stated as follows: Given that the pair (A, B) is controllable, find F such that all eigenvalues of $A + BF$ are placed at the origin. This can be achieved by the following steps:

1. Define characteristic polynomial of A

$$p(s) = \det(sI - A) = s^n + \alpha_{n-1}s^{n-1} + \alpha_{n-2}s^{n-2} + \ldots + a_0$$

2. Define A_c, B_c which are in canonical controllable form:

$$A_c = \begin{bmatrix} -\alpha_{n-1} & -\alpha_{n-2} & \cdots & -\alpha_1 & -\alpha_0 \\ 1 & 0 & \cdots & 0 & 0 \\ 0 & \ddots & & & \vdots \\ \vdots & & \ddots & 0 & \\ 0 & & 0 & 1 & 0 \end{bmatrix}, \quad B_c = \begin{bmatrix} 1 \\ 0 \\ \vdots \\ \\ 0 \end{bmatrix} \tag{7.10}$$

Note that the first row of A_c contains the coefficients of the characteristic polynomial in descending order with negative signs.

3. Define Γ, Γ_c, T where

$$\Gamma = \begin{bmatrix} B & AB & A^2B & \cdots & A^{n-1}B \end{bmatrix} \tag{7.11}$$

$$\Gamma_c = \begin{bmatrix} B_c & A_cB_c & A_c^2B_c & \cdots & A_c^{n-1}B_c \end{bmatrix} \tag{7.12}$$

$$T = \Gamma_c^{-1}\Gamma \tag{7.13}$$

4. Obtain the state-feedback matrix F

$$F = \begin{bmatrix} \alpha_{n-1} & \alpha_{n-2} & \cdots & a_0 \end{bmatrix} \tag{7.14}$$

The algorithm described above is developed in order to comply with the standard pole placement design approach involving Ackermann's formula. Initially, a transformation T is required such that the controllable canonical form of the pair (A, B) is obtained (7.10). This form is favourable since the characteristic polynomial of A is known and A_c and B_c are sparse. A state feedback matrix F is required such that

$$A_c + B_cF_c = \begin{bmatrix} -\alpha_{n-1} & -\alpha_{n-2} & \cdots & -\alpha_1 & -\alpha_0 \\ 1 & 0 & \cdots & 0 & 0 \\ 0 & \ddots & & & \vdots \\ \vdots & & \ddots & 0 & \\ 0 & & 0 & 1 & 0 \end{bmatrix} + \begin{bmatrix} 1 \\ 0 \\ \vdots \\ \\ 0 \end{bmatrix} \begin{bmatrix} f_1 & f_2 & \cdots & f_n \end{bmatrix}$$

$$= \begin{bmatrix} f_1 - \alpha_{n-1} & f_2 - \alpha_{n-2} & \cdots & f_{n-1} - \alpha_1 & f_n - \alpha_0 \\ 1 & 0 & \cdots & 0 & 0 \\ 0 & \ddots & & & \vdots \\ \vdots & & \ddots & 0 & \\ 0 & & 0 & 1 & 0 \end{bmatrix}$$

so that

$$\det\left|sI - A_c - B_cF_c\right| = s^n + \left(\alpha_{n-1} - f_1\right)s^{n-1} + \left(\alpha_{n-2} - f_2\right) + \ldots + \left(a_0 + f_n\right) \tag{7.15}$$

which is the closed-loop characteristic polynomial. Setting this equal to s^n gives:

$$F_c = \begin{bmatrix} f_1 & f_2 & \cdots & f_n \end{bmatrix} = \begin{bmatrix} \alpha_{n-1} & \alpha_{n-2} & \ldots & a_0 \end{bmatrix} \tag{7.16}$$

Now that F_c is determined, the inverse transformation T^{-1} is required to obtain F. If we assume that $F_c = FT^{-1}$ is the inverse transformation, then using $A_c = TAT^{-1}$ and $B_c = TB$ gives:

$$A_c + B_c F_c = TAT^{-1} + TBFT^{-1} = T\left[A + BF\right]T^{-1} \tag{7.17}$$

so that $A_c + B_c F_c$ and $A + BF$ have the same characterictic polynomial s^n. The original transform T is known to be equation (7.13) [Antsaklis and Mitchell 1998]. The problem of selecting H so that $A + HC$ has all eigenvalues at the origin is dual to the state feedback problem described above.

STEP 5: Formulation of optimisation problem in terms of linear constraints

First partition the closed-loop equations by using the Youla parametrisation as:

$$\begin{bmatrix} z_1 \\ z_2 \end{bmatrix} = \begin{bmatrix} y \\ u \end{bmatrix} = \begin{bmatrix} T_1^1\left(z^{-1}\right) \\ T_1^2\left(z^{-1}\right) \end{bmatrix} - \begin{bmatrix} T_2^1\left(z^{-1}\right) \\ T_2^2\left(z^{-1}\right) \end{bmatrix} Q\left(z^{-1}\right) T_3\left(z^{-1}\right) \nu\left(z^{-1}\right) \tag{7.18}$$

where y and u are the regulated outputs. Since in this case $T_1\left(z^{-1}\right)$ is stable, this can be alternatively written as:

$$\begin{bmatrix} y \\ u \end{bmatrix} = \begin{bmatrix} T_1^1\left(z^{-1}\right) \\ T_1^2\left(z^{-1}\right) \end{bmatrix} - \begin{bmatrix} T_2^1\left(z^{-1}\right) T_3\left(z^{-1}\right) \\ T_2^2\left(z^{-1}\right) T_3\left(z^{-1}\right) \end{bmatrix} Q\left(z^{-1}\right) \nu\left(z^{-1}\right) \tag{7.19}$$

Hence the transfer function between ν and y for the first regulated output y can be written as:

$$T(z^{-1}) = \frac{y(z^{-1})}{\nu(z^{-1})} = T_1^1\left(z^{-1}\right) + T_2^1\left(z^{-1}\right) T_3\left(z^{-1}\right) Q(z^{-1}) \tag{7.20}$$

The following terms have been replaced accordingly in order to simplify equation (7.20):

$$b\left(z^{-1}\right) = T_1^1\left(z^{-1}\right), \quad c(z^{-1}) = T_2^1\left(z^{-1}\right) T_3\left(z^{-1}\right), \quad q(z^{-1}) = Q(z^{-1})$$

to get:

$$T(z^{-1}) = \frac{y(z^{-1})}{\nu(z^{-1})} = \frac{b(z^{-1}) + c(z^{-1})q(z^{-1})}{a(z^{-1})} \tag{7.21}$$

Here, $a(z^{-1})$ is the denominator and $q\left(z^{-1}\right)$ is the free parameter. i.e. any H_2 function. It is up to the designer to choose $q\left(z^{-1}\right)$ to optimise $T(z^{-1})$. Note also that under the assumption made earlier (all eigenvalues of $A + B_2F$ and $A + HC_2$ placed at the origin), $a(z^{-1}) = 1$. This choice is only made for convenience (since it simplifies the exposition) and the problem *can be* solved for arbitrary pole locations (inside the unit circle).

Now assume that ν is a (discrete) impulse, so that $\nu(z^{-1}) = 1$. The degree of both $b\left(z^{-1}\right)$ and $c\left(z^{-1}\right)$ will be *r*, where *r* is the number of state variables. Also, $a\left(z^{-1}\right) = 1$ because the eigenvalues of $A + B_2F$ and $A + HC_2$ are placed at the origin. Parametrise $q\left(z^{-1}\right)$ as a finite-impulse-response (FIR) filter of arbitrary degree *p*, i.e.

$$q(z^{-1}) = q_0 + q_1 z^{-1} + q_2 z^{-2} + \cdots + q_p z^{-p} \tag{7.22}$$

Also write

$$b(z^{-1}) = b_0 + b_1 z^{-1} + b_2 z^{-2} + \cdots + b_r z^{-r}$$
$$c(z^{-1}) = c_0 + c_1 z^{-1} + c_2 z^{-2} + \cdots c_r z^{-r}$$
$$y(z^{-1}) = y_0 + y_1 z^{-1} + y_2 z^{-2} + \cdots y_N z^{-N}$$

Then, in equation (7.21):

$$\begin{aligned} y(z^{-1}) &= b(z^{-1}) + c(z^{-1})q(z^{-1}) \\ &= b_0 + b_1 z^{-1} + \ldots + b_r z^{-r} + (c_0 + c_1 z^{-1} + \ldots + c_r z^{-r})(q_0 + q_1 z^{-1} + \ldots + q_p z^{-p}) \\ &= b_0 + b_1 z^{-1} + \ldots + b_r z^{-r} + c_0 q_0 + \left(c_0 q_1 + c_1 q_0\right) z^{-1} + \left(c_0 q_2 + c_1 q_1 + c_2 q_0\right) z^{-2} + \ldots + c_r q_p z^{-r-p} \end{aligned} \tag{7.23}$$

The multiplication of polynomials $c\left(z^{-1}\right)$ and $q\left(z^{-1}\right)$ can be implemented in matrix form as a multiplication by a Toeplitz matrix. Thus, the order of $y\left(z^{-1}\right)$ in equation (7.23) is *r*+*p*, i.e.

$$\deg[y(z^{-1})] = N = r + p \text{ and } y_k = 0 \text{ for } k > N = r + p .$$

Equation (7.21) can be written in matrix form as:

$$\begin{bmatrix} y_0 \\ y_1 \\ \vdots \\ y_r \\ \vdots \\ y_n \\ \vdots \\ \vdots \\ y_{p+r} \end{bmatrix} = \begin{bmatrix} b_0 \\ b_1 \\ \vdots \\ b_r \\ 0 \\ 0 \\ \vdots \\ 0 \\ 0 \end{bmatrix} + \begin{bmatrix} c_o & 0 & 0 & 0 & \cdots & 0 & 0 & 0 & 0 \\ c_1 & c_0 & 0 & 0 & \cdots & 0 & 0 & 0 & 0 \\ \vdots & \ddots & \ddots & & \cdots & 0 & 0 & 0 & 0 \\ c_r & c_{r-1} & \cdots & \cdots & \cdots & c_1 & c_0 & 0 & 0 \\ 0 & \ddots & \ddots & \ddots & \cdots & \ddots & \ddots & \ddots & 0 \\ 0 & 0 & c_r & c_{r-1} & \cdots & \cdots & \cdots & c_1 & c_0 \\ 0 & 0 & 0 & \ddots & \cdots & \ddots & \ddots & \ddots & c_1 \\ 0 & 0 & 0 & 0 & \cdots & 0 & 0 & c_r & c_{r-1} \\ 0 & 0 & 0 & 0 & \cdots & 0 & 0 & 0 & c_r \end{bmatrix} \begin{bmatrix} q_0 \\ q_1 \\ \\ \vdots \\ \vdots \\ \\ q_p \end{bmatrix} \tag{7.24}$$

Note that the response is forced to be deadbeat, i.e y_{p+r} is the last non zero value of the regulated output. This means that the controller makes the output zero after $p+r$ samples. This is due to the restriction on $q\left(z^{-1}\right)$ which was taken to be an FIR filter and may lead to a conservative solution unless r is taken to be large. Ideally r should be selected to make NT, a reasonable transient before the structure is fully stabilised. It is expected (but need to be established formally) that for large N the deviation from optimality can be made arbitrarily small. The equations can be written compactly in matrix form $y = b + Cq$ where q contains the coefficients of $q\left(z^{-1}\right)$ and C is a Toeplitz matrix. The same procedure is followed for the second regulated output.

STEP 6: Formulation into a linear programming problem

Since all constraints are linear, the minimisation of the peak response of the regulated signal can be formulated as a linear programming problem of the form:

$$\min C^T x \text{ subject to } Ax \le b \tag{7.25}$$

Let δ be the maximum output of the regulated signal (acceleration) that we wish to minimise. Then:

$$-\delta \le y(k) \le \delta \quad \text{for all} \quad 0 \le k \le N \tag{7.26}$$

Now, $y_k = c_k{}^T x + \hat{b}_k$, where $c_k{}^T$ denotes the k-th row of the C-matrix of equation (7.24), and $\hat{b}_k$ is defined as:

$$b_k = b_k \text{ for } 0 \le k \le r \text{ and } b_k = 0 \text{ for } k > r \tag{7.27}$$

Thus, separating the two equations we can write:

$$-c_k{}^T q - \delta \le \hat{b}_k \quad \text{and} \quad c_k{}^T q - \delta \le -\hat{b}_k \quad \text{for all } 0 \le k \le N$$

The optimal solution is the minimum value of $\delta = | y_{\max} |$ for which equation (7.21) is valid. The constraints can be represented compactly in matrix form as:

$$\begin{bmatrix} \mathbf{-1} & C \\ \mathbf{-1} & -C \end{bmatrix} \begin{bmatrix} \delta \\ \mathbf{q} \end{bmatrix} \le \begin{bmatrix} \hat{\mathbf{b}} \\ \mathbf{-\hat{b}} \end{bmatrix} \tag{7.28}$$

where $\mathbf{1}$ represents a column-vector of p ones, C is the $(p+r)\times p$ matrix of equation (7.24), $\hat{\mathbf{b}}$ is the vector of p terms of equation (7.24), q is an n-dimensional vector containing the unknown coefficients q_i and δ is a scalar. Setting

$$\mathbf{x} = \begin{pmatrix} \delta \\ \mathbf{q} \end{pmatrix}$$

the problem is now in the standard linear-programme form:

$$\min \delta = \begin{bmatrix} 1 & 0 & \cdots & 0 \end{bmatrix} \mathbf{x}$$

subject to:

$$\begin{bmatrix} \mathbf{-1} & C \\ \mathbf{-1} & -C \end{bmatrix} \mathbf{x} \le \begin{bmatrix} \hat{\mathbf{b}} \\ \mathbf{-\hat{b}} \end{bmatrix} \tag{7.29}$$

The solution to the problem will result in the optimal peak-value of the regulated signal and the coefficients of the optimal $q(z^{-1})$, from which the optimal controller can be recovered via a bilinear transformation corresponding to the Youla parametrisation (see section 3.6.5). Note that the optimal δ is the variable to be minimised, i.e the maximum absolute value of the acceleration signal.

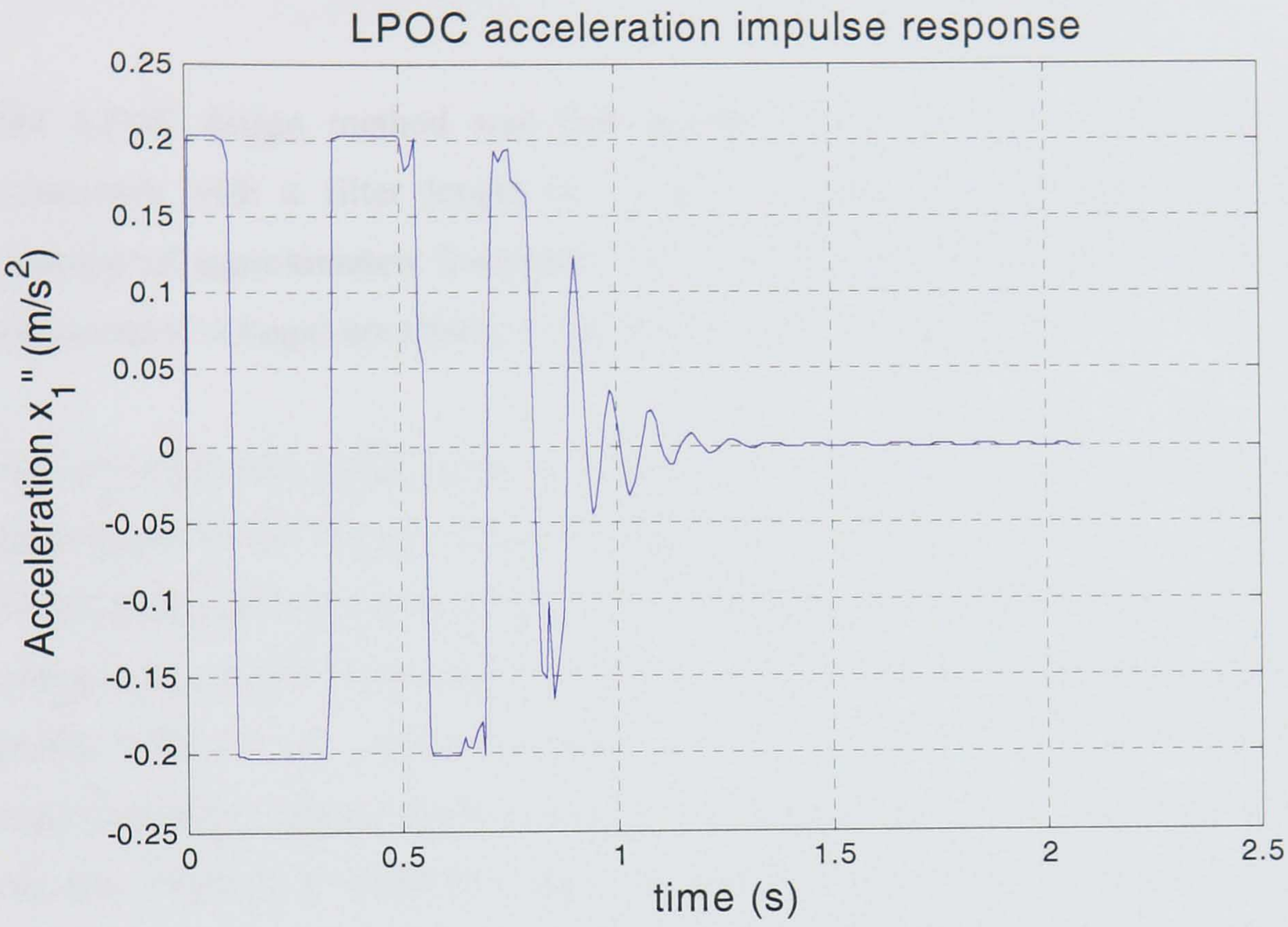

Figure 7.4 LPOC acceleration impulse response

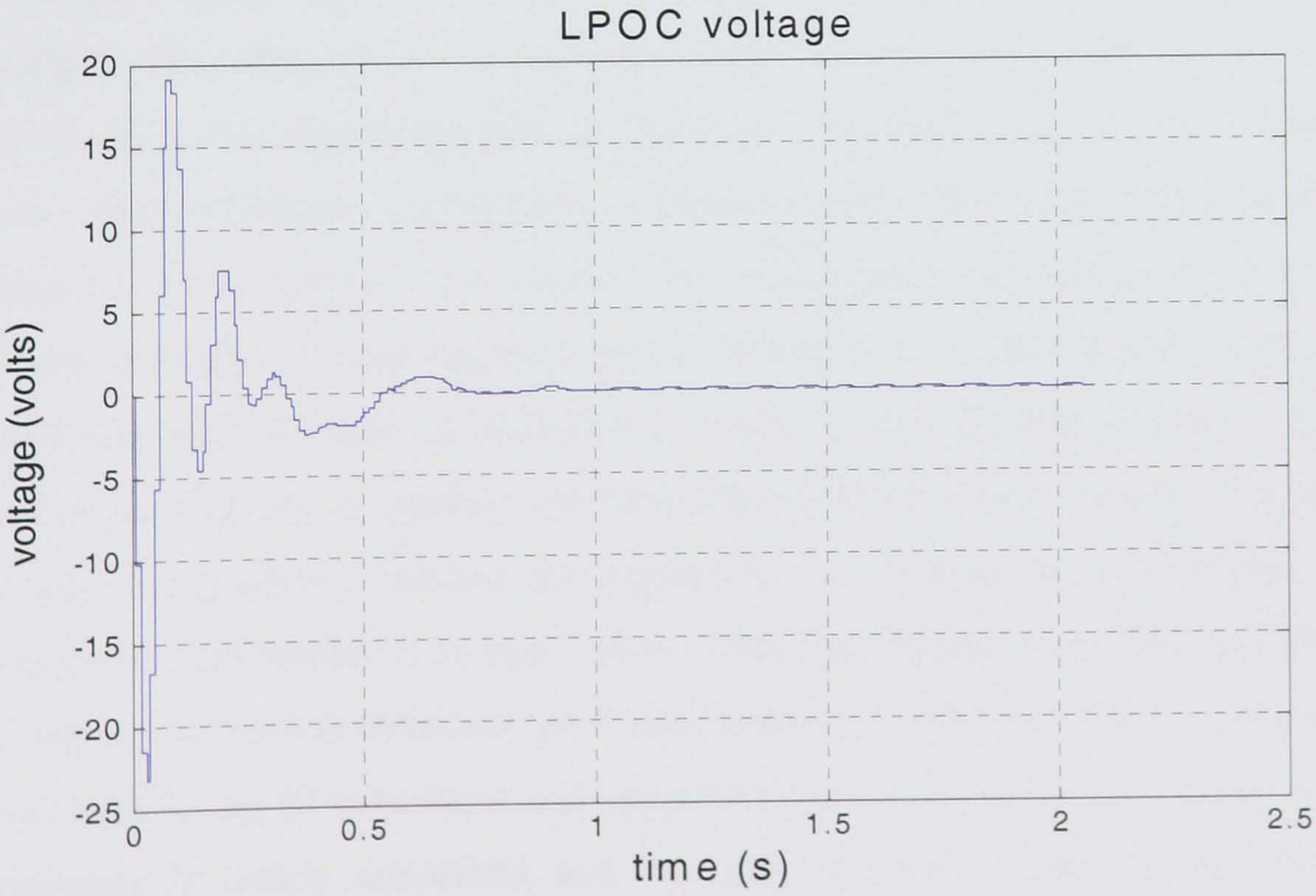

Figure 7.5 LPOC control effort for impulse load

Comparison between LPOC and LQR		
	$\ddot{x}_{max}\,(m/s^2)$	u_{max} (Volts)
LPOC	0.21	22
LQR	13	16.15

Table 7.2.

The LPOC design method was first applied to the structure without any control constraints with a filter length of $r = 200$ samples, corresponding to a deadbeat response of approximately 2 seconds. The two regulated signals (1st floor acceleration and actuator voltage) are shown in Figures 7.4 and 7.5 respectively.

The unconstrained LPOC method yields excellent results in terms of optimising the peak signal level. The maximum acceleration is extremely low, $0.21 m/s^2$ (about 100 times smaller than the peak acceleration resulting from the LQR design, while the peak voltage control level increased by a factor of 1.25). However, the resulting acceleration profile (Figure 7.4) clearly indicates that the response is unrealistic for practical implementation. The acceleration reaches its peak positive value of 0.21 m/s^2 extremely fast and swings to its minimum negative value 0.21 m/s^2 almost 10 ms later, requiring a huge slew-rate from the actuator. Subsequently, the acceleration fluctuates between the two extreme values for a few cycles of progressively increasing frequency before decaying to zero after about 1.5 seconds, (half a second earlier than the set deadbeat horizon) exhibiting highly-damped oscillations. This behaviour can be explained as follows: The maximum acceleration is reached very fast (first peak) because the disturbance is an impulse. To counter the acceleration increasing excessively, the controller produces a large negative force, followed by a large positive force a few milliseconds later, to limit acceleration increase in the opposite direction. After the maximum acceleration is reached, the controller's primary goal is to keep it at the same level and thus gradually reduces the applied forces. Finally, the acceleration reaches zero as the system settles to its equilibrium. Thus the method works theoretically in the sense that it succeeds to minimise peak acceleration, as indicated by the flat regions of the acceleration signal at positive and negative peaks of the same magnitude. However, the response is clearly unrealistic and thus the controller cannot be implemented in practice. The high rate of the control signal (especially in the early part of the response)

means that even if this control profile could be generated by the actuator, the resulting closed-loop system would have an unrealistically large bandwidth, and hence the system would have poor stability margins and would be highly susceptible to model uncertainties.

STEP 7: Imposing Constraints

In the above formulation, the peak value of the regulated output is minimised for an impulsive loading without any constraints on the size or rate of the control input. This is unrealistic and may result in highly discontinuous control signals that would be difficult to implement or could cause stability problems, especially in the presence of model uncertainty, due to the potentially excessive bandwidth of the closed-loop system. Thus, some constraints need to be added in order to make the design more realistic. The first constraint limits the magnitude of the control signal, i.e. we require that:

$$|u_k| \leq u_{\max} \text{ for all } k \geq 0$$

Now note that from the Youla parametrisation with $u\left(z^{-1}\right)$ as the second regulated output we can write:

$$u\left(z^{-1}\right) = T_1^2(z^{-1}) - T_2^2(z^{-1})T_3(z^{-1})q(z^{-1})$$

which may be written in the more convenient form:

$$u\left(z^{-1}\right) = \beta(z^{-1}) + \gamma(z^{-1})q(z^{-1}) \tag{7.30}$$

Note again that $\beta(z^{-1}), \gamma(z^{-1})$ and $q(z^{-1})$ are polynomials in z^{-1} (the first two due to special type of parametrisation, and the third due to restriction of $q(z^{-1})$ in the class of FIR filters). Similarly to the last section, the equation can be written in matrix form:

$$\begin{bmatrix} u_0 \\ u_1 \\ \vdots \\ u_r \\ \vdots \\ \vdots \\ \vdots \\ \vdots \\ u_{p+r} \end{bmatrix} = \begin{bmatrix} \beta_0 \\ \beta_1 \\ \vdots \\ \beta_r \\ 0 \\ 0 \\ \vdots \\ 0 \\ 0 \end{bmatrix} + \begin{bmatrix} \gamma_0 & 0 & 0 & 0 & \cdots & 0 & 0 & 0 & 0 \\ \gamma_1 & \gamma_0 & 0 & 0 & \cdots & 0 & 0 & 0 & 0 \\ \vdots & \ddots & \ddots & & \cdots & 0 & 0 & 0 & 0 \\ \gamma_r & \gamma_{r-1} & \cdots & \cdots & \cdots & \gamma_1 & \gamma_0 & 0 & 0 \\ 0 & \ddots & \ddots & \ddots & \cdots & \ddots & \ddots & \ddots & 0 \\ 0 & 0 & \gamma_r & \gamma_{r-1} & \cdots & \cdots & \cdots & \gamma_1 & \gamma_0 \\ 0 & 0 & 0 & \ddots & \cdots & \ddots & \ddots & \ddots & \gamma_1 \\ 0 & 0 & 0 & 0 & \cdots & 0 & 0 & \gamma_r & \gamma_{r-1} \\ 0 & 0 & 0 & 0 & \cdots & 0 & 0 & 0 & \gamma_r \end{bmatrix} \begin{bmatrix} q_0 \\ q_1 \\ \\ \vdots \\ \vdots \\ \\ q_p \end{bmatrix} \tag{7.31}$$

where the β_i and γ_i are the coefficients of the polynomials $\beta(z^{-1})$ and $\gamma(z^{-1})$ of equation (7.30), respectively. Writing the equation in compact form $u = \hat{\beta} + \Gamma q$ as before, and its k-th row as $u_k = \hat{\beta}_k + \gamma_k{}^T q$, the constraints $|u_k| \le u_{\max}$ for all k, may be expressed by a pair of linear inequalities:

$$-\gamma_k{}^T q \le u_{\max} + \hat{\beta}_k \quad \text{and} \quad \gamma_k{}^T q \le u_{\max} - \hat{\beta}_k \text{ for all } k$$

or in matrix form as:

$$\begin{pmatrix} \mathbf{0} & -\Gamma \\ \mathbf{0} & \Gamma \end{pmatrix} \begin{pmatrix} \delta \\ \mathbf{q} \end{pmatrix} \le \begin{pmatrix} u_{\max}\mathbf{1} + \hat{\boldsymbol{\beta}} \\ u_{\max}\mathbf{1} - \hat{\boldsymbol{\beta}} \end{pmatrix} \tag{7.32}$$

These can be augmented with the inequalities of the previous section (7.29) and solved via a standard linear programme to minimise δ.

When the system was optimised and simulated with the above constraints, the voltage showed a non-linear profile with very large accelerations rates. Therefore, in order to make the response more realistic an extra constraint needs to be added in the change of voltage, Δu (slew-rate constraint). Now,

$$\begin{aligned} \Delta u_k &= u_{k+1} - u_k = \hat{\beta}_{k+1} + \gamma^T{}_{k+1} q - (\hat{\beta}_k + \gamma^T{}_k q) \\ &= (\hat{\beta}_{k+1} - \hat{\beta}_k) + (\gamma^T{}_{k+1} - \gamma^T{}_k) q \end{aligned}$$

and we require

$$|\Delta u_k| \leq (\Delta u)_{\max} \quad \text{for all } k \geq 0$$

This may be written as a pair of linear inequalities:

$$(\gamma^T{}_{k+1} - \gamma^T{}_k)q \leq (\Delta u)_{\max} - (\hat{\beta}_{k+1} - \hat{\beta}_k)$$

and

$$-(\gamma_{k+1}{}^T - \gamma_k{}^T)q \leq (\hat{\beta}_{k+1} - \hat{\beta}_k) + (\Delta u)_{\max}$$

for all samples *k*, or, in matrix form as:

$$\begin{pmatrix} \mathbf{0} & -(\bar{\Gamma} - \tilde{\Gamma}) \\ \mathbf{0} & \bar{\Gamma} - \tilde{\Gamma} \end{pmatrix} \begin{pmatrix} \delta \\ \mathbf{q} \end{pmatrix} \leq \begin{pmatrix} (\Delta u)_{\max}\mathbf{1} - (\bar{\boldsymbol{\beta}} - \tilde{\boldsymbol{\beta}}) \\ (\Delta u)_{\max}\mathbf{1} + (\bar{\boldsymbol{\beta}} - \tilde{\boldsymbol{\beta}}) \end{pmatrix} \tag{7.33}$$

where $\bar{\Gamma}$ and $\bar{\boldsymbol{\beta}}$ denote the matrix Γ and the vector $\boldsymbol{\beta}$ with the first row eliminated (respectively), while $\tilde{\Gamma}$ and $\tilde{\boldsymbol{\beta}}$ denote the matrix Γ and vector $\boldsymbol{\beta}$ with the last row eliminated (respectively). The inequalities can now be augmented to the previous set of linear inequalities, and solved in a linear programme to impose additional rate constraints on the control signal.

$$\begin{bmatrix} \mathbf{1} & C \\ -\mathbf{1} & -C \\ \mathbf{0} & \Gamma \\ \mathbf{0} & -\Gamma \\ \mathbf{0} & -(\bar{\Gamma} - \tilde{\Gamma}) \\ \mathbf{0} & \bar{\Gamma} - \tilde{\Gamma} \end{bmatrix} \begin{bmatrix} \delta \\ \mathbf{q} \end{bmatrix} \leq \begin{bmatrix} \hat{\mathbf{b}} \\ -\hat{\mathbf{b}} \\ u_{\max}\mathbf{1} + \hat{\boldsymbol{\beta}} \\ u_{\max}\mathbf{1} - \hat{\boldsymbol{\beta}} \\ (\Delta u)_{\max}\mathbf{1} - (\bar{\boldsymbol{\beta}} - \tilde{\boldsymbol{\beta}}) \\ (\Delta u)_{\max}\mathbf{1} + (\bar{\boldsymbol{\beta}} - \tilde{\boldsymbol{\beta}}) \end{bmatrix} \tag{7.34}$$

An LQR design was first carried out for comparison purposes. The design involves a quadratic cost-function consisting of two penalty terms, acceleration and control effort. Both weighting factors were set to 1, penalising equally the two terms. The design was carried out both in continuous and discrete-time (with a sampling rate of 100 *Hz*), producing almost identical results.

Subsequently, the LPOC design was carried out with control constraints on the peak control signal and its rate. The peak-magnitude control signal constraint was set at 16 Volts, similar to the peak LQR and the maximum control rate at of 40 Volts/*s*. The two regulated signals resulting from the two designs (LQR and constrained LP) are shown in Fig 7.6 and 7.7. The main results of all simulations are also summarised in Table 7.3.

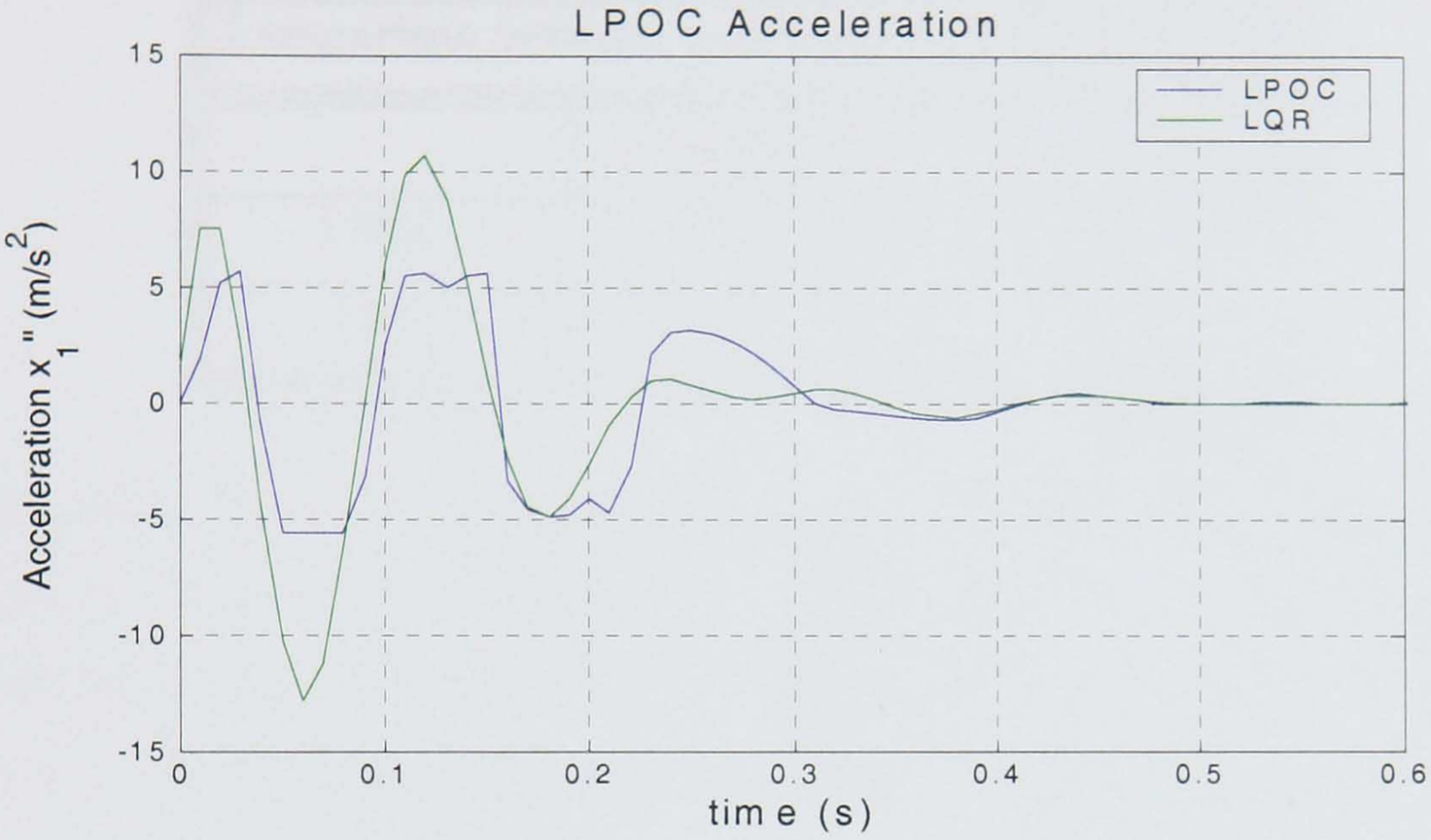

Figure 7.6 Constrained LPOC and LQR (acceleration)

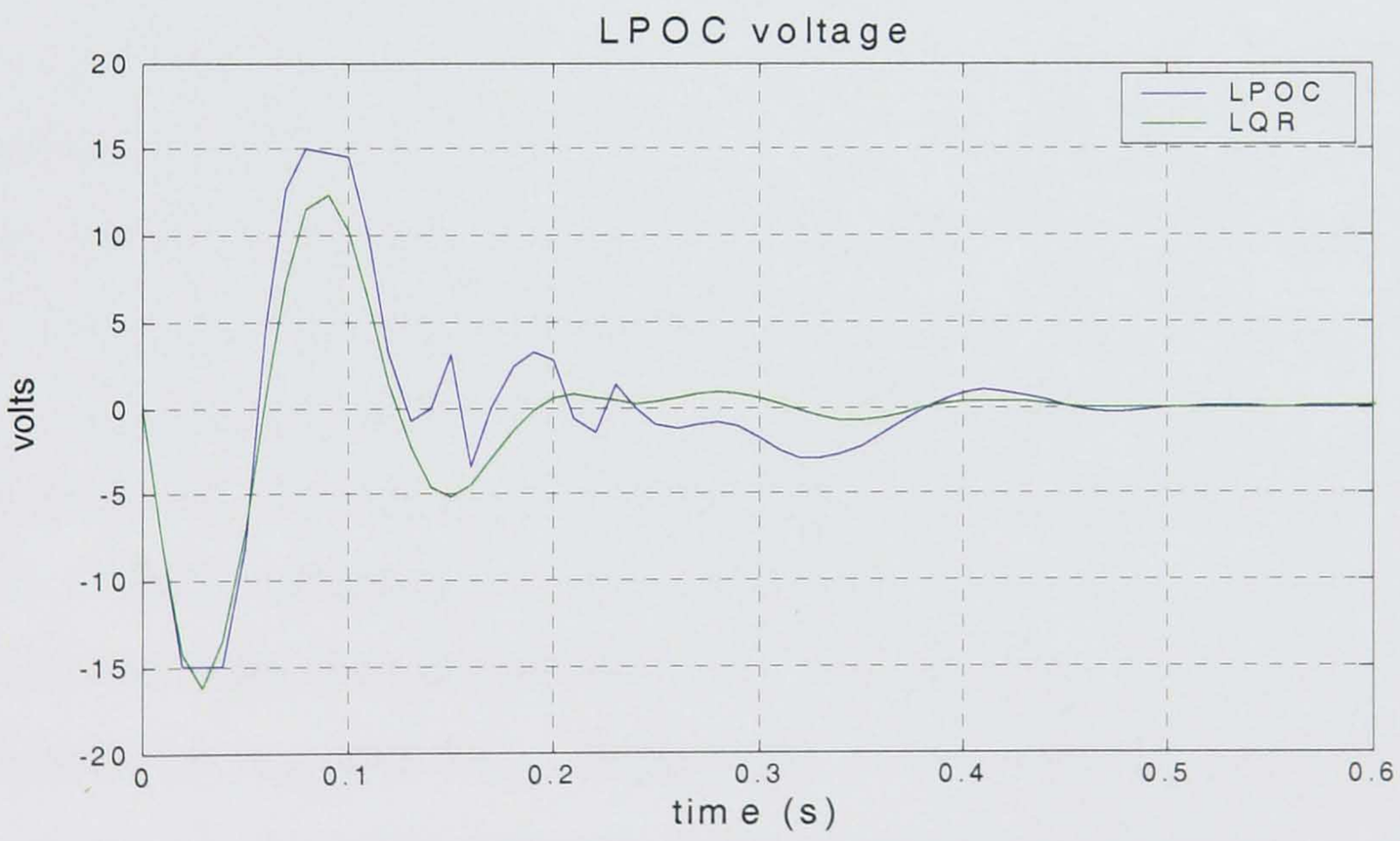

Figure 7.7 Constrained LPOC and LQR (voltage)

Setting an acceptable limit in the rate of change of the control signal $\Delta u_{\max} = 40$ Volts/s which is about ten times less than the fast rates of the early response observed in Figure 7.4, the response of the system to the impulsive loading becomes acceptable. The maximum acceleration for the constrained LP design is almost 2.5 times less than the

peak value obtained by LQR, while the controller peak signal (16 Volts) is slightly less than the peak value obtained from the LQR design (16.15 Volts). This improvement is made despite the fact that the LQR controller is based on state-feedback (all four states assumed measurable), whereas the LPOC uses output feedback only (first-floor acceleration being the only measurement).

Comparison between constrained LPOC and LQR		
	$\ddot{x}_{max}\ (m/s^2)$	u_{max} (Volts)
LPOC	5.5	16
LQR	13	16.15

Table 7.3

The simulations have been repeated several times for different set of parameters. The aim was to observe if the performance improves or not by changing the design variables, the number N of time steps, the sample time (T_s), the maximum allowable voltage u_{max} and the maximum allowable change in voltage Δu_{max}. The result are summarised in the tables 7.4 to 7.6.

The minimisation is very sensitive to the parameters used and if it is over-constrained, or the number of samples is too high or too low, the linear programming may either fail or may not reach an optimum solution. In the first table the number of samples used is varied. For more than 100 samples the solution is the same, signifying that 100 samples (or $1s$) is the minimum time required for the minimisation horizon to reduce the maximum peak and settle to zero. For 50 samples the maximum acceleration increases from 10 to 17 m/s^2, indicating that this settling-time requirement is too stringent. The second and third tables show the maximum acceleration and control effort as a function of the constraint on u_{max} and Δu_{max}, respectively. As the maximum permissible voltage and rate of change of voltage increases the maximum acceleration reduces. At some point no further reduction of peak response is possible; this is the minimum possible acceleration that this system can have.

Observing the maximum acceleration and voltage while the parameters vary is important at later phases when the design is used for a different disturbance input, i.e.,

an earthquake signal. Furthermore, the design is very sensitive even to minor changes in the parameters. If the sampling time is changed from 10 *ms* to 20 *ms*, by setting constraints $u_{\max} = 30\ Volts$ and $\Delta u_{\max} = 100$ Volts/s, the maximum acceleration is 2 m/s^2; by doubling $u_{\max}$ and $\Delta u_{\max}$ the maximum acceleration becomes 0.4 m/s^2. In previous examples by relaxing the constraints, i.e., for larger values of $u_{\max}$ and $\Delta u_{\max}$ there was no difference in the outcome

LPOC results as a function of number of samples						
Samples (N)	500	400	200	100	50	20
Permissible u_{max}	1000	1000	1000	1000	1000	1000
Permissible $\Delta u_{\max}$	30	30	30	30	30	30
$Y_{\max}$	10.22	10.21	10.23	10.23	17.18	95.48
$u_{\max}$	59.56	59.31	58.65	59.83	60	102.75

Table 7.4

LPOC results as a function of constraint on u_{max}										
Samples (N)	200	200	200	200	200	200	200	200	200	200
Permissible u_{max}	1000	500	200	100	60	50	40	30	20	15
Permissible $\Delta u_{\max}$	30	30	30	30	30	30	30	30	30	30
$Y_{\max}$	10.2	10.2	10.2	10.2	10.2	10.2	14.3	20.6	26.8	35.6
$u_{\max}$	58.6	59.6	59.8	59.1	59.7	49.6	40.3	32.1	20	15

Table 7.5

LPOC results as a function of constraint on $\Delta u_{\max}$								
Samples (N)	200	200	200	200	200	200	200	200
Permissible u_{max}	100	1000	1000	1000	1000	1000	1000	1000
Permissible $\Delta u_{\max}$	1000	1000	500	200	100	50	30	10
$Y_{\max}$	2.46	2.73	2.66	2.84	2.66	2.68	10.23	32.26
$u_{\max}$	54.14	53.86	53.93	53.74	53.92	53.91	58.65	31.01

Table 7.6

7.4. LPOC controller design

The preceding section derives and describes the optimisation algorithm. From the formulation of the problem the solution is obtained and simulated but without having directly obtained the controller. Here, the controller is derived. From [Francis 1987] the set of all (proper real-rational) controllers K stabilising G is parametrised by:

$$K = (Y - MQ)(X - NQ)^{-1} = (\tilde{X} - Q\tilde{N})^{-1}(\tilde{Y} - Q\tilde{M}),\ Q \in \Re H_\infty \qquad (7.35)$$

The state space realisations of all functions is given in section 3.6.5, (page 68). The controller is of the form:

$$K = J(K,Q) = K_{11} + K_{12}Q(I - K_{22}Q)^{-1}K_{21} \qquad (7.36)$$

with state-space realisation [Francis 1987]

$$K = \left[\begin{array}{c|cc} A + B_2F + HC_2 + HD_{22}F & -H & B_2 + HD_{22} \\ \hline F & 0 & I \\ -(C_2 + D_{22}F) & I & -D_{22} \end{array}\right] \qquad (7.37)$$

The LPOC optimal controller is obtained by substituting Q_{opt} into (7.36) where Q_{opt} is the FIR filter obtained form the solution of the linear programme.

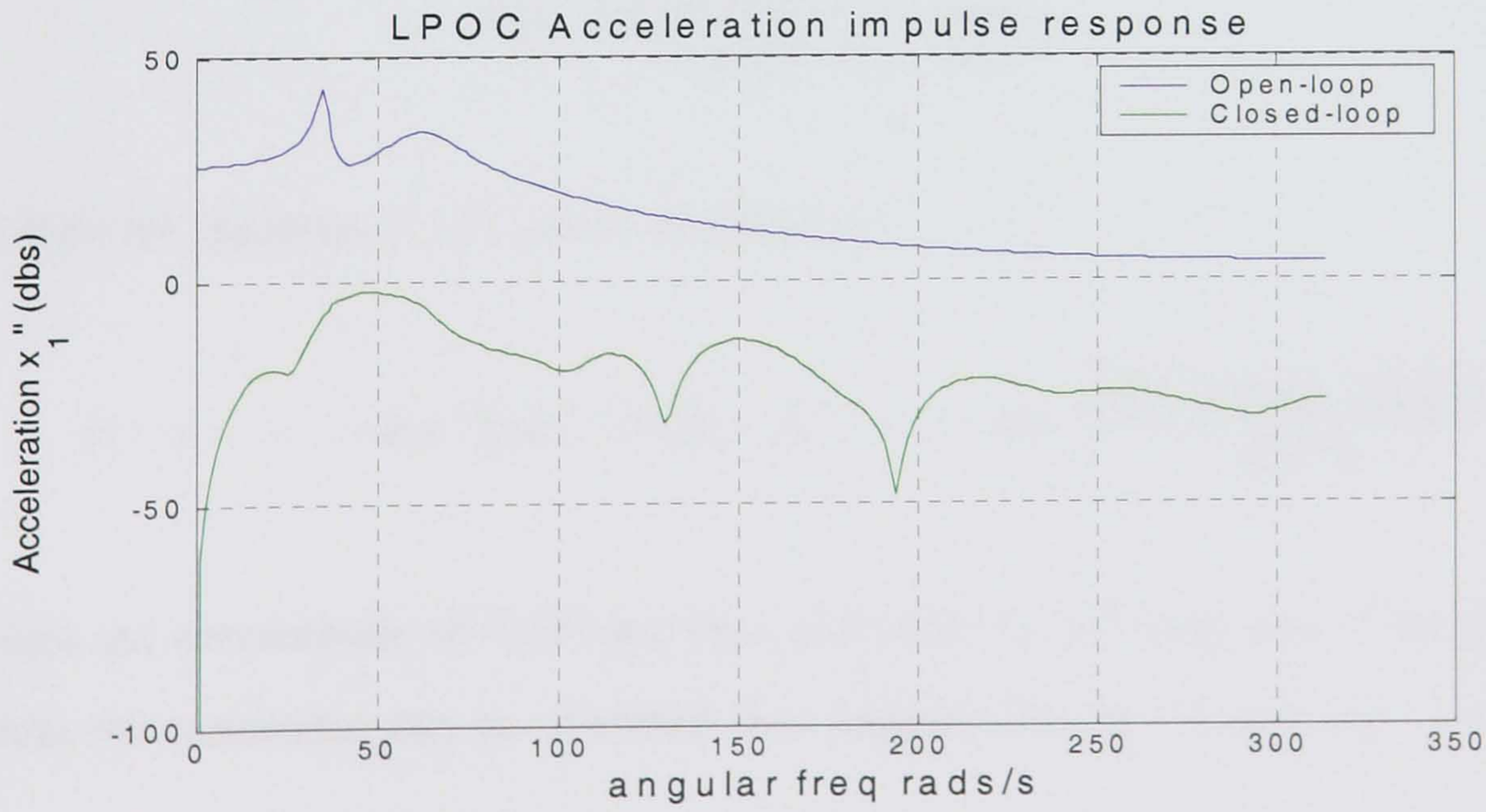

Figure 7.8 Passive and LPOC frequency responses

The frequency response in figure 7.8 shows that the closed-loop system reduces significantly the gain over all frequencies. This suggests that the controller will be effective for arbitrary disturbance inputs, not just an impulse.

7.5. Model reduction

The order of the controller is equal to the number of time steps N, in this case 204. This, results to computational difficulties and complex models and should be reduced for practical purposes. A model reduction technique was used, (balanced truncation method, [Zhou and Doyle 1998]). The model reduced responses were similar to the original ones, but with larger peaks, i.e. the method was unable to keep the peak responses low. By removing the high order parts of the controller the performance was significantly reduced. This suggests that more complex model reduction techniques emphasising approximation over a sufficiently large bandwidth should be investigated.

7.6. Design with alternative disturbance models

Apart form impulsive loadings different types of disturbance inputs can be incorporated in the design. Here, the necessary modifications in the LPOC design procedure are outlined when the disturbance signal has a general z-transform of the form:

$$\nu\left(z^{-1}\right)=\frac{\beta_0+\beta_1 z^{-1}+\ldots+\beta_m z^{-1}}{1+\alpha_1 z^{-1}+\ldots+\alpha_l z^{-1}} \tag{7.38}$$

In this case, equation (7.21), can be modified to:

$$\left(1+\alpha_1 z^{-1}+\ldots+\alpha_l z^{-1}\right) y(z^{-1})=\left(\beta_0+\beta_1 z^{-1}+\ldots+\beta_l z^{-1}\right)\frac{b(z^{-1})+c(z^{-1})q(z^{-1})}{a(z^{-1})} \tag{7.39}$$

where the denominator of (7.38) has been moved to the left hand side of the equation, while the numerator can be absorbed into polynomials $b\left(z^{-1}\right)$ and $c\left(z^{-1}\right)$ (thereby

increasing their order). By placing the poles at the origin we still have $a(z^{-1})=1$. Transforming to the time domain by inverting the transform gives:

$$\left(y_k+\beta_1 y_{k-1}+\ldots+\beta_i y_{k-i}\right)y(z^{-1})=\tilde{b}(z^{-1})+\tilde{c}(z^{-1})q(z^{-1}) \tag{7.40}$$

which can be written in matrix form as:

$$\begin{bmatrix} 1 & & & & \\ \alpha_1 & 1 & & & \\ \vdots & \alpha_1 & 1 & & \\ \alpha_l & & & \ddots & \\ & \ddots & & \ddots & \\ & & \alpha_l & & 1 \end{bmatrix}\begin{bmatrix} y_1 \\ y_2 \\ \\ \vdots \\ \\ y_n \end{bmatrix}=\begin{bmatrix} b_1 \\ \\ \vdots \\ \\ b_i \end{bmatrix}+\begin{bmatrix} c_1 & & \\ & \ddots & \\ & \ddots & \\ & & c_1 \end{bmatrix}q \tag{7.41}$$

or, in more compact form, as:

$$Ay=\boldsymbol{b}+C\boldsymbol{q} \tag{7.42}$$

On noting that matrix A has full column rank for $l<n$, this can be solved as:

$$y=\left(A^TA\right)^{-1}A^T\boldsymbol{b}+\left(A^TA\right)^{-1}A^TC\boldsymbol{q} \tag{7.43}$$

The same procedure is followed for the second regulated output. The problem is now formulated in its original form and the design procedure can be resumed from step 4. Note here, that this modification increases the complexity of the model, thus reducing the ability of the linear programming solver.

7. Three-storey building simulations with LPOC and LQR

The LPOC technique was applied to the design of the 3 storey building described in Chapter 5, the objective being to minimise the 1st floor accelerations which is assumed to be the only measurement. The following values were used for the simulation: $T_s=0.015s.$, $u_{\max}=0.2Volts$, $\Delta u_{\max}=0.2Volts/s$, $N=200$). The responses compare favourably with those obtained by LQR and are shown in Figure 7.9 and 7.10. Note that

LPOC is capable of achieving significant reduction in peak acceleration levels using a significantly reduced (peak) level voltage.

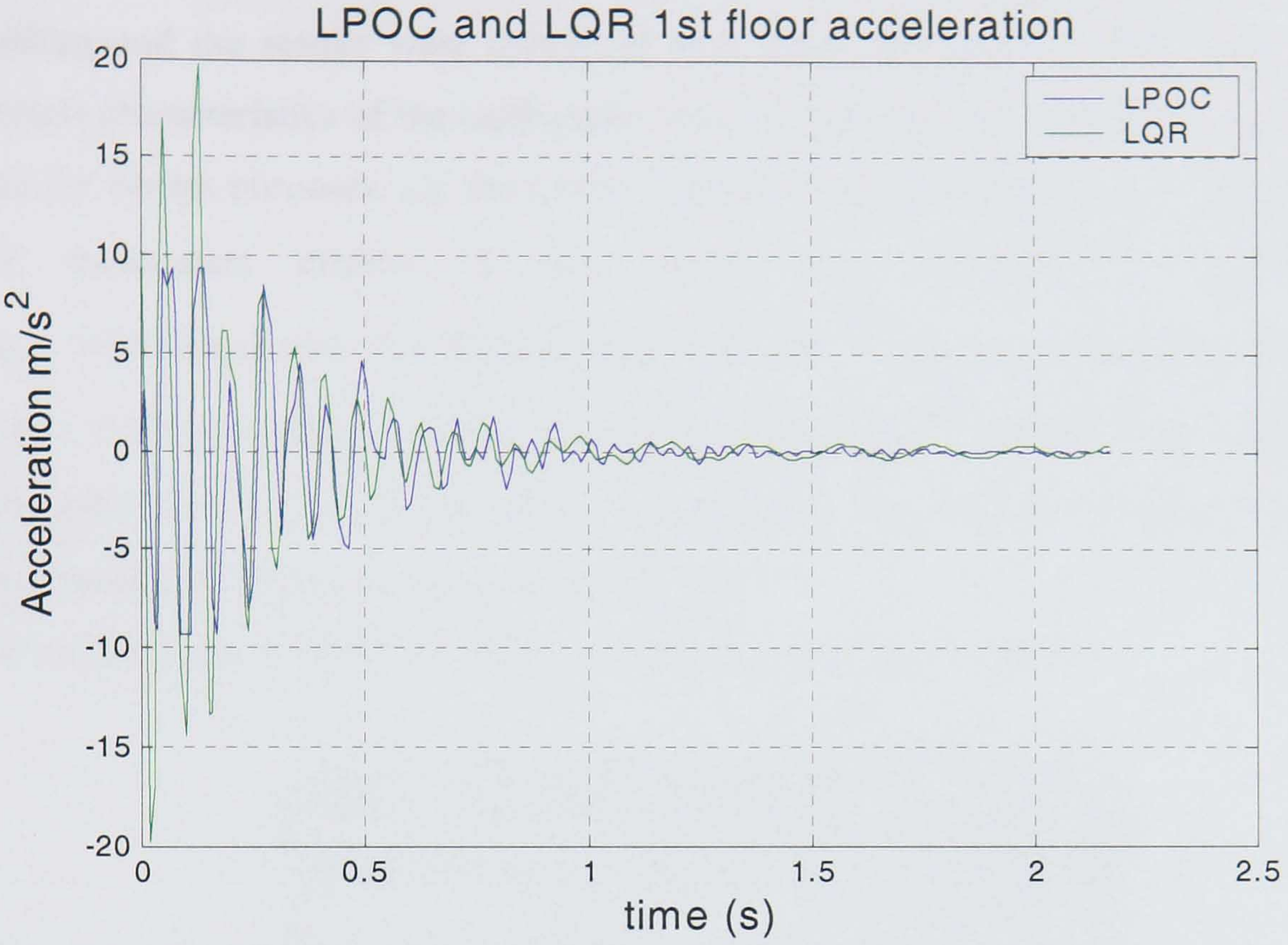

Figure 7.9 Acceleration of 3-storey building (LPOC and LQR)

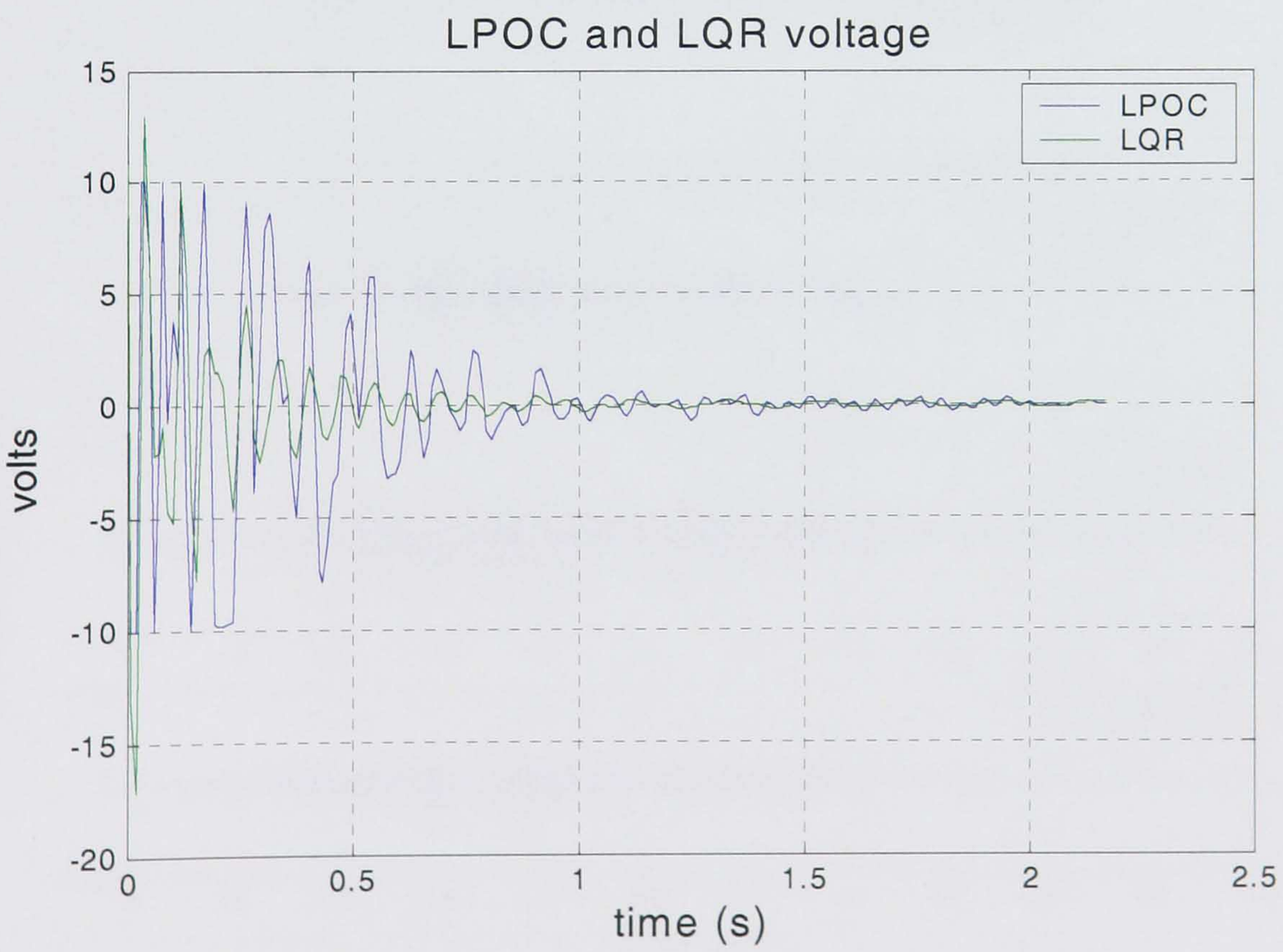

Figure 7.10 Voltage of 3-storey building (LPOC and LQR)

7. 8. Earthquake-signal response

The LPOC controller was tested for an earthquake signal disturbance on the one-storey building and the results were compared with those obtained by LQR. Note that the spectral characteristics of the earthquake were initially assumed unknown and were not used for design purposes, i.e. the LPOC controller was designed for an impulsive load. The parameters chosen in this design are: $T_s = 0.015\,s$, $u_{\max} = 0.2\,Volts$, $\Delta u_{\max} = 0.3\,Volts/s$ and $N = 200$ samples. The control penalty of the LQR design was set to $\rho = 0$ to impose no direct penalty on the control energy. With these design parameters similar peak levels of the control signal are obtained and therefore the two methods can be compared in a meaningful way.

The results are summarised in Figures 7.11 and 7.12 and in Table 7.7.

LPOC and LQR responses for earthquake		
	$\ddot{x}_{\max}$ (m/s^2)	$u_{\max}$ (Volts)
LPOC	56	145
LQR	106	137

Table 7.7

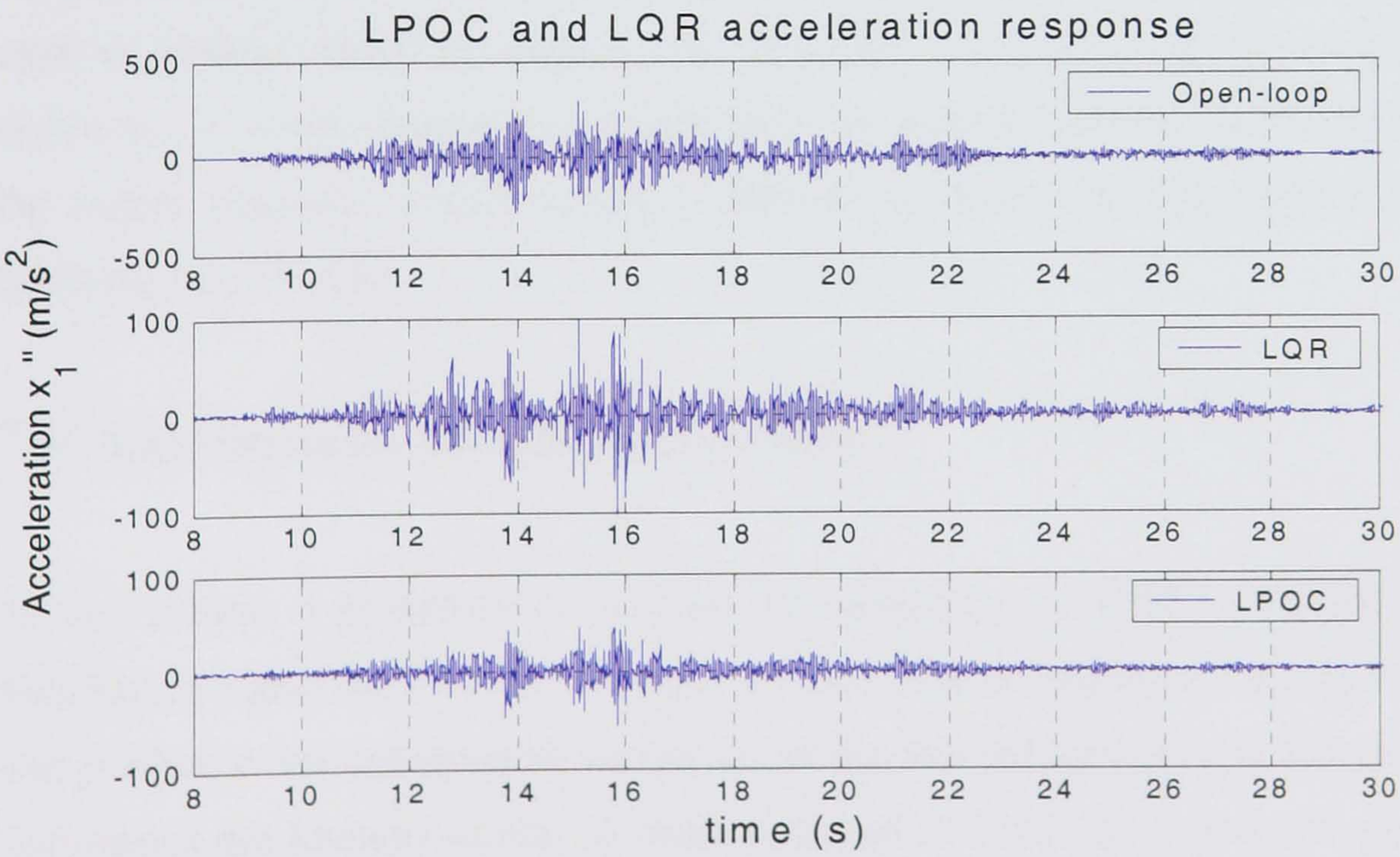

Figure 7.11 Earthquake response (LPOC and LQR)

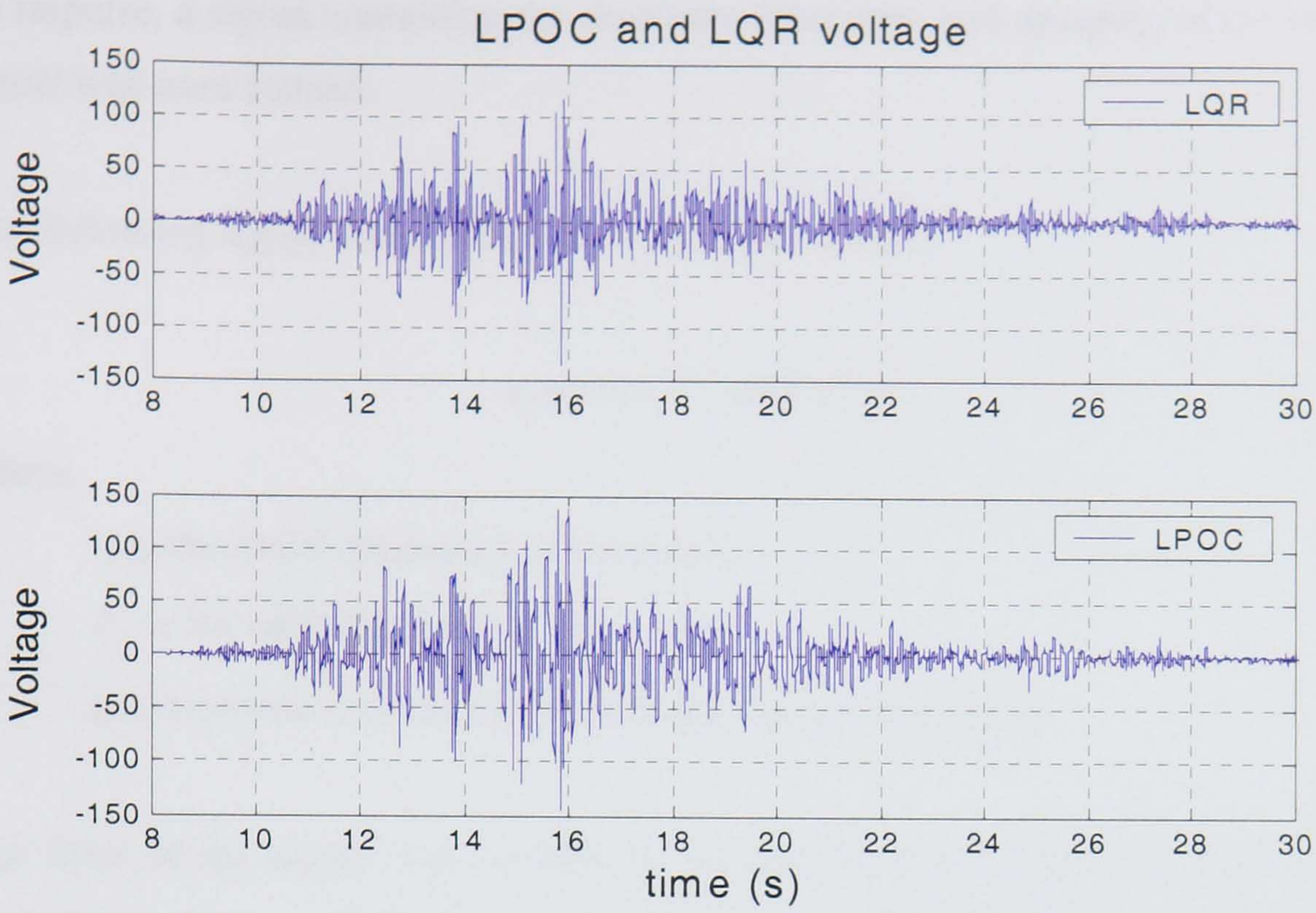

Figure 7.12 Voltage for earthquake response (LPOC and LQR)

The Matlab simulations show that the LPOC algorithm is still very effective, since it achieves lower peak acceleration levels for similar levels of control input. Note that in this example it is not possible to impose direct constrains on the maximum control effort and its slew rate, because these are valid only for the designed input, i.e. an impulse. The two constraints here are similar to the penalty terms used in LQR and are used as indirect means of shaping the controller. Note also that the design is very sensitive, i.e. small changes in the constraints or sample time can significantly change the output response, which makes it difficult to draw safe conclusions about the performance of LPOC.

7.9. Earthquake identification filter

In this section a procedure is outlined for designing an LPOC controller using a disturbance signal model which is more realistic than an impulse. It is hoped that this will produce a less conservative design (assuming that the spectral characteristics of the disturbance are known) similar to those achieved in LQR. As it was not numerically feasible to use the earthquake signal itself (Loma Prieta) as the design input in place of

an impulse, a signal containing the dominant frequency and damping of the earthquake signal was used instead.

The following signal was assumed as a disturbance input:

$$u_f(n) = e^{-aT_s n}\sin\left(\omega T_s n\right) \tag{7.44}$$

where,

ω is the radial frequency of the signal,

T_s is the sampling interval used, and

a is a constant controlling exponential decay (damping).

The form of the signal was decided by considering the spectrum of the Loma-Prieta earthquake. The constants a and ω are chosen such that the filter has an attenuation rate and dominant frequency similar to this spectrum. The filter is of low order and is a rather crude representation of the z-transform of the earthquake signal:

$$Z[u_f(n)] = Z\left[e^{-aT_s n}\sin\left(\omega T_s n\right)\right] = \frac{ze^{-\alpha T_s}\sin\left(\omega T_s\right)}{z^2 - 2e^{-\alpha T_s}\cos\left(\omega T_s\right)z + e^{-2\alpha T_s}} \tag{7.45}$$

The block diagram of the combined system is shown below.

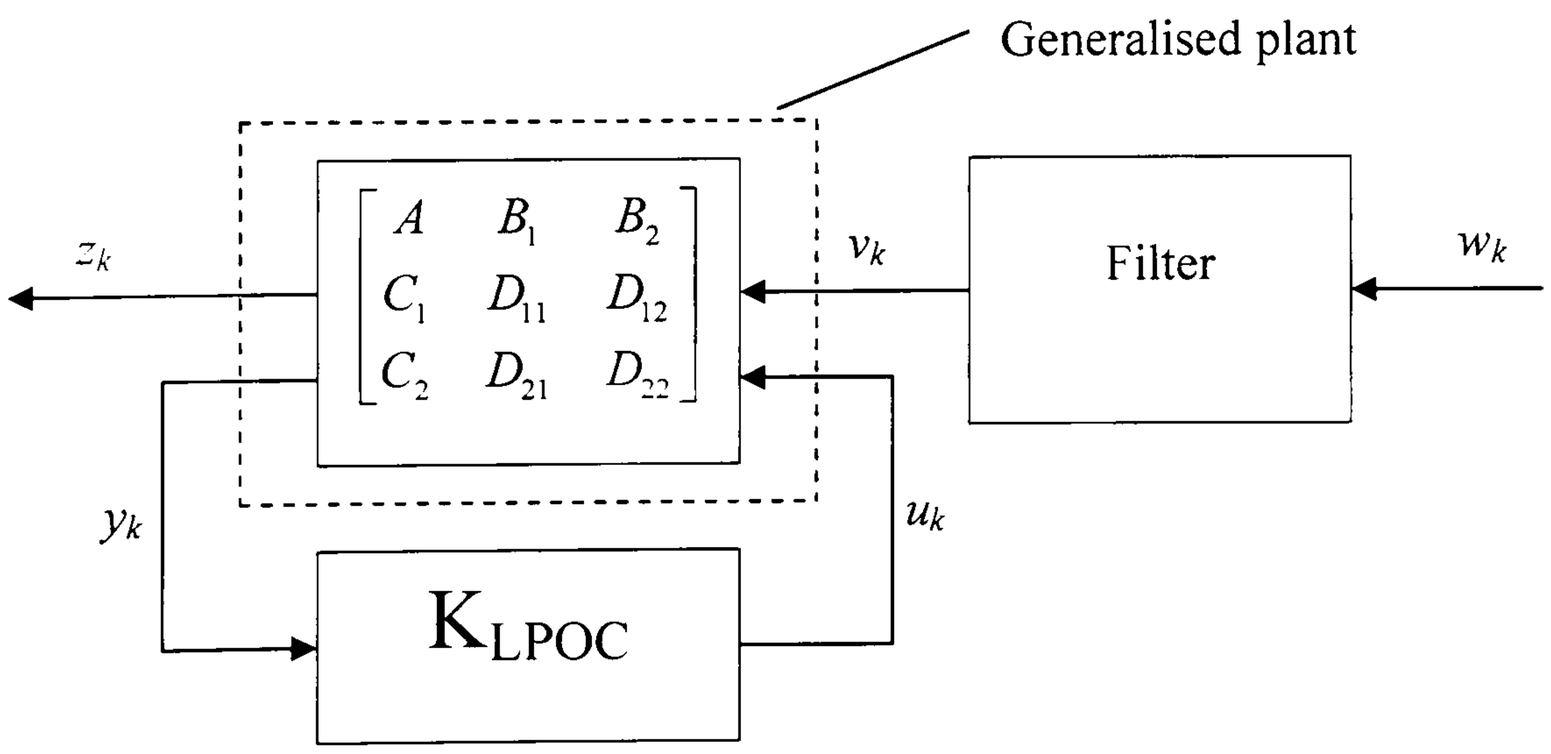

Figure 7.13 Block diagram of system with filter

where w_k is the external disturbance (which can be assumed to be an impulse) and v_k is the disturbance representing $u_f(n)$; the remaining terms have their usual meaning. The state space model of the generalised plant, including the filter dynamics is:

$$\begin{bmatrix} x_k \\ x_{k+1}^f \end{bmatrix} = \begin{bmatrix} A & B_1 C_f \\ 0 & A_f \end{bmatrix} \begin{bmatrix} x_k \\ x_{k+1}^f \end{bmatrix} + \begin{bmatrix} B_1 D_f \\ B_f \end{bmatrix} w_k + \begin{bmatrix} B_2 \\ 0 \end{bmatrix} u_k$$
$$\begin{bmatrix} z_k \\ y_k \end{bmatrix} = \begin{bmatrix} C_1 & D_{11} C_f \\ C_2 & D_{21} C_f \end{bmatrix} \begin{bmatrix} x_k \\ x_k^f \end{bmatrix} + \begin{bmatrix} D_{11} D_f \\ D_{21} D_f \end{bmatrix} w_k + \begin{bmatrix} D_{12} \\ D_{22} \end{bmatrix} u_k \tag{7.46}$$

Corresponding to a new generalised plant:

$$P_f(z) = \left[\begin{array}{cc:cc} A & B_1 C_f & B_1 D_f & B_2 \\ 0 & A_f & B_f & 0 \\ \hdashline C_1 & D_{11} C_f & D_{11} D_f & D_{12} \\ C_2 & D_{21} C_f & D_{21} D_f & D_{22} \end{array}\right]$$

Under the standard assumptions the pair (A, B_2) must be controllable and the pair (A, C_2) observable. Considering the state-space realisation of the new generalised plant it can be seen that the modes of the filter, $\lambda_i(A_f)$ are now uncontrollable from the second input u_k. Thus, it is impossible to reproduce the previous design method (which requires that all eigenvalues of the A-matrix are moved to the origin via an appropriate state-feedback matrix F), unless the eigenvalues of A_f are already located at zero, which can simply be accommodated by approximating the filter by a Moving Average (MA) model. The following parameters were used for the design: $T_s = 0.015s$, $u_{\max} = 0.3\ Volts$, $\Delta u_{\max} = 0.5\ Volts/s$, $N = 200$, $\omega = 25$, $a = 10$. The LPOC problem was formulated and solved for an impulsive disturbance; since, however, the filter has been absorbed inside the generalised plant, the optimisation is performed for $u_f(n)$. The resulting acceleration profile had a peak value of 0.19 m/s^2 (similar to the acceleration of the original problem) and low damping, decaying to zero in about 2 seconds.

The design was subsequently tested for a SDOF system using an earthquake signal as an input. The design incorporating the filter was found to have slightly superior performance compared to the simple LPOC. Thus, the general LPOC method can still be improved by taking into account information related to the expected spectrum of the disturbance. The design was carried out with the following parameters: $T_s = 0.015s$, $u_{\max}$=0.3 $Volts$, $\Delta u_{\max}$=1 $Volts/s$, $N = 200$, $\omega = 35 rads/s$ and $a = 10$. Because the order of the problem is further increased a SDOF system is used. Here the disturbance is the Loma-prieta earthquake signal. The simulation results of the two designs are shown in Figures 7.14 and 7.15.

Comparison of LPOC and LPOC with filter for earthquake signal		
	$\ddot{x}_{\max}\left(m/s^2\right)$	u_{max} (Volts)
LPOC	2.86	2.64
LPOC with filter	1.81	3.32

Table 7.8

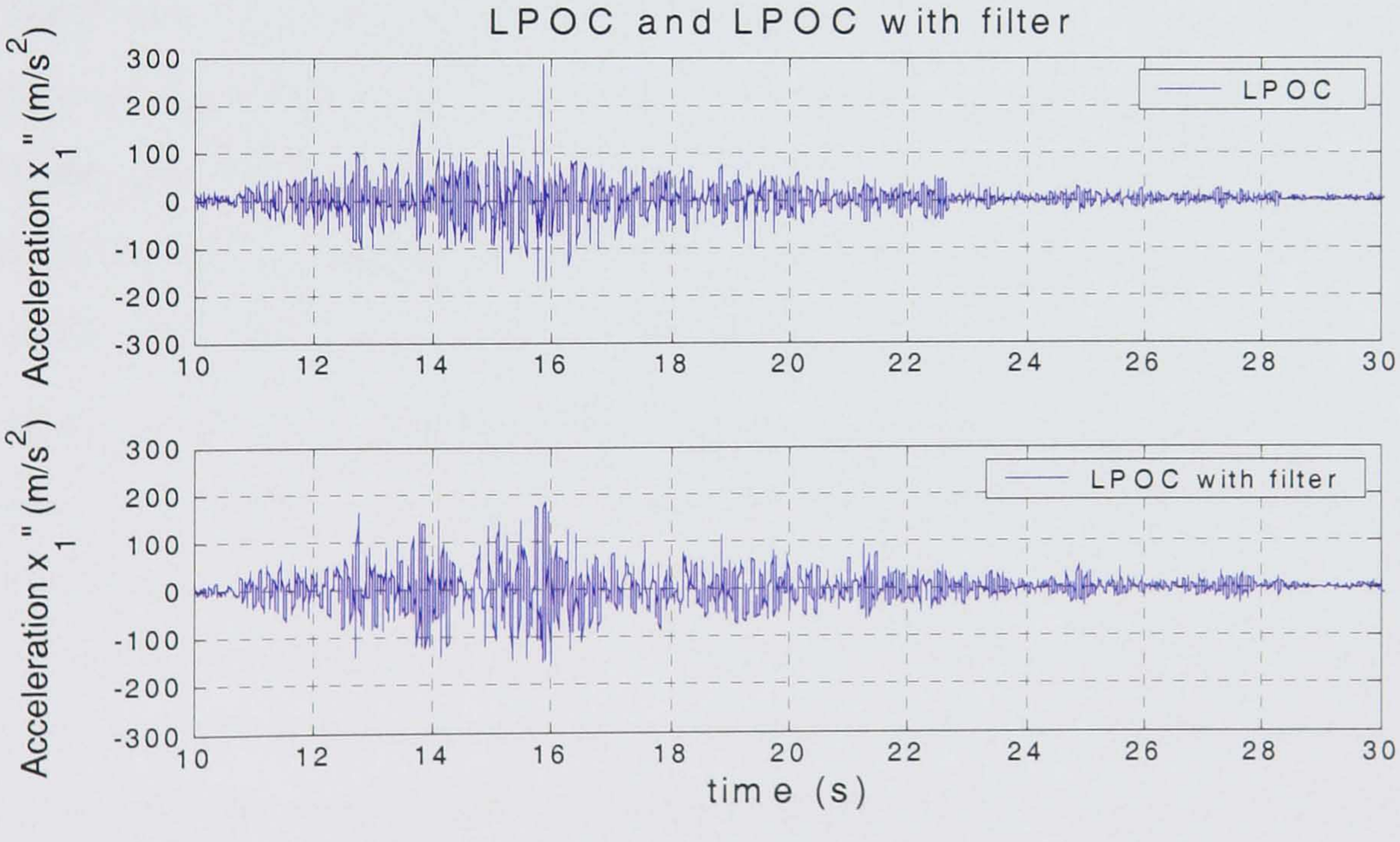

Figure 7.14 Earthquake acceleration response for LPOC and LPOC with filter

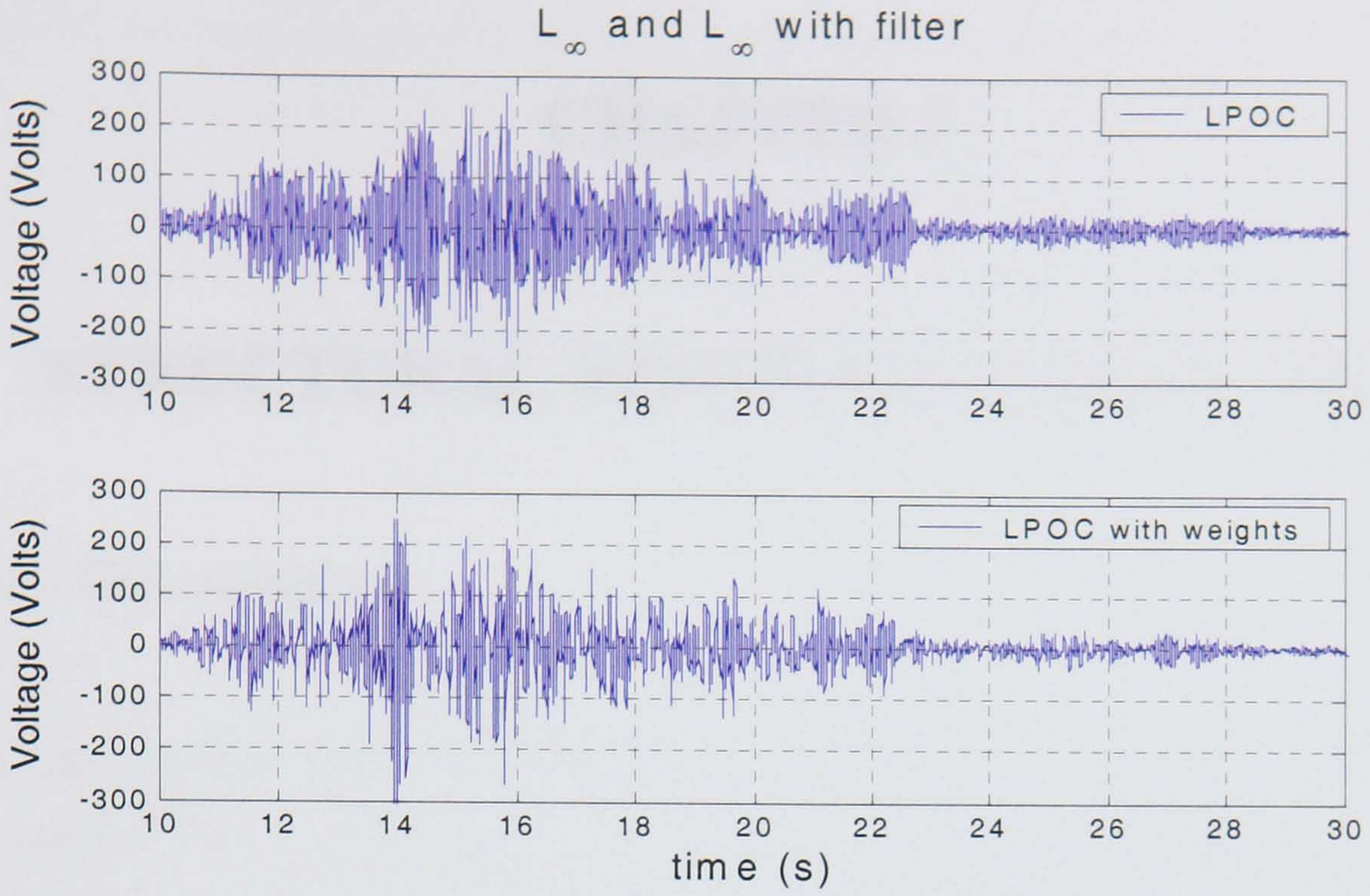

Figure 7.15 Earthquake response for LPOC and LPOC with filter (voltage)

7.10. Summary

The purpose of this chapter was to develop an algorithm aiming to minimise the maximum output peak responses of a system. The proposed method minimises the l_∞ norm of the impulse response of the system, i.e. the maximum peak of the regulated output. A modification of the Youla parametrisation was used in a discrete-time framework to characterise all deadbeat stable closed-loop systems via a free stable matrix FIR parameter, $Q(z)$. This allows the problem to be solved via finite-dimensional Linear Programming. To make the design more realistic linear constraints have been added involving the maximum value of the control signal and its rate. Simulation results show that the method compares favourably with LQR when minimisation of peak acceleration response is the main objective, for similar peak voltage levels. Similar results were obtained for different simulation studies, e.g. real earthquake signals and higher-order (three-storey) models. The method was extended to address a number of issues related to the design including controller model reduction, design for general disturbance models (rather than impulsive loading) and filter-augmentation techniques. Overall the design approach is promising although a number of issues related to robustness and numerical tractability need further investigation.

CHAPTER 8

STRUCTURAL STIFFNESS ESTIMATION

8. 1. Introduction

An open problem in civil engineering is the estimation of the stiffness matrix of existing structures. This is important in old structures or monuments where no structural information is known, or structures requiring strengthening after earthquakes, blasts or other kind of loadings. The stiffness matrix depends on the geometry of a structure and the individual stiffness of each member. Obtaining the stiffness matrix of a new structure is normally a straightforward task because the member stiffness and geometry is known. This is not the case in existing structures where the exact geometry and member strengths are unknown. Measuring experimentally the stiffness matrix of a building is a very complicated task. The stiffness of a particular member can be estimated by testing the strength of this element via non-destructive methods, but the exact geometry is typically not known. Even if the geometry of a building and the stiffness of each member is known, the overall stiffness matrix may still be unknown due to model non-linearities and interconnections between members. Experimental stiffness estimation requires the use of a vibration generator attached to the structure. Firstly, the frequencies and modes of vibration need to be determined and then forced vibration response data are taken by exciting the structure at various locations, which are subsequently analysed in the time or frequency domains.

An experimental method of estimating the stiffness matrix of a structure that does not require any knowledge about the structural geometry is to apply a known force (or set of forces) F and measure the displacement vector X. Then the stiffness matrix can be obtained from $F - KX = 0$, where $K \in R^{n \times n}$. The stiffness matrix K can be computed if at least n different forces are applied and the corresponding displacements measured. If the structure is not perfectly linear, or if there are errors in the measurements of F or X

then the estimates may not be accurate. Noise is always present in natural systems, and errors in measurement are unavoidable, especially when the system is very stiff and large forces are required to produce small displacements. Here the positive semi-definite Procrustes Problem (PSDPP) is used which is valid for versions of the problem with positive (semi-)definite stiffness matrices. The advantages that this method offers is that it takes into account the special form of the matrix K and that it gives good estimates when model uncertainties and errors are present.

History: Originally, the problem was used in the area of statistics and economics in estimation problems relating to covariance matrices [Gower and Dijksterhuis 2004]. Later, the general Procrustes problem was used as a least-squares approximation problem and [Allwright 1988] introduced the Positive Semi-Definite Procrustes problem by using convex analysis. The solution has also been employed in the area of optimisation as the means of approximating inverse Hessian matrices in quasi-Newton algorithms.

Outline: The first part of this chapter briefly describes the Procrustes problem and explains its application to civil engineering, namely stiffness matrix estimation. The mathematical background behind the problem is outlined, the original Procrustes algorithm formally defined and its solution is derived analytically. Two different algorithms are used for solving the Procrustes problem. The second part shows applications of the method for the main structural engineering stiffness matrix form. It includes the standard problem when the stiffness matrix is positive definite, when it has a special tridiagonal form common among buildings and when it is tridiagonal and positive-semi definite where the alternating projection method is used. The Procrustes problem is solved both for static and dynamic loadings; in the latter case an earthquake signal is assumed to excite the structure and all measurements at regular time samples are recorded. Finally, a case study is presented where the stiffness matrix of a building undergoing structural control is not accurately known. An adaptive control scheme is used, in which the on-line stiffness coefficient estimates are used to tune an on-line LQR controller.

8. 2. Background theory and definitions

Here, some definitions required for the Procrustes solutions are stated. Some basic concepts of convex sets and cone theory are also described for better understanding of the techniques described in subsequent chapters.

1. Frobenious norm

The Frobenious norm of a matrix $A \in \Re^{m \times n}$ is defined as:

$$\|A\|_F = \sqrt{\sum_{i=1}^{m}\sum_{j=1}^{n}|a_{ij}|^2} = \mathrm{tr}\left(A^T A\right)^{1/2} \tag{8.1}$$

This is the square root of the sum of the squares of all elements.

2. Trace function

The trace of a square matrix $A \in \Re^{n \times n}$ is the sum of the diagonal elements i.e.

$$\text{If } A = \begin{bmatrix} a_{11} & \cdots & a_{1n} \\ \vdots & \ddots & \vdots \\ a_{n1} & \cdots & a_{nn} \end{bmatrix} \text{ then } \mathrm{tr}(A) = \sum_{i=1}^{n} a_{ii} = a_{11} + a_{22} + \cdots + a_{nn}$$

3. Positive semi-definite, positive definite matrices

Let A be a square matrix and **x** a vector with at least 1 non-zero entry, then

$$\text{If } x^T Ax > 0 \ \ \forall x \qquad A \text{ is positive definite} \tag{8.2}$$

$$\text{If } x^T Ax \geq 0 \ \ \forall x \qquad A \text{ is positive semi-definite} \tag{8.3}$$

By definition, any stiffness matrix is positive definite.

4. The vec operator

If $A \in \Re^{n \times n}$ than the *vec* operator makes the matrix into a vector of n^2 elements by placing each column (or row) below the other. i.e.

$$\text{If } A=\begin{bmatrix} a_{11} & \cdots & a_{1n} \\ \vdots & \ddots & \vdots \\ a_{n1} & \cdots & a_{nn} \end{bmatrix} \text{ then } \text{vec}(A)=\begin{pmatrix} a_{11} & \ldots & a_{n1} & \ldots & \ldots & a_{1n} & \ldots & a_{nn} \end{pmatrix}$$

If A is symmetric, then $\text{vec}(A)$ denotes the vector of coordinates of $\text{vec}(A)$ with respect to a basis set $\{w_1, w_2, \ldots, w_n\}$ where w_i are all orthonormal. Also the following identities hold true:

$$\text{vec}(A) = W\,\overline{\text{vec}}(A) \tag{8.4}$$

and

$$\overline{\text{vec}}(A) = W^T \text{vec}(A) \tag{8.5}$$

where W is the matrix comprising of all the basis vectors w_i. Here $r = n(n+1)/2$.

5. Kronecker product

The Kronecker product of two matrices A and B is obtained by multiplying each element of matrix A by matrix B. The result will be a "large" matrix. The Kronecker product is defined for any two matrices of any dimensions, i.e.

If $A = a_{ij} \in \Re^{m\times n}$ and $B = b_{ij} \in \Re^{p\times q}$ then,

$$A \otimes B = \begin{pmatrix} a_{11}B & a_{12}B & \cdots & a_{1n}B \\ a_{21}B & a_{22}B & \cdots & a_{2n}B \\ \vdots & \vdots & \ddots & \vdots \\ a_{n1}B & a_{n2}B & \cdots & a_{nn}B \end{pmatrix} \text{ where } A \otimes B \in \Re^{mp\times nq} \tag{8.6}$$

An important property of the *vec* operator involving the Kronecker product is that: [Allwright 1988]

$$\text{vec}(ABC) = (A \otimes C^T)\text{vec}(B) \tag{8.7}$$

6. Singular value decomposition

Singular value decomposition (SVD) is a useful tool in linear algebra. Singular values are similar to eigenvalues and provide significant information about the matrix gain

along various directions. The matrix is decomposed into a product of three new matrices, one of which is sparse and gives the singular values in descending order along the diagonal. A singular value of a matrix A is the square root of the eigenvalue of A times its complex conjugate transpose denoted by A^*. Thus, all singular values are non-negative.

$$\sigma(A) = \sqrt{\lambda(AA^*)}$$

Let $A \in C^{m\times n}$, then there exist two unitary matrices U and V such that

$$U = [u_1, u_2, \ldots, u_n] \in C^{n\times n}$$
$$V = [v_1, v_2, \ldots, v_m] \in C^{m\times m} \tag{8.8}$$

such that A can be written as:

$$A = U\Sigma V^*, \quad \text{where } \Sigma = \left[\begin{array}{ccc|c} \sigma_1 & & 0 & 0 \\ & \ddots & & \\ 0 & & \sigma_r & \\ \hline 0 & & & 0 \end{array}\right] \tag{8.9}$$

Here, the vectors $\{u_i\}$ and $\{v_i\}$ are orthonormal, r is the rank of A, $[u_1, u_2, \ldots, u_r]$ is an orthonormal basis of $\text{Range}(A)$ and $[v_{r+1}, v_{r+2}, \ldots, v_n]$ is an orthonormal basis of $\text{Ker}(A)$.

7. Convex sets

Consider the two diagrams of figure 8.1. The first represents a convex set and the second a non-convex set. Geometrically, a convex set is one in which the straight line segment joining any two points of the set lies inside this set.

If x and y are different points in $\Re^n$, the set of points of the form

$$(1-\lambda)x + \lambda y = x + \lambda(y - x) \qquad \lambda \in \Re \tag{8.10}$$

defines a line through x and y. If $(1-\lambda)x + \lambda y \in C$ for all $\lambda \in \Re$ and all $x, y \in \Re^n$, then the equation defines an affine set [Rockafellar 1970]. A simple test for convexity also exists: If,

$$(1-\lambda)x+\lambda y \in C \quad \text{for} \quad 0 \le \lambda \le 1 \tag{8.11}$$

whenever $x \in C$ and $y \in C$, then the set $C \subseteq \Re^n$ is convex.

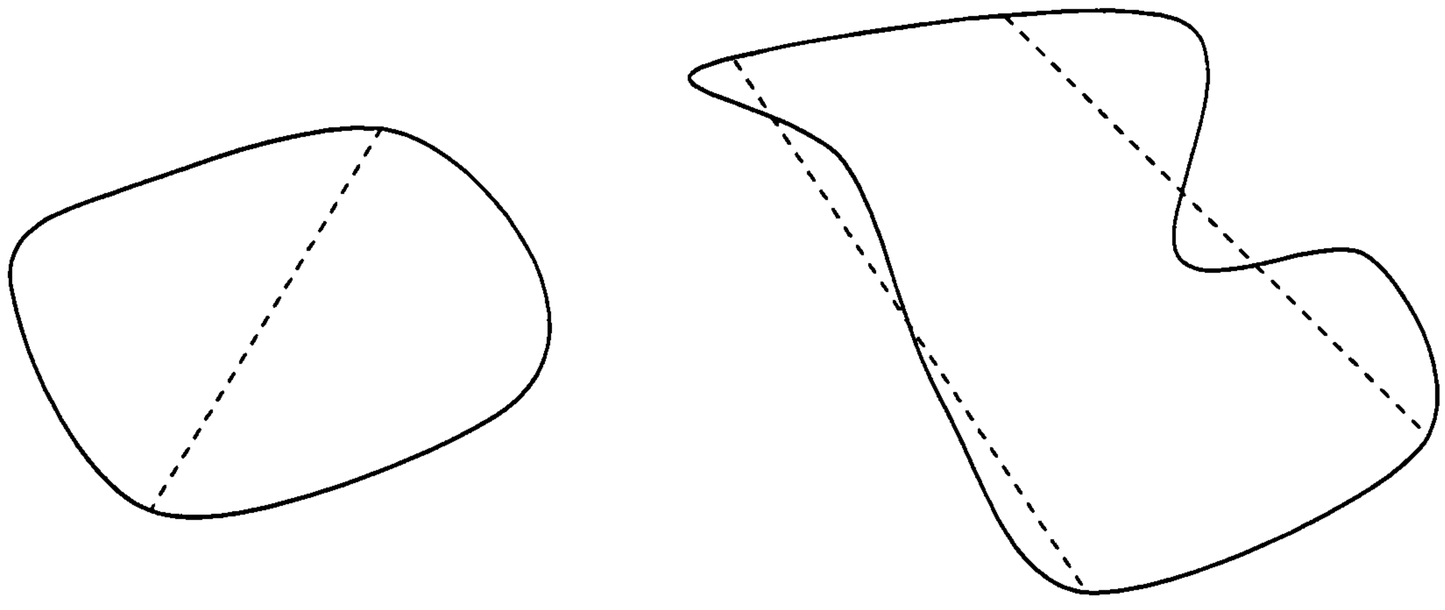

Figure 8.1.a) Convex set b) Non-convex set

Convex hull. A convex hull of a set is the smallest possible set that is convex and contains the set. The non-convex set of figure 8.2.a) can become convex by enlarging it. Subsequently, the figure in diagram 8.2.b) is its convex hull, i.e. the smallest convex set containing the original (non-convex) set.

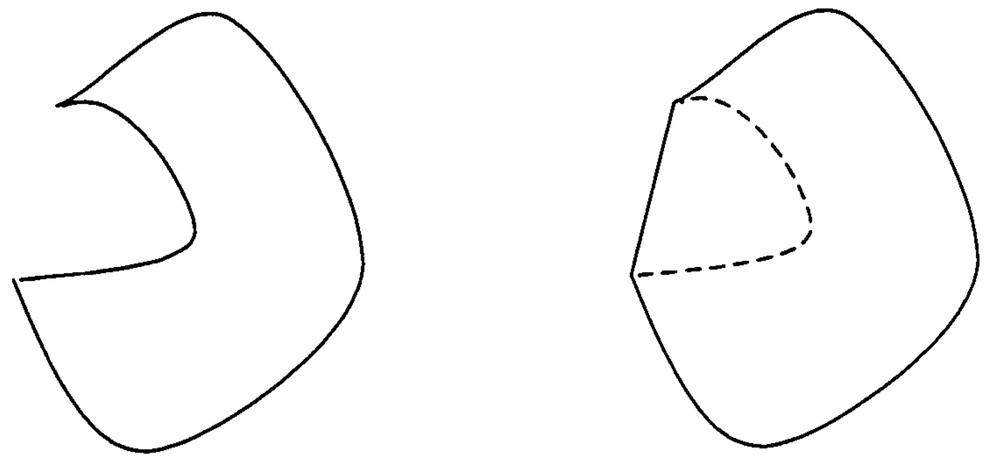

Figure 8.2 a) Non-convex set b) Convex hull

8. Cone theory

A set $K \subseteq \Re^n$ is a *cone* if it is closed under positive scalar multiplication, i.e. $\lambda x \in K$ when $\lambda x \in K$ and $\lambda > 0$. Geometrically, cones contain all half lines through the points emanating from the origin. A set F in $\Re^n$ is a convex cone if F is a proper, convex subset of $\Re^n$ that is not a singleton set and there exists a point V in F such that $\text{Ray}[V, X) \subset F$ for all $X \in F, X \neq V$. Each point V in F with this ray property is a

vertex of the cone. Cones are closely related to convex sets since they appear very often in optimisation, including the Procrustes problem. Not all cones are convex, as shown in

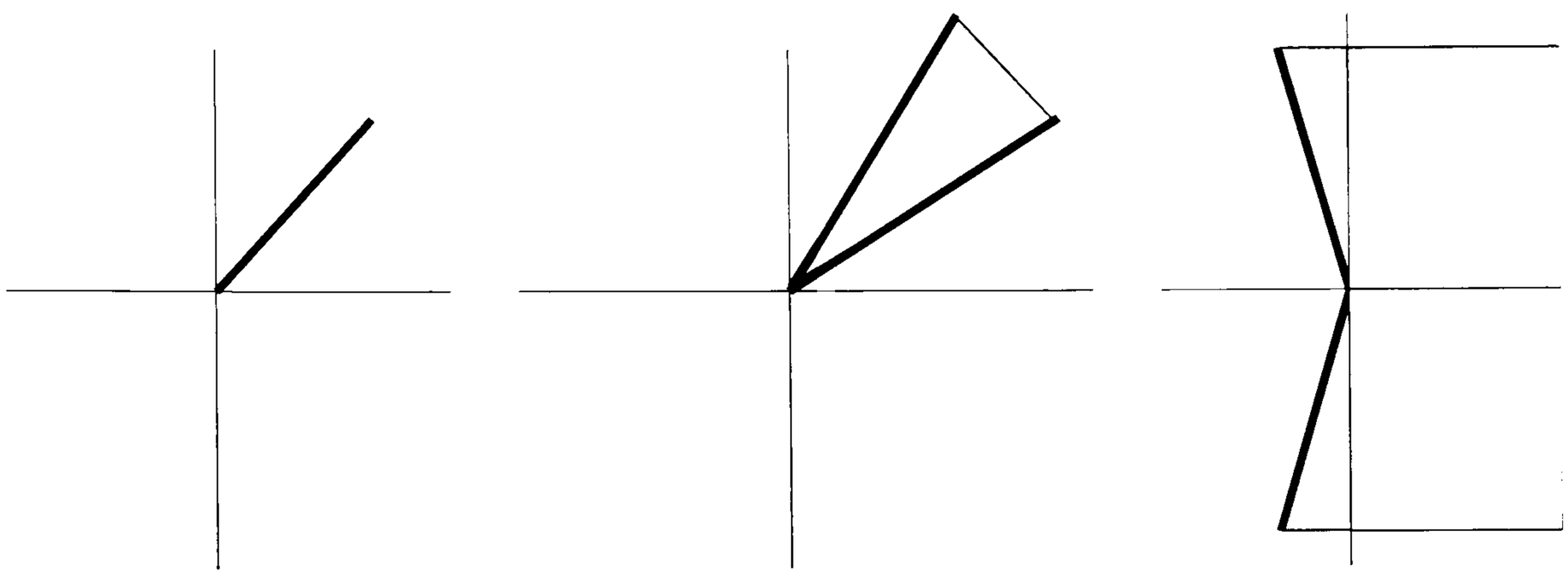

Figure 8.3.a) Convex cone (line) b) Convex cone c) Non-convex cone

in figure 8.3 where all three are cones but only the first two are convex cones.

Formally, a set is a convex cone if

$$\Gamma_1, \Gamma_2 \in F \Rightarrow \zeta\Gamma_1 + \xi\Gamma_2 \in F \text{ for all } \zeta, \xi > 0 \tag{8.12}$$

8. 3. Positive Semi Definite Procrustes Problem (PSDP)

The original Procrustes optimisation problem is formulated as:

$$\min_{A \in S_+^n} \left\| F - AG \right\|_F \tag{8.13}$$

where $A \in \Re^{n \times n}$, $F, G \in \Re^{n \times m}$ and A is positive semi-definite. It is normally assumed that $m \geq n$ and that $Rank(G) = n$. Then:

$$\begin{aligned} \min_{A \in S_+^n} \left\| F - AG \right\|_F &= \min_{A \in S_+^n} \left\| \text{vec}(F) - \text{vec}(AG) \right\|_2 \\ &= \min_{A \in S_+^n} \left\| \text{vec}(F) - \left(I \otimes G^T \right) \text{vec}(A) \right\|_2 \qquad \text{from (8.7)} \\ &= \min_{A \in S_+^n} \left\| \text{vec}(F) - (I \otimes G^T) WW^T \text{vec}(A) \right\|_2 \end{aligned} \tag{8.14}$$

Here, W is the orthogonal matrix obtained from r basis vectors $\{w_r\}$ and $S_{\leq}^{n}$ denotes the set of all $n \times n$ positive semi-definite matrices. To illustrate let A be:

$$A = A^T = \begin{bmatrix} a_{11} & a_{12} & a_{13} \\ a_{12} & a_{22} & a_{23} \\ a_{13} & a_{23} & a_{33} \end{bmatrix} \tag{8.15}$$

Note that because A is symmetric $a_{ij} = a_{ji}$. Here, if A $n \times n$, A is defined by exactly $r = n(n+1)/2$ elements. By using the *vec* operator for a 3×3 matrix:

$$\text{vec}(A) = \begin{bmatrix} a_{11} \\ a_{12} \\ a_{13} \\ a_{21} \\ a_{22} \\ a_{23} \\ a_{13} \\ a_{23} \\ a_{33} \end{bmatrix} = a_{11}\begin{bmatrix} 1 \\ 0 \\ 0 \\ 0 \\ 0 \\ 0 \\ 0 \\ 0 \\ 0 \end{bmatrix} + a_{12}\begin{bmatrix} 0 \\ 1 \\ 0 \\ 1 \\ 0 \\ 0 \\ 0 \\ 0 \\ 0 \end{bmatrix} + a_{22}\begin{bmatrix} 0 \\ 0 \\ 0 \\ 0 \\ 1 \\ 0 \\ 0 \\ 0 \\ 0 \end{bmatrix} + a_{13}\begin{bmatrix} 0 \\ 0 \\ 1 \\ 0 \\ 0 \\ 0 \\ 1 \\ 0 \\ 0 \end{bmatrix} + a_{23}\begin{bmatrix} 0 \\ 0 \\ 0 \\ 0 \\ 0 \\ 1 \\ 0 \\ 1 \\ 0 \end{bmatrix} + a_{33}\begin{bmatrix} 0 \\ 0 \\ 0 \\ 0 \\ 0 \\ 0 \\ 0 \\ 0 \\ 1 \end{bmatrix} \tag{8.16}$$

If now the vectors are normalised to unit length,

$$vec(A) = \begin{bmatrix} a_{11} \\ a_{12} \\ a_{13} \\ a_{21} \\ a_{22} \\ a_{23} \\ a_{13} \\ a_{23} \\ a_{33} \end{bmatrix} = a_{11}\begin{bmatrix} 1 \\ 0 \\ 0 \\ 0 \\ 0 \\ 0 \\ 0 \\ 0 \\ 0 \end{bmatrix} + a_{12}\sqrt{2}\begin{bmatrix} 0 \\ 1/\sqrt{2} \\ 0 \\ 1/\sqrt{2} \\ 0 \\ 0 \\ 0 \\ 0 \\ 0 \end{bmatrix} + a_{22}\begin{bmatrix} 0 \\ 0 \\ 0 \\ 0 \\ 1 \\ 0 \\ 0 \\ 0 \\ 0 \end{bmatrix} + a_{13}\sqrt{2}\begin{bmatrix} 0 \\ 0 \\ 1/\sqrt{2} \\ 0 \\ 0 \\ 0 \\ 1/\sqrt{2} \\ 0 \\ 0 \end{bmatrix} + a_{23}\sqrt{2}\begin{bmatrix} 0 \\ 0 \\ 0 \\ 0 \\ 0 \\ 1/\sqrt{2} \\ 0 \\ 1/\sqrt{2} \\ 0 \end{bmatrix} + a_{33}\begin{bmatrix} 0 \\ 0 \\ 0 \\ 0 \\ 0 \\ 0 \\ 0 \\ 0 \\ 1 \end{bmatrix} \tag{8.17}$$

The r vectors $\{w_r\}$ are now orthonormal and can be used to define matrix $W = [w_1\, w_2\, w_3 \ldots w_r]$. Note that $W^T W = I_r$ since the columns of W are orthonormal. Further WW^T projects orthogonally any n^2-dimensional vector onto $vec(S^n)$, so in particular $WW^T \xi = \xi$ for every $\xi \in vec(S^n)$.

Now, the terms of equation (8.14) can be replaced accordingly:

$$f = vec(F) \qquad H = \left(I \otimes G^T\right) W \qquad W^T vec(A) = \overline{vec}(A) \tag{8.18}$$

Apply singular value decomposition, to matrix H; this gives:

$$H = \begin{bmatrix} U_1 & U_2 \end{bmatrix} \begin{bmatrix} \Sigma \\ 0 \end{bmatrix} \begin{bmatrix} V^T \end{bmatrix} \text{ here } U_1 \in R^{mn \times r},\ U_2 \in R^{mn \times mn-r},\ \Sigma \in R^{r \times r}$$

$$H = \begin{bmatrix} U_1 & U_2 \end{bmatrix} \begin{bmatrix} \Sigma V^T \\ 0 \end{bmatrix} \tag{8.19}$$

Now let $P = [U_1 \quad U_2]$ and $L = \Sigma V^T$. Then,

$$H = P \begin{bmatrix} L \\ 0 \end{bmatrix} \tag{8.20}$$

and f can be factored accordingly to get:

$$f = P \begin{bmatrix} u^T \\ l^T \end{bmatrix} \Rightarrow f P^T = \begin{bmatrix} u \\ l \end{bmatrix} \tag{8.21}$$

By substituting equation (8.18) back to (8.14) we obtain:

$$\min_{A \in S_\Sigma^n} \left\| F - AG \right\|_F = \min_{A \in S_\Sigma^n} \left\| \mathrm{vec}(F) - (I \otimes G^T) WW^T \mathrm{vec}(A) \right\|_2$$

$$= \min_{A \in S_\Sigma^n} \left\| f - H \overline{\mathrm{vec}}(A) \right\|_2 \qquad \text{(from (8.20)}$$

$$= \min_{A \in S_\Sigma^n} \left\| P^T f - P^T P \begin{bmatrix} L \\ 0 \end{bmatrix} \overline{\mathrm{vec}}(A) \right\|_2$$

$$= \min_{A \in S_2^n} \left\| \begin{bmatrix} u \\ l \end{bmatrix} - \begin{bmatrix} L \\ 0 \end{bmatrix} \overline{\text{vec}}(A) \right\|_2 \qquad \text{(from (8.21)}$$

$$= \min_{A \in S_2^n} \left\| \begin{matrix} u - L\overline{\text{vec}}(A) \\ l \end{matrix} \right\|_2$$

hence,

$$\min_{A \in S_2^n} \|F - AG\|_F = \left(\min_{A \in S_2^n} \left\| u - L\overline{\text{vec}}(A) \right\|_F^2 + \|l\|_2^2 \right)^{1/2} \tag{8.22}$$

Now, if we define $L\overline{\text{vec}}(A) = k$ the minimisation problem is reduced to:

$$\min_{A \in S_2^n} \|F - AG\|_F = \min_{k \in K} \|u - k\|_F + \min \|l\|_2^2 \tag{8.23}$$

Here, K is the convex cone:

$$K = \text{cone}\left[LW^T \Omega \right] \tag{8.24}$$

where

$$\Omega = conv\{\Psi\} \qquad \Psi = \left\{ \text{vec}\left(\text{B}^2\right) : B \in U \right\} \subset R^{n^2}$$

and, l is a constant, which does not affect the minimisation and represents a "fixed" cost. Graphically, the minimisation problem is equivalent to finding the distance of u to the cone K.

8. 4. Algorithms for Solving the Procrustes Problem

The solution of the Procrustes problem is not straightforward and several algorithms have been developed for its implementation. Two methods will be used here, one developed by Allwright (1988) called the proximal point algorithm for conical cones and the steepest descent method based on Woodgate (2006).

Proximal point algorithm for conical hulls [Allwright 1988] Recall that the Procrustes minimisation problem has been reduced to:

$$\min_{k\in K}\left\|u-k\right\|_F, \quad \Gamma = LW^T\Omega, \quad K = \text{cone}\left[\Gamma\right]$$

where K, u, L and W are as defined previously. An acceptable approximation $\bar{k}$ (arbitrarily close to the exact optimal) can be found using the following facts:

- There exists a $\pi \in R_>$ such that for any point x in Γ there is a point $y \in \Gamma$ which is in the ray through 0 and x for which $\|y\| \geq \pi$
- For each $g \in R^r$ a member of $\arg\min\left\{g^T\gamma : \gamma \in \Gamma\right\}$ can be found.

The algorithm follows the steps as given in [Allwright 1988]:

1. Select parameters by choosing:

   $\varepsilon \in (0,\infty)$

   $\overline{k_0} \in \text{cone}\left[\Gamma\right]$, an initial estimate of $\bar{k}$

2. Initialise variables:

   $k_0 :=$ minpoint$\left[u, \text{cone}\left[\left\{\overline{k_0}\right\}\right]\right]$

   $\hat{b}_{-1} := 0$

   $i = 0$

3. Decide when to stop the iteration:

Find a $y_i \in \arg\min_{y\in s} \nabla u\left(k_i\right)^T\left(y_i - k_i\right)$,

by finding

$$y_i \in \arg\min_{y\in s} \nabla u\left(k_i\right)^T \gamma$$

and setting

$$y_i = \begin{Bmatrix} \eta\gamma_i & \text{if } \nabla u(k_i)^T\gamma \\ k_i & \text{otherwise} \end{Bmatrix}$$

Compute a lower bound b_i for $u(\hat{k})$:

$$b_i := u(k_i) + \nabla u(k_i)^T\left(y_i - k_i\right)$$

Compute $\hat{b}_i$:

$$\hat{b}_i := \max\left\{\bar{b}_{i-1}, b_i\right\}$$

If

$$\left[u(k_i) + \|l\|^2\right] \le (1+\varepsilon)^2\left[\hat{b}_i + \|l\|^2\right]$$

Then set $\bar{k} = k_i$ and stop, else continue.

4. Choose next iterand

$$k_{i+1} := \text{minpoint}\left[u, \text{cone}\left[\text{line}\left\{k_i, y_i\right\}\right]\right]$$

$$i = i + 1$$

The algorithm is proved to converge (see [Allwright 1988]).

Steepest descent algorithm

The steepest descent algorithm finds the nearest local minimum of a function. It starts at a point P_0 and moves along the direction of the negative gradient of the function i.e. $-\nabla f(P_i)$ until reaching points P_{i+1}. The steepest descent method is valid only when the gradient can be computed. Recall the original Procrustes problem of (8.13); this is minimised for those symmetric matrices A that satisfy:

$$AGG^T + GG^T A = Q \tag{8.25}$$

where

$$Q = FG^T + GF^T \tag{8.26}$$

A solution is suggested by [Woodgate 2006], in which A is factored in the form $A = E^T E$, which characterises all symmetric positive semi-definite matrices. Thus the problem becomes:

$$\min\left\|F - E^T EG\right\| \tag{8.27}$$

and solved over a "free" E. Although the cost function is not convex in terms of E and in fact possesses many local minima, it is shown in [Woodgate 2006] that any local minimum is actually also global, a fact which is assumed here without proof. Thus the

algorithm will solve the problem if it succeeds to converge to any local minimum. This can be guaranteed by careful choice of step-length. The steepest-descent algorithm is used based on the following iteration for computing matrix E:

$$E_{i+1} = E_i - \omega_i D_i \tag{8.28}$$

where D_i is the search direction, given by the negative gradient,

$$D_i := \nabla_E f(E_i) \tag{8.29}$$

For $\omega > 0$ (sufficient small), $f(E_{i+1}) < f(E_i)$ for all $\omega_i \in (0, \omega)$ iff $\nabla_E f(E_i) \neq 0$. The gradient can be calculated as [Woodgate 2006],

$$D_i = E_i L(E_i) = E_i E^T{}_i E_i G G^T + G G^T E_i^T E_i - Q \tag{8.30}$$

and

$$f(E_i) = \frac{1}{2} tr\left\{F^T F + \left(E_i^T E_i\right)^2 G G^T - E_i^T E_i Q\right\} \tag{8.31}$$

The steepest descent algorithm will converge if ω_i is chosen sufficiently small. However, if ω_i is chosen too small, this can make convergence to the optimum solution slow. Standard techniques exist for adapting the step-length according to the (estimated) distance from the optimal point, so that large step-lengths are initially used and progressively reduced as the optimal point is approached. In the present implementation the step-length was chosen by an "Armijo"-type rule which minimises the cost function along the descent direction, and, although not necessarily most efficient in terms of computation time, performed well in practice.

8. 5. Stiffness Matrix

Assembly of stiffness matrix: The $k_{i,j}$ coordinate of a stiffness matrix of a structural system, represents the force corresponding to coordinate i due to a unit displacement of coordinate j. Consider for instance the simplest form of a structure, a uniform prismatic

bar of length L, elastic Modulus E and cross-sectional area A. The bar has one node at each end (figure 8.4). In order to find the first entry K_{11}, a unit displacement is applied at one end of the bar, and the load applied at that end is calculated.

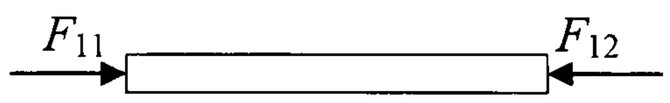

Figure 8.4 Forcer on a bar

The elementary formula for stretching a bar an amount δ is:

$$\delta = \frac{FL}{AE} \Rightarrow F = \frac{AE}{L}\delta \tag{8.32}$$

Now, $F_{i,j}$ is the force at node i associated with a displacement at node j, and u_i is the displacement of node i. Assume as a sign convention that loads and displacements are positive to the right. Here a negative force is applied at node 2 to produce a positive displacement at node 1. Hence,

$$F_{11} = -F_{21} = \frac{AE}{L}u_1 \quad \text{and} \quad F_{12} = -F_{22} = \frac{AE}{L}u_2 \tag{8.33}$$

By taking a unit displacement $u_1 = u_2 = 1$, we can write the above equations in matrix form:

$$\begin{bmatrix} F_{11} & F_{12} \\ F_{21} & F_{22} \end{bmatrix} = \frac{AE}{L}\begin{bmatrix} 1 & -1 \\ -1 & 1 \end{bmatrix} \times 1 = k\begin{bmatrix} 1 & -1 \\ -1 & 1 \end{bmatrix} \tag{8.34}$$

because the stiffness of a bar is $k = AE/L$. Therefore the stiffness matrix of the bar in figure 8.4 is:

$$K = k\begin{bmatrix} 1 & -1 \\ -1 & 1 \end{bmatrix} \tag{8.35}$$

Consider now a more complicated structural system with m elements and n nodes (figure 8.5.a). This is a typical lumped mass representation of a building. Assume that

there is only one degree of freedom per node, in the horizontal direction. The stiffness matrix will be an n by n matrix generated by the individual stiffness matrices of the member elements. The stiffness matrix of any element of uniform stiffness k_1 between any two nodes i and j as obtained for the bar above, is:

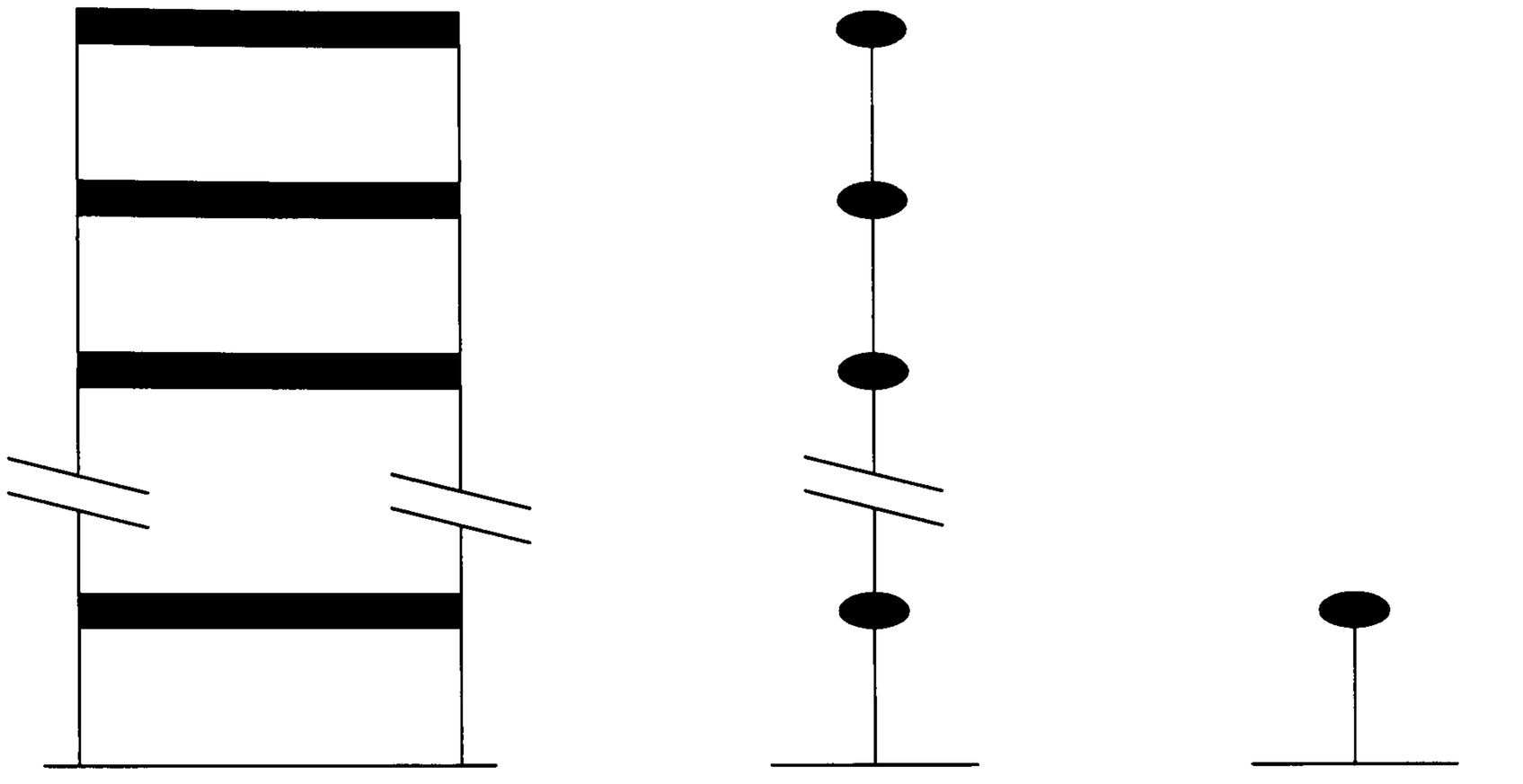

Figure 8.5 a) Building b) building idealisation c) SDOF system

$$K_{i,j} = \begin{bmatrix} k_1 & -k_1 \\ -k_1 & k_1 \end{bmatrix} \tag{8.36}$$

The stiffness matrix of the lowest element of figure (8.5.c.), between the lowest node and the support is different. The $k_{1,1}$, $k_{1,2}$ and $k_{2,1}$ terms are as above but the $k_{2,2}$ term changes. The force required to displace it is also restricted by the support between the element and the ground of stiffness k_s. Therefore its stiffness matrix is:

$$K_{1,2} = \begin{bmatrix} k_1 & -k_1 \\ -k_1 & k_1 + k_s \end{bmatrix} \tag{8.37}$$

Hence, the stiffness of the whole structure of n floors is:

$$K = K_1 + K_2 + \ldots + K_i + \ldots + K_n$$

or,

$$K=\begin{bmatrix} k_1 & -k_1 & & & \\ -k_1 & k_1 & & & \\ & & & & \\ & & & & \end{bmatrix}+\begin{bmatrix} & & & & \\ & k_2 & -k_2 & & \\ & -k_2 & k_2 & & \\ & & & & \end{bmatrix}+\begin{bmatrix} & & & & \\ & & & & \\ & & k_i & -k_i & \\ & & -k_i & k_i & \end{bmatrix}+\begin{bmatrix} & & & & \\ & & & & \\ & & & k_n & -k_n \\ & & & -k_n & k_n+k_5 \end{bmatrix}$$

and so,

$$K=\begin{bmatrix} K_1 & -K_1 & & & & & & & \\ -K_1 & K_1+K_2 & -K_2 & & & & & & \\ & -K_2 & K_2+K_3 & -K_3 & & & & & \\ & & -K_3 & \ddots & \ddots & & & & \\ & & & \ddots & \ddots & -K_i & & & \\ & & & & -K_i & K_i+K_{i+1} & -K_{i+1} & & \\ & & & & & -K_{i+1} & \ddots & \ddots & \\ & & & & & & \ddots & \ddots & -K_n \\ & & & & & & & -K_n & K_n+K_s \end{bmatrix} \quad (8.38)$$

with those elements not explicitly shown being equal to zero.

Characteristics of lumped mass structural building stiffness matrix: The $k_{i,j}$ coordinate of a stiffness matrix of a structural system, represents the force corresponding to coordinate i due to a unit displacement of j. Therefore, by definition,

1. If node i and node j are not connected by any element of some stiffness k, then $k_{i,j}=0$.
2. The main diagonal of the stiffness matrix is always positive, since a negative value would mean that a force at a point produces a displacement of that point in the opposite direction, which is unreasonable.
3. The stiffness matrix is always symmetric if the relationship between applied loads and resulting deformation is linear. This means that a force at i has the same effect (produces the exact same deflection) on j as a force on j has on i.
4. An unsupported or inadequately supported structure has a singular stiffness matrix and is positive semi-definite. This is a mechanism in civil Engineering terms because the structure is not connected to any supports. Hence, any external force

will make the whole structure move. If supports are sufficient to prevent all possible rigid body motion the stiffness matrix is non-singular and positive-definite.

5. Finally, if each node is connected only to at most two consecutive members, then $k_{i,j}=0$, for $|i-j|>1$. This means that between two members i and j that are not adjacent, as in the case of a building, the $k_{i,j}$ component is zero.

8. 6. Solution for the Building Structural Stiffness Problem

Consider now the stiffness matrix of an n storey building without any bracing, and the members being connected vertically one on top of the other like the one of figure (8.5). The stiffness matrix can be decomposed as shown below:

$$K=\begin{bmatrix} k_1 & -k_1 & & & \\ -k_1 & k_1+k_2 & -k_2 & & \\ & -k_2 & \ddots & \ddots & \\ & & \ddots & k_{n-2}+k_{n-1} & -k_{n-1} \\ & & & -k_{n-1} & k_{n-1}+k_n \end{bmatrix}$$

or

$$K=k_1\begin{bmatrix} 1 & -1 & & \\ -1 & 1 & & \\ & & & \\ & & & \end{bmatrix}+k_2\begin{bmatrix} & & & \\ & 1 & -1 & \\ & -1 & 1 & \\ & & & \end{bmatrix}+\ldots+k_n\begin{bmatrix} & & & \\ & & & \\ & & & \\ & & & 1 \end{bmatrix} \qquad (8.39)$$

Here, K is the overall stiffness matrix and k_i the stiffness of the i-th element. The stiffness matrix is split into a sum of n simpler matrices containing only ones, each multiplied by k_i. These coefficient matrices will be denoted by C_i. Now,

$$\|F-KX\|_F^2=\|F-k_1C_1X-k_2C_2X-\ldots-k_nC_nX\|_F^2$$
$$=trace\left\{\left(F-k_1C_1X-k_2C_2X-\ldots-k_nC_nX\right)^T\left(F-k_1C_1X-k_2C_2X-\ldots-k_nC_nX\right)\right\}$$

For simplicity define $P_i=k_iC_i$; expanding the above equation we have:

$$\|F-KX\|_F^2=trace\left\{F^TF\right\}+\sum_{i=1}^{n}k_i tr\left\{F^TP_i+P_i^TF\right\}-\sum_{i=1}^{n}k_i^2 tr\left\{P_iP_i^T\right\}+\sum_{i\neq j}k_ik_j tr\left\{P_iP_j^T+P_jP_i^T\right\}$$

This can be written in matrix form as:

$$\left\|F - KX\right\|_{\mathrm{F}}^2 = \mathrm{trace}\left\{F^T F\right\} - \begin{bmatrix} \mathrm{tr}\left\{F^T P_1\right\} & \mathrm{tr}\left\{F^T P_2\right\} & \cdots & \mathrm{tr}\left\{F^T P_n\right\} \end{bmatrix} \begin{bmatrix} k_1 \\ k_2 \\ \vdots \\ k_n \end{bmatrix},$$

$$+ \begin{bmatrix} k_1 & k_2 & \cdots & k_n \end{bmatrix} \begin{bmatrix} \mathrm{tr}\left\{P_1^T P_1\right\} & \mathrm{tr}\left\{P_1^T P_2\right\} & \cdots & \mathrm{tr}\left\{P_1^T P_n\right\} \\ \mathrm{tr}\left\{P_2^T P_1\right\} & \mathrm{tr}\left\{P_2^T P_2\right\} & \cdots & \mathrm{tr}\left\{P_2^T P_n\right\} \\ \vdots & \vdots & \ddots & \vdots \\ \mathrm{tr}\left\{P_n^T P_1\right\} & \mathrm{tr}\left\{P_n^T P_2\right\} & \cdots & \mathrm{tr}\left\{P_n^T P_n\right\} \end{bmatrix} \begin{bmatrix} k_1 \\ k_2 \\ \vdots \\ k_n \end{bmatrix}$$

which can be written in compact form as:

$$\left\|F - KX\right\|_F^2 = \alpha + \beta^T k + k^T \Phi k := J\left(k\right) \tag{8.40}$$

where we have defined:

$$\alpha = \mathrm{trace}\left\{F^T F\right\},$$

$$\beta = \begin{bmatrix} tr\left\{F^T P_1\right\} & tr\left\{F^T P_2\right\} & \cdots & tr\left\{F^T P_n\right\} \end{bmatrix}^T,$$

$$\Phi = \begin{bmatrix} tr\left\{P_1^T P_1\right\} & tr\left\{P_1^T P_2\right\} & \cdots & tr\left\{P_1^T P_n\right\} \\ tr\left\{P_2^T P_1\right\} & tr\left\{P_2^T P_2\right\} & \cdots & tr\left\{P_2^T P_n\right\} \\ \vdots & \vdots & \ddots & \vdots \\ tr\left\{P_n^T P_1\right\} & tr\left\{P_n^T P_2\right\} & \cdots & tr\left\{P_n^T P_n\right\} \end{bmatrix}$$

and

$$k^T = \begin{bmatrix} k_1 & k_2 & \cdots & k_n \end{bmatrix}$$

The aim now is to find k that minimises the above function. There are two types of solution available.

Assume that the problem is unconstrained, i.e. that the positive definiteness assumption $k_i > 0$ is automatically satisfied. Then:

$$\frac{\partial J(k)}{\partial k} = \nabla J(k) = \beta + 2\Phi k = 0 \tag{8.41}$$

$$\Rightarrow k = -\frac{1}{2}\Phi^{-1}\beta \tag{8.42}$$

For a realistic solution $k_i \geq 0$ for all i, i.e. all the entries of the k vector must be non-negative. This cannot always be guaranteed by the unconstrained solution above, e.g. if the stiffness of one member is significantly lower than the stiffness of the other members and the error measurement in X (or F) is large.

The second solution takes account of the constraints and involves quadratic programming, which is a very powerful tool for solving quadratic optimisation problems. Here, the only constraint is that all k_i values are positive. The problem is stated as:

$$\min J(k) = \beta^T k + k^T \Phi k \text{ subject to } k_i > 0 \tag{8.43}$$

Several examples have been tested with Matlab using quadratic programming and estimation by simple matrix inversion, i.e. $K = FX^{-1}$ (for square X only, i.e. for a fixed number of measurements equal to the number of stiffness parameters). First, valid F and X vectors were generated for a given "true" stiffness matrix K. The K matrix was estimated exactly with both methods. Next, random error terms were introduced in X, (or F) and K was estimated. The estimated stiffness matrix was close to the original K as the error size was reduced and/or the number of measurements was increased. For large error terms negative estimates of K could be obtained via the first method but not when quadratic programming was used.

8.7 Solution for the Positive Definite Case

To test the effectiveness of the Procrustes algorithm two matrices $K \in \Re^{n \times n}$ and $F \in \Re^{n \times m}$ were generated with K symmetric positive definite and $m \geq n$. The force matrix F was calculated by the equation $F = KX$ and then the stiffness matrix was estimated using the F and X matrices. Both algorithms were tested (proximal point and steepest descent). The stiffness matrix K was estimated with high accuracy (99.96%)

with both methods. Next, error terms in the displacement matrix X were introduced in the order of 10%. The results produced by the Procrustes algorithm were compared with those from simple matrix inversion $K = FX^{-1}$ (for $m = n$ only).

The Procrustes algorithm produced significantly better estimates than estimation via matrix inversion. Furthermore, the matrix obtained was always positive (semi-) definite as opposed to the matrix obtained by matrix inversion, which in some cases was not. Finally, by adding more measurements, i.e. increasing the number of columns of the displacement matrix X, the stiffness matrix estimation error consistently reduced. The results are summarised below for both algorithms. It was not clear (and beyond the scope of this work) to compare which method converged faster and with higher precision, a task that could have been undertaken via statistical analysis of the results. [Woodgate 2006], suggests a third method, the modified Newton algorithm, which in theory converges faster than either of the two methods used; however, because the two algorithms showed fast convergence rates and a satisfactory precision, the modified Newton algorithm was not implemented.

Convergence rate of Procrustes algorithm compared to matrix inversion

Method	Original K	$K = FX^{-1}$	Procrustes (3 measurements)	Procrustes (10 measurements)
Proximal point	$\begin{bmatrix}1.5 & 1.2 & 1.1\\ 1.2 & 1.2 & 0.9\\ 1.1 & 0.9 & 0.9\end{bmatrix}$	$\begin{bmatrix}1.68 & 1.49 & 0.65\\ 0.92 & 0.67 & 1.82\\ 1.30 & 1.36 & 0.39\end{bmatrix}$	$\begin{bmatrix}1.53 & 1.19 & 1.1\\ 1.19 & 1.21 & 1.01\\ 1.1 & 1.01 & 0.93\end{bmatrix}$	$\begin{bmatrix}1.49 & 1.24 & 1.07\\ 1.24 & 1.32 & 0.82\\ 1.07 & 0.82 & 0.99\end{bmatrix}$
Steepest descent	$\begin{bmatrix}1.5 & 1.2 & 1.1\\ 1.2 & 1.2 & 0.9\\ 1.1 & 0.9 & 0.9\end{bmatrix}$	$\begin{bmatrix}1.60 & 1.26 & 1.16\\ 1.12 & 1.14 & 0.79\\ 1.26 & 0.56 & 1.07\end{bmatrix}$	$\begin{bmatrix}1.64 & 1.15 & 1.21\\ 1.15 & 1.27 & 0.67\\ 1.21 & 0.67 & 1.01\end{bmatrix}$	$\begin{bmatrix}1.50 & 1.14 & 1.12\\ 1.14 & 1.22 & 0.84\\ 1.12 & 0.84 & 0.90\end{bmatrix}$

Table 8.1

8.8. The Tridiagonal Positive Definite Case - Alternating Projections

The third case of structural stiffness matrix form is that of a symmetric, positive semi-definite and tridiagonal matrix but without any special dependencies between its elements. This stiffness matrix form is common in elastic structures. If the original Procrustes algorithm is used, the estimated matrix will not be tridiagonal in general. In order to employ this additional information the alternating projection algorithm will be used.

Let $S_{\geq}^{n}$ be the convex cone of all positive semi-definite matrices and T the subspace of all tridiagonal matrices. Then the optimisation problem described in the previous paragraph can be formulated as:

$$\inf_{A \in S_{\geq}^{n} \cap T} \left\| F - AG \right\|_{F}.$$

The objective is to find the projection onto the intersection of the two convex sets $S_{\geq}^{n}$ and T, which will give the optimal positive semi-definite and tridiagonal stiffness matrix K. This can be achieved by the alternating projection algorithm, where at first a positive semi-definite matrix is obtained followed by a tridiagonal matrix, followed again by a positive semi-definite, matrix etc. until the solution converges. The algorithm is shown graphically in figure 8.6. The cone represents the set of positive semi-definite matrices and the oval shape is the set of the tridiagonal matrices (which is in fact a subspace). The solution will alternate from PSD to Tridiagonal until the intersection is reached, which is the solution of the problem.

Alternating projection algorithm

The method of alternating projection is a powerful tool for determining best approximations from a closed convex set K, if it is the intersection of two or more closed convex sets. Although this is difficult to achieve in detail, calculating the two individual projections is straightforward. The algorithm was originally developed to calculate projections onto the intersection of (closed) convex sets. For two subspaces,

the rate of convergence of the algorithm depends on the "angle" between the two subspaces. The proof of this result is given in [Deutsch, 2001]. The important points are summarised below for the case of two subspaces:

Von Neumann's Theorem. Let M_1 and M_2 be closed subspaces in the Hilbert space X. Then for each $x \in X$,

$$\lim_{n\to\infty}\left(P_{M_2}P_{M_1}\right)^n(x) = P_{M_1\cap M_2}(x) \tag{8.44}$$

Angle between two subspaces

The rate of convergence of the alternating projection algorithms depends solely on the angle between the two subspaces. If the angle is large the rate of convergence is fast as well.

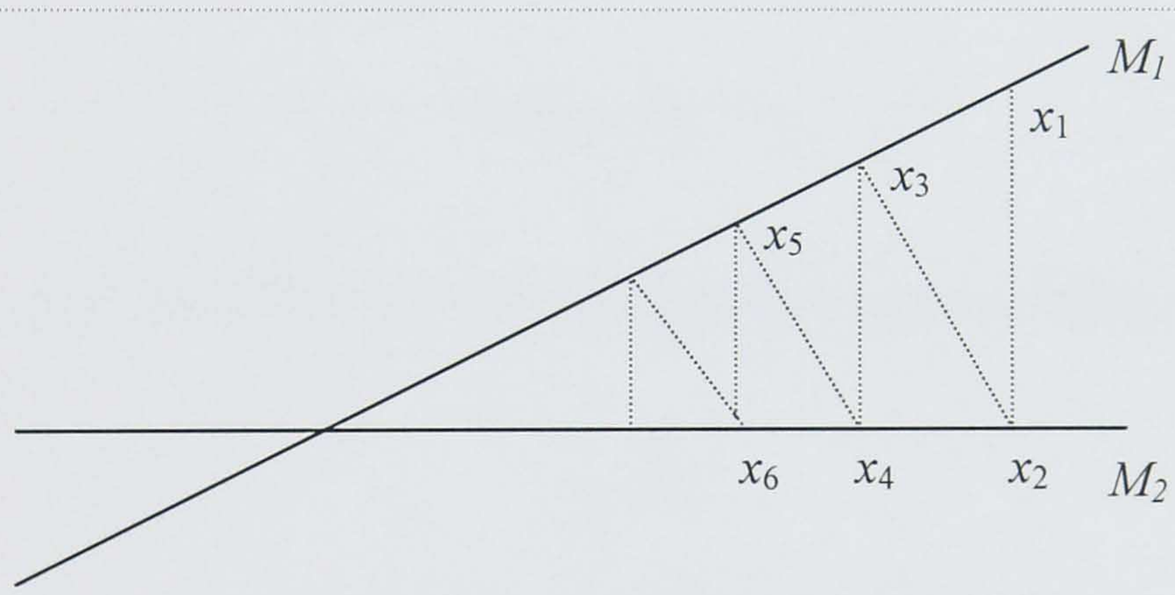

Figure 8.7 Alternating projection

Theorem [Deutsch, 2001]: Let M_1 and M_2 be closed subspaces in the Hilbert space X and $c = c\left(M_1, M_2\right)$. Then for each $x \in X$,

$$\left\|\left(P_{M_2}P_{M_1}\right)^n(x) - P_{M_1\cap M_2}(x)\right\| \le c^{2n-1}\left\|x - P_{M_1\cap M_2}(x)\right\| \le c^{2n-1}\|x\| \tag{8.45}$$

for $n = 1, 2, 3, \ldots$ Moreover, the constant c is the smallest possible constant in the above inequality independent of x.

Dykstra's algorithm: [Deutsch, 2001]

In this section the Dykstra algorithm is used. This result proves that best approximations can be computed via an iterative procedure, if an algorithm exists to project onto individual subspace or closed convex set. Here, the set of all PSD matrices is a convex cone as explained in an earlier section while the set of symmetric matrices with a triangular structure is a subspace of the vector space of all symmetric matrices (and thus also closed and convex).

The algorithm proceeds in cycles. Let $P_{k_n}(x)$ be projection onto the intersection of the n-th convex set K_n, $n=1,2,\ldots,r$, where r is the total number of convex sets. Now assume that $[n]=n \bmod (r)$, x depends on $P_{k_n}(x)$ and on an error term e_n generated as the algorithm proceeds, i.e.

$$x_i = P_{k_n}(x_{[n]+1} + e_{n-r}) \tag{8.46}$$

and

$$e_n = x_{n-1} + e_{n-r} - x_n \tag{8.47}$$

Also, e_{-1} and e_0 are initially set to 0. The first few steps are shown for the case on two convex sets:

$n=0$ $\quad x_0 = 0$

$\quad e_{-1} = 0$

$n=1$ $\quad x_1 = P_{k_1}(x_0 + e_{-1})$

$\quad e_1 = x_0 + e_{-1} - x_1$

$n=2$ $\quad x_2 = P_{k_2}(x_1 + e_0)$

$\quad e_2 = x_1 + e_0 - x_2$

$n=3$ $\quad x_3 = P_{k_1}(x_2 + e_1)$

$\quad e_3 = x_2 + e_1 - x_3$

etc.

The algorithm is shown graphically below for the case of two convex sets:

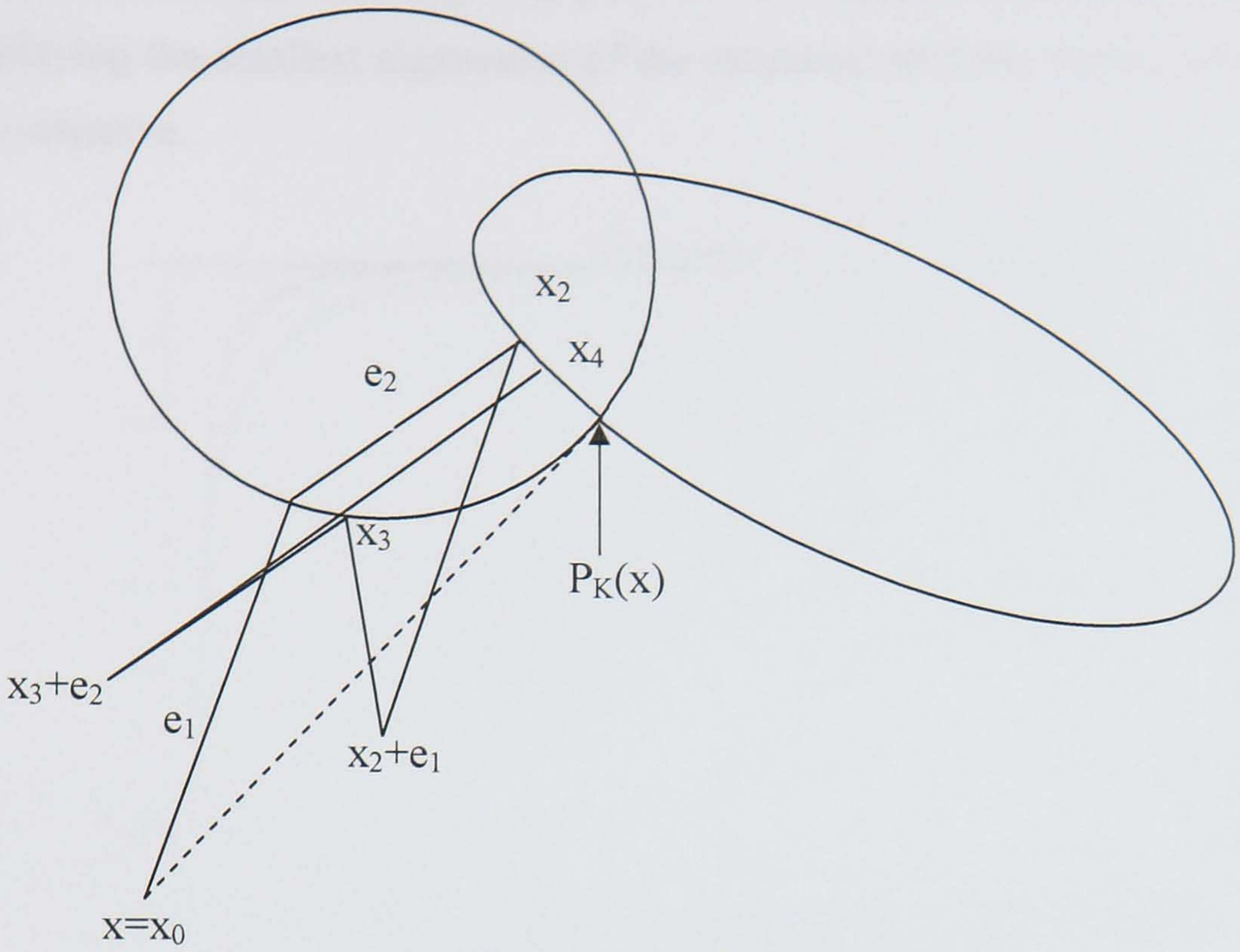

Figure 8.8 Dykstra algorithm

The Procrustes problem has been solved with Dykstra's algorithm. The two convex sets in this case correspond to, (i) $S_{\geq}^{n}$, the convex cone of symmetric positive semi-definite matrices and, (ii) the set of all symmetric matrices with triangular structure (actually a subspace). The first projection can be performed using either the proximal point algorithm described earlier or via steepest descent. The second projection is straightforward and can be performed using the projection operator WW^T defined earlier followed by setting to zero all elements a_{ij} with $|i-j|>1$.

To test the results, positive definite triangular stiffness matrices K were generated randomly, together with corresponding force and displacement matrices F and X (either error free or corrupted by measurement noise error terms) and subsequently it was attempted to estimate the stiffness matrix from the data using the two algorithms described earlier. The alternating projection algorithm was terminated after either a fixed number of iterations or when a tolerance criterion involving a norm of the difference between two consecutive estimates generated during the algorithm was satisfied. The matrices produced at the odd iteration steps were positive semi-definite but not necessarily triangular, while the opposite conditions were satisfied at the even-numbered steps. However, as the algorithm converged to the optimal solution both sets

of conditions were satisfied. The positive semi-definite condition was monitored by displaying the smallest eigenvalue of the estimated stiffness matrix which needs to be non-negative.

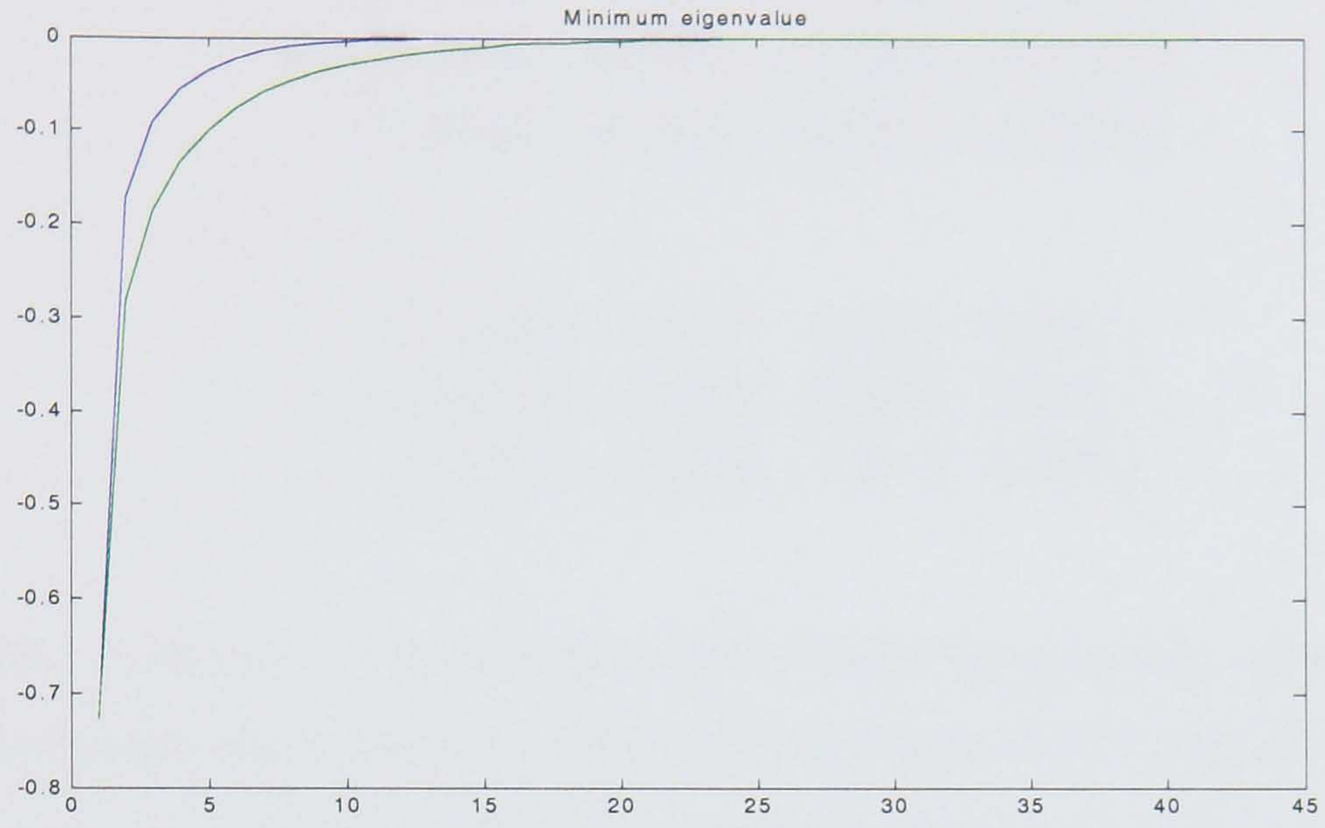

Figure 8.9 Minimum eigenvalue for proximal point and steepest descent

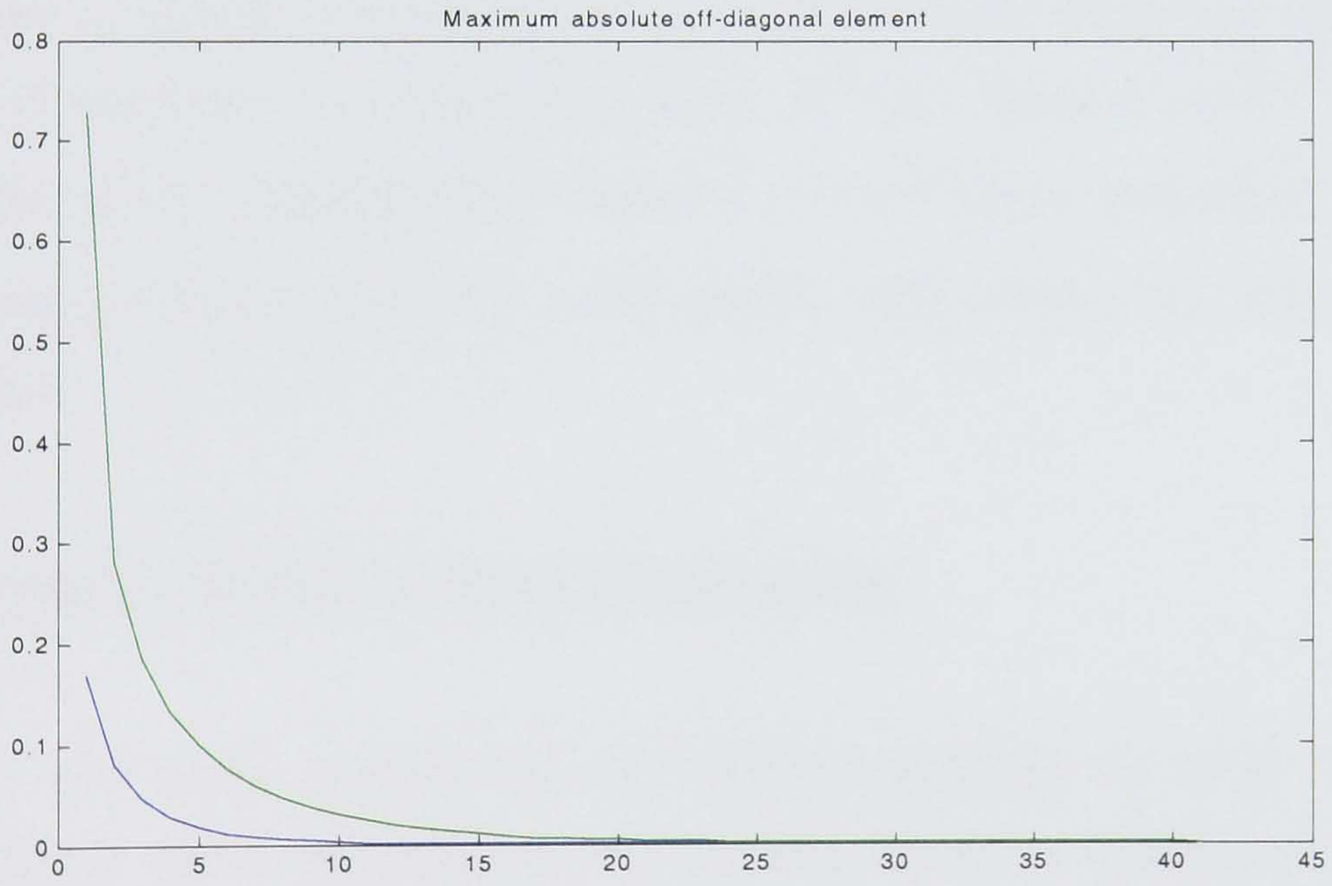

Figure 8.10: Maximum absolute value of estimated element $|K_{ij}|, |i-j|>1$ for proximal point and steepest descent

Figures 8.9 and Figure 8.10 display the minimum eigenvalue and the maximum absolute value of the entries in the (i,j)-th positions with $|i-j|>1$, generated during a typical algorithm (using both methods). It can be seen that the both algorithms converge

towards a solution which is both positive semi-definite and triangular. The force and displacement vectors used in the example were chosen as:

$$F = \begin{bmatrix} 0.1326 & -1.5804 & -1.0246 & -0.4293 \\ 1.5929 & -0.0787 & -1.2344 & 0.0558 \\ 1.0184 & -0.6817 & 0.2888 & -0.3679 \end{bmatrix}$$

and

$$X = \begin{bmatrix} -0.4650 & 2.1122 & 1.0378 & 0.3155 \\ 0.3710 & -1.3573 & -0.3898 & 1.5532 \\ 0.7283 & -1.0226 & -1.3813 & 0.7079 \end{bmatrix}$$

respectively. Although in this case the method using the proximity algorithm (deemed to have converged when the norm between the estimate and the solution is smaller than 10^{-5}) appears to converge slightly faster than steepest descent (i.e. in 15 rather than about 20 iterations) the overall results were mixed and thus no firm conclusions could be drawn in general concerning the convergence rates of the two methods, either in terms of iterations or computation time. It was noted, however, that unless the projection onto $S_{\geq}^{n}$ (using either method) was calculated reasonably accurately, the alternating projection algorithm could exhibit small oscillations and a non-monotonic behaviour.

8.9 Dynamic Stiffness Matrix Estimation

Making real scale experiments on existing buildings in order to measure the displacement and hence calculate the stiffness matrix is difficult in practise. Let us assume that a building, or a part of a structure is damaged due to an earthquake, a blast or a fire that has resulted in failure of a member or weakness of a part of the structure. Alternatively, assume that there is an ancient building or monument whose stiffness matrix is not known or that it has degraded through time. Performing actual experiments on site is very difficult and transporting the building at a different location is either not possible or too expensive. Typically, it is easy to apply a force on a member and measure its displacement, but in order to measure the displacement of all the nodes of a structure a very large force has to be applied. Furthermore, typical stiffness values of

buildings are at least in the order of 10^6 *N/m*, which means that a force of $1KN$ will produce displacements in the order of 1 *mm*. Therefore, in order to obtain realistic data, large forces are needed to provide reasonable displacements and reduce the error in measurement. One alternative way to overcome this practical obstacle is to let nature provide the forces. If the structure is in a region of frequent earthquakes or large winds then if the structure is provided with sensors, during the earthquake many recordings can be taken, and an estimate of the stiffness matrix can be obtained. A further advantage of this method is that from a dynamic response many more measurements can be recorded and more accurate estimates can therefore be obtained. Here, the measurements are dynamic but this does not change significantly the stiffness matrix calculation, provided the developed stresses do not exceed the elastic limit.

Let us assume that the stiffness matrix of a building is required. The acceleration of the earthquake, the epicentre and hypocentre and hence distance to the site are all known. Also the energy lost from the earthquake until it reaches the site is known as well. Finally assume that accelerometers are placed on every floor, together with displacement and velocity sensors (alternatively acceleration data may be used to obtain velocity and displacement data).

Now, the force on the building from the earthquake is F,

$$F = M\ddot{x} + C\dot{x} + Kx \tag{8.48}$$

and hence

$$(F - M\ddot{x} - C\dot{x}) - Kx = 0 \tag{8.49}$$

Assume that the only unknown in this equation is K. The above equation can be formulated as a Procrustes problem used to estimate K. An example was performed in Matlab where the exact stiffness was obtained from the Procrustes algorithm and direct matrix inversion, from only a few measurements matching the order of the system but without injecting any measurement noise.

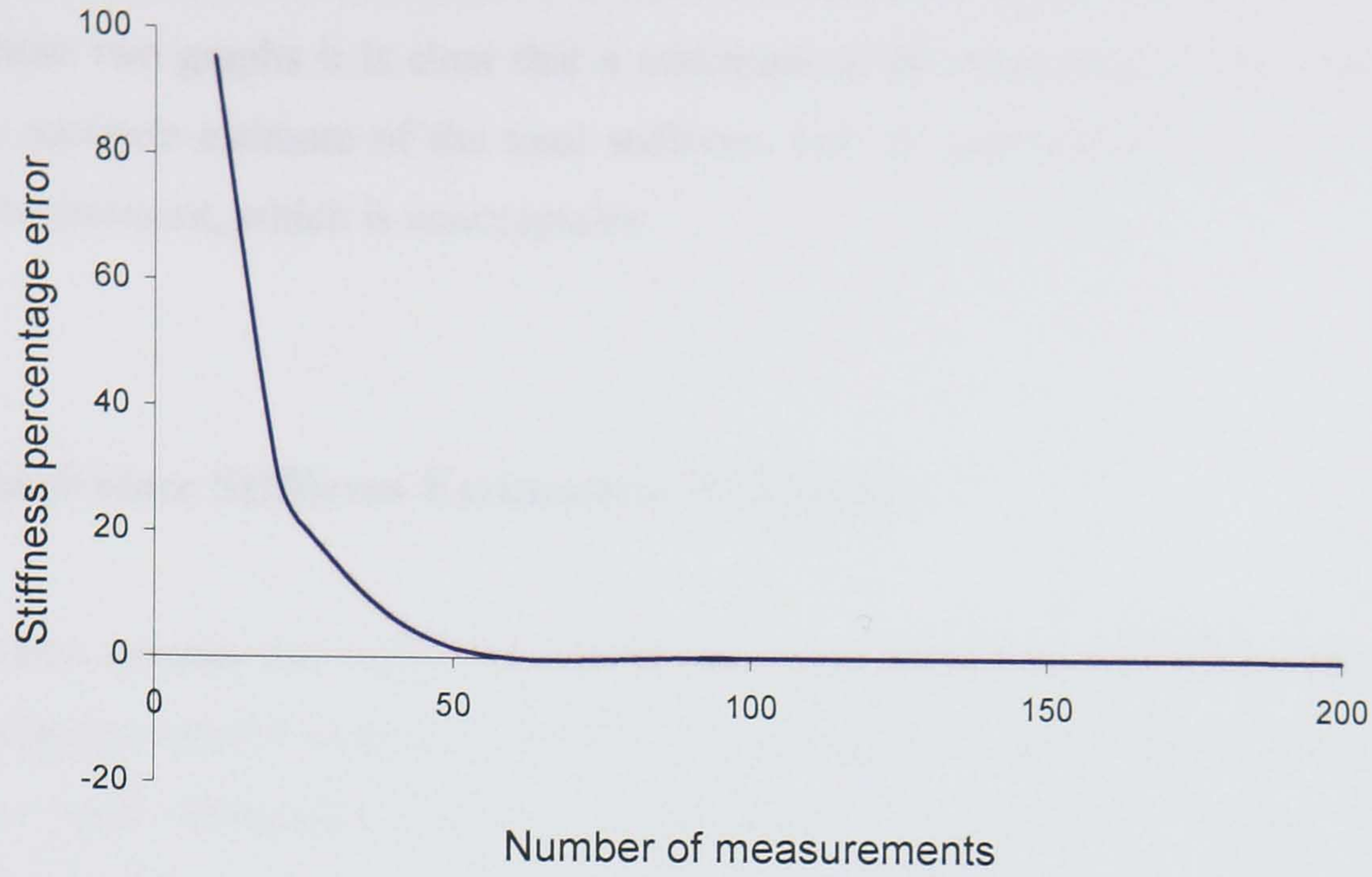

Figure 8.11: Percentage estimation error vs number of measurements

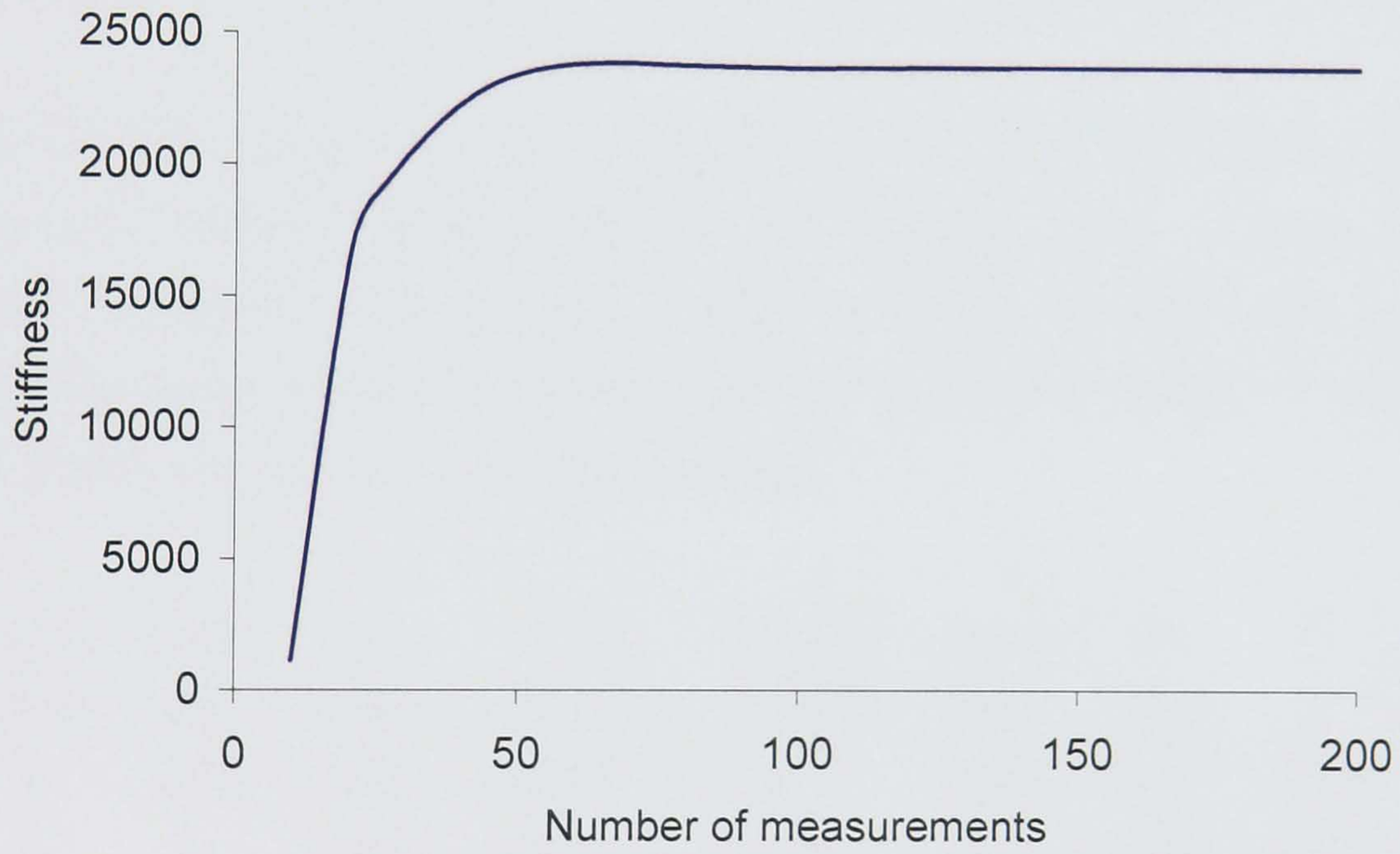

Figure 8.12: Total stiffness estimation vs number of measurements

Next, errors in the measurements were introduced of the order of ±1%. Now, the estimated stiffness matrix was quite inaccurate when direct matrix inversion was used. In order to estimate the stiffness parameters accurately, several measurements were obtained and thus F and X become matrices with many more columns than rows. The accuracy of the method depends largely on the number of measurements taken. Graph 8.12 shows the total stiffness error as a function of the number of measurements. The

estimate of the sum of the stiffness of all floors is also shown (true value is 23800 N/m). From these two graphs it is clear that a minimum of 40 measurements are required to give an accurate estimate of the total stiffness. For 25 measurements there is a 20% error measurement, which is unacceptable.

8.10 Real-time Stiffness Estimation Example

This section extends the work of the previous section in the area of stiffness estimation via an adaptive control example. Consider for example that part of a structure has failed due to a large earthquake and as a consequence the structure is weaker. The new stiffness matrix is not known, although it is required for any kind of control design. In order to reinforce the structure an active controller is employed. The controller's dual purpose is to protect the structure and also to help estimate the new stiffness matrix.

Because the exact stiffness is unknown, an initial stiffness matrix is assumed, which is also used for controller design purposes. The structure is the 3-storey building considered in chapters 5 and 6 and uses an LQR controller. The initial stiffness matrix K_i used for the design and the real stiffness matrix (K_r) are shown below. The real floor stiffness is 40% less than the one initially assumed.

$$K_i = \begin{bmatrix} 18600 & -2600 & 0 & 0 \\ -2600 & 5200 & -2600 & 0 \\ 0 & -2600 & 5200 & -2600 \\ 0 & 0 & -2600 & 2600 \end{bmatrix} \quad K_r = \begin{bmatrix} 23960 & -1560 & 0 & 0 \\ -1560 & 3120 & -1560 & 0 \\ 0 & -1560 & 3120 & -1560 \\ 0 & 0 & -1560 & 1560 \end{bmatrix}$$

Graph 8.13 shows the results of four different simulations. The first one is the response of the structure to an impulsive loading without any controller (passive response). The second one shows the "expected" response, i.e. the response we expect to observe if the structure had the initially assumed stiffness matrix. The third response is the "real" response of the active system, which is unstable. Thus, by using incorrect parameters for the design an unstable closed-loop system is produced. The fourth simulation shows the "ideal" response, which is what we would get if the correct stiffness was known at

the design stage (and the LQR controller was designed with the same weighting matrices). The "real" control input (figure 8.14) is also constantly increasing which is an indication of an unstable design.

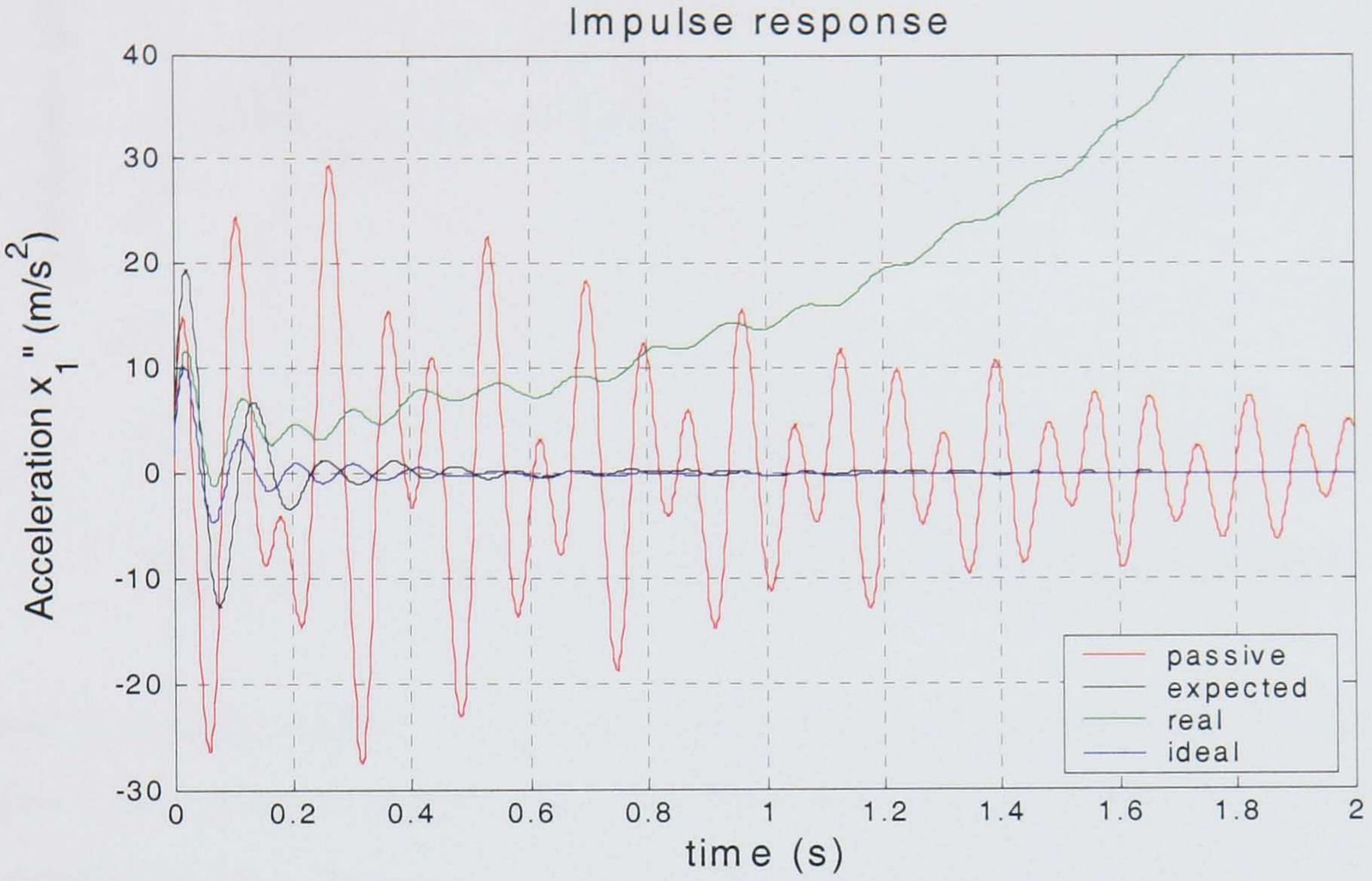

Figure 8.13 Acceleration (passive, expected real and ideal)

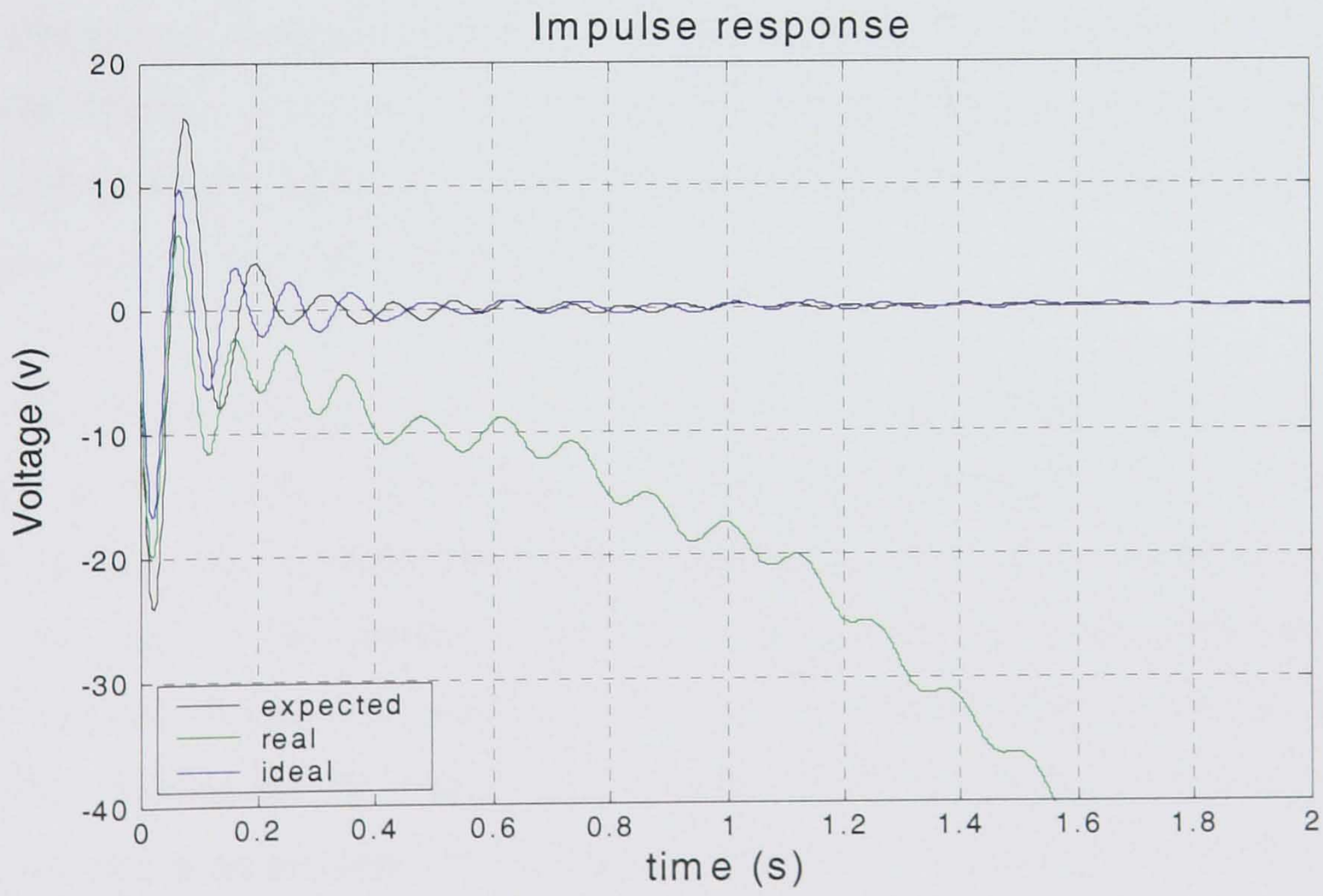

Figure 8.14 Voltage (passive, expected real and ideal)

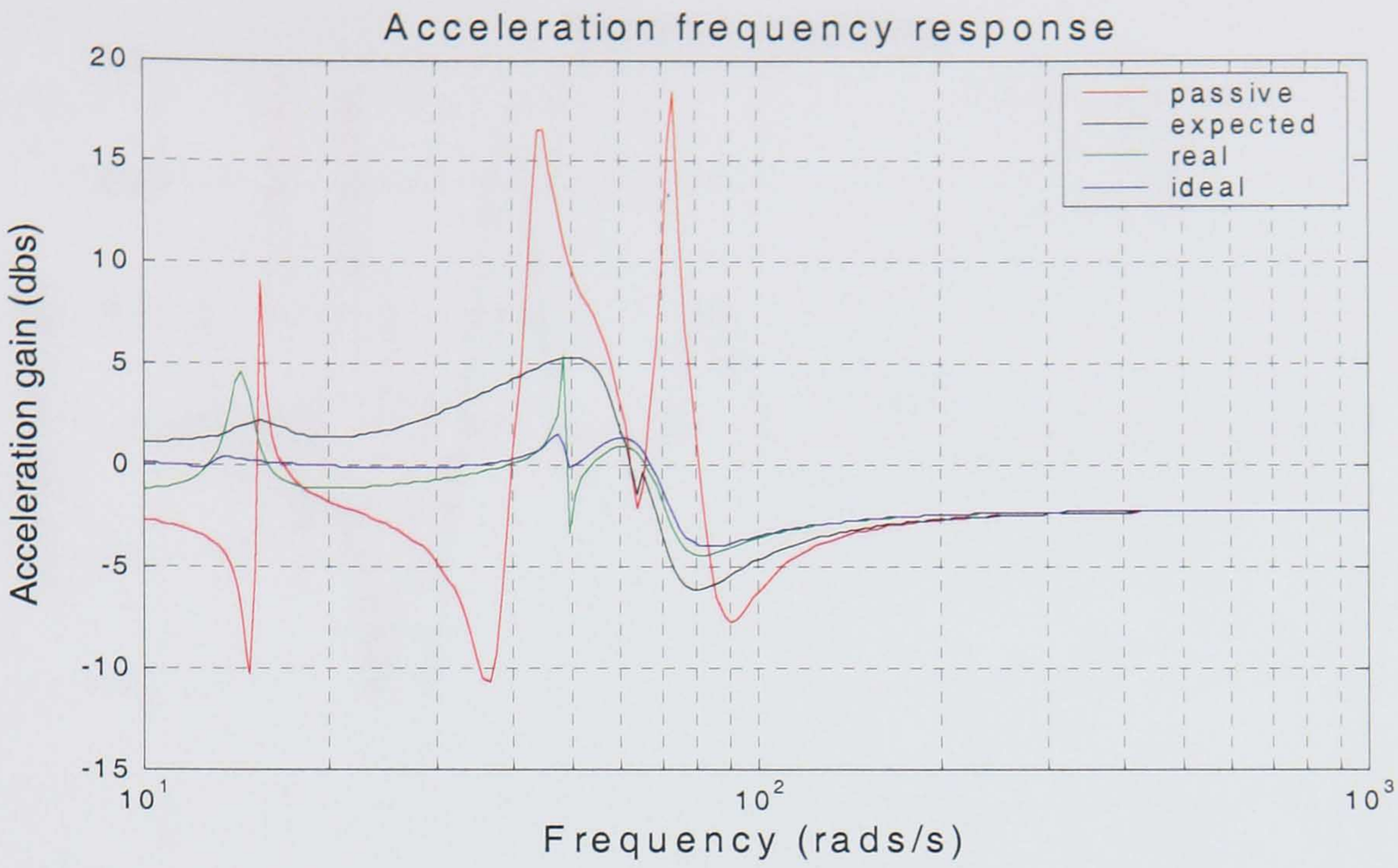

Figure 8.15 Frequency bode plots (passive, expected real and ideal)

Next, an online stiffness matrix estimation scheme was employed, as described in section 10. In order to obtain an accurate estimate of the stiffness matrix, at least 30-50 measurements are required (see section 8.9), corresponding to a period of 0.5 seconds for a sampling period of 10ms used here. Using this time the system operates in closed loop with the controller designed on the basis of the wrong (initial) stiffness estimates and thus the response starts to show increasing amplitudes of oscillation as the closed-loop is unstable. At time $t = 0.5s.$ the controller is switched to the one redesigned using the stiffness matrix estimates. The simulations of the responses of the displacements of the four floors are shown in figure 8.16.

An alternative method is to use an adaptive control scheme where after each measurement is taken, the stiffness is estimated and an online LQR controller is re-designed and the corresponding control signal applied for the next sampling interval. The drawback of this method is that each sampling interval a new estimation and an LQR control design are needed, tasks which are both time-consuming (although possibly feasible for the sampling rate used). Since a number of measurements are required before an accurate estimate can be obtained, a "forgetting-factor" type estimate of the form:

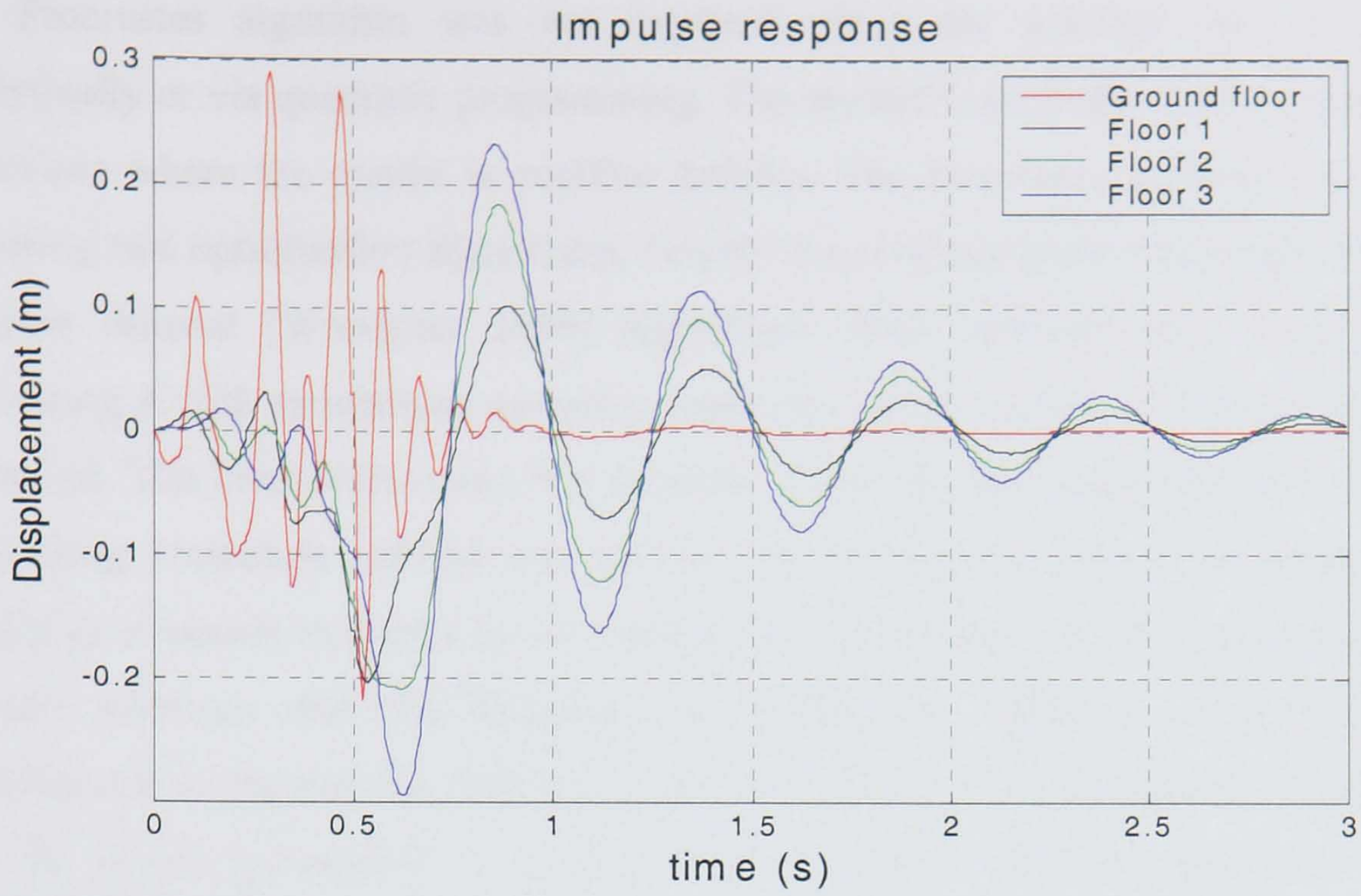

Figure 8.16 Floor displacements using adaptive control scheme

$$K = \frac{20K_i + nK_e}{20 + n} \tag{8.50}$$

can be used. This combines the initial estimate with the new estimates obtained in real time. As the sampling index increases, the initial estimates are progressively discounted and replaced with the more accurate estimates, based on the real-time response of the system.

8.11 Summary

This chapter considers the estimation of stiffness matrices by using the Procrustes approximation method. When the stiffness matrix is unknown, by applying a force F and measuring the resulting displacement vector X, the stiffness matrix K can be obtained. The Procrustes method is a strong optimisation tool when uncertainty in measurements is present and when a-priori knowledge of the stiffness matrix form is available. Three forms of structural stiffness matrices common among structures have been considered. The simplest one is a special form present in buildings where the stiffness matrix is tridiagonal with only as many variables as the number of floors. Here,

the Procrustes algorithm was not required; since the solution can be obtained analytically or via quadratic programming. The second form is the most general among structures where the matrix is positive definite. The Procrustes method was used by choosing two optimisation algorithms, namely the proximal point [Allwright 1988] and steepest descent [Woodgate 2006] algorithms. Both methods were successful for estimating K with satisfactory accuracy, especially as the number of measurements was increased. The third form is one that is positive semi-definite and tridiagonal. Here, the alternating projection method was applied for solving the estimation problem. This algorithm proceeds in cycles by successive projections onto the cone of positive semi-definite matrices and the subspace of tri-diagonal matrices, respectively, until convergence to the optimal estimate is obtained. The main advantage of the method is that its theory guarantees convergence to the global optimum and also provides estimates of the convergence rate.

In the last part of the chapter, the estimation scheme was expanded from the static to the dynamic loading case. Instead of applying a set of static forces and measuring the set of corresponding displacements, during an earthquake sensors can be used to measure these forces and displacements continuously. Thus, a much larger number of measurements can be obtained and a better stiffness estimate results. The work of the chapter concludes with an adaptive controller design example. Here, active control is applied to a structure with poorly known stiffness properties. A fixed LQR controller designed with the wrong parameters is shown to be unstable. However, if on-line estimation is used and the estimates are used to re-design the controller, stability and performance (vibration suppression) of the design can be recovered.

CHAPTER 9

BENCHMARK PROBLEM CASE STUDY

9.1. Introduction

The last part of the thesis is a case study. The previous examined control design methods, LQG, H_∞, LPOC and passive control are applied and verified into a realistic full-scale structure. Certain aspects relevant to controller implementation are discussed in detail. In the previous chapters emphasis was given into the optimality of a controller in terms of reducing structural deflections and accelerations or control effort. Here, the main objective is to determine if a design method is applicable to a real life problem, e.g when time-delays, large scale-models or multi-objectives are taken into account. A more sophisticated finite-element structural model was obtained for the structure used in this chapter. Finally, the chapter contains a more complete set of results related to comparison of different design methods than those presented in previous chapters.

Benchmark problems: The structure chosen for control design is a benchmark problem. It was introduced by a committee of researchers with the objective of having a common set of criteria under consideration when testing different design techniques or algorithms. There have been three generations of benchmark structures so far: The first generation was a three-storey regular building implementing an AMD or an ATC system. The 2nd generation of benchmark problems included an Earthquake-excited 20-storey building and a 76-story building subject to wind loading. The first building required apart from controller design the specification of the best type of actuators along with the number and location of actuators and sensors used and the latter had a TMD or AMD at the top floor. The third generation of benchmark problems includes bridges and non-linear buildings models. They are 3, 9 or 20-storey non-linear building, a wind excited 76-storey building, a cable stayed bridge and a smart base isolation problem. The complexity of the benchmark problems increases and although the first generation problems were set mainly for comparison of various schemes, the purpose of the last two generation problems is to verify the stability of control algorithms.

For this study two benchmark problems were used, the first for the 3-storey building using AMD. Then an active control scheme for a 76-storey building with wind loading was designed, to investigate issues arising in large and complex structures.

Benchmark problems have been extensively used by many researchers since their introduction in 1998. They have been widely accepted by the scientific community and they constitute an official method of measuring the performance of various design methods for structural control. There are special Benchmark sessions in structural control conferences and special Benchmark issues in journals (e.g. the special issue in Journal of Earthquake Engineering and Structural Dynamics, Volume 27, issue 11).

The advantage that benchmark problems offer is that the models usually correspond to real or designed buildings. Furthermore the assessment criteria are realistic because they are applied in the way they would be applied in a real problem, e.g. by including saturation actuation levels, time delays and any other limiting factors arising in real-time active structural control. Also, the state space models used are typically obtained from extensive finite element analysis, or from experimental data.

The benchmark problem in structural control was introduced in 1998 by [Spencer et al. 1998] It represents a structural control problem that can be used to evaluate several control algorithms. The structural model used was one that had been fully designed but not built [Chung et al. 1989], [Chung et al. 1988], [Dyke et al. 1994b]. The evaluation model was derived by using experimental data at the structural dynamics and control earthquake engineering laboratory at Notre Dame University.

The aim of Benchmark problems was to have a unique/common model and design framework for researchers so that valid comparisons between proposed new design methods or algorithms can be made. Several issues such as model reduction, time delays, saturation, multi objective design, limit sensors, noise are taken into account. The researcher needs to design a suitable controller, which is simulated for real earthquake measurements and random signals of certain type. The results are evaluated by several criteria, including peak and RMS values of displacement, velocities and accelerations of the building floors and the actuator.

9.2. 1st Benchmark problem-3 storey AMD

9.1.1. Model description

Experimental model: The structure is a regular 3-storey, single bay steel model subject to 1-dimensional motion. The structural frame has a mass of 77 Kg and the floors 227 Kg distributed evenly. The height of the frame is 158 cm. A scale time factor of 0.2 was used, which means that the modes have 5 times lower periods than the full-scale structure. The other model quantities have been reduced accordingly: $F = 1:60$, mass $= 1:200$, $T = 1:2$, displacement $= 4:29$, acceleration $= 7:2$.

The control scheme used was an AMD placed on the 3rd floor. It consists of a servo-actuated hydraulic cylinder of 3.8 *cm* diameter and maximum displacement (stroke) of 30.5 *cm*. The mass of the AMD was 5.2 *Kg*, 1.7% of the total mass of the structure. Sensors are placed on each floor measuring the acceleration of the ground, every floor and the acceleration and displacement of the AMD device. Note that the designer has the option of measuring displacements and velocities as well, or to assume any combination of the above measurements.

Evaluation model:

The State space description of the model is given by:

$$\dot{x} = Ax + Bu + E\ddot{x}_g \tag{9.1}$$

$$y = C_y x + D_y u + F_y \ddot{x}_g + v \tag{9.2}$$

$$z = C_z x + D_z u + F_z \ddot{x}_g \tag{9.3}$$

where, x is the state vector

$y = \left[x_m, \ddot{x}_1, \ddot{x}_2, \ddot{x}_3, \ddot{x}_m, \ddot{x}_g \right]$, is the measured output vector

$z = \left[x_1, x_2, x_3, x_m, \dot{x}_1, \dot{x}_2, \dot{x}_3, \dot{x}_m, \ddot{x}_1, \ddot{x}_2, \ddot{x}_3, \ddot{x}_m, \ddot{x}_g \right]$, is the regulated output vector

A is the system dynamic matrix reduced by model reduction

B is the control input matrix

E is the exogenous ground excitation matrix

C is the measurement matrix

D is the control input feedthrough matrix

F is the exogenous feedthrough matrix

$\ddot{x}_g$ is the exogenous input (disturbance)

The full model has 28 states but it is reduced to 10 states after appropriate model reduction. Note that the 10 states do not directly correspond to physical states, e.g. the 4th state does not correspond to the floors' acceleration, velocity or displacement of a certain floor. Therefore the designer cannot obtain the physical state-variables from the A matrix. The only known information is the measured and regulated output signal.

Stationary random process input: The excitation inputs are two historic earthquake records and a random input. The random signal is a stationary random process with a spectral density defined by the following Kanai-Tajimi spectrum

$$S_{\ddot{x}_g\ddot{x}_g}(\omega) = \frac{S_0\left(4\zeta_g^2\omega_g^2\omega^2 + \omega_g^4\right)}{\left(\omega^2 - \omega_g^2\right)^2 + 4\zeta_g^2\omega_g^2\omega^2} \tag{9.4}$$

where ω_g and ζ_g are within the following ranges: $20rad/s \le \omega_g \le 120rad/s$ and $0.3 \le \zeta_g \le 0.75$. For comparison purposes the spectral intensity is chosen such that the RMS value of the ground acceleration takes a constant value of $\sigma_{\ddot{x}_g} = 0.12g$.

$$S_0 = \frac{0.03\zeta_g}{\pi\omega_g\left(4\zeta_g^2 + 1\right)}g^2 s. \tag{9.5}$$

Evaluation criteria This Benchmark problem has 10 evaluation criteria, which include RMS and peak responses, for the 2 real earthquake and the one random excitation signal. They include accelerations, displacements and velocities of the floors and the mass driver. Therefore the design methods are evaluated for all possible aspects. The five first evaluation criteria are for RMS responses for the random excitation signal.

The first criterion is the non-dimensional measure of:

$$J_1 = \max_{\omega_g,\zeta_g}\left\{\frac{\sigma_{d_1}}{\sigma_{x_3}}, \quad \frac{\sigma_{d_2}}{\sigma_{x_3}}, \quad \frac{\sigma_{d_3}}{\sigma_{x_3}}\right\} \tag{9.6}$$

It measures the ability of the system to minimise the interstorey drifts relative to the 3rd floor displacement of the uncontrolled structure. Here, σ_{d_i} is the interstorey drift between two adjacent floors, where usually the maximum displacement occurs at the lower floor. σ_{x_3} is the worst-case stationary RMS 3rd floor displacement of the uncontrolled structure, occurring when $\omega_g = 37.3\,rad/s$ and $\zeta_g = 0.3$.

The second criterion is the maximum absolute floor acceleration divided by the worst-case stationary RMS 3rd floor acceleration of the uncontrolled building (occurring again when $\omega_g = 37.3\,\text{rad/s}$ and $\zeta_g = 0.3$).

$$J_2 = \max_{\omega_g,\zeta_g}\left\{\frac{\sigma_{\ddot{x}_1}}{\sigma_{\ddot{x}_3}}, \quad \frac{\sigma_{\ddot{x}_2}}{\sigma_{\ddot{x}_3}}, \quad \frac{\sigma_{\ddot{x}_3}}{\sigma_{\ddot{x}_3}}\right\} \tag{9.7}$$

The next three evaluation criteria involve the actuator, and are given by the ratio of its displacement, velocity and acceleration to the uncontrolled building's 3rd floor displacement, velocity and acceleration, respectively. The actuator displacement provides a measure of the physical size of the control device. The actuator velocity provides a measure of the control power required and the absolute acceleration is a measure of the magnitude of the forces required for the actuator to execute the commanded control action. The evaluation criteria can be expressed as:

$$J_3 = \max_{\omega_g,\zeta_g}\left\{\frac{\sigma_{x_m}}{\sigma_{x_3}}\right\} \tag{9.8}$$

$$J_4 = \max_{\omega_g,\zeta_g}\left\{\frac{\sigma_{\dot{x}_m}}{\sigma_{\dot{x}_3}}\right\} \tag{9.9}$$

$$J_5 = \max_{\omega_g,\zeta_g}\left\{\frac{\sigma_{\ddot{x}_m}}{\sigma_{\ddot{x}_3}}\right\} \tag{9.10}$$

The other five evaluation criteria involve peak responses. Here, the input is a historic earthquake record. The records used are the NS record of the 1940 El Centro and the NS 1968 Hachinohe earthquake. The time scale for the earthquakes is increased by a factor of 5 and the magnitude decreased by a factor of 3.5 because the building is small-scale. Both earthquakes are considered and the performance index is always the worst case scenario of the two responses. The evaluation criteria are similar to the 5 first ones but now involve peak responses rather than RMS responses. The first index is the ratio of the maximum interstorey drift relative to the 3rd floor displacement of the uncontrolled building:

$$J_6 = \max_{\substack{ELCentro\\Hachinohe}}\left[\max\left\{\frac{x_1}{x_3},\quad \frac{x_2-x_1}{x_3},\quad \frac{x_3-x_2}{x_3}\right\}\right] \tag{9.11}$$

The next performance index is the maximum peak acceleration of the three floors normalised by the third floor acceleration of the uncontrolled building, i.e:

$$J_7 = \max_{\substack{ELCentro\\Hachinohe}}\left[\max\left\{\frac{\ddot{x}_1}{\ddot{x}_3},\quad \frac{\ddot{x}_2}{\ddot{x}_3},\quad \frac{\ddot{x}_3}{\ddot{x}_3}\right\}\right] \tag{9.12}$$

The last three evaluation criteria are given by the ratio of the actuators' displacement, velocity and acceleration normalised by the 3rd floor uncontrolled displacement, velocity and acceleration respectively:

$$J_8 = \max_{\substack{ELCentro\\Hachinohe}}\left[\max\frac{x_m}{x_3}\right] \tag{9.13}$$

$$J_9 = \max_{\substack{ELCentro \\ Hachinohe}} \left[\max \frac{\dot{x}_m}{\dot{x}_3} \right] \tag{9.14}$$

$$J_{10} = \max_{\substack{ELCentro \\ Hachinohe}} \left[\max \frac{\ddot{x}_m}{\ddot{x}_3} \right] \tag{9.15}$$

Simulation model: The input passes through a multiplexer to the plant, specified as a continuous state space LTI model given in equation (9.1). Out of the 13 regulated states, equation (9.3) (displacement velocities or accelerations of each floor and AMD and acceleration of ground excitation) only 6 are taken as measurements: $(\ddot{x}_1, \ddot{x}_2, \ddot{x}_3, \ddot{x}_m, x_m, \ddot{x}_g)$, of which only the 4 accelerations are measured from sensors, i.e. $(\ddot{x}_1, \ddot{x}_2, \ddot{x}_3, \ddot{x}_m)$. Note that the designer has the choice of using different measurements by connecting the appropriate states to be measured to the multiplexer. Sensor noise is added, with the user having the ability to specify the noise level. Next, the signal is limited in amplitude, discretised and quantised. Thus, the designer needs simply to input the state space form of a discrete controller. A saturation level of maximum control voltage is specified and a unit delay of 1 sample period is imposed to make the design more realistic. The signal is then fed back to the plant.

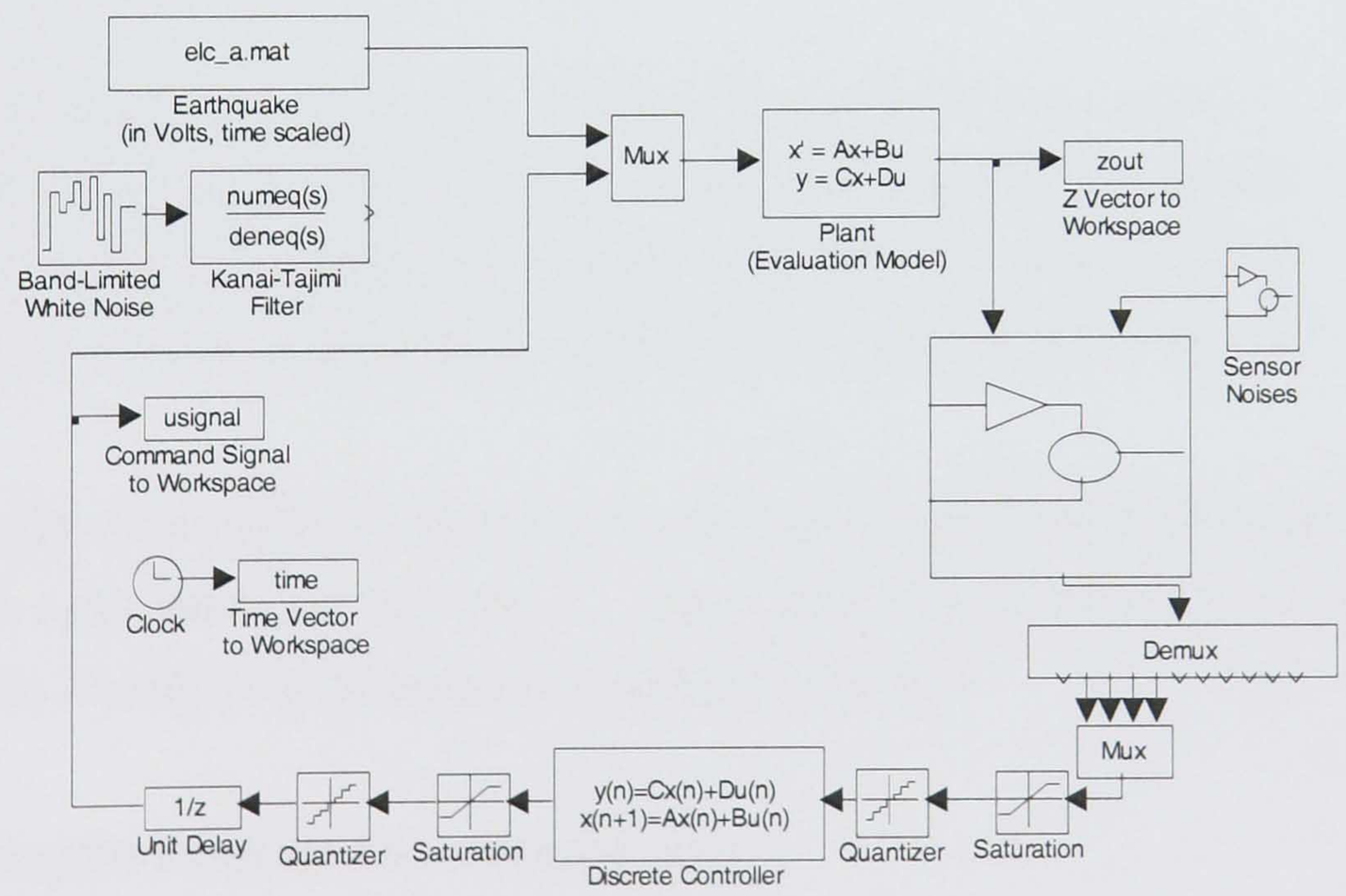

Figure 9.1 1st Benchmark problem, Simulink model

9.2.2. Control design

LQR design

A sample controller has been designed for this benchmark problem by S. Dyke. The objective of the LQR is to minimise the following performance index:

$$\hat{J}(u) = \int_0^{\infty} \left(x^T Q x + u^T R u + 2 x^T N u \right) dt \tag{9.16}$$

subject to plant dynamic constraints $\dot{x} = Ax + Bu + E\ddot{x}_g$. Here, u is the control effort measured in terms of actuator displacement. **x** includes 3 regulated outputs which are the accelerations of each floor $(\ddot{x}_1, \ddot{x}_2, \ddot{x}_3)$. In the above equation the first term represents the states whose weighted energy is to be optimised, the second term the control effort and the last term represents various cross-terms between state and control variables. The appropriate Q, R and N matrices are chosen such that the given control problem can be formulated in the standard LQR problem formulation.

In our case the 4 quadratic optimisation terms are:

$$\begin{aligned}
\ddot{x}_1 &= \rho_1 C_1^T x + \rho_1 D_1 u \Rightarrow \ddot{x}_1^2 = \rho_1^2 x^T C_1 C_1^T x + \rho_1^2 2 x^T C_1 D_1 u + \rho_1^2 D_1^2 u^2 \\
\ddot{x}_2 &= \rho_2 C_2^T x + \rho_2 D_2 u \Rightarrow \ddot{x}_2^2 = \rho_2^2 x^T C_2 C_2^T x + \rho_2^2 2 x^T C_2 D_2 u + \rho_2^2 D_2^2 u^2 \\
\ddot{x}_3 &= \rho_3 C_3^T x + \rho_3 D_3 u \Rightarrow \ddot{x}_3^2 = \rho_3^2 x^T C_3 C_3^T x + \rho_3^2 2 x^T C_3 D_3 u + \rho_3^2 D_3^2 u^2 \\
\ddot{x}_m &= \rho_4 C_4^T x + \rho_4 D_4 u \Rightarrow \ddot{x}_m^2 = \rho_4^2 x^T C_4 C_4^T x + \rho_4^2 2 x^T C_4 D_4 u + \rho_4^2 D_4^2 u^2
\end{aligned} \tag{9.17}$$

where C_i and D_i are obtained from the known measurement and feedthrough matrices. Here, the LQR does not take the F_y matrix into account which is an acceptable assumption. Finally, ρ_i is the penalty term of each objective.

By summing the 4 objective functions we have:

$$\begin{aligned}
&\sum_{i=1} \rho_i x_i^2 = \rho_1 \ddot{x}_1^2 + \rho_2 \ddot{x}_2^2 + \rho_3 \ddot{x}_3^2 + \rho_4 \ddot{x}_m^2 = x^T \left(\rho_1^2 C_1 C_1^T + \rho_2^2 C_2 C_2^T + \rho_3^2 C_3 C_3^T + \rho_4^2 C_4 C_4^T \right) x + \\
&+ 2 x^T \left(\rho_1^2 C_1 D_1 + \rho_2^2 C_2 D_2 + \rho_3^2 C_3 D_3 + \rho_4^2 C_4 D_4 \right) u + \left(\rho_1^2 D_1^2 + \rho_2^2 D_2^2 + \rho_3^2 D_3^2 + \rho_4^2 D_4^2 \right) u^2
\end{aligned} \tag{9.18}$$

from which the matrices Q, R and N can be obtained as

$$Q = \rho_1^2 C_1 C_1^T + \rho_2^2 C_2 C_2^T \rho_3^2 C_3 C_3^T + \rho_4^2 C_4 C_4^T$$
$$R = \rho_1^2 C_1 D_1 + \rho_2^2 C_2 D_2 + \rho_3^2 C_3 D_3 + \rho_4^2 C_4 D_4 \quad (9.19)$$
$$N = \rho_1^2 D_1^2 + \rho_2^2 D_1^2 + \rho_3^2 D_1^2 + \rho_4^2 D_1^2$$

The penalty terms $\rho_1 = \rho_2 = \rho_3 = 1$ were initially assumed for the design, placing equal emphasis to all three acceleration minimisation objectives. The penalty term on the control effort is set to $\rho_4 = 50$. This is the minimum penalty for a valid solution of the LQR problem. This is because for a lower value of ρ_4 the standard LQR assumptions are not satisfied and the closed-loop system is unstable. The results obtained are identical to the ones from the sample controller designed by Dyke. Note that for a stabilising controller, the standard assumptions of LQR theory must be satisfied:

- The pair (A, B) is stabilisable
- $R > 0$ and $Q - NR^{-1}N^T \geq 0$
- $(Q - NR^{-1}N^T, A - BR^{-1}N^T)$ has no unobservable modes on the imaginary axis

LQG design

Here, the state space equations are assumed to be of the form:

$$\dot{x} = Ax + Bu + \Gamma\omega \quad (9.20)$$
$$u = Cx + Du + \nu \quad (9.21)$$

where ω and ν are unknown errors and disturbances modelled as white noise signals (zero-mean, stochastic processes uncorrelated in time, see section 5.3.3). A state estimator was added at this point. This is an exact replica of the existing system. The sensors are accelerometers that measure the acceleration at each floor. The remaining states (displacement and velocity variables) are estimated. Covariance matrices are chosen as $W = 25$, $V = 1$, $N = 0$ for all sensors. The optimal Kalman filter has a state equations given as:

$$\dot{\hat{x}} = A\hat{x} + Bu + H(C\hat{x} - Cx) \tag{9.22}$$

$$\hat{y} = C\hat{x} + Du \tag{9.23}$$

The 10 performance indices obtained with LQG control are summarised below in Figure 9.2

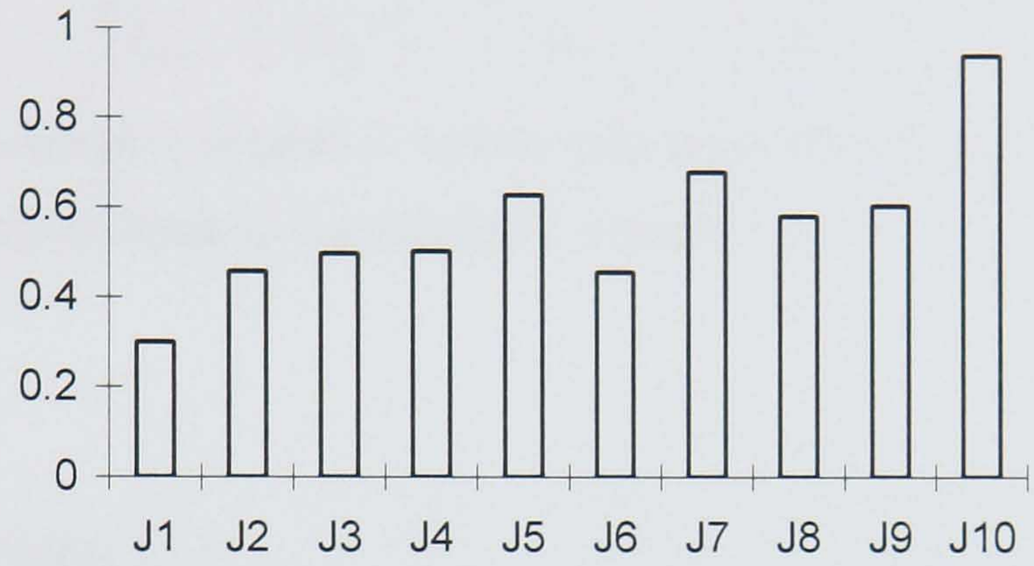

Figure 9.2 Benchmark 1 LQG performance indices

H_∞ control

The second design method uses an H_∞ controller. The method has been described in section 3.6.4 and applied in chapter 5. Here, only the important aspects for the design will be outlined. Recall equations (9.1) to (9.3) below, where (9.1) is the state vector, (9.2) is the measured output and (9.3) is the regulated output. Both the vector of regulated and measured variables are defined to be the three floor accelerations together with the actuator's acceleration. A penalty is included for the control effort, like in the LQR case, to account for the relative importance of each optimisation objective. Here, the meaning of the penalty is different then in LQR because the minimisation norm corresponds to a different quantity then in LQR. The penalty term is adjusted only for the control effort, assuming a unity penalty for the floor accelerations. The generalised plant is obtained by writing the state equations, driven by the vector of external disturbance and the control signal. The output variables are the vector of (appropriately weighted) regulated signals and the measured signals.

$$\begin{bmatrix} \ddot{x}_1 \\ \ddot{x}_2 \\ \ddot{x}_3 \\ \ddot{x}_m \\ \dot{x}_1 \\ \dot{x}_2 \\ \dot{x}_3 \\ \dot{x}_m \end{bmatrix} = \begin{bmatrix} \rho_1 C_1 \\ \rho_2 C_2 \\ \rho_3 C_3 \\ 0 \\ C_1 \\ C_2 \\ C_3 \\ C_m \end{bmatrix} x + \begin{bmatrix} \rho_1 D_{11} \\ \rho_2 D_{12} \\ \rho_3 D_{13} \\ \rho_4 \\ D_{11} \\ D_{12} \\ D_{13} \\ D_{14} \end{bmatrix} u + \begin{bmatrix} \rho_1 F_{11} \\ \rho_2 F_{12} \\ \rho_3 F_{13} \\ 0 \\ F_{11} \\ F_{12} \\ F_{13} \\ F_{14} \end{bmatrix} \ddot{x}g$$

The objective is to design a controller, which minimises the infinity norm of the transfer function from the disturbance to the regulated outputs, i.e:

$$\min_{K \in s} \left\| \begin{bmatrix} T_{\ddot{x}_1} \\ T_{\ddot{x}_2} \\ T_{\ddot{x}_3} \\ T_{\ddot{x}_m} \end{bmatrix} \right\| = \min_{K \in s} \max_{\omega \in \Re} \{ \sqrt{\left| T_{\rho_1 \ddot{x}_1, \nu(j\omega)} \right|^2 + \left| T_{\rho_2 \ddot{x}_2, \nu(j\omega)} \right|^2 + \left| T_{\rho_3 \ddot{x}_3, \nu(j\omega)} \right|^2 + \left| T_{\rho_m \ddot{x}_m, \nu(j\omega)} \right|^2} \}$$

$$= \min_{K \in s} \max_{\omega \in \Re} \{ \rho_1^2 \left| T_{\ddot{x}_1, \nu}(j\omega) \right|^2 + \rho_2^2 \left| T_{\ddot{x}_2, \nu}(j\omega) \right|^2 + \rho_3^2 \left| T_{\ddot{x}_3, \nu}(j\omega) \right|^2 + \rho_m^2 \left| T_{\ddot{x}_m, \nu}(j\omega) \right|^2 \} \quad (9.24)$$

which, represents the weighted sum of the energy of the three regulated signals. A stable controller is obtained that stabilises the closed-loop system. It was discretised using Tustin's transformation and finally simulated. Several values of penalty on the control effort have been applied and the evaluation results for $\rho = 20$ are shown in figure 9.3.

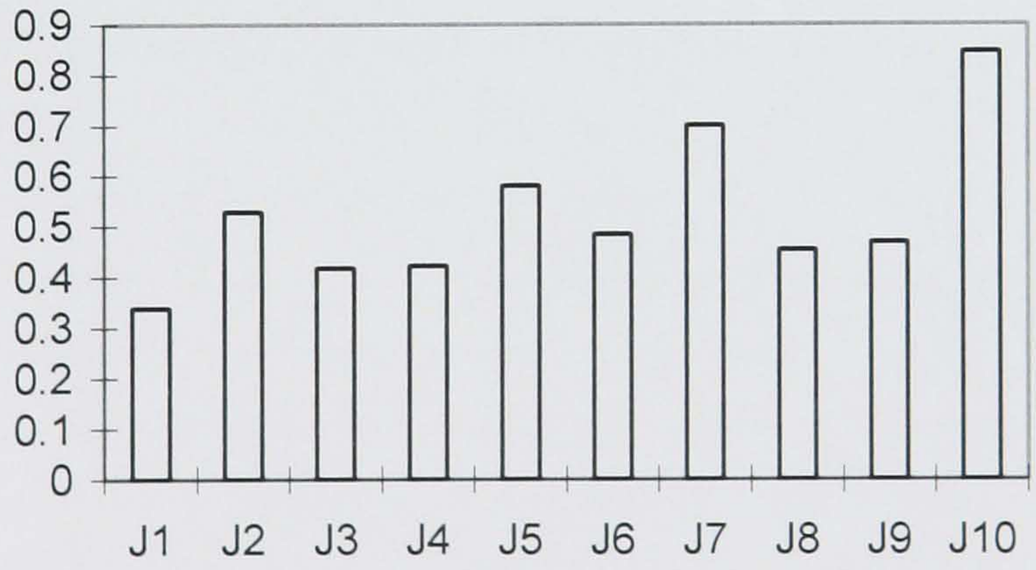

Figure 9.3 Benchmark 1 H_∞ performance indices

LQR with identification filter

The next design is an LQR controller with the addition of an identification filter. The filter forces the controller to place more emphasis to the frequencies of the input where most of the energy is concentrated. When the input is the earthquake, the Fourier transform of the earthquake is obtained and so the distribution of frequencies is known. By increasing the order of the filter the accuracy is increased, but so is the order and complexity of the controller. Figures 9.4 and 9.5 show the spectral density of the two earthquakes, El Centro and Hachinohe. Some modifications in Simulink were needed before obtaining these responses. The El Centro earthquake record runs for 10 seconds and consists of 2500 uniform samples, thus T_s=0.004 s which was the assumed sampling interval of the controller. Similarly, the Hachinohe earthquake record runs for 7.2 seconds and consists of 3600 samples; thus the controller sampling time in this case was changed to T_s=0.002 s from the original value of T_s=0.001 s. A 3rd order filter was found adequate for capturing the spectrum of the two signals. If is was required to maintain the original sampling interval, interpolation of the data records would have been performed – however this was not done as the two new sampling rates are adequate.

The controller designed using the filter reduced control effort but increased the accelerations, displacements and velocities of the each floors. As a consequence a higher control penalty of $\rho = 80$ was used.

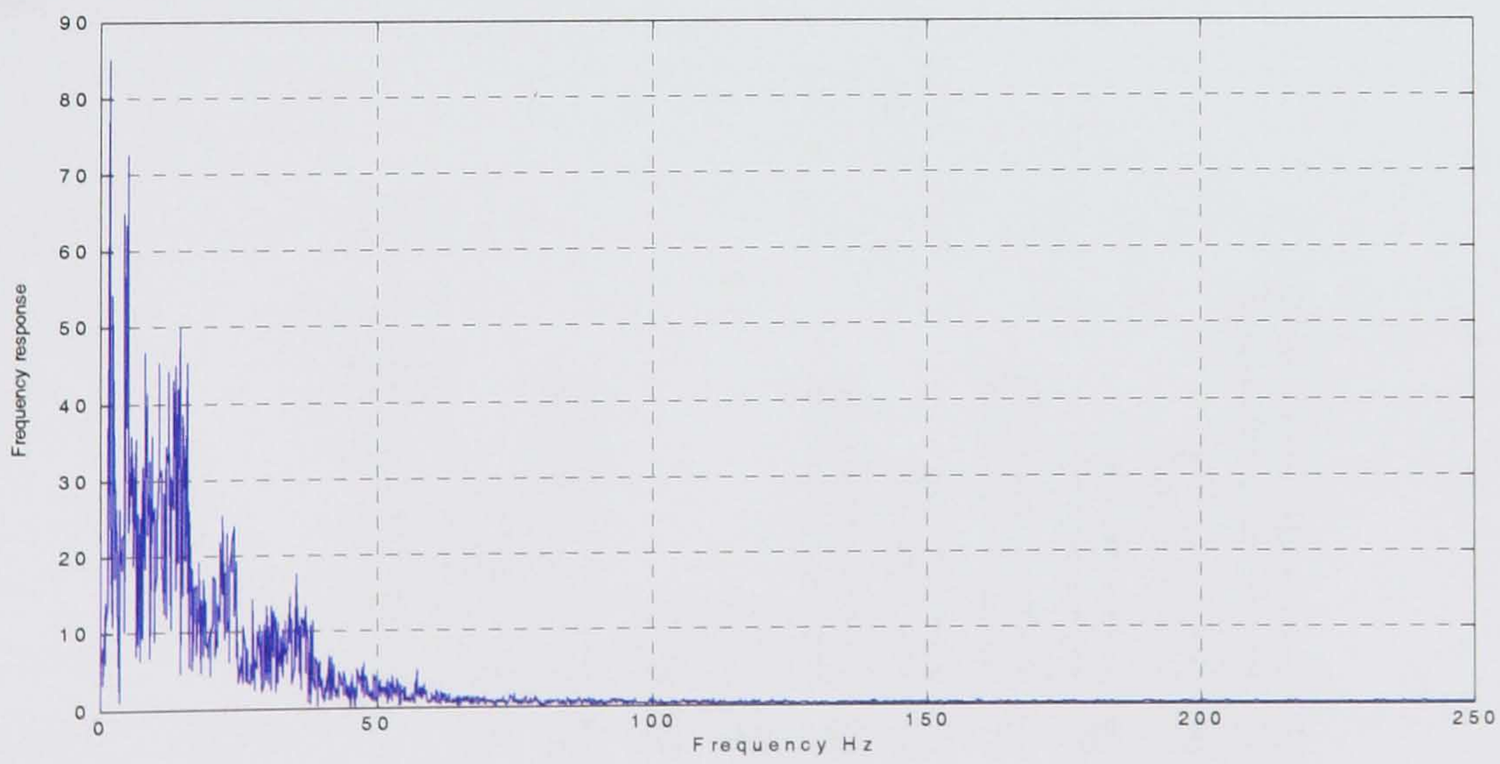

Figure 9.4 Hachinohe earthquake signal Fourier transform

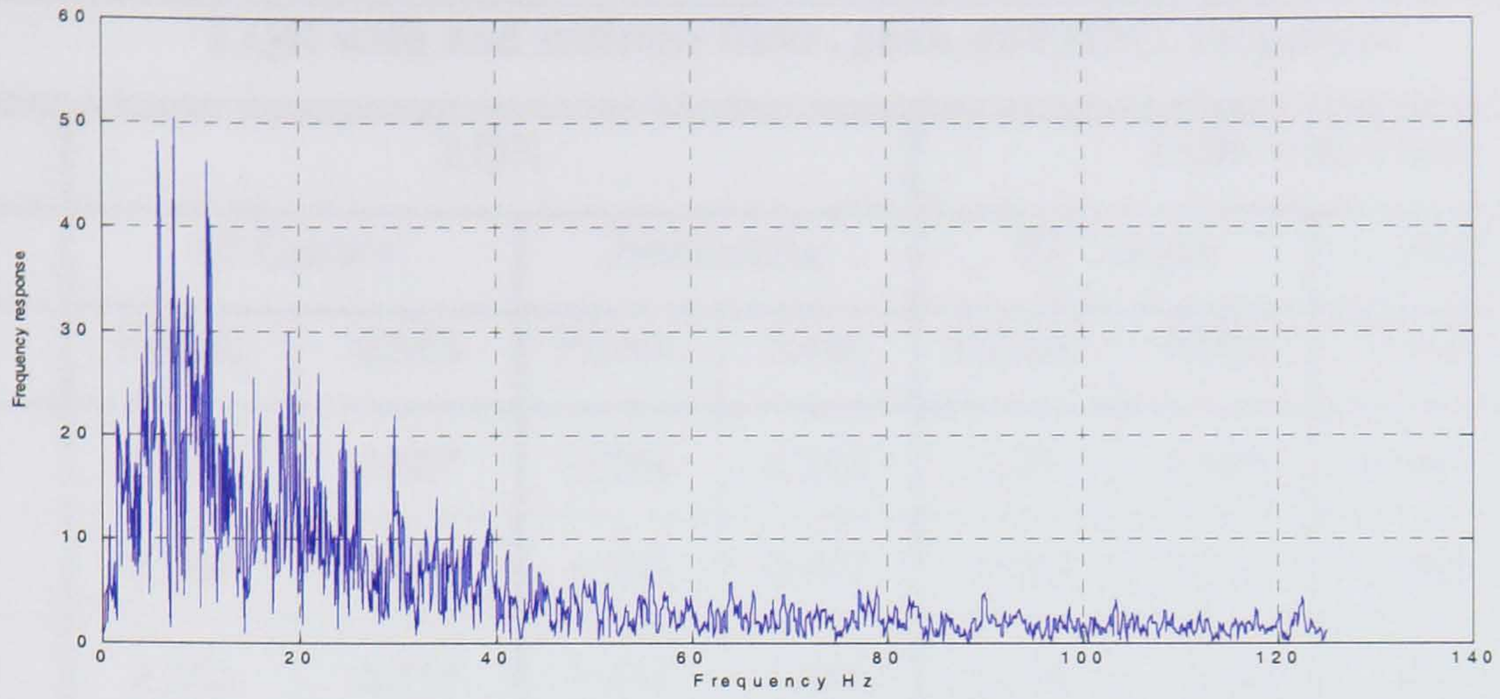

Figures 9.5 El Centro earthquake Fourier transform

The performance indices have not been improved by the addition of the filter. To investigate further the reason for this all the peak and RMS values of the 12 measured indices for the two earthquake records with and without the filter were considered (table 9.1). Clearly the filter has almost no effect when considering the EL Centro EQ, but has improved the performance when considering the Hachinohe EQ. This can be explained because the Hachinohe Earthquake has a narrow frequency band and thus the filter considerably improves performance. In contrast, the EL Centro spectrum has a wide-band and therefore any kind of frequency weighted filter is of little use. The filtered LQR design cannot deteriorate compared to the simple LQR as suggested by the performance indices. This is because the performance indices are obtained by comparing each individual floor for both EQ records and taking the worst case. This combination leads the filtered LQG to be worse for some indices than the simple LQG design.

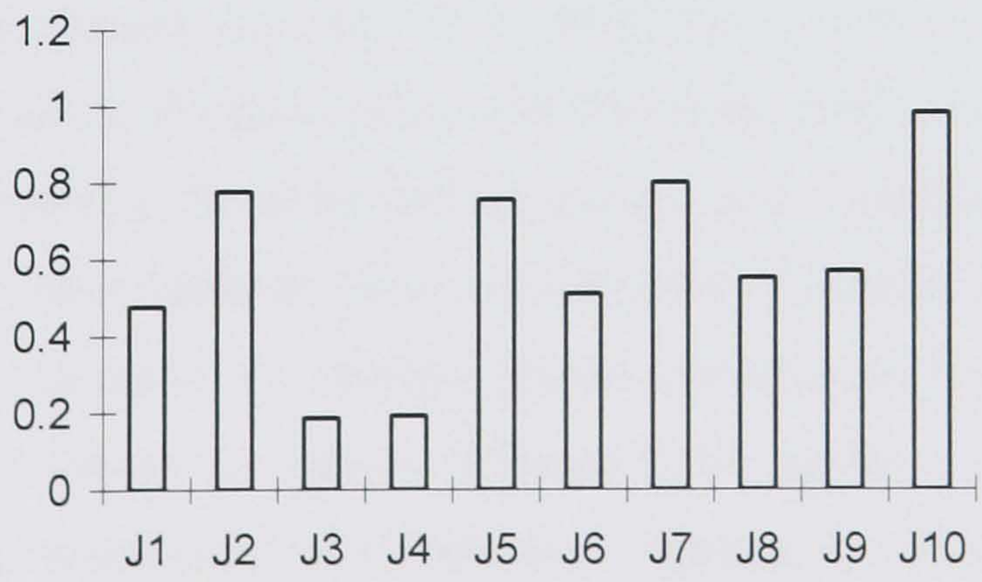

Figure 9.6 Benchmark 1 LQR with identification filter evaluation indices

LQR with and without filter, peak and RMS responses								
	LQR				LQR with Filter			
	El Centro		Hachinohe		El Centro		Hachinohe	
	PEAK	RMS	PEAK	RMS	PEAK	RMS	PEAK	RMS
x_1	1.355	0.507	0.756	0.269	1.37	0.528	0.847	0.321
x_2	2.164	0.78	1.195	0.417	2.193	0.814	1.368	0.503
x_3	2.252	0.717	1.217	0.398	2.298	0.752	1.453	0.5
x_m	2.006	0.884	1.111	0.456	1.894	0.837	0.746	0.365
$\dot{x}_1$	50.42	18.51	27.78	9.672	52.12	19.29	33.59	11.61
$\dot{x}_2$	77.67	28.39	43.33	15.11	78.55	29.72	50.13	18.34
$\dot{x}_3$	78.2	26.38	44.16	14.25	79.38	27.58	49.51	17.94
$\ddot{x}_m$	79.36	32.82	45.49	16.88	74.58	31.04	30.35	13.47
$\ddot{x}_1$	1.854	0.713	1.307	0.39	1.926	0.745	1.321	0.473
$\ddot{x}_2$	2.879	1.076	1.635	0.582	2.898	1.127	1.845	0.704
$\ddot{x}_3$	3.275	1.007	1.866	0.551	3.458	1.054	2.196	0.694
$\ddot{x}_m$	4.837	1.433	3.457	0.812	5.053	1.435	2.808	0.859

Table 9.1

LPOC control

A LPOC was initially designed but is not included here because it cannot be fairly evaluated in this Benchmark problem. The LPOC has a high-order controller which cannot be accomodated by the Benchmark specifications. Furthermore, only one design objective can be included in the minimisation function and a minimum sampling time of 0.1-0.2 *s*., while the other methods have 3 minimisation functions and 10 ms sampling time. The LPOC is designed for specific known disturbances but in the benchmark problem it will be evaluated for various different input signals. Finally, the evaluation criteria are based on "worst-case" of all indices as opposed to LPOC that targets mainly one objective function.

9.2.3 Summary of results

A first generation three storey benchmark structure was designed using several methods which are evaluated. The evaluation criteria were very broad and included as many aspects as possible. Peak and RMS responses subject to two different earthquakes and a filtered random excitation were included. The accelerations and displacement of all floors were included together with the acceleration, velocity and displacement of the controller as well. Finally, the model was made as realistic as possible by including time delay, controller saturation and sensor noise. The design methods used were LQG, H_∞ and frequency weighted LQG.

The LQG and H_∞ methods seem to produce the most effective controllers. They have very similar responses and hence evaluation indices. The RMS responses are broadly similar, slightly lower for the accelerations and displacement variables (evaluation indices J1 and J2) with H_∞ , but also slightly larger control effort measures (evaluation indices J3 to J5). The peak responses are similar with H_∞ requiring a larger control effort to achieve the same level of performance as LQG. On the whole LQG has a marginally better performance, but H_∞ controllers are typically very effective when uncertainty is included in the model as they tend to sacrifice nominal for robust performance. No uncertainty was included in this study and therefore the nominal performance of the H_∞ controller is considered to be good. In both methods the designer has the choice of penalising further the control effort to improve the efficiency of the design.

The weighted LQG evaluation criteria are different to simple LQG. A much lower control effort was initially achieved, thus resulting in much higher displacements and accelerations. By tuning the control penalty coefficients the two designs could be made to have similar evaluation indices for a more direct comparison of the results like with H_∞. This was not done because by penalising the control effort in the weighted LQG design performance would deteriorate significantly and the comparison would not have been valid. In the two previous designs the building performance indices (J1, J2, J6 and J7) were roughly proportional as were the controller indices (J3-J5 and J8 to J10). Here the controller displacements and velocities were low but the controller accelerations

were large which suggests some inconsistency in the objective function formulation, and a less robust design.

Overall the two traditional design methods produced good and consistent results. The weighted LQG design produced the best performance for some indices but also the worst in others. This is because the latter controller was designed under strict assumptions and hence cannot perform as well when these fail to apply of when additional performance criteria are taken into account. As explained earlier, the weighted LQG is expected to perform better than LQG when the disturbance signal has spectral characteristics reflected accurately by the identification filter (which is absorbed in the plant dynamics) but its worst-case performance over many different evaluation criteria and disturbance signals can be inferior. The inability to design a LPOC proves that, in its current state of development, it cannot safely be used in real applications although it has the ability to minimise responses effectively in some circumstances as shown in chapter 7.

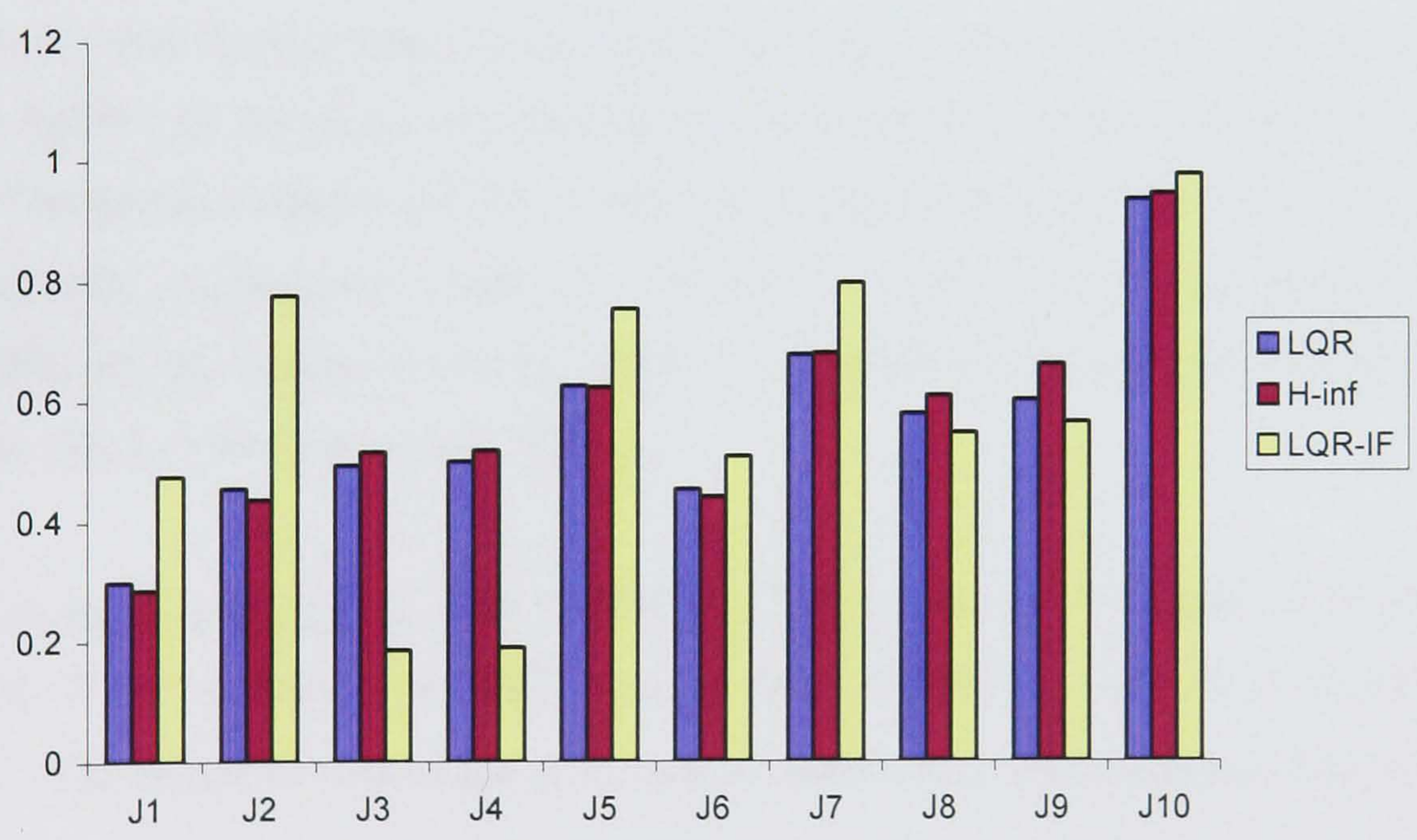

Figure 9.7. Benchmark 1 evaluation indices

9.3. 76-storey benchmark wind excited building

9.1.1. Model description

The second model used is the 76-storey wind excited building representing an office tower in Melbourne. It was fully designed but finally not build due the economic recession. A control device was proposed because the building was slender and therefore wind sensitive. The controller should preferably be an AMD or a TMD at the top floor, but semi-active control schemes can also be included on other floors as well.

Wind forces and earthquake forces are approximately represented in a similar way in civil engineering, i.e. as a horizontal force acting perpendicular to the face of the building. This representation can be an oversimplification for a realistic designs. Sometimes, only one side is assumed to need earthquake protection because the other side is less vulnerable due to the presence of shear walls or other means of protection.

In case of wind loading there is the along and across wind excitation and as a result control systems in two directions are needed. For simplicity only one controller is used here, although the combined effect of both the along and across wind makes the design problem more challenging. Finally, the effects of torsion and of controller-structure interaction are not considered in this study. All background information related to this model is taken from [Yang et al. 1997b1].

Model-building description: The building is 306*m* tall and is made of reinforced concrete. It has a mass of 153,000 tons, volume 520,000 m^3 and mass density 300 Kg/m^3. The height to width ratio is 7:3 and therefore it is wind sensitive. The building consists of a concrete core and concrete frame. The frame was designed to carry the static load and part of the wind load and the core to withstand the wind load. The axis of elastic centre coincides with the axis of mass centre to avoid coupled lateral-torsional motions. There are 24 columns at the perimeter building, spaced equally at 6.5*m*. Each side is 42 *m* long. The columns are connected with beams of dimensions 400 *mm* by 900 *mm*. On top of the beam is the lightweight floor that uses steel beams with a metal deck and a 120 *mm* slab. The compressive strength of concrete used was 60 *Mpa* and the

modulus of elasticity 40 *Gpa*. Finally, the concrete core is at the centre with width 21 *m* by 21 *m*.

The building was modelled using finite element analysis as a vertical cantilever beam. It is assumed that the portion of building between 2 adjacent floors is a classical beam element of uniform thickness. The model consists of 76 translation and 76 rotation degrees of freedom, two per floor. The rotational DOF were removed leaving only the 76 translation DOFs representing the displacements in the lateral direction of each floor. If the controller is included (AMD or TMD) one extra degree of freedom results. The damping ratios of the first 5 modes were assumed to be 1%, while the fundamental mode is 0.16 *Hz*.

For design purposes a control system (TMD or AMD) is added in the top floor producing one more DOF. The default mass of the TMD is 765 *tons*, which is 0.5% of the total mass of the building. Its frequency is tuned to that of the fundamental mode, 0.16 *Hz*, and a large damping is assumed. In the case where the controller is included (AMD and TMD) the 77-DOF system is reduced to a 24-DOF system accordingly. The selected floors for model reduction are floors 3, 6, 10, 13, 16, 20, 23, 26, 30, 33, 36, 40, 43, 46, 50, 53, 56, 60, 63, 66, 70, 73, 76 and the controller mode of the active system.

Evaluation model

Numerically, it is very time consuming to work with the 76 DOF models and therefore model reduction was performed. A method described by [Karrem 1981], [Wu et al. 1998] was used where the eigen-properties of the selected states of the original system are represented in the reduced order system. The 76 DOF system is reduced to a 23 DOF system whereby the first 46 complex modes are retained. When the control system is included (TMD or AMD) the 77 DOF system is reduced to a 24 DOF system. The SS model is given by:

$$\dot{x} = Ax + Bu + EW \tag{9.25}$$

$$y = C_y x + D_y u + F_y W + v \tag{9.26}$$

$$z = C_z x + D_z u + F_z W \tag{9.27}$$

where

$\dot{x}$ is the state vector

u is the scalar control force

W is the wind load vector

y is the measured output with

$$y = \left[\dot{x}_1, \dot{x}_{30}, \dot{x}_{50}, \dot{x}_{55}, \dot{x}_{60}, \dot{x}_{65}, \dot{x}_{70}, \dot{x}_{75}, \dot{x}_{76}, \dot{x}_m, \ddot{x}_1, \ddot{x}_{30}, \ddot{x}_{50}, \ddot{x}_{55}, \ddot{x}_{60}, \ddot{x}_{65}, \ddot{x}_{70}, \ddot{x}_{75}, \ddot{x}_{76}, \ddot{x}_m\right]$$

z is the regulated output $z = \left[\bar{x}, \dot{\bar{x}}, \ddot{\bar{x}}\right]$ where

$\bar{x} = \left[x_1, x_{30}, x_{50}, x_{55}, x_{60}, x_{65}, x_{70}, x_{75}, x_{76}, x_m\right]$ and $\dot{\bar{x}}$ and $\ddot{\bar{x}}$ are defined accordingly

A is the system dynamic matrix reduced from 77 by 77, to 24 by 24.

B is the control input matrix

E is the exogenous ground excitation matrix

C is the measurement matrix

D is the control input feedthrough matrix

F is the exogenous feedthrough matrix

ν is the noise

Note that systems dynamics matrix A is substantially different when considering the 23 DOF system and the 24 DOF system. In order to further reduce the computational time the wind load vector W is reduced. It is assumed to be a lumped load acting precisely on the floors used. Therefore the dimensions of E is reduced to 48 by 24 (or 46 by 23 for the passive model). The designer needs to decide the type of actuator used, the location and their number. The default program assumes an AMD or TMD on the top floor. If the designer wishes he can place the actuator at a different floor, or even use multiple TMD's or multiple semi-active devices placed at several floors, but the program needs to be altered appropriately. Finally, the designer can choose the number and location of sensors. A discrete controller needs to be designed of the form:

$$x_c(k+1) = f_1\left[x_c(k), \tilde{y}(k), u(k), k\right] \tag{9.28}$$

$$u(k) = f_2\left[x_c(k), \tilde{y}(k), k\right] \tag{9.29}$$

where $x_c(k), \tilde{y}(k), u(k)$ are vectors corresponding to the states of the compensator, selected measurement output vector and the control force, respectively. The maximum size of the compensator is limited to 12.

Wind model: An earthquake can be represented by a horizontal force on the basement of a building, even for models requiring great accuracy. In reality wind loads have a widely varying and complex behaviour. The simplest way is to represent it as a constant or linear varying horizontal force acting in the face of the building. The wind load depends on the average wind velocity and a fluctuating component, which can be modelled as a stationary random process. The wind load is also related to the response of the structure, but this interaction can be ignored. The static load due to the average wind velocity can be ignored as well. In order to reduce the computation effort only the along-wind motion will be considered and not the across-wind motion. Finally, there is no coupled lateral torsional motion because the axis of elastic centres and axis of mass centre coincide. These assumptions allow for a realistic model without placing too much effort in computing more detailed wind excitation models.

The along wind fluctuation component model used has the Davenport wind-load spectrum, used also in the Canadian design code. The (i, j) element of the 2-sided cross-power spectral density matrix $S_{w'w'}$ can be represented as [Simiu and Scanlan 1986],

$$S_{w_i w_j}(\omega) = \frac{8\overline{w}_i \overline{w}_j k_0 V_r^2}{\overline{V}_i \overline{V}_j |\omega|} \frac{\left(\frac{600\omega}{\pi V_r}\right)^2}{\left[1+\left(\frac{600\omega}{\pi V_r}\right)^2\right]^{\frac{4}{3}}} \exp\left(-\frac{c_1|\omega|}{2\pi}\frac{|h_i - h_j|}{V_r}\right) \tag{9.30}$$

where ω is in rad/s

V_r is the reference mean wind velocity in *m/s* at 10 meters above the ground

c_1 is a constant,

h_i is the height of the i-th floor,

k is a constant depending on the surface roughness of the ground and

$$\overline{w}_j = E\left[w_j(t)\right] = 0.5\rho A_j C_D \overline{V}_j^2 \tag{9.31}$$

where ρ is the air density,

C_D is the drag coefficient

A_j is the tributary area for the j-th story unit and

$\overline{V_t}$ is the mean wind velocity which is assumed to follow a power law:

$$\overline{V} = V_g \left(\frac{h_t}{h_g} \right)^{\alpha} \tag{9.32}$$

where h_g is the gradient height, V_g being the average wind velocity at the gradient height [Simiu and Scanlan 1986] and α is a parameter taking values between 0.15 and 0.5. The parameters used for this benchmark problem are: $K_0 = 0.03$, $c_1 = 7.7$, $\alpha = 0.4$, $\rho = 1.25 Kg/m^3$, $C_D = 1.2$, $h_g = 300m$. The tributary areas and heights of each wind load locations are shown in figure 9.8:

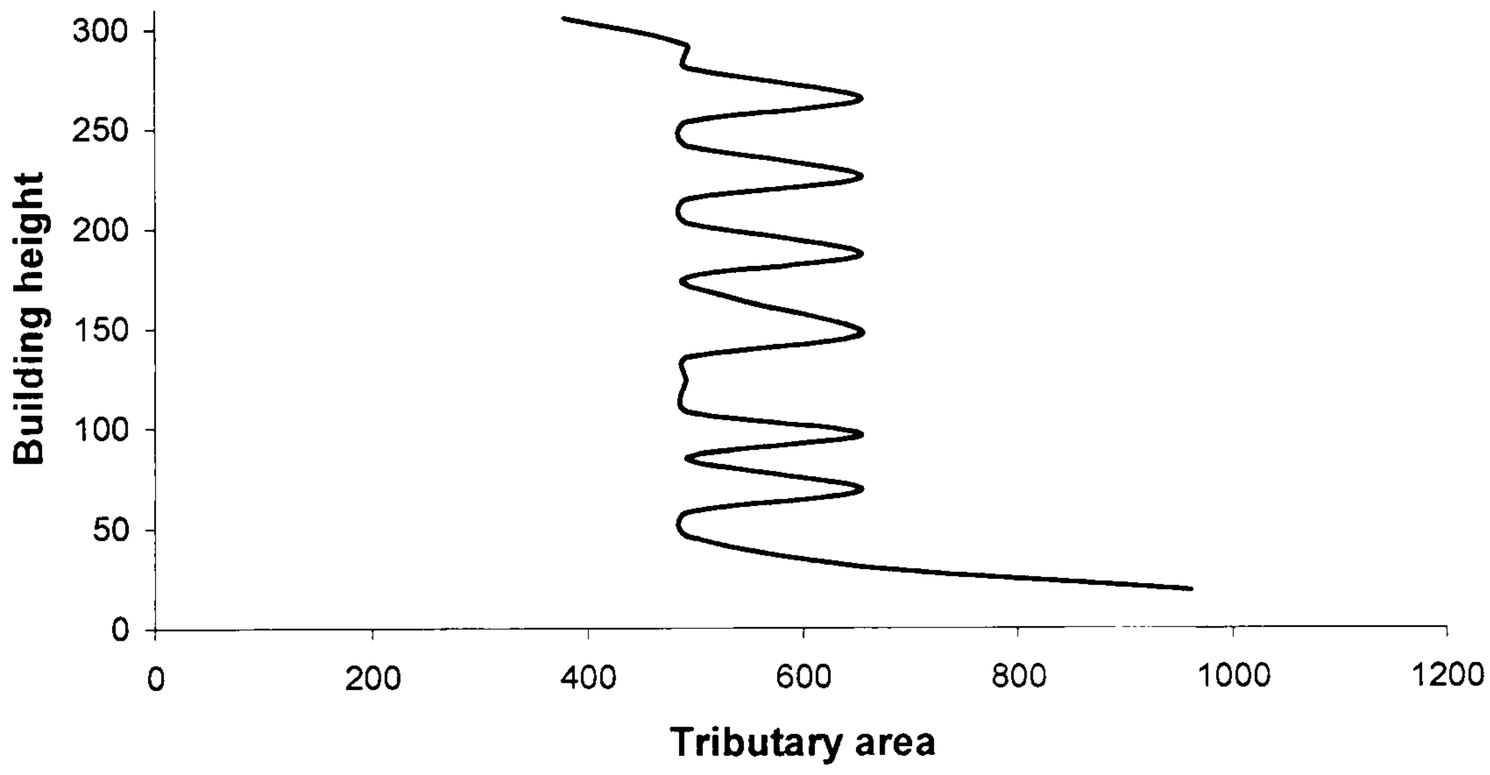

Figure 9.8 Tributary areas as a function of building height

Evaluation criteria: In this benchmark problem there are 12 performance evaluation criteria. As in the 1st benchmark problem half of these are based on RMS response values and the other half on peak response values. The RMS responses are obtained from the stochastic analysis and the peak responses are obtained from a deterministic analysis. The stochastic analysis uses the cross-power spectral density matrix and random vibration analysis. The deterministic response analysis uses a set of 23 sample functions (time histories) of wind loads which was simulated by Yang et al [Yang et al. 1997a].

To reduce the computational time only the responses of some of the floors is calculated, namely the ones that are contained in the output vector z. The performance indices are calculated from these measurements only. As the main objective of the control system is to reduce the occupant's discomfort, the first criterion is the ability to reduce the maximum floor accelerations:

$$J_1 = \max\left\{\frac{\sigma_{\ddot{x}1}}{\sigma_{\ddot{x}75o}}, \frac{\sigma_{\ddot{x}30}}{\sigma_{\ddot{x}75o}}, \frac{\sigma_{\ddot{x}50}}{\sigma_{\ddot{x}75o}}, \frac{\sigma_{\ddot{x}55}}{\sigma_{\ddot{x}75o}}, \frac{\sigma_{\ddot{x}60}}{\sigma_{\ddot{x}75o}}, \frac{\sigma_{\ddot{x}65}}{\sigma_{\ddot{x}75o}}, \frac{\sigma_{\ddot{x}70}}{\sigma_{\ddot{x}75o}}, \frac{\sigma_{x75}}{\sigma_{\ddot{x}75o}}\right\} \qquad (9.33)$$

The denominator is the RMS acceleration of the 75th floor without the controller. The numerator is the RMS acceleration of the *i*-th floor. This index does not have dimensions. The last floor is not considered in the index because there are no occupants in it.

The second criterion is the average percentage reduction from the 50th floor and above:

$$J_2 = \frac{1}{6}\sum\left(\frac{\sigma_{\ddot{x}i0} - \sigma_{\ddot{x}i}}{\sigma_{\ddot{x}i0}}\right) \quad \text{for} \quad i = 50, 55, 60, 65, 70, 75 \qquad (9.34)$$

where $\sigma_{\ddot{x}i0}$ is the uncontrolled RMS acceleration of the ith floor and $\sigma_{\ddot{x}i}$ is RMS acceleration of the *i*-th floor with control. The next two evaluation criteria measure the ability of the controller to minimise displacements. The dimensionless indices are the same ones used to define the first two indices but for displacements:

$$J_3 = \max\left\{\frac{\sigma_{x1}}{\sigma_{x76o}}, \frac{\sigma_{x30}}{\sigma_{x76o}}, \frac{\sigma_{x50}}{\sigma_{x76o}}, \frac{\sigma_{x55}}{\sigma_{x76o}}, \frac{\sigma_{x60}}{\sigma_{x76o}}, \frac{\sigma_{x65}}{\sigma_{x76o}}, \frac{\sigma_{x70}}{\sigma_{x76o}}, \frac{\sigma_{x75}}{\sigma_{x76o}}, \frac{\sigma_{x76}}{\sigma_{x76o}}\right\} \qquad (9.35)$$

$$J_4 = \frac{1}{7}\sum\left(\frac{\sigma_{xi0} - \sigma_{xi}}{\sigma_{xi0}}\right) \quad \text{for} \quad i = 50, 55, 60, 65, 70, 75, 76 \qquad (9.36)$$

Here σ_{xi} is the RMS displacement of the i-th floor and σ_{xi0} is the uncontrolled RMS displacement of the ith floor.

The last two RMS evaluation criteria involve the controller's response. They measure the control effort in terms of actuator displacement and velocity.

$$J_5 = \frac{\sigma_{xm}}{\sigma_{x76o}} \tag{9.37}$$

$$J_6 = \frac{\sigma_{\dot{x}m}}{\sigma_{\dot{x}76o}} \tag{9.38}$$

where $\sigma_{\dot{x}m}$ is the RMS actuator velocity measured as the relative velocity between the ATMD and the top floor. These indices are also dimensionless. The maximum RMS force and stroke applied by the actuator are taken as: $\sigma_u \geq 100KN$ and $\sigma_{xm} \geq 100KN$ respectively. The displacement of the actuator corresponds to the physical size of the control device and its velocity to the control power it requires.

The other evaluation criteria are based on the deterministic response analysis. The indices are the same but now involve peak responses. J7 and J8 are a measure of the ability of the controller to minimise building accelerations and J9 and J10 the ability of the controller to minimise building displacements:

$$J_7 = \max\left\{\frac{\ddot{x}_1}{\ddot{x}_{75o}}, \frac{\ddot{x}_{30}}{\ddot{x}_{75o}}, \frac{\ddot{x}_{50}}{\ddot{x}_{75o}}, \frac{\ddot{x}_{55}}{\ddot{x}_{75o}}, \frac{\ddot{x}_{60}}{\ddot{x}_{75o}}, \frac{\ddot{x}_{65}}{\ddot{x}_{75o}}, \frac{\ddot{x}_{70}}{\ddot{x}_{75o}}, \frac{\ddot{x}_{75}}{\ddot{x}_{75o}}\right\} \tag{9.39}$$

$$J_8 = \frac{1}{6}\sum_i \left(\frac{\ddot{x}_{io} - \ddot{x}_i}{\ddot{x}_{io}}\right) \quad \text{for } i = 50,55,60,65,70,75 \tag{9.40}$$

$$J_9 = \max\left\{\frac{x_1}{x_{76o}}, \frac{x_{30}}{x_{76o}}, \frac{x_{50}}{x_{76o}}, \frac{x_{55}}{x_{76o}}, \frac{x_{60}}{x_{76o}}, \frac{x_{65}}{x_{76o}}, \frac{x_{70}}{x_{76o}}, \frac{x_{75}}{x_{76o}}, \frac{x_{76}}{x_{76o}}\right\} \tag{9.41}$$

$$J_{10} = \frac{1}{7}\sum_i \left(\frac{x_{io} - x_i}{x_{io}}\right) \quad \text{for } i = 50,55.60,65.70.75.76 \tag{9.42}$$

where x_i = peak displacement of ith floor

$\ddot{x}_i$ = peak acceleration of ith floor

x_{io}= peak displacement of ith floor without control

$\ddot{x}_{io}$ = peak acceleration of ith floor without control

The last two evaluation criteria measure the displacement and velocity of the controller. They are an indication of the control effort required by the controller to achieve the buildings response minimisations.

$$J_{11} = \frac{x_{pm}}{x_{p76o}} \tag{9.43}$$

$$J_{12} = \frac{\dot{x}_{pm}}{x_{p76o}} \tag{9.44}$$

where x_{pm} is the peak stroke of the actuator and $\dot{x}_{pm}$ is the peak velocity of the actuator. The maximum control force and stroke allowed is: $\max|u(t)| \le 300KN$ and $\max|x_m(t)| \le 75\ cm$ respectively.

Design constraints for the ATMD

Some implementation constraints are imposed on the control design in order to make the benchmark problem realistic. They are discussed below as given by the 2nd generation Benchmark problems authors [Yang et al. 1997b].

1. Theoretically, the acceleration and velocity of every floor can be measured and given to the feedback controller. As explained earlier only the accelerations and velocities of the 10 floors of the reduced order model of y are measurable. From these 20 measurable variables a maximum of 6 sensors are permitted. The designer has the choice of deciding the location of the sensors.
2. Because the accuracy of measured velocity may be unsatisfactory, velocity feedback can be obtained by passing the measured acceleration feedback through a filter as described in [Spencer et al. 1998].
3. The controller is digital and has a sampling time of $\Delta t = 0.001s$
4. A computational time-delay of $1ms$ is assumed in the implementation of the imposed controller. It is considered only in the deterministic response analysis.

5. The measurement noise is modelled as Gaussian rectangular pulse process of width $2ms$ and a two-sided spectral density of $10^{-9} m^2 / s^3 / Hz$.
6. In order to limit computational resources, the compensator for the controller can have a maximum of 12 states.
7. Every controller is evaluated using the reduced order evaluation model, i.e the 24 DOF with W24 model.
8. The controller is required to be stable
9. The natural frequency and damping ratio of the ATMD or TMD are design parameters chosen by the designer.
10. The robustness of the controller should be discussed.

9.3.2. Control design

Passive: The model reduction is performed such that the eigen properties of the original system are represented accurately. Hence, the first 46 complex modes are retained. Also the 5 first damping values are assumed to be one. From passive analysis the first 10 frequencies and damping values are obtained (see table 9.2). When running the simulation the designer chooses the following parameters: Uncertainty in stiffness matrix, integration step and total integration time (and sampling time). The first ten frequencies and damping ratios are obtained, and the peak and RMS accelerations, velocities and displacements of the 10 selected floors (regulated output z) are calculated. The displacement of the building is shown in figure 9.9

This 2nd generation benchmark problem gives the designer the choice of implementing apart from active controllers, a TMD as well. It can be placed anywhere on the building but common practise is to put TMD's on the top floors. Hence, it is placed on the 76th storey. A design having a TMD is already included in the benchmark files where the TMD is in the 76th floor. The default values for the TMD are, mass 500 *Kg*, damping ratio 0.2 and tuning ratio 1.

With the introduction of the damper an extra mode is included, of frequency similar to that of the 1st mode but with large damping (18%). As a consequence the damping

Mode frequencies and damping ratios		
Mode	Frequency (Hz)	Damping Ratio
1	0.1600	1.0000
2	0.7651	1.0000
3	1.9921	1.0000
4	3.7899	1.0000
5	6.3945	1.0000
6	9.4577	1.1410
7	13.2481	1.3951
8	17.5136	1.7231
9	22.8172	2.1574
10	28.2235	2.6147

Table 9.2 Mode frequencies and damping ratios

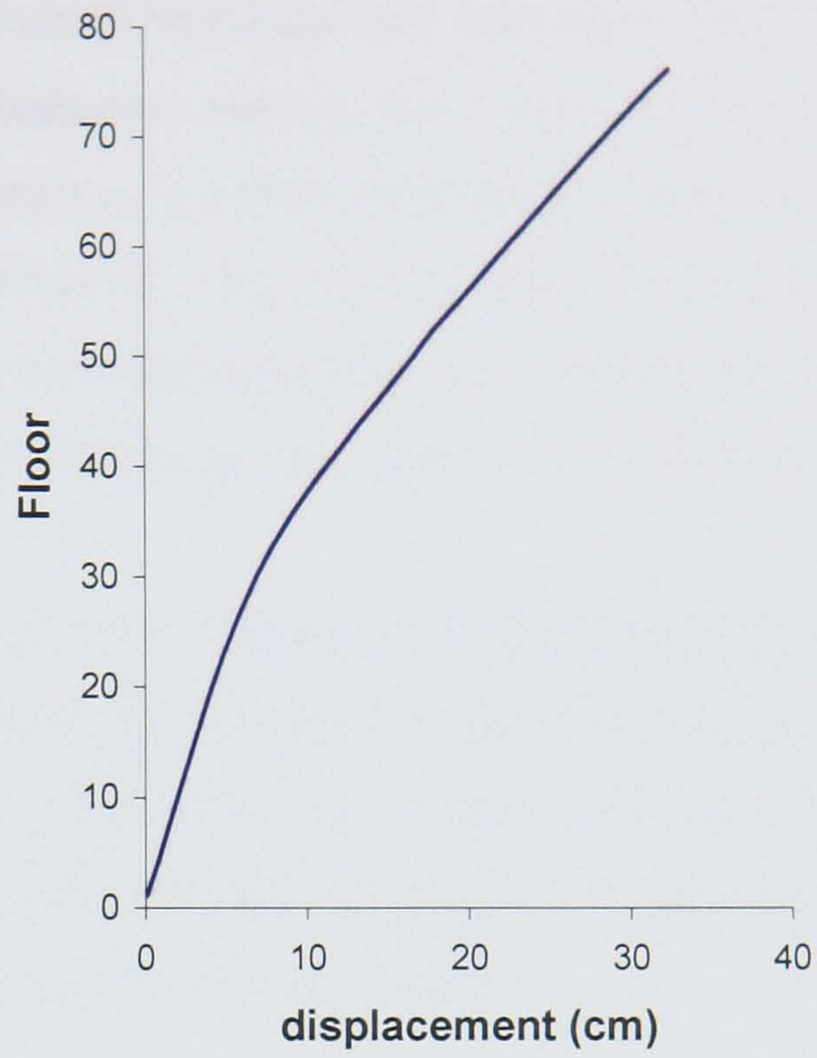

Figure 9.9 TMD building displacement

values of the first mode is increased from 1 to 2.88. All other damping values for the remaining modes are increased as well by a small margin.

The mass of the TMD is 3.3% of the total mass of the building. The peak displacement of the top floor was reduced by 21.4% and the peak acceleration of the top floor by 34.2%. Larger reduction of the RMS values were recorded.

LQR control

A sample controller was designed by [Yang et al. 1997b] that used LQG control. The objective of the LQR is to minimise an index, equation (9.16) subject to plant dynamic constraints given in equations (9.25), (9.26), and (9.27).

Here, subscript r denotes a model reduced to a 12 dimensional state vector x_r where $x_r = [x_{16}, x_{30}, x_{46}, x_{60}, x_{76}, x_m, \dot{x}_{16}, \dot{x}_{30}, \dot{x}_{46}, \dot{x}_{60}, \dot{x}_{76}, \dot{x}_m]$. Reducing the number of states is necessary in order to comply with the sixth restriction on the maximum size of

the compensator being 12. The Linear Quadratic Gaussian controller will have as many states as the state vector x and the state order reduction technique was used again where the first 12 complex modes were retained. The measured output y_r has 3 terms, which is the number of sensors used. The measurement noise v_r is a three dimensional vector, z_r is the 30-dimensional regulated output and matrices C_{zr}, D_{zr}, F_{zr}, C_{yr}, D_{yr} and F_{yr} are defined accordingly. Here, the wind load W and the measurement noise v_r are assumed to be uncorrelated Gaussian white noise vector processes but different components within the W matrix can be correlated.

Returning to equation (9.16) u is the control effort and x includes 30 regulated outputs. The first term represents the states to be optimised, the second term the control effort and N is the cross-term. The appropriate Q, R and N matrices are chosen such that the given control problem can be put in the standard LQR problem formulation. A different path was chosen than the one selected by the benchmark problems authors.

The quadratic optimisation terms are:

$$x_i = \rho_i C_i^T x + \rho_i D_i u \Rightarrow \ddot{x}_i^2 = \rho_i^2 x^T C_i C_i^T x + \rho_i^2 2x^T C_i D_i u + \rho_i^2 D_i^2 u^2 \qquad (9.45)$$

where x_i is any regulated output, C_i and D_i are obtained form the known measurement and feedthrough matrices. Here, it is assumed that the F_y matrix is zero, a valid assumptions because the input is white noise. Also ρ is the penalty term on each objective. A unity penalty factor was used for all floor displacements and for the first five floor velocities and accelerations. The four higher floors are less important and therefore a high penalty was used for velocity and acceleration (10^5). Finally, a low penalty ($\rho = 0.15$) was used for the displacement acceleration and velocity of the actuator.

By summing the 30 objective functions we have:

$$\begin{aligned}\sum_i x_i = x_1^2 + x_2^2 + x_3^2 + \ldots + \ddot{x}_{30}^2 = x^T \left(\rho_1^2 C_1 C_1^T + \rho_2^2 C_2 C_2^T + \rho_3^2 C_3 C_3^T + \ldots + \rho_{30}^2 C_{30} C_{30}^T\right) x \\ +2x^T \left(\rho_1^2 C_1 D_1 + \rho_2^2 C_2 D_2 + \rho_3^2 C_3 D_3 + \ldots + \rho_{30}^2 C_{30} D_{30}\right) u \\ +\left(\rho_1^2 D_1^2 + \rho_2^2 D_2^2 + \rho_3^2 D_3^2 + \ldots + \rho_{30}^2 D_{30}^2\right) u^2 (2) \qquad (9.46)\end{aligned}$$

and therefore the matrices Q, R and N are obtained. By substituting them in equation 1. equation 2 is obtained.

$$Q = \sum \rho_i^2 C_i C_i^T$$
$$R = \sum \rho_i^2 C_i D_i \qquad (9.47)$$
$$N = \sum \rho_i^2 D_i^2$$

Here ρ_i takes the following values in ascending order of i, i.e. $\rho = [1\ 1\ 1\ 1\ 1\ 1\ 1\ 1\ 1\ 1\ 0.15\ 1\ 1\ 1\ 1\ 1\ 10^5\ 10^5\ 10^5\ 10^5\ 10^5\ 0.15\ 1\ 1\ 1\ 1\ 1\ 10^5\ 10^5\ 10^5\ 10^5\ 0.15]$ The values used are the ones suggested by the authors of the benchmarks problem. The results are the same as the ones by [Yang et al. 1997b] and they are shown in figure 9.10. In addition, the standard assumptions of LQR theory must be satisfied:

- The pair (A, B) is stabilisable.
- $R > 0$ and $Q - NR^{-1}N^T \geq 0$
- $(Q - NR^{-1}N^T, A - BR^{-1}N^T)$ has no unobservable modes on the imaginary axis.

LQG design

The state space equations is given by equations 9.20 and 9.21. The sensors are accelerometers that can measure the acceleration at every floor and controller, but here three measurements are used. The other displacement and velocities are estimated. The parameters are $V = 0.1$ for all sensors, $N = 0$ and $W = 25$, is a 24 by 24 matrix with values depending on the excitation power spectral density matrix and the frequency where the spectral peak occurs. The optimal Kalman filter equation with state equations is given by equation 9.22.The 12 performance indices are shown in figure 9.10.

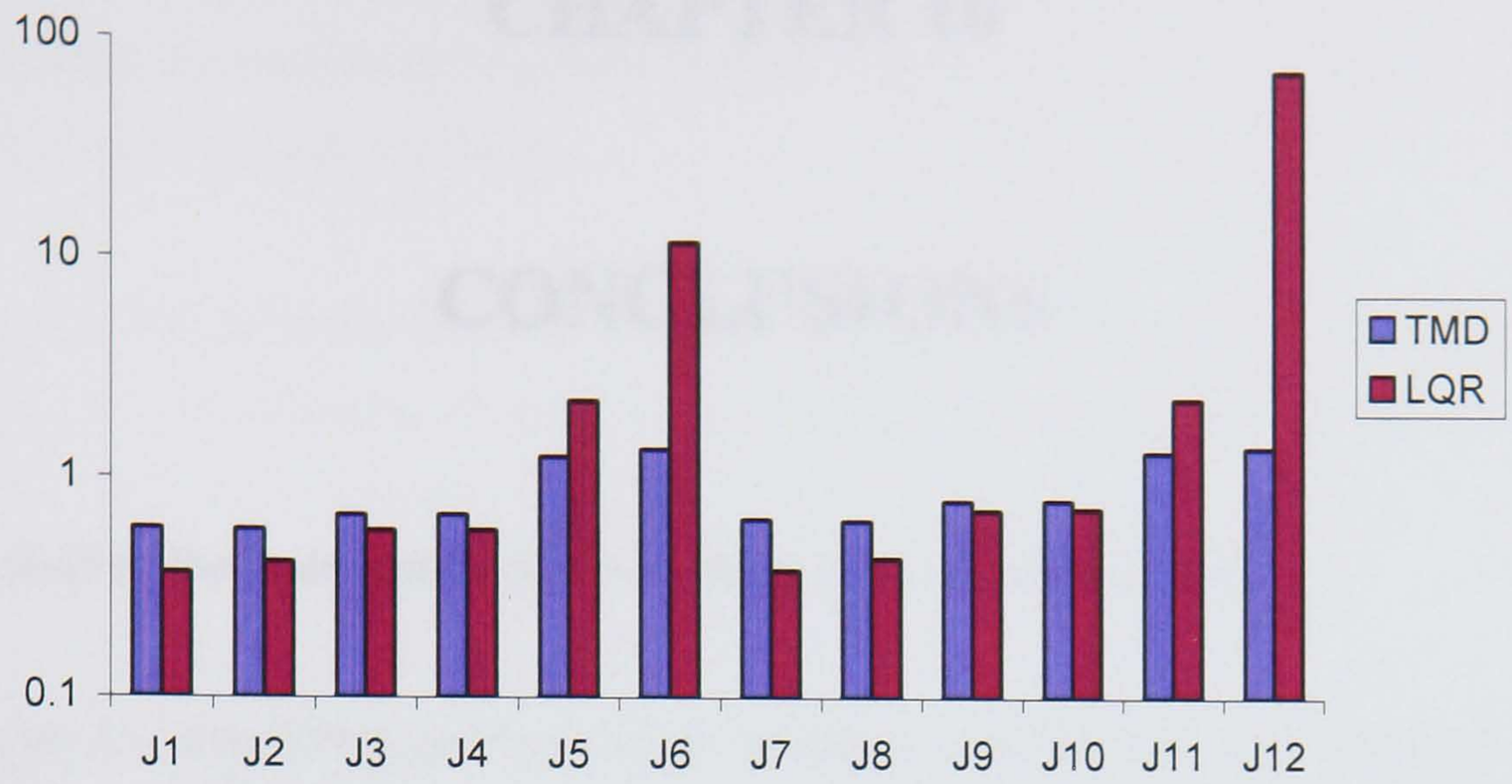

Figure 9.10 Benchmark 2 evaluation indices (TMD, LQG)

9.4. Summary

The purpose of this chapter was to evaluate the various design methods in a more realistic design example. Two benchmark problems were used, one three storey building for earthquakes and wind-loads and a 76-storey wind excited tower. The models were obtained with more sophisticated finite element analysis and the design included aspects such as time delays, saturation of control signals, quantisation effects in digital control, large-scale models and their approximation, multiple design objectives, etc. The designs were evaluated in terms of peak and RMS responses of several floors for various inputs.

The main results obtained from the chapters 5 and 6 about LQR and H_∞ control were confirmed here. This was not the case with the identification filter where the evaluation indices were of similar or lower level. This shows that although various techniques can be used to improve the performance of a system, when it comes to large models with several evaluation criteria robust designs are more effective.

CHAPTER 10

CONCLUSIONS

In this chapter the main results of the research work are summarised.

In chapter 4 a simplified passive energy dissipation mechanism was analysed using the popular TMD device. An idealised frame-pendulum model was used to examine the conditions under which this device can be effective for passive vibration control. It was shown that although the frequency of the additional mode introduced by the pendulum cannot coincide with the frequency of the frame's mode, judicious selection of the design parameters can achieve resonance and effective energy dissipation. In addition, the concept of inelastic deformations has also been analysed. TMD's target specific structural modes. Earthquake resistant structures are specifically designed to perform large inelastic deformations during earthquakes which in conjunction with cyclic loading can cause permanent stiffness degradation and an effective shift in the structure's characteristic frequencies, thus making TMD's less efficient. This concept was demonstrated by a simple example involving a non-linear simulation and the limitations of TMD's (and modal controllers in general) were discussed.

In chapter 5 an LQR controller was designed, incorporating a model of a known earthquake signal into the plant dynamics, identified from its spectral characteristics. As expected, the controller performed considerably better for this particular earthquake signal compared to the standard LQR design, by reducing peak and RMS accelerations by a factor of five, with virtually no increase in control effort. This is a remarkable improvement and proves that there is potentially a significant improvement margin for active control algorithms, especially in cases where the class of disturbances is known, when controllers are designed for specific design objectives or when they target specific modes. This conclusion, however, is no longer valid when considering large-scale models with non-linearities, multiple objectives or disturbances with poorly known spectral content, as demonstrated by the benchmark

problems of Chapter 9. Thus, one of the most challenging design issues in this area is the derivation of realistic and accurate models of earthquake signals related to specific geological and regional conditions.

The Linear Programming Optimal Controller of chapter 7 and the optimal controller involving an identification filter of chapter 5 had considerably better performance than LQR and H_∞ controllers when peak minimisation of regulated signals was the main objective. However, this was no longer the case when these controllers were evaluated in the benchmark problems presented in chapter 9, where performance was assessed by many different criteria and practical limitations of controller implementation were also taken into account (e.g. average and worst-case criteria, controller order, control signal saturation, time-delays, quantisation effects, etc); in contrast LQR or H_∞ designs produced the best and most consistent results and exhibited roughly the same level of performance. Thus, robust designs provided by LQG or H_∞ control methods are still central to general structural control problems, especially in the presence of model uncertainty or unknown disturbances.

An algorithm (LPOC) was proposed which minimises the maximum peak response of regulated outputs, an objective which is highly relevant for structural engineering. The proposed method achieves this goal by placing direct time-domain constraints on the maximum control effort and on its slew-rate. The response is deadbeat and the finite minimisation horizon after which the steady-state is reached can also be determined by the designer. By placing the poles of the closed-loop system to zero in the z-plane, the stability of the system is automatically guaranteed. If the exact type of disturbance is known (and there is no plant uncertainty) the algorithm produces the optimal solution over all deadbeat controllers and in the limit (as the deadbeat horizon tends to infinity) over all discrete stabilising controllers. The disturbance input was initially assumed to be an impulse (which in a sense is the worst type of loading) although extensions to different types of input are possible. The optimisation problem is solved via linear programming subject to constraints on the control signal and its rate which can be used to produce smooth responses and limit the bandwidth of the closed-loop system. Potential problems with the method which need further investigation include computational limitations for problems of high complexity and the high degree of the resulting controller, although model reduction can often be

applied successfully. Enhancing the robustness properties of the design and the extension of the method to sets of disturbances (perhaps with known spectral characteristics) are two issues that require further investigation.

One possible way for connecting the two approaches is to tune on-line a robust controller using information collected in real-time about the model's parameters or the characteristics of the disturbance signal. In this thesis, this approach is followed in Chapter 8, where the stiffness parameters of a structure (initially assumed to be highly uncertain) are estimated on-line using a novel estimation algorithm and subsequently used to re-design a discrete-time LQR controller at each sampling interval. The simulation results show that the adaptive scheme in this case is able to stabilise the structure (which would have been unstable if the initial stiffness parameters were used for designing a fixed LQR controller) and also to reduce the amplitude of vibrations. Conceivably, a similar approach can be followed for estimating the spectral characteristics of the disturbance signal as well, or other important characteristics. Although this general approach seems promising, more work is needed to ensure fast convergence of the estimation scheme and the stability of the resulting adaptive control system in the presence of noisy measurements and system-model discrepancies.

Further work/future direction of research:

- The LPOC designed in chapter 7 is only capable with dealing with small model sizes and stronger linear programming solvers are required for larger scale problems. A full robustness analysis of the method is also necessary. The designed controller is stable but has sharp peaks suggesting that it is sensitive to model uncertainties and non-linearities. This obstacle can be overcome by combining the LPOC with other design methods or by adding frequency weights. Specifically, a combination of the dead-beat parametrisation approach with both linear (for control magnitude and rate) and quadratic performance objectives (reminiscent of LQG) could prove promising, although it would require more complex computations based on quadratic programming. In its present form, the algorithm is generally very sensitive, i.e.

by slightly changing certain design parameters a substantially different response is obtained in some cases. Finally, large order controllers are obtained using the method and controller-model reduction is not always effective in maintaining the same performance levels. Thus, specialised model-reduction algorithms which approximate directly important time-domain characteristics can be investigated.

- In chapter 4 a design involving a frame-pendulum model was analysed. When a simple non-linear stiffness model for the frame was considered, the energy dissipation by the pendulum was considerably lower because the period of the frame increased, thus deviating considerably from the period of the pendulum. During large or moderate earthquakes the non-linear behaviour of steel cannot be avoided. More accurate non-linear models should be considered to model the exact pendulum-frame behaviour. If precise conclusions can be drawn, the tuning of passive controllers can be re-assessed to include this characteristic. The non-linear stiffness model can also be included in the design and simulation of active control schemes.

- The overall nominal performance of LQG methods was marginally better than that obtained by H_∞ controllers. This was not surprising, as H_∞ controllers are typically used due to their robust characteristics, i.e. to account for unmodelled dynamics and parametric uncertainty, often present in structural control applications. Thus, the design with H_∞ control can be conservative, and be outperformed by LQG controllers, as far as nominal performance is concerned. It is worth investigating whether, under model uncertainty, the robust performance of H_∞ controllers can actually surpass that of LQG controllers.

- In chapter 5 an LQR controller incorporating an identification filter of a recorded earthquake signal was designed. As expected, the controller performed considerably better for this particular signal compared to simple LQR, by reducing peak and RMS accelerations by a factor of five. This is a marked improvement and proves that there may be significant margins

available in active control algorithms, when a-priori knowledge is taken into account. However, recorded earthquake signals often have different spectral characteristics, so a detailed modelling work is needed to define appropriate disturbance models (perhaps location specific) which are not too specialised and can thus be used in practice.

- An important assumption made throughout this work (with the exception of the two case studies) is that actuators can react instantaneously to a controller's command. This is not true in practice, especially when large levels of actuation power are needed. Typically, from the start of an earthquake at a remote location until the waves reach a structure, considerable time may pass. Thus, placing sensors at distant locations from the structure which is to be protected may provide valuable "pre-view" information on an incoming earthquake, which can be used to (partially) compensate the actuator's delay, or even pre-empt its response by means of feed-forward action. Provided practical implementation issues can be addressed, such a scheme could prove to be highly effective in the area of active vibration control of civil engineering structures.

References

Agrawal and Yang 2000

Agrawal AK, Yang JN. July 2000. Compensation of time-delay for control of civil engineering structures. *Journal of Earthquake Engineering and Structural Dynamics,* (p.37-62).

Allwright 1988

Allwright J. C., May 1988. Positive semidefinite matrices: Characterization via conical hulls and least-squares solution of a matrix equation. *SIAM Control and Optimization* **26** (3) pp. 537-556,

Allwright 2003

J.C.Allwright, 2003. "*Discrete-Time Systems and Computer Control*. MSc Lectures notes, Imperial College.

Almazan et al 2001

José L. Almazán, Juan C. De la Llera, Nov 2001. Analytical model of structures with frictional pendulum isolators. *Journal of Earthquake Engineering and Structural Dynamics,* (p 305-332)

Alt et al 2000

T. R. Alt, F. Jabbari, J. N. Yang, Jan 2000. Control design for seismically excited buildings: sensor and actuator reliability. *Journal of Earthquake Engineering and Structural Dynamics*, (p 241-257).

Antsaklis and Mitchell 1998

Antsaklis, P. J., and Michel, A. N., 1998. *Linear Systems.* McGraw-Hill.

Arup ARUP website. Available at http://www.arup.com/millenniumbridge/ [Internet]

Baker et al 1999

G., A.Baker, E.A.Johnson and B.F. Spencer, Jr., 1999. Control strategies for a structural control benchmark study: Verification by experiment. *13th ASCE Engineering Mechanics Conference*

Chang et al 2001

Shih-Po Chang, Nicos Makris, Andrew S. Whittaker, Andrew C. T. Thompson, Nov. 2001. Experimental and analytical studies on the performance of hybrid isolation systems. *Journal of Earthquake Engineering and Structural Dynamics* (p 421-443).

Chu et al 2001

S. Y. Chu, T. T. Soong, C. C. Lin, Y. Z. Chen, Nov 2001. Time-delay effect and compensation on direct output feedback controlled mass damper systems. *Journal of Earthquake Engineering and Structural Dynamics,* (p 121-137)

Chung et al 1988

Chung L. L., Reinhorn A.M., Soong T. T., 1988. Experiments on active control of seismic structures, *Journal of Engineering Mechanics* **114** (2)

Chung et al. 1989

Chung L. L., Lin R. C., Soong T. T., Reinhorn A.M., 1989. Experimental Study of Active Control for MDOF Seismic Structures. *Journal of Earthquake Engineering and Structural Dynamics* **115** (8) p. (1609-1629)

Clough and Penzien 1993

Ray W. Clough, Joseph Penzien *Dynamics of structures.* McGraw-Hill International Editions

Constantinou 1994

Michael Constantinou, 1994. Application of Fluid Viscous Dampers to Earthquake Resistant Design. Research Accomplishments, 1986-1994. Buffalo: National Center for Earthquake Engineering Research, Available at: http://mceer.buffalo.edu/publications/resaccom/94-SP02/rsconvert.asp?f=rsa7_fvd.html (Last cited in 2004)

Cook 1995

Robert D. Cook 1995. *Finite element method for stress analysis.* John Wiley & Sons.

Coveney et al 2001

Coveney VA, Johnson DE, Kulak RF, 2000. Modeling the free oscillation of a building supported on high damping rubber isolators in seismic Engineering. 100, The *ASME Pressure Vessels and Piping Conference*, **1**, Nitzal ME (ed.) U.S.A.;

Dahleh and Bobillo 1995

M.A. Dahleh and J.J. Diaz Bobill, 1995. *Control of uncertain systems: A linear programming approach*, Prentice-Hall, Englewood-Cliffs, New Jersey.

D'Amato and Rotea 1997

F. J. D'Amato Mario A. Rotea Oct. 1999. Limits of achievable performance and controller design for the structural control benchmark problem. *IEEE*

D' Amato and Rotea 1999

Fernando J. D'Amato, Mario A. Rotea, Jan. 1999. Limits of achievable performance and controller design for the structural control benchmark problem. *Journal of Earthquake Engineering and Structural Dynamics*, (p 1203-1224)

Damatty 2002

A. A. El Damatty, April 2002. Studies on the Application of Tuned Liquid Dampers (TLD) to Upgrade the Seismic Resistance of Structures. ICLR Research Paper Series – No. 17.

Davis and Vinter 1985
M. H. A. Davis, R. Vinter, 1985. *Stochastic Modelling and Control.* Clapham and Hall

Deutsch, 2001
Frank Deutsch, 2001. *Best Approximation in Inner Product Spaces*. Springer-Verlag.

DIS Available at http://www.dis-inc.com/default.htm [Internet]

Djajakesukma et al 2002
S. L. Djajakesukma, B. Samali, H. Nguyen, January 2002. Study of a semi-active stiffness damper under various earthquake inputs, *Journal of Earthquake Engineering and Structural Dynamics*, (p 1757-1776)

Dyke et al 1994a
S.J. Dyke, B.F. Spencer, Jr., P. Quast, M.K. Sain, D.C. Kaspari Jr. and T.T. Soong, Aug. 1994. Experimental verification of acceleration feedback control strategies for an active tendon system. Report of the National Center for Earthquake Engineering Research, Buffalo.

Dyke et al 1994b
S. J. Dyke, B.F. Spencer, Jr., P. Quast, D.C. Kaspari, Jr., and M.K. Sain, 1996 Implementation of an active mass driver using acceleration feedback control. *Microcompurets in Civil Engineering* **11**, 305-323.

Elnashai 2001
S. Elnashai, 2001. *Earthquake Engineerirng Design.* MEng Lecture notes, Imperial College.

Erberik and Sucuoglou
Erberik and H. Sucuoglu, 2004. System energy dissipation in deteriorating systems through low-cycle fatigue. *Journal of Earthquake Engineering and Structural Dynamics*, p. 49-67.

Eurocode 8 1998
Eurocode 8, 1998. *Earthquake resistant design of structures*.

Firdaus et al 2003
Firdaus E. Udwadia, Hubertus F. von Bremen, Ravi Kumar, Mohammad Hosseini, Jan. 2003. Time delayed control of structural systems, *Journal of Earthquake Engineering and Structural Dynamics*, (p 495-535).

Forrai et al 2003
A. Forrai, S. Hashimoto, H. Funato, K. Kamiyama, June 2003. Robust active vibration suppression control with constraint on the control signal: application to flexible structures. *Journal of Earthquake Engineering and Structural Dynamics*, (p 1655-1676).

Francis 1987

Bruce A. Francis, 1987. *Lecture Notes in Control and Information Sciences, A course in H, Control Theory*. Springer-Verlag

Glover and Doyle 1988

Glover K. and Doyle J.C., 1988. State-space formulae for all stabilizing controllers that satisfy an H∞ norm bound and relation to risk sensitivity. *Systems and Control Letters*, **11**, 167-72.

Gower and Dijksterhuis 2004

J. Gower and B. Dijksterhuis 2004. *Procrustes Problem*. Oxford University Press

Hall 2006

Steven R. Hall, 2006. *Feedback Control*. MIT, Lecture notes. Available at http://web.mit.edu/16.31/www/Fall06/index.html[Internet]

Hamdan and Nayfesh 1989

Hamdan, A.M.A. and Nayfeh, A.H., 1989. Measure of modal controllability and observability for first- and second order linear systems. *Journal of Guidance, Control and Dynamics,* **12** (5), 768.

Hatada and Smith 1997

Tomohiko Hatada and H.Allison Smith, June 1997. Development and Application of Nonlinear Controller Using Variable Damping Design *Proceedings of the American Control Conference*

Housner et al 1997

G.W.Housner, L.A. Bergman, T.K. Caughey, A.G. Chassiakos, R.O. Claus, S.F. Masri, R.E, Skelton, T.T. Soong, B.F. Spencer and J.T.P.Yao, Sep. 1997. Structural control: Past, present and future. *Journal of Engineering Mechanics*,

Hsiung and Chopra 2002

Wen-Hsiung Lin, Anil K. Chopra, June 2002. Earthquake response of elastic SDF systems with non-linear fluid viscous dampers. *Journal of Earthquake Engineering and Structural Dynamics*, (p 1623-1642).

Johnson et al 2003

Jerod G. Johnson, Lawrence D. Reaveley, Chris Pantelides, Feb. 2003. A rooftop tuned mass damper frame *Journal of Earthquake Engineering and Structural Dynamics*, (p 965-984).

Karrem 1981

Kareem, A. 1981. Wind excited Response of Buildings in Higher Modes. *ASCE Journal of Structural Division*, **107**, (ST4), pp. 701-796.

Kelly 1991

James M. Kelly, Jan. 1991. Base isolation: Origins and development." *EERC News*, **12**, (1), January 1991 Available at http://nisee.berkeley.edu/lessons/kelly.html [Internet]

Koshika et al 1996

N.Koshika,M. Sakamoto, I. Fukushima, T Kobori, Dec. 1996. Analytical study on active and non-linear control for large earthquakes" Proceedings of the 35th *Conference on Decision and Control*, Kobe Japan.

Li 2002

Chunxiang Li, Jan. 2002. Optimum multiple tuned mass dampers for structures under the ground acceleration based on DDMF and ADMF, *Journal of Earthquake Engineering and Structural Dynamics*, p 897-919.

Li and Liu 2002

Chunxiang Li, Yanxia Liu, Feb. 2002. Active multiple tuned mass dampers for structures under the ground acceleration, *Journal of Earthquake Engineering and Structural Dynamics*, (p 1041-1052).

Li 2003

Chunxiang Li, Feb 2003 Multiple active-passive tuned mass dampers for structures under the ground acceleration. *Journal of Earthquake Engineering and Structural Dynamics*, (p 949-964).

LIM et al 2003

A. W. Lim, T. Y. Chung, S. J. Moon, July 2003. Adaptive bang-bang control for the vibration control of structures under earthquakes. *Journal of Earthquake Engineering and Structural Dynamics* (p 1977-1994)"

Limebeer et al 1987

Limebeer D.J.N. and Hung Y.S. 1987. An analysis of the pole-zero cancellations in H_α optimal control problems of the first kind. *SIAM Journal on Control and Optimisation*

Limongelli 2003

M. P. Limongelli, Mar. 2003. Optimal location of sensors for reconstruction of seismic responses through spline function interpolation. *Journal of Earthquake Engineering and Structural Dynamics*, (p 1055-1074).

Lynch 1993

Jerome Peter Lynch, Sep. 1998. *Active structural control research at Kajima corporation*. Available at http://eil.stanford.edu/publications/jerry_lynch/nsfkajima.pdf [Internet]

Maciejowski 1989

J.M. Maciejowski, 1989. *Multivariable Feedback Design*. Addison Wesley Publishing Company.

Min et al 2001

Kyung-Won Min, Jae-Seung Hwang, Sang-Hyun Lee, Lan Chung, Sep. 2001. Probabilistic approach for active control based on structural energy. *Journal of Earthquake Engineering and Structural Dynamics*, (p 2301-2318).

Nishimura and Kojima 1991

H. Nishimura and Akihito Kojima, 1991. "Seismic Isolation Control" *IEEE Control Systems*.

Pearson

J.P.Pearson (11). *Notes on l-1 Optimal Control*. Department of Electrical and Computer Engineering Rice University, Houston.

Philips and Harbor 1996

Charles L. Philips, R. D. Harbor, 1996. *Feedback Control Systems*. Prentice Hall 3rd Edition.

Pinho 2001

R. Pinho, 2001. *Seismic Design of Reinforced Concrete*. MEng Lecture Notes, Imperial College.

Rana et al 1997

R.Rana, H.Gupta and T.Singh, Oct. 1997. Application of controllability measure for actuator placement in a civil engineering structure. Proceedings of the 1997 *IEEE International Conference on Control Applications*.

Rockafellar 1970

R. Tyrell Rockafellar, 1970. *Convex analysis*. Princeton Landmarks.

Simiu and Scanlan 1986

Simiu, E. and Scanlan, R.H., 1986. *Wind Effects on Structures*, 2nd Ed., John Wiley & Sons Inc.

Singh et al 2002

Mahendra P. Singh, Sarbjeet Singh, Luis M. Moreschi, Jan 2002. Tuned mass dampers for response control of torsional buildings. *Journal of Earthquake Engineering and Structural Dynamics*, (p 749-769).

Slotine and Li 1991

Jean Jacques E. Slotine Weiping Li, 1991. *Applied Non-Linear Control*. Prentice Hall.

Soong 1990

T.T. Soong, 1990. *Active Structural Control: Theory and Practise*. Longman Scientific and Technical.

Spencer and Sain 1997

Spencer, B.F., Jr. and Sain, M.K.1997. Controlling Buildings: A new Frontier in feedback. *IEEE Control Systems Magazine*, **17** (6), 19-35.

Spencer 2002

B.F.Spencer Jr. Smart Damping Technologies for Dynamic Hazard Mitigation. Available at http://www.pwri.go.jp/eng/ujnr/joint/34/paper/22spence.pdf [Internet]

Spencer et al 1998

A. F. Spencer Jr., S. J. Dyke, H. S. Deoskar, Jan 1999. Benchmark problems in structural control: part I - Active Mass Driver system, *Journal of Earthquake Engineering and structural dynamics* (p 1127-1139).

Stubberud et al. 1994

A. J. Stubberud, I. J. Williams, J. J. DiStefano, 1994, *Schaum's Outline of Feedback Control Systems*. McGraw-Hill

Sun et al 2003

Qing Sun, Ling Zhang, Jinxiong Zhou, Qingxuan Shi, Sep. 2003. Experimental study of the semi-active control of building structures using the shaking table. *Journal of Earthquake Engineering and Structural Dynamics,* (p 2353-2376).

Sznaier 1995

Mario Sznaier, July 1995. A mixed l_∞-H_∞ optimization approach to robust controller design. *SIAM Control and Optimization* **33** (4) p. 1086-1101.

Sznaier et al 2003

Mario Sznaier, Takesh Amishama, and Tamer Inanc, March 2003. *H2* control with domain constraints: Theory and applications. *IEEE Transactions on Automatic Control*, Volume. 48, No.3,

Tsai et al 2003

A. S. Tsai, Tsu-Cheng Chiang, Bo-Jen Chen, Shih-Bin Lin, May 2003. An advanced analytical model for high damping rubber bearings. *Journal of Earthquake Engineering and Structural Dynamics,* (p 1373-1387).

Wang 2002

Wang, Yen-Po, 2002. "Fundamentals of Seismic Base Isolation" Available at Http://www.ncree.gov.tw/itp2002/09_FundamentalsOfSeismicBaseIsolation.pdf [Internet]

Wellstead 1979

P.E. Wellstead, 1979. *Introduction to physical systems Modelling.* Academic Press.

WIKI n.d Available at http://en.wikipedia.org/wiki/Taipei_101 [Internet]

Wong and Yang 2003

K.K.F. Wong and Rong Yang, Nov 2003. Predictive Instantaneous Optimal Control of Inelastic Structures during Earthquakes. *Journal of Earthquake Engineering and Structural Dynamics*. (2179-2195).

Woodgate 1996

Woodgate K., Nov. 2006. A new algorithm for the positive semi-definite procrustes problem.

Wu et al 1998

Wu, J. C., Yang, J.N. and Schmitendorf, W., 1998. Reduced order H-infinity and LQR control of seismic-excited buildings. *Journal of Engineering Structures.*

Xing et al 2001

Liping Xing, Eizaburo Tachibana, Yutaka Inoue, Nov. 2001. Optimal placement of sensors on buildings subjected to intermediate-storey excitation according to QN control method. *Journal of Earthquake Engineering and Structural Dynamics*, (p 1-13).

YANG

Available at http://cee.uiuc.edu/sstl/education/buildingsum.htm Page designed by Guangqiang Yang [Internet]

Yang et al 1997a

Yang, J.N., Wu, J.C., Samali, B. and Agrawal, A.K., 1997b. "A Benchmark Problem for Response Control of Wind-Excited Tall Buildings" Benchmark Problem Package Available at http://www.eng.uci.edu/civil/civileng.html

Yang et al 1997b

Yang, J.N., Wu, J.C., Samali, B. and Agrawal, A.K. (1997b) "A Benchmark Problem for Response Control of Wind-Excited Tall Buildings" Benchmark Problem Package Available at http://www.eng.uci.edu/civil/civileng.html

Youla et al 1976

Youla D.C., H.A. Jabr, and J.J. Bongiorno Jr., 1976. Modern Wiener-Hopf design of optimal controllers: part II, IEEE *Trans. Automation Control* **AC-21**, pp 319-338

Zhang and Ivan 2001a

Yunfeng Zhang, W. D. Iwan, Nov 2001. Active interaction control of civil structures. Part 1: MDOF systems. *Journal of Earthquake Engineering and Structural Dynamics*, p. 161-178.

Zhang and Ivan 2001b

Yunfeng Zhang, W. D. Iwan, Nov 2001. Active interaction control of civil structures. Part 2: MDOF systems. *Journal of Earthquake Engineering and Structural Dynamics*, (p 179-194).

Zhou and Doyle 1998

Kemin Zhou with J.C. Doyle, 1998. *Essentials of Robust Control.* Prentice Hall.